Univerzita Karlova

Přírodovědecká fakulta

Studijní program: Molekulární a buněčná biologie, genetika a virologie

Mgr. Alena Náprstková

Proteiny ALBA v reprodukčním vývoji rostlin

ALBA proteins in plant reproductive development

Disertační práce

Školitel: Prof. RNDr. David Honys, PhD.

Praha, 2025

Prohlášení

Prohlašuji, že jsem závěrečnou práci zpracovala samostatně a že jsem uvedla všechny použité informační zdroje a literaturu. Tato práce ani její podstatná část nebyla předložena k získání jiného nebo stejného akademického titulu.

V Praze, 24. 11. 2025

Funding

This study was financially supported from Czech Science Foundation/GAČR (grants No. 18-02448S, 23-07000S, and 24-10653S), from Ministry of Education, Youth and Sports/MEYS (project LUC25133 TRANSHEAT), and the project TowArds Next GENeration Crops, reg. no. CZ.02.01.01/00/22_008/0004581 of the ERDF Programme Johannes Amos Comenius. Microscopy was performed at the Imaging Facility of the IEB AS CR, supported by MEYS CR LM2023050 'Czech-BioImaging' and IEB AS CR.

Acknowledgements

My deepest thanks belong to my supervisor, Prof. RNDr. David Honys, PhD, who allowed me to study and gain experience in multiple roles connected with my work in the Pollen Biology lab at IEB AS CR and teaching at Charles University. I would like to express my sincere gratitude for the exceptional opportunity and trust in allowing me to demonstrate my lecture skills and lead a practical course. Moreover, the possibility of participating in various international conferences always stimulated my dedication, which was further supported by the opportunity to lead multiple students. Next, I would like to highlight the support I received from my colleagues and former colleagues in the Pollen Biology lab. My special thanks belong to RNDr. Jan Fíla, PhD., for thesis editing and Mgr. Karel Raabe for the trust and for enhancing my skills in molecular cloning and microscopic techniques. There, I would like to emphasize the importance of continuous learning in microscopy, as presented by Ing. Kateřina Malínská, PhD. (the Imaging Facility of the IEB AS CR) and RNA processing and sequencing by Ing. Karel Müller, PhD. (the Transcriptomics and Cloning Facility of the IEB AS CR). My appreciation also belongs to PharmDr. Jindřiška Angelini, PhD., for lending the microtome and to my sister, Bc. Dagmar Náprstková, for her assistance with R-based statistics.

There, I would like to express my sincere admiration for my family's comprehension and support, especially to my partner for their unceasing patience, endurance, and encouragement, as well as to our friends for their unexpected insights and advice. My last dedicated thanks go to the members of the Czech kyudo federation for their essential positivity. I hope my family members who cannot see this thesis would be proud.

Abstract

ALBA proteins with an affinity to nucleic acids form a conserved family among all domains of life. In eukaryotic evolution, their homologs split into two subfamilies: shorter Rpp20-like (which possess the Alba domain) and longer forms represented by the Rpp25-like subfamily (in which additional domains are recognized). Plant genomes typically encode a higher number of *ALBA* genes, which are introduced through chromatin dynamics and reorganization. Although the roles of *ALBA* homologs in plants have been intensively studied, their functions and importance have not yet been fully clarified. This study aims to find their implementation in the reproduction of *Arabidopsis*, particularly in the male gametophyte. Initial experiments uncovered expression patterns of the family in generative organs, followed by protein localizations during pollen development. Further experiments were based on colocalization assays with selected markers for various types of ribonucleoprotein particles (RNPs) in pollen. Concurrently, the Alba family was investigated in connection with the cellular heat stress response in reproductive organs with an emphasis on the male gametophyte. The uniform behavior of ALBA proteins corresponds to their action in dimeric or multimeric complexes. Surprisingly, the acquired results revealed subtle variations between ALBAs, indicating their involvement in different steps of RNA metabolism and cell adaptation to stress. Additionally, loss-of-function mutations of *ALBA* genes result in only a mild plant phenotype, whereas significant overexpression of just one *ALBA* homolog can lead to fertility reduction. Collectively, the achieved results highlighted the impact of ALBA proteins in maintaining cellular homeostasis and during plant reproduction.

Keywords

Arabidopsis thaliana, ALBA proteins, flowering, pollen, heat stress, colocalization, confocal microscopy, overexpression, phenotypic defects

Abstrakt

Proteiny ALBA, které mají afinitu k nukleovým kyselinám, tvoří rodinu konzervovanou napříč všemi říšemi organismů. V evoluci eukaryot došlo k jejich rozdělení do dvou podrodin; kratší, podobné Rpp20 (které mají pouze doménou Alba) a delší, podobné Rpp25 (obvykle obsahují další přídatné domény). V rostlinných genomech se obvykle vyskytuje větší množství genů *ALBA*, které vznikly důsledkem dynamiky a přestaveb chromatinu. Přestože jsou rostlinné homology intenzivně studovány, důležitost jejich funkce zatím není zcela ozřejměna. Tato práce si klade za cíl vysvětlení jejich vlivu na rozmnožování huseníčku, především studuje jejich úlohu ve vývoji samčího gametofytu. První pokusy vedly k popisu transkripční aktivity Alba rodiny v generativních orgánech následované lokalizacemi proteinů ve vývoji pylu. Návazné experimenty byly založeny na kolokalizaci s vybranými markerovými proteiny, které značí různé typy ribonukleoproteinových částic (RNP) v pylu. Současně byla rodina proteinů Alba studována ve spojení s buněčnou odpovědí na teplotní stres v reprodukčních orgánech s důrazem na samčí gametofyt. Podobnosti pozorované v chování proteinů ALBA jsou v souladu s jejich působením v dimerních nebo multimerních komplexech. Získané výsledky překvapivě odhalily drobné odchylky pozorované mezi homology, podle kterých lze předpokládat jejich zapojení v metabolismu RNA na různých úrovních a v buněčné adaptaci na stres. Navíc ztrátové mutace v genech *ALBA* mají jen nepatrný vliv na fenotyp rostlin, zatímco významná nadprodukce i jen jednoho z nich zpravidla vede až ke snížení schopnosti reprodukce. Dohromady tyto výsledky poukazují na význam proteinů ALBA pro udržení buněčné homeostáze a rozmnožování rostlin.

Klíčová slova

huseníček rolní, proteiny ALBA, kvetení, pyl, stres způsobený vysokými teplotami, kolokalizace, konfokální mikroskopie, nadexprese, nestandardní morfologie

Content

List of used abbreviations

3' UTR	-	3' untranslated region
5' UTR	-	5' untranslated region
ALBA	-	ACETYLATION LOWERS BINDING AFFINITY protein
ALBA	-	*ACETYLATION LOWERS BINDING AFFINITY* nucleic acid
AP1	-	APETALA 1
BR	-	Biological replicas
BC1	-	Backcrossed first, uniform generation
BC2	-	Backcrossed second, segregating generation
Ct values	-	Cycle threshold values
C-terminal	-	carboxy-terminal
CO	-	CONSTANS
DAG	-	days-after-germination
ddH_2O	-	double-distilled water
dsDNA	-	double-stranded DNA
eIF4E	-	EUKARYOTIC INITIATION FACTOR 4E
eIF4E1	-	EUKARYOTIC INITIATION FACTOR 4E1
EPP	-	EDTA/puromycin-resistant particles
FLC	-	FLOWERING LOCUS C
FP, FPs	-	Fluorescent Protein, Fluorescent Proteins
FT	-	FLOWERING LOCUS T
GAF1	-	GAMETOPHYTE DEFECTIVE 1
GB	-	GoldenBraid
GC	-	Generative cell
GFP	-	GREEN FLUORESCENT PROTEIN
GI	-	GIGANTEA
GUS	-	β-GLUCURONIDASE
KanFastR	-	Kanamycin and FastRed resistance cassette
MGU	-	Male germ unit
ML	-	Maximum likelihood
MYB	-	
HS	-	Heat stress
IDR, IDRs	-	Intrinsically distorted region, Intrinsically distorted regions
IF3-C	-	C-terminal part of the bacterial TRANSLATION INITIATION FACTOR 3
K16	-	Lysine 16
LFY	-	LEAFY

LLP, LLPs	-	Liquid-liquid phase separation/separations
LP, LPs	-	Laser power, Laser powers
MGU	-	Male germ unit
mRNP	-	Messenger ribonucleoprotein particle
NLS	-	Nuclear localization signal
nosT	-	Nopaline synthase Terminator
oexALBA	-	*proCsWMV::ALBA4-6-GFP::nosT*
oexALBA1	-	*proCsWMV::ALBA1-GFP::nosT*
oexALBA2	-	*proCsWMV::ALBA2-GFP::nosT*
oexALBA4	-	*proCsWMV::ALBA4-GFP::nosT*
oexALBA5	-	*proCsWMV::ALBA5-GFP::nosT*
oexALBA6	-	*proCsWMV::ALBA6-GFP::nosT*
oexGFP	-	*proCsWMV::GFP*
oexGUS-GFP	-	*proCsWMV::GUS-GFP*
PABP	-	POLY (A)-BINDING PROTEIN
PABP3	-	POLY (A)-BINDING PROTEIN 3
PABP5	-	POLY (A)-BINDING PROTEIN 5
PMI	-	Pollen mitosis I
PB, PBs	-	Processing body, Processing bodies
RGG	-	Arginine-Glycine-Glycine
RFP	-	RED FLUORESCENT PROTEIN
Ribo-BiFC	-	80S ribosome visualized by BiFC
RNase P/MRP	-	Ribonuclease P/MRP
RNPs	-	Ribonucleoprotein particles
Rpp20	-	RIBONUCLEASE P PROTEIN SUBUNIT P20
Rpp25	-	RIBONUCLEASE P PROTEIN SUBUNIT P25
SC	-	Sperm cell
ROS	-	Reactive oxygen species
RT	-	Room temperature
RT-qPCR	-	Reverse transcription quantitative PCR
SAM	-	Shoot apical meristem
SC, SCs	-	Sperm cell, Sperm cells
SG, SGs	-	Stress granule, Stress granules
SOC1	-	SUPRESSOR OF OVEREXPRESSION OF CONSTANS 1
SpoVS	-	SPORULATION PROTEIN VS
ssDNA	-	Single-stranded DNA
T1	-	Transgenic first, uniform generation

T2	-	Transgenic second, segregating generation
T3	-	Transgenic third generation
Ta	-	Annealing temperature
TL	-	Transmitted light
TSF	-	TWIN SISTER OF FLOWERING LOCUS T
TR	-	Technical replicas
TU, TUs	-	Transcription unit, Transcription units
VC	-	Vegetative cell
YFP	-	YELLOW FLUORESCENT PROTEIN

1. Introduction

Homologs of the AlbA superfamily encode an ancient group of proteins with nucleic acid-binding capability found in all domains of life. In evolution, the highly conserved branch is divided into two paralogous families, most likely during the primary diversification of the Archaea and Bacteria domains. Further analysis of *ALBA* genes within the archaeo-eukaryotic lineage uncovered highly diverse sequences in Eukaryotes compared to Archaea. Accelerated differentiation within the eukaryotic family depends on pleiotropic functions related to RNA processing and metabolism (Aravind et al., 2003). All members of the large family possess a characteristic functional structure, the nucleic acid-binding Alba domain (Pfam PF01918). This domain mediates the formation of ALBA complexes, which can include dimers, tetramers, and oligomers (Guo et al., 2003; Tanaka et al., 2012; da Costa et al., 2017; Chan et al., 2018; Wang et al., 2019). Moreover, this functional motif shares a key fold with multiple ancient domains found in various proteins and enzymes that have an affinity for nucleic acids and are regulated by temperature (Biou et al., 1995; Guo et al., 2003; Aravind et al., 2003).

1.1. ALBA proteins distribution among Eukaryotes

In evolution, plant genomes underwent genome duplications and rearrangements that introduced gene multiplication and promoted their diversification, including Alba domain-containing genes Plant Alba domain separated from plasmodials over 1800 million years ago, followed by differentiation of protein subfamilies, Rpp20-like and Rpp25-like, about 200 million years later. Genes within the eukaryotic family share a motif characteristic for the Alba domain, which is variable in length and sequence features. Rpp20-like consists of shorter genes that harbor solely an Alba domain, whereas the Rpp25-like subfamily groups longer genes with additional structures, including RNA-binding arginine-glycine-glycine (RGG) repeats. The first diverging branches of eukaryotic Rpp20-like subgroup are formed by sequentially distant homologs of unicellular organisms, *Plasmodium* and *Theileria,* followed by a common branch of plants and other plasmodial homologs. The most recently diverged members of the subfamily comprise *ALBA* genes from Fungi and Metazoa. On the other hand, Rpp25-like members from the plant kingdom are more closely related to metazoan homologs, which enable the grouping of plasmodial, plant, and metazoan genes separately. In bacteria, the absence of a sequence-related bacterial *ALBA* group and the dispersion of bacterial homologs across the archaeal branch indicate their acquisition through horizontal transfer from Archaea (Jagadeesh et al., 2024).

The proportion of the Alba family remarkably differs between species, from a single copy per subfamily in humans (Guerrier-Takada et al., 2002) and unicellular parasites (Mani et al., 2011; Gissot

et al., 2013; Dupé et al., 2014) through small gene families found in *Plasmodium* (Goyal et al., 2012) to expanded numbers in plant genomes comprising up to twenty members in monocot *Zea mays* (Verma et al., 2018; Jagadeesh et al., 2024). The size of ALBA proteins varies significantly according to the content of additional motifs and domains accumulated throughout evolution. The first studies revealed and described sequences within a narrow range of 90–95 amino acids characteristic of archaeal species (Aravind et al., 2003). Interestingly, a marginal portion of eukaryotic homologs comprises products ranging from 150 to 4508 amino acids (Jagadeesh et al., 2024). The length variability of the Alba domain and the presence of extra domains, such as the thioredoxin-like fold, TAXi_N-TAXi_C, HHH_5, TULP, and RGG motifs, initiate variations between species and allow discussions of ALBA functional plasticity (Aravind et al., 2003; Wai et al., 2021; Jagadeesh et al., 2024).

Moreover, the massive expansion of gene numbers and sequence variety in plants hardly reflects identical roles, as small gene families or even sole members emphasize their variability at all levels (Honkanen et al., 2016). Further studies revealed interesting sequence relationships within subgroups in phylogenetically unrelated plant species. The Rpp20-like subfamily possesses highly conserved sequences shared by the green algae *Chlamydomonas*, basal angiosperm *Amborella*, and dicot *Vitis* (grape wine), while Rpp25-like homologs associate with *Amborella* and monocot plants. Unlikely, the Rpp20-like subfamily in moss *Physcomitrella* clusters with monocots, but Rpp25-like members are more related to dicot tomato (Wai et al., 2021). A model plant, Arabidopsis, encodes six *ALBA* genes with typical motifs and domain content, which are equally divided into two subfamilies: Rpp20-like, comprising *ALBA1* (At1g29250), *ALBA2* (At2g34160), and *ALBA3* (At3g04620), accompanied by Rpp25-like, which consists of *ALBA4* (At1g20220), *ALBA5* (At1g76010), and *ALBA6* (At3g07030). Two genes from each subfamily form highly similar pairs (*ALBA1* and *ALBA2*, *ALBA4* and *ALBA5*), followed by more diversified sequences of *ALBA3* and *ALBA6* (Goyal et al., 2016; Verma et al., 2018). In the tomato genome, *ALBA* genes are divided into distinct subgroups. The enlarged Alba family comprises eight members, five genes of the Rpp20-like subfamily (*ALBA2*, *ALBA3*, *ALBA6*, *ALBA7*, and *ALBA8*) and three of the Rpp25-like subfamily (*ALBA1*, *ALBA4*, and *ALBA5*) (Wai et al., 2021). Although most plants possess *ALBA* genes with a typical structure of the Alba domain, some sequences contain unique motifs and do not belong to either of these categories (Verma et al., 2014; Wai et al., 2021). One of the fundamental studies on plants identified nine genes in the genome of monocot rice, *Oryza sativa*. From them, eight genes with a characteristic structure are equally distributed in the Rpp20-like subfamily (*OsALBA3-5* and *OsALBA8*) and the Rpp25-like subfamily (*OsALBA1*, *OsALBA2*, *OsALBA6*, and *OsALBA9*). Although *OsALBA7* has an atypical sequence, it carries a specific domain arrangement similar to that of plasmodial *ALBA3* (Verma et al., 2014; Verma et al., 2018). The exposed variability and diversification of *ALBA* genes among the eukaryotic lineage, especially within plant species, highlight their adaptability and flexibility in the evolutionary process.

1.2. Alba domain

Archaeal and eukaryotic clades diverged in distinct sequence motifs but maintained the core structure of the domain, which consists of the Alba fold found in multiple proteins (Aravind et al., 2003; Jagadeesh et al., 2024). Three distant families were identified to share a similar topology of the Alba fold, despite low sequence similarity in the bacterial lineage (Aravind et al., 2003; Rigden et al., 2008; Jagadeesh et al., 2024). The first of them is the bacterial IF3-C fold, which recognizes tRNA structures and binds rRNA in *Bacillus stearothermophilus* (Biou et al., 1995; Wardleworth et al., 2002; Hada et al., 2008), although it is common to various RNA-binding proteins such as RIBOSOMAL PROTEIN S8, DNAse I, methyltransferases, thiouridine and pseudouridine synthases (Koonin et al., 2001; Aravind et al., 2001; Wardleworth et al., 2002). The number and variety of these proteins highlight the importance of fold conservation in nucleic acid-binding factors, which play a considerable role in RNA processing and metabolism (Aravind et al., 2003). The second group, with a similar topology, comprises proteins of the Sporulation stage V, specifically the SPORULATION PROTEIN VS (SpoVS), and the last family involves the RNA-binding protein YHBY. In the archaeo-eukaryotic lineage, the Alba fold is presumed to have evolved from the YhbY fold, which shares a basic loop responsible for tRNA selection and mRNA recognition (Biou et al., 1995; Wardleworth et al., 2002; Aravind et al., 2003; Jagadeesh et al., 2024). The RNA-binding ability is original to ALBA proteins initially introduced to form complexes with small RNAs regulated by lysine deacetylation, despite studies depicting their DNA-binding affinity (Lurz et al., 1986; Wardleworth et al., 2002; Aravind et al., 2003; Jelinska et al., 2005).

The Alba domain or Alba fold is highly conserved across archaeo-eukaryotic lineage and consists of four β-sheets and two α-helices in β1-α1-β2-α2-β3-β4 order. Elongated β3- and β4-sheets at the carboxy-terminus (C-terminal) of the domain are connected by a flexible loop, which facilitates direct interaction with the minor groove of DNA in archaeon *Sulfolobus solfataricus* (Bell et al., 2002; Wardleworth et al., 2002; Zhao et al., 2003; Chou et al., 2003; Aravind et al., 2003). The DNA affinity of archaeal members is secured by a lysine residue (K16) in ALBA1/SSO10B1, which is necessary for recognition and association with 12 bp of the double-stranded DNA (dsDNA) (Xue et al., 2000; Wardleworth et al., 2002; Jelinska et al., 2005). The DNA-protein interaction is mediated by a dimerization-formed central hydrophobic core with acetylated K16 and non-acetylated lysine 17. The reversible acetylation state is regulated by SIR2 deacetylase (Bell et al., 2002; Wardleworth et al., 2002). The binding affinity of these complexes to DNA is further controlled by histone acetyltransferases and other proteins such as SSO10B2 and SAC7D (Lu et al., 2013). The lysine residues are found within a highly conserved α/β structure at an extended N-terminal β fold in most members (Bell et al., 2002; Aravind et al., 2003; Nag et al., 2024). Although members of both Archaea and Eukarya lineages lack the K16 acetylation target in their amino acid sequences, this indicates its

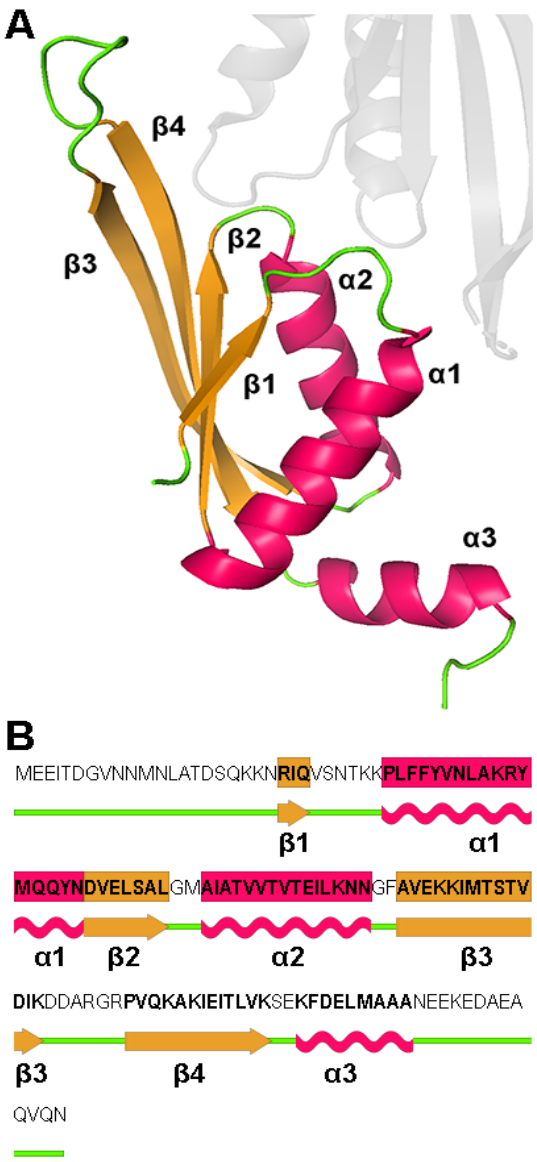

Figure 1: Structure of AtALBA2. (**A**) The protein model based on X-ray structure was obtained from the Protein Data Bank available at DOI: https://doi.org/10.2210/pdb1VM0/pdb. A single strain is shown in colors; β-sheets in orange, α-helixes in pink, and distorted regions in green. The order of secondary structures is marked by numbers from the amino- to the C-terminal end of the protein structure. (**B**) The complete protein sequence encoded by AT2G34160 was obtained from TAIR (www.arabidopsis.org), and secondary structures are highlighted in the sequence, accompanied by a scheme of the structures below.

non-universal role in regulation (Aravind et al., 2003; Jagadeesh et al., 2024). In *Aeropyrum pernix K1*, ALBA1 homologs dimerize purely by hydrophobic interactions between two α1-helices that are stabilised by the coordination of phenylalanine on the dimer's surface. Disruption of ApALBA1 by the F60A mutation revealed that the amino acid sequence of the α1-helices is not essential for the dimer, as supported by the low sequence identity (only 36%) of this region (Laurens et al., 2012).

In eukaryotes, additional amino-terminal (N-terminal) α-helix and β-sheet are typical for yeast POP6/7 homologs, and an extra structure of β-sheets and α-helices was identified between β3 and β4 loops in fungi. An additional C-terminal α-helix extension (α3) is characteristic of the Rpp20-like subfamily in plants (Figure 1), and two ALBA3/4 proteins in *Plasmodium* (Jagadeesh et al., 2024). According to these findings, the most conserved region of the Alba fold is located between the β1-sheet and the α2-helix, which carries essential sequence motifs and residues. The lysine-rich motif KKP/TKK is encoded within the α1-helix in PfALBA3 and OsALBA1, which facilitates DNA affinity (Goyal et al., 2012; Verma et al., 2014). Further in the center of the domain is a highly conserved glycine residue (G43/G77) in the β2-sheet, shared among the archaeo-eukaryotic lineage, which is responsible for RNA binding (Verma et al., 2014; Jagadeesh et al., 2024). Moreover, the β2-sheet and α2-helix create a stable cluster in plants (Jagadeesh et al., 2024).

The Rpp20-like subfamily characteristically comprises members with an extended synapomorphic C-terminal motif with the FDXH sequence (where H represents a hydrophobic residue, typically L). This signature was found in the prevalent number of ALBA proteins in yeasts, vertebrates, nematodes, insects, protozoan parasites, and related proteins identified in plants, including AtALBA1-3. Next, the C-terminal extension of the Rpp25-like subfamily typically possesses the GYQXP signature, also found in AtALBA4-6 (Aravind et al., 2003; Mani et al., 2011).

1.3. RGG domain

Many members of the Rpp25-like subfamily have an extended low-complexity region that lacks a defined three-dimensional structure. Encoded sequence motifs comprise highly repetitive signatures that typically generate intrinsically disordered regions (IDRs) with the ability to form secondary structures through intermolecular interactions (Emenecker et al., 2020). IDRs are responsible for the multivalence of molecules (protein or RNA) that is necessary for phase separation *in vitro*. This attribute is provided by the interactions of structured domains, domain-IDRs, and IDR-motifs, which promote the accumulation of various compounds called scaffolds (Figure 2). Liquid-liquid phase separation (LLP) secures cytoplasmic compartmentalization without an endomembrane system that is essential for intracellular organization (Gomes et al., 2019; Emenecker et al., 2020). These subcellular aggregates are typically referred to as ribonucleoprotein particles (RNPs), cellular bodies, or foci, all of which share a common feature of spatial biomolecule concentration (Banani et al., 2017; Emenecker et al., 2020). In plants, several granules are described in the cytoplasm, for example, processing bodies (PBs) (Maldonado-Bonilla, 2014) and stress granules (SGs) (Hamada et al., 2018; Emenecker et al., 2020).

The Rpp25-like homologs typically comprise approximately 200–300 amino acids, containing RGG trinucleotide repeats that extend their C-terminal ends (Reichel et al., 2024). The created RGG box is known for its RNA-binding properties, specifically recognizing guanine-rich secondary structures that form rigid G-quadruplexes (Vasilyev et al., 2015; Ozdilek et al., 2017). It is presented in the sequences of multiple proteins involved in RNA biogenesis and processing, as well as DNA-damage-induced cell death, reviewed in (Thandapani et al., 2013). RGG-box affinity to RNA is regulated by protein arginine methyltransferase, which specifically modifies arginine residues (Kiledjian et al., 1992; Liu et al., 1995; Darnell et al., 2001; Mani et al., 2011). According to these characteristics, the RGG domain could be involved in ALBA protein accumulation and granule formation (Baron et al., 2012).

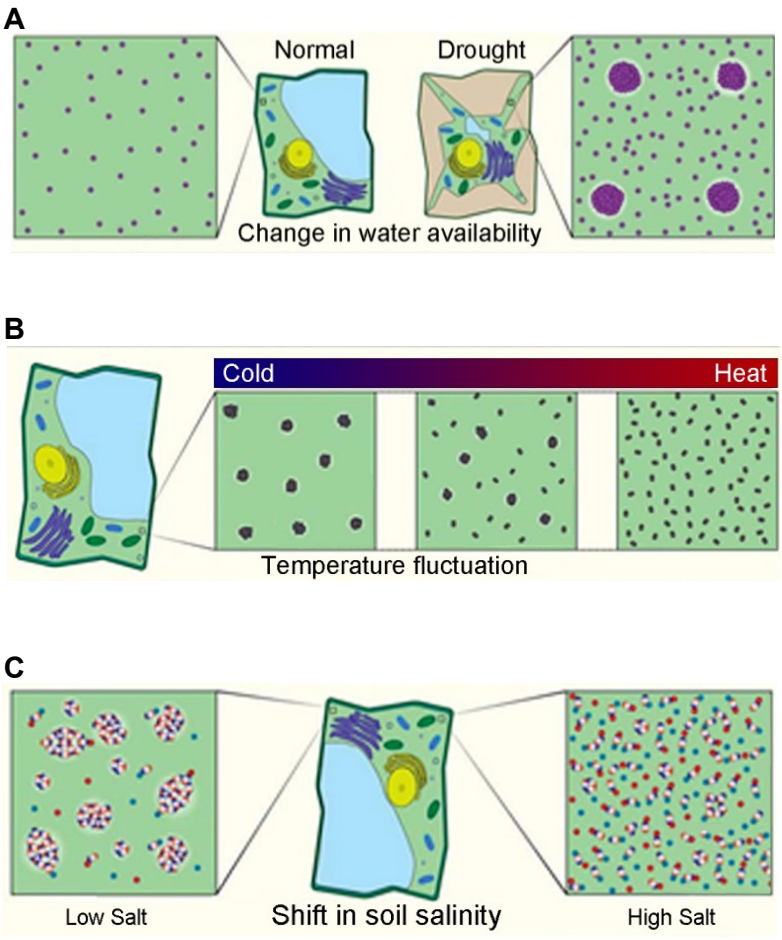

Figure 2: Phase separation and material aggregation upon cellular responses to stress conditions. This scheme shows three putative ways of phase separation processes induced by stress conditions. Water accessibility influences the concentration of biomolecules in the cytoplasm, leading to their aggregation and protection during drought (**A**). Temperature changes can enhance the aggregation or dissolution of biomolecules. Their fluctuation and partial aggregation could be disrupted and affect cellular processes (**B**). Osmotic stress caused by a shift in cell cytoplasm salinity content can disrupt native accumulations of related compounds (**C**). The figure is based on (Emenecker et al.,

1.4. Molecular processes

ALBA proteins play multiple roles in cell processes, depending on the characteristics of individual residues, sequence motifs, simple folds, and complex domains that are responsible for molecular interactions. The first documentation of ALBA subcellular localization was performed in onion epidermal cells that transiently expressed *OsALBA1*, C-terminally fused with GFP. The visualization displayed a predominant signal distribution in the cytoplasm, accompanied by a lower level fraction in the nucleus (Verma et al., 2014). Recently, three homologs were examined in tomato; *ALBA4-6* were fused with *GFP* and transiently expressed in rice protoplasts. The signal indicates a predominant localization in the cytoplasm, supplemented by nuclear presence (Wai et al., 2021). In Arabidopsis, transiently expressed *ALBA1* and *ALBA2* were localized in the cytoplasm (C-terminal GFP fusions) or in the nucleus (GFP-ALBA2), although they were previously isolated from the nucleolar fraction (Palm et al., 2016; Yuan et al., 2019). In the nucleus, ALBA1 and ALBA2 form homodimers and a heterodimer at active sites of DNA where they recognize and stabilize R-loops, DNA-RNA hybrids accompanied by ssDNA (Santos-Pereira et al., 2015; Yuan et al., 2019).

In Arabidopsis stable lines, ALBA proteins are localized in the cells' cytoplasm of young tissues, including growing rosettes, roots, and flower buds (Náprstková, 2016; Wang et al., 2019). The available data indicate that the closest homologs of each family, ALBA1 and ALBA2, and ALBA4 and ALBA5, are localized in the cells' cytoplasm of the root tips (Náprstková, 2016; Wang et al., 2019). However, further studies have connected members of both families (ALBA2 and ALBA4) with mRNA via interaction with ECT2 *in vivo* (Reichel et al., 2024). The multivalent ECT2-ALBA-mRNA complex likely serves as a molecular scaffold for material accumulation and phase separation in the cytoplasm. Moreover, ALBA4 predominantly binds *3′ UTRs* of the same mRNA set as ALBA2. ALBA4 preferentially recognizes pyrimidine-rich motifs of uridine tracts that are tightly neighbored by m^6A, which is occupied by ECT2 (Fray et al., 2015; Reichel et al., 2016; Arribas-Hernández et al., 2021; Reichel et al., 2024). This post-transcriptional modification affects RNA processing, modification, localization, stability, and translatability, which are provided by RNA-binding proteins (RBPs) (Hentze et al., 2018). The reading of m^6A is reportedly mediated by the Alba domain, which induces theories of the C-terminal IDR role in the process. The RGG domain importance is reflected by the severity of homozygous *alba456*$^{+A/+A,+T/+T,\ \ +T/+T}$ mutant phenotypic defects compared with *alba123* mutant (Tong et al., 2022; Reichel et al., 2024). Moreover, ALBA4 and ALBA6 are further involved in RNA metabolism and heat stress response in the cytoplasm (Gosai et al., 2016; Reichel et al., 2016; Tong et al., 2022; Jagadeesh et al., 2024). The Alba-family members are comprehensively regulated at several levels, from transcription to translation and protein interactions with family members and other proteins (Verma et al., 2014). Although the summary functional diversity of ALBA proteins across all kingdoms of life highlights their capability and progressivity in adapting to the current requirements of a cell, the major function of plant subfamilies may be based on genome maintenance and manifestation (Jagadeesh et al., 2024).

The initial references to *ALBA* genes in plants were based on sequence homology with known orthologs, followed by correlations of their behavior with protozoan parasites, humans, and yeast. Most studies have been dedicated to simple unicellular organisms, such as *Trypanosoma*, *Plasmodium*, and *Leishmania* (Subota et al., 2011; Chêne et al., 2012). Among a group of parasitic species, the Alba family comprises small gene families that encode proteins involved in RNA metabolism and translation, with a predominant localization to the cytoplasm (Mair et al., 2010; Mani et al., 2011; Dupé et al., 2014). Upon stress, ALBA proteins aggregate in nuclear or cytoplasmic RNPs (Fetzer et al., 2002; Hua et al., 2004). In *Trypanosoma brucei*, all ALBA proteins can form heterodimers; however, the cytoplasmic localization of the Rpp20-like subfamily is facilitated by interaction with the Rpp25-like subfamily, bridged by RNA (Mani et al., 2011). Starvation and heat stress (HS) trigger their accumulation in cytoplasmic foci (Cassola et al., 2007; Kramer et al., 2008). The aggregates are commonly found in several organisms, typically referred to as PBs and SGs (Buchan et al., 2009; Subota et al., 2011). Upon starvation stress, ALBA proteins fully colocalize

with the SG marker but partially overlap with the PB marker signal. PBs consist of translation repressors, mRNA decay machinery, and translationally inactive RNAs with variable fates that can be either stabilized or degraded, depending on the type of transcript (Decker et al., 2012; Aizer et al., 2014; Jang et al., 2019). In contrast, elevated temperature merely alters the ALBA localization pattern, resulting in even lower co-occurrence with heat stress-induced SGs (Subota et al., 2011). SGs most likely facilitate the effective translation of stress-related transcripts by selectively regulating the synthesis or degradation of hosted poly(A) mRNAs, accompanied by RNA-binding proteins and translation initiation factors (Anderson et al., 2009; Buchan et al., 2009; Vanderweyde et al., 2013; Iserman et al., 2020).

In *Trypanosoma cruzi*, all members of the Alba family are expressed during the parasite life cycle, although their amount varies at the protein level, indicating post-transcriptional regulation. Both members of the Rpp25-like subfamily play a canonical role in RNA processing in later developmental stages. In contrast, diversified members of the Rpp20-like subfamily are presumably involved in different processes (Matiz-González et al., 2024). In *Toxoplasma gongii*, the encoded ALBA heterodimer recognizes various mRNAs, including its own, and regulates the translation of specific transcripts involved in differentiation and stress response. Moreover, their molecular function relies on the translatability of *ALBA2,* which depends on *3′ UTR* recognition by the ALBA dimer and interaction partners, such as ssDNA and ssRNA-binding TgSSOSSB. TgALBAs exhibit a dual localization pattern that varies according to the actual ontogenetic stage. In the extracellular form of the parasite, both proteins accumulate in perinuclear foci colocalizing with the endoplasmic reticulum and RNP markers, although they are randomly distributed in the cytoplasm of intracellular stages (Gissot et al., 2013; Boulila et al., 2014).

A similar role of ALBA proteins has been described in *Leishmania*. In the promastigote stage, ALBA3 regulates the stability of stage-specific β-amastin transcripts, which encode putative virulence factors in the cytoplasm. Recognition of β-amastin *3′ UTRs* provides transcripts destabilization underpinning the importance of ALBA3 precise regulation, which is mandatory for maintaining high target content (Dupé et al., 2014; Pérez-Díaz et al., 2017). Cell differentiation is induced by a heat shock (from 25 °C to 37 °C), triggering the re-localization and enrichment of ALBA1 (Rpp20-like subfamily) and ALBA3 (Rpp25-like subfamily) in the flagellum and nucleolus (Dupé et al., 2015). The nucleolar localization initially confirmed by the NOP10 marker was further supported by its increased accumulation at nucleolar rearrangements under stress conditions (Olson, 2004; Boisvert et al., 2007). This suggests diversification of ALBA roles in *Leishmania*, especially through mRNA translatability and maintenance in RNPs throughout development. ALBA protein cytoplasmic localization is restored in fully differentiated amastigotes, indicating ALBA shuttling (Dupé et al., 2015).

Although ALBA proteins have been studied in two plasmodial species, their localization and function greatly vary. Although they are restricted to cytoplasmic RNA-related processes in *P. berghei*, *P. falciparum* has adopted the most prominent nuclear position in transcription regulation (Acharya et al., 2025). In *P. berghei* oocytes, maternal mRNAs are accumulated and stored for further fertilization processes. In these aggregates, called P granules, transcripts are bound to the translation machinery, including eIF4E and PABPs, in contrast to PBs, which lack the factors responsible for RNA degradation (Mair et al., 2010). Despite this, *PfALBA3* and *PfALBA6* are constitutively expressed throughout all asexual blood stages. ALBA3 is localized to nuclear foci with variable distribution, fluctuating from peripheral appearance at ring stages to dispersed localization in the trophozoite and the schizont stages. The dynamics of ALBA3 are modulated by an acetylation state and SIR2A deacetylase activity at the nuclear periphery of telomeric and subtelomeric regions associated with Telomere-Associated Repetitive Elements (TARE1 and TARE6) in ring stages (Freitas-Junior et al., 2005; Mancio-Silva et al., 2008; Tonkin et al., 2009; Chêne et al., 2012; Goyal et al., 2012). On the contrary, ALBA6 is predominantly localized in the cytoplasm, with a small portion in the nucleus, and its roles are connected with DNase activity and the maintenance of cell homeostasis under stress (Nag et al., 2024). Altogether, ALBA proteins play various roles necessary for protozoan development and reproduction under both standard and stress conditions. Their sequestration to RPBs depends on starvation, temperature stress, and pH, but also responds to DNA damage induced by oxidative stress (Zadow et al., 2025).

Similar to PfALBA6, the sole homologs of ALBA proteins in yeast and humans, RPP20/POP7 and RPP25/POP6, form a heterodimer targeted to the nucleolus. The dimer associates with a multisubunit enzyme with nuclease activity, ribonuclease P/MRP (RNase P/MRP) holoenzyme, which is involved in tRNA maturation and RNA polymerase III regulation (Guerrier-Takada et al., 2002; Aravind et al., 2003; Welting et al., 2004; Reiner et al., 2006; Welting et al., 2007). An extremely stable RPP20/RPP25 heterodimer specifically binds pre-tRNA, which is required for tRNA maturation processes to ensure the RNase P complex´s canonical function (Kouzuma et al., 2003; Aravind et al., 2003; Hada et al., 2008; Hands-Taylor et al., 2010; Reiner et al., 2011; Pérez-Díaz et al., 2017). Although the association of the ALBA heterodimer with the cleavage complex is dynamic and does not participate in further accumulation and pre-ribosomal complex formation, it is involved in pre-rRNA processing before the ribosome subunits boundary (Welting et al., 2006; Welting et al., 2007). RPP20/RPP25 contact with RNase P is mediated by RPP25 recognition of the P3 domain of the H1 RNA compound (Pluk et al., 1999; Van Eenennaam et al., 2002; Guerrier-Takada et al., 2002; Welting et al., 2004) , whereas RPP20 selects additional interactors according to current conditions (Li et al., 2001; Altman et al., 2001; Hua et al., 2004). In yeast, the POP6/POP7 heterodimer stabilizes a flexible secondary structure of the P3 domain (Perederina et al., 2010) and recruits POP1 (Fagerlund et al., 2015). Although the *5′ UTR* processing of pre-tRNA and transcription regulation could bridge ALBA

protein counterparts in humans and yeast, their plasticity suggests non-canonical role differentiation. The yeast heterodimer likely stabilizes more than one lncRNA restricted to RNaseP/MRP, but also binds non-coding RNA and telomerase subunits (Lemieux et al., 2016).

The ALBA proteins were originally isolated from the hyperthermophilic crenarchaeon *Sulfolobus acidocaldarius*. Despite their cell abundance, the identified basic 10kDa proteins could dimerize and bind short DNA fragments *in vitro* even at low concentrations (Lurz et al., 1986; Wardleworth et al., 2002; Aravind et al., 2003; Jelinska et al., 2005; Laurens et al., 2012). Formed dimers facilitate DNA stabilization, which depends on the modulation of their double-stranded DNA (dsDNA)-binding affinity (Laurens et al., 2012). The binding time of ALBA1 proteins to the nucleic acid increases with fragment length and expanding number of nucleation sites, which improves oligomer formation (Bell et al., 2002; Zhao et al., 2003; Marsh et al., 2005; Jelinska et al., 2005; Lu et al., 2013). While the emerging DNA-protein interactions belong to the strongest identified nucleic acid-protein boundaries, they can be impaired by protein acetylation, which led to the name origin (ALBA, Acetylation Lowers Binding Affinity) (Xue et al., 2000; Wardleworth et al., 2002; Bell et al., 2002). Homodimer structure and concentration are crucial for chromatin remodelation and condensation into helices, up to loop formation, in a temperature-dependent manner. The conformation of the ALBA1 dimer changes at 45 °C, which is the standard growth temperature for thermophilic Archaea, in order of chromatin maintenance (Cui et al., 2003; Jelinska et al., 2005). Dimers influence the access of transcription factors to DNA by regulating DNA topology. Additionally, the heterodimerization of ALBA1 with lowly expressed ALBA2 generates the next regulation level, which is most probably implemented in *S. solfataricus* cell development and stress responses (Lurz et al., 1986; Forterre et al., 1999; Xue et al., 2000; Bell et al., 2002; Jelinska et al., 2005; Laurens et al., 2012). Moreover, ALBA roles diversified even within the genus, as indicated by the ALBA/SSO10B association with ribosomes, particularly bound to RNA in *S. shibatae* (Guo et al., 2003; Jelinska et al., 2005; Guo et al., 2013; Goyal et al., 2016). A detailed protein investigation identified specific interaction partners, including 16S and 23S rRNAs and mRNA molecules, with a plausible role in RNA protection and maintenance (Guo et al., 2003; Jelinska et al., 2005). In contrast to their essential role in crenarchaeon survival, their impact on euryarchaeon growth is minimal, as reflected by their absence in *Methanosarcina* and haloarchaea (Forterre et al., 1999; Pavlov et al., 2002; Bell et al., 2002; Liu et al., 2009; Goyal et al., 2016).

1.5. Impact of *ALBA* genes to developmental processes

In multiple species, ALBA proteins are involved in various cellular processes that impact development and stage transitions. In plants, the ALBA protein's role is crucial for growth and reproduction, regardless of the weak phenotypic aberrations observed in single mutant lines of Arabidopsis

(Honkanen et al., 2016; Magwanga et al., 2019; Wang et al., 2019). The nutrient intake of stable mutants can be influenced by the reduced length of root hairs observed in *alba4* and *alba5, as* well as the shortened rhizoids in mutants of the moss *Marchantia polymorpha* (Honkanen et al., 2016). The same phenotypic defect was observed in transient knockdowns of *ALBA4* and *ALBA5* in cotton, *Gossypium hirsutum* (Magwanga et al., 2019). Multiple mutant analyses revealed an increased number of phenotypic defects in Arabidopsis (Wang et al., 2019; Tong et al., 2022). The triple mutant of the Rpp25-like subfamily *alba456* can be delayed in growth, including flowering. An expression analysis revealed affected transcription of genes involved in metabolism, particularly upregulation of factors involved in mineral intake. The enriched activity of *ALBA* genes supports these results in root tips, as well as the localization of proteins to the cytoplasm (Wang et al., 2019; Tong et al., 2022). Above six homologs, *ALBA1* and *ALBA4* are the most active orthologs in a sporophyte, especially in the root tips, cotyledons, and leaves primordia, though the male gametophyte exhibits almost a particular expression pattern of *ALBA3* (Borg et al., 2011; Wang et al., 2019). Nevertheless, further characterization of *alba1245* and *alba456* mutants revealed additional defects in trichome branching, which were assigned to the loss of the Alba domain. The pronounced phenotype of the *alba456* triple mutant is presumably caused by the loss of the RGG domain (Tong et al., 2022; Reichel et al., 2024). In rice, all nine *ALBA* genes are expressed in various organs, with notable differences between moderately active *ALBA1* and *ALBA7*, and almost inactive *ALBA2*, *ALBA3*, *ALBA5,* and *ALBA9*, as well as highly abundant *ALBA4*, *ALBA6,* and *ALBA8*, especially in reproductive organs (Verma et al., 2018). Moreover, m^6A methylation of mRNA can pronounce the phenotypic defects connected with successful embryogenesis in plants (Zhong et al., 2008; Geula et al., 2015). Consequently, ALBA proteins are involved in cell differentiation and ontogenesis from the earliest stages until reproduction.

1.6. Plant reproduction

Plants represent sessile organisms without a chance to escape unfavorable conditions. To survive and ensure the survival of their offspring, comprehensive molecular and metabolic pathways are required for their acclimation and adaptation to various stresses (Wada et al., 2010; Kazan et al., 2016; Takeno, 2016). Sexual reproduction is ensured by flowering, a process that involves the emergence of buds and flowers, which can be organized into an inflorescence. A perfect flower and inflorescence architecture is essential for effective seed production (Huijser et al., 2011). Flowering is promoted by the interplay of precisely regulated pathways that terminate the vegetative stage and induce a transition to the generative phase of development. These mechanisms integrate the endogenous state (autonomous pathway, age, the circadian clock, sugar deposit, and phytohormone balance) with environmental stimuli (vernalization, temperature, photoperiod, and light intensity). Competence for flowering is achieved when acquired signals transduced to the transcription level induce morphological changes in the shoot apical meristem (SAM) (Eimert et al., 1995). Therefore, the separation and identification

of a particular pathway is unusually challenging (Wada et al., 2010; Riboni et al., 2013; Blümel et al., 2015; Teotia et al., 2015; Takeno, 2016; Laanen et al., 2023).

The efficiency of signal interplay is crucial for offspring production and maintaining population stability (Jung et al., 2009; Tsuji, 2017). Potential time shifts can compensate the impact of a stressful environment in two ways: by premature flowering to prevent stress or by outlasting the stress before reproduction (Jung et al., 2009; Wada et al., 2010). Early flowering can reduce the number of seeds and their viability due to underdevelopment, yet still increase seed production in adverse conditions (Huijser et al., 2011). Arabidopsis plants cultivated under long days display an accelerated transition to flowering, promoted by salicylic acid and ROS signaling, low nitrate concentrations, and high temperatures (Park et al., 2016). In contrast, there are several inputs that delay the transition to flowering, increasing the probability of reproductive failure (Sunkar et al., 2007; Kazan et al., 2016). In Arabidopsis, flowering can be delayed by abiotic stresses, including salinity, cold, and drought (Park et al., 2016). Nevertheless, regulators of flowering time can integrate responses to abiotic stresses, especially tolerance to drought, cold and ABA signaling, in various ways (Wuriyanghan et al., 2009; Han et al., 2013; Ying et al., 2014).

In Arabidopsis, at least four major pathways interconnect a few important genes that perceive and process recognized signals. Here, some of them are briefly mentioned to illustrate the complexity of processes controlling competence for reproduction. The master regulators that promote the transition to flowering are GIGANTEA (GI), CONSTANS (CO), FLOWERING LOCUS T (FT), and other factors (Simpson et al., 2002; He et al., 2005). GI integrates signals from the circadian clock and light quality, specifically red light via PHYB and blue light via CRYPTOCHROME, which activate transcription of *CO* and *FT* (Fowler et al., 1999; Park et al., 1999; Mizoguchi et al., 2005; Kim et al., 2007; Martin-Tryon et al., 2007). Moreover, GI is a hub for several environmental responses, connecting flowering with a tolerance to drought (Han et al., 2013; Riboni et al., 2013), cold (Cao et al., 2005), and salt (Kim et al., 2013), mechanisms that are not characteristic of the circadian clock signaling cascade. Before activation, *CO* is repressed by cold stress or the flowering repressor CONSTANS-LIKE 9 (COL9). Once CO appears, it directly promotes the transcription of the following florigen genes: FLOWERING LOCUS T (*FT*) and TWIN SISTER OF FT (*TSF*) (Suárez-López et al., 2001; Yamaguchi et al., 2005; Yoo et al., 2007; Jang et al., 2009). The expression of *FT* is enabled by vernalization, a period of cold temperatures, which inhibits the transcription of the FLOWERING LOCUS C (*FLC*) (Searle et al., 2006). The transcription of *FT* is further enhanced by blue light photoreceptors (Ito et al., 2012) and the drought stress response mediated by abscisic acid (Riboni et al., 2013). The established FT-TSF complex promotes SUPPRESOR OF OVEREXPRESSION OF CONSTANS 1 (SOC1) transcription and stimulates expression of the floral meristem identity genes LEAFY (LFY) and APETALA 1 (AP1) (Mizoguchi et

al., 2005; Chao et al., 2014; Park et al., 2016). LFY and AP1 form a complex to finally activate the floral homeotic genes required for the organ identity (Mizoguchi et al., 2005).

In Arabidopsis, floral organs continuously emerge in concentric rings from the outermost to the innermost whorl. Initially, four green sepals emerge in the first whorl, followed by four white petals that evolve in the second whorl (Figure 3). Throughout bud growth, sepals enclose the floral bud cavity and protect the inner whorls against harsh conditions. In the third and fourth whorls are differentiated structures carrying developing gametophytes, with six stamens surrounding a gynoecium represented by a pistil in the center. Stamens consist of filaments and anthers in which the pollen grains are developed. Ovules evolve in the pistil formed by the fusion of two carpels enclosing and protecting the inner cavity. The distal part of the carpels differentiates into a style, which is morphologically isolated from the cap of the papillae cells. The released pollen grains are trapped by papillae, germinate, and grow through the central part of the pistil toward ovules.

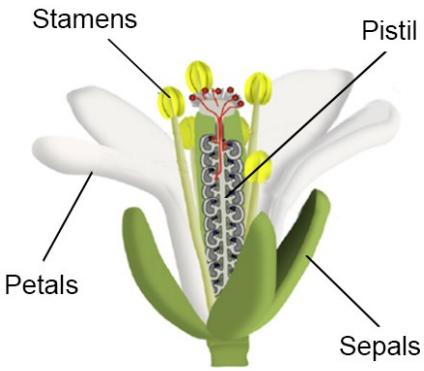

Figure 3: Schematic illustration of the Arabidopsis flower. The main parts of a complete flower are arranged in four whorls: outermost green sepals and petals protecting two inner whorls, stamens and pistils. Pollen grains develop in stamens until maturation. The released grains adhere to the receptive pistils, rehydrate, and germinate. Elongating pollen tubes grow through the pistil to reach the ovules. The figure was obtained and modified according to (Dresselhaus et al., 2012).

1.6.1. Female gametophyte

A central part of the pistil is interconnected by the placenta, which gives rise to ovule primordia (Figure 4). Initiated outgrowth emerges, elongates, and differentiates into the funiculus, chalaza, and the nucellus (Skinner et al., 2004). In Arabidopsis, a single nucellar cell differentiates into a megasporocyte, which undergoes meiosis to create haploid megaspores (megasporogenesis) (Irene Julca et al., 2021). Only the chalazal megaspore proceeds with three sequential karyokineses to finally form an embryo sac by delayed cytokinesis, while others degrade (Vijayan et al., 2021). Simultaneously, integuments emerge from the chalazal epidermis and overgrow the developing embryo sac up to the micropyle (Robinson-Beers et al., 1992). The fully matured embryo sac consists of seven precisely distributed cells; the egg cell surrounded by two synergids at the micropylar pole, three antipods at the chalazal pole, and central cell fulfilling most of the embryo sac volume.

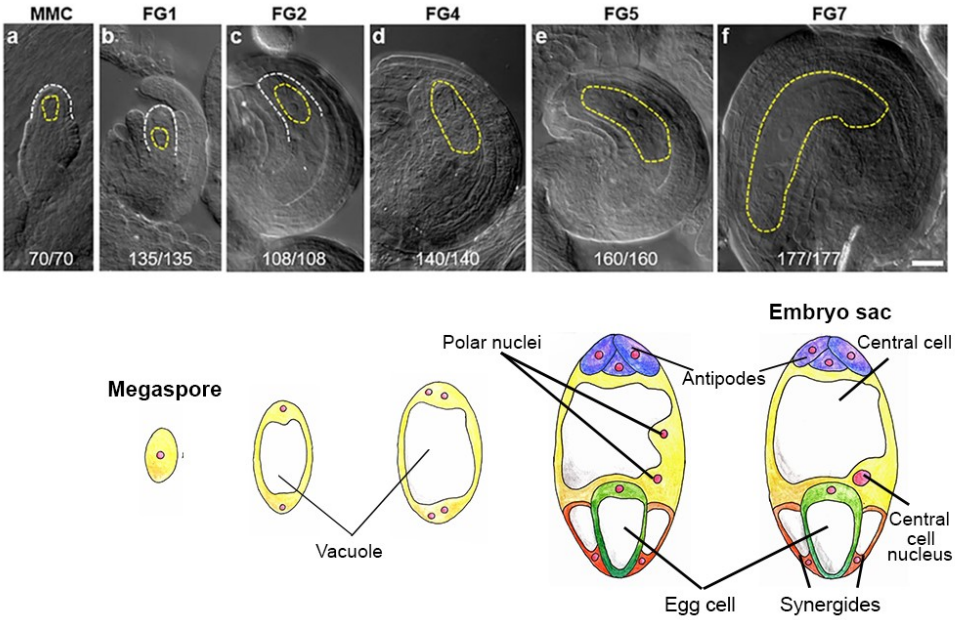

Figure 4: Overview of ovule and female gametophyte development. The placenta gives rise to an ovule primordium, which develops until full maturation. Megasporocytes undergo meiosis (**a**), a single haploid megaspore is overgrown by integuments (**b**). The megaspore goes through three rounds of mitosis to create a female gametophyte, which changes orientation within an ovule to reach the final (inverted) position (**c-f**). The fully developed embryo sac (bottom) consists of two synergids accompanied by an egg cell at the micropylar pole, three antipods at the opposite (chalazal) pole and a central cell. The diploid nucleus of the central cell is formed by two polar nuclei fusion. Ovule development was acquired from (Park et al., 2024).

The matured ovule communicates with a pollen tube growing through the transmitting tract from the stigma, through the style into the ovary. Sperm cells are delivered to the ovule by a pollen tube and reach the female gametophyte via the micropylar entrance (Figure 5). The attracted pollen tube usually

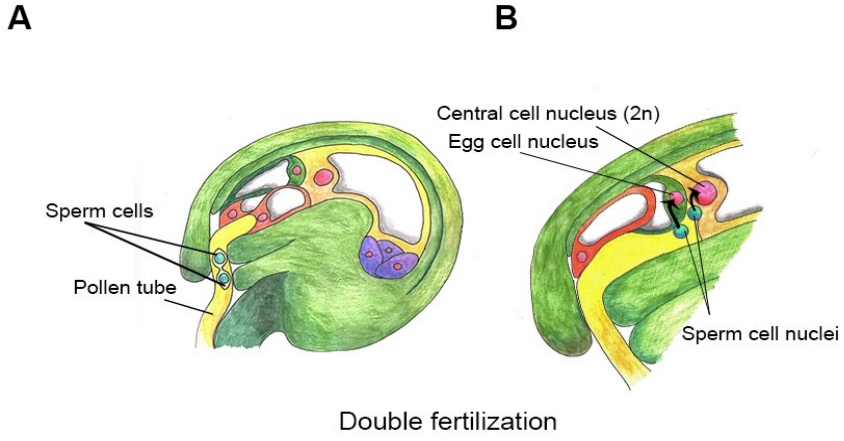

Figure 5: Schematic overview of double fertilization in Arabidopsis. The pollen tube penetrates the ovule through the micropyle to deliver sperm cells for double fertilization (**A**). The released sperm cells fuse with the egg cell and central cell nuclei to create the diploid embryo and the triploid endosperm, respectively (**B**).

bursts in a synergid cell and releases sperms cells which fuse with the egg cell and the central cell to facilitate double fertilization. Successful fertilization creates a diploid zygote that develops into an embryo, a new sporophyte, and a triploid endosperm that provides embryo nutrition up to seed maturation (Drews et al., 1998; Dresselhaus et al., 2012; Sze et al., 2021; Park et al., 2024).

1.6.2. Male gametophyte

In the third whorl of the Arabidopsis flower, evolved stamens are present. Initiated primordia grow and develop into an elongated filament carrying an anther up to the stigma. During the expansion, anthers differentiate into multiple specific layers responsible for pollen development, which comprises two consecutive phases, microsporogenesis and microgametogenesis (Ma, 2005; Hafidh et al., 2021). The predominant contribution of these processes belongs to the innermost anther´s layer, the tapetum. Tapetal cells undergo morphological and physiological changes along with sporogenous cells (Scott et al., 2004). The material secreted by the tapetum is crucial for the formation of specialized pollen cell wall and nutrient accumulation (Bedinger, 1992; Scott et al., 2004). Developing pollen accumulates resources containing protective substances essential for pollen vitality, along with reserves necessary for the further energy-consuming metabolism of the growing pollen tube (Pacini, 1996; Pacini et al., 2006). The fully matured haploid male gametophyte in angiosperms represents a unique structure with maximal reduction comprising two or three cells: the vegetative cell (VC) and the generative cell (GC) (bicellular pollen) or the VC and two sperm cells (SC) (tricellular pollen).

Microsporogenesis (Figure 6) begins with diploid microsporocytes that undergo synchronized meiosis, resulting in the formation of four haploid microspores connected by a callose into tetrads (Scott et al., 2004). Calases secreted by the tapetal cells release independent haploid microspores, which enlarge due to the intake of vacuole volume. This process is absolutely inevitable for the initiation of microgametogenesis by asymmetric pollen mitosis I, which is precisely regulated and produces prominent VC and minor GC with distinct fates essential for pollen fertility (Eady et al., 1995; Honys et al., 2006). The GC is early in two-celled pollen, surrounded by the VC that fulfills the significant volume of the young pollen and supports an origin of the male germ line up to fertilization (Eady et al., 1995; Berger et al., 2011; Russell et al., 2015). The VC is transcriptionally very active, which is provided by relaxed chromatin underpinning its nuclear character and irregular shape. The storage of accumulated substances is guaranteed by the synthesis of mRNA, proteins, lipids, and sugars that change the cytoplasmic properties (Bedinger, 1992; Nepi et al., 2001; Pacini et al., 2006; Honys et al., 2009; Hafidh et al., 2011; Hafidh et al., 2021). The specific developmental program established in the bicellular pollen produces uniform and unique gene expression profiles (Park et al., 1998; Honys et al., 2004; Becker et al., 2007). The amount of produced non-coding RNAs and transcripts increases up to nine to twenty times compared to the initial state (Tupý, 1982). The pollen

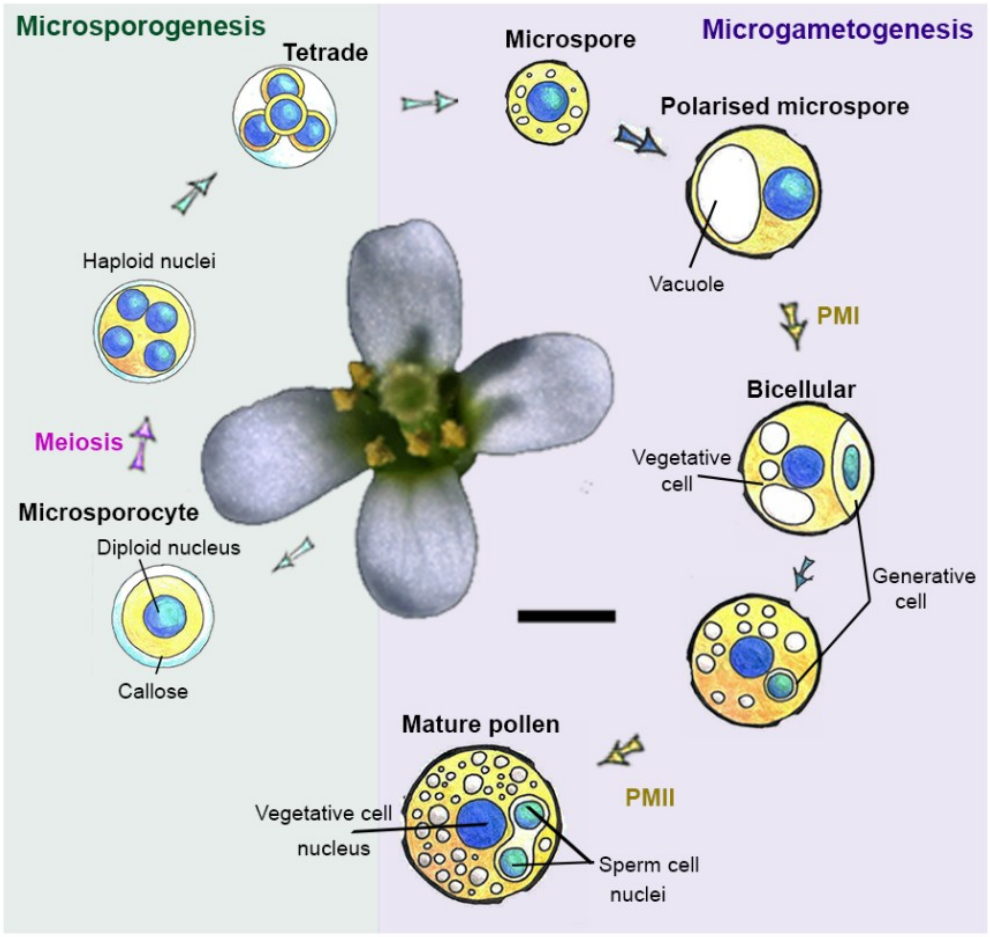

Figure 6: Schematic of pollen development. Pollen grains are produced in anthers by two developmental processes. Microsporogenesis: Microsporocytes undergo meiosis as a result of four haploid microspores covered by callose. Microgametogenesis: Microspores undergo two sequential mitotic divisions, producing bicellular pollen (PMI), which consists of the VC and the GC. The GC divides in PMII, resulting in two SCs. A mature pollen grain is filled by the VC cytoplasm, which contains two sperm cells (Guo et al., 2019; Hafidh et al., 2021).

transcriptomic description was expanded by translatomic (Lin et al., 2014) and sequestromic data that followed the late developmental stages with post-transcriptional regulation and mRNA storage (Hafidh et al., 2018).

The GC nucleus is highly condensed and occupies a marginal volume of the cell surrounded by a minimal portion of the cytoplasm. In pollen mitosis II, the GC equally divides and produces two SCs connected with the VC nucleus, forming a male germ unit (MGU) (Twell, 2011; McCue et al., 2011; Berger et al., 2011). The cell cycle activates the R2R3 MYB transcription factor DUO POLLEN 1 (DUO1), which promotes mitosis and facilitates sperm cell fate through its targets including DUO1-ACTIVATED NUCLEIC ACID BINDING PROTEIN (DAN1), later named ALBA3 (Eady et al., 1995; Borges et al., 2008; Brownfield et al., 2009; Borg et al., 2011; Borg et al., 2015).

The Alba domain of ALBA3 is essential for homodimer formation and ssRNA-binding affinity, especially the presence of lysine 46 and leucine 90 (L90) residues within the domain are crucial for the RNA affinity. Moreover, the loss of L90 in the *alba3-2* L90S mutant caused the downregulation of genes related to pollen development, germination, and pollination. Dysregulation of these processes proceeds to silique shortening and reduced seed sets, reducing the fertility of *alba3-2* mutants (Ci et al., 2025).

The progamic phase of pollen development is initiated by pollen release from anthers (Hafidh et al., 2021). Once the desiccated pollen grain successfully lands on the stigma, it immediately begins to interact with papillae cells that enable grain hydration (Windari et al., 2021). The VC undergoes rapid molecular changes, polarizes, reorganizes organelles, and starts to germinate (Parton et al., 2001; Voigt et al., 2005). Pollen germination induces unique transcriptional activity for the emerging pollen tube and its first hours of growth, followed by intriguing translation in the later stages (Čapková et al., 1988). Since the processes are separated in time, the newly synthetized transcripts are transferred to large, translationally inactive ribonucleoprotein granules – EDTA/puromycin-resistant particles (EPPs) discovered later (Honys et al., 2009). EPPs' analysis revealed that their content is characteristically connected with protein synthesis; matured ribosomal subunits, rRNAs, and mRNAs covered by factors involved in their transport and localization including ALBA proteins. The pollen tube provides SCs transport to an ovule, preceded by an intense molecular dialogue between male and female reproductive tissues, resulting in double fertilization, which ends the progamic phase (Pacini, 1996; Dresselhaus et al., 2013; Hafidh et al., 2016). Altogether, pollen grains represent a highly specialized niche with a unique cell composition, making them an ideal model system for investigating molecular and cellular processes.

1.7. Stress response

Sessile plants have to face seasonal challenges and continuously varying environmental conditions that remarkably influence plant fitness and fertility. In particular, abiotic stresses significantly reduce seed production, which is essential for yield (Barnabás et al., 2008; Bokszczanin et al., 2013). In evolution, plants have developed a range of defense mechanisms in response and adaptation to stress stimuli. These processes are regulated by specific transcription, translation, and post-translational programs that can adapt to adverse conditions of the habitat to maintain cell homeostasis, plant survival and reproduction (Conrath, 2011; Krasensky et al., 2012; Tanou et al., 2012; Ohama et al., 2017). Nevertheless, the efficiency of compound accumulation plays a comprehensive role, which secures an immediate response. Aggregate formation and regulation depend on temperature, pH, salinity, and other factors affecting plant growth and reproduction rate. Therefore, the possible plant-specific

molecular mechanisms of coping with abiotic stresses remain to be researched (Emenecker et al., 2020).

ALBA proteins were connected with various stress responses in evolutionarily diversified organisms. In plant species, members of the widely multiplied Alba family are influenced by abiotic stress conditions (Reichel et al., 2016; Verma et al., 2018; Magwanga et al., 2019). The original data highlighted the involvement of rice homologs in responses to stress conditions and phytohormone treatments in seedlings (Verma et al., 2014; Verma et al., 2018). In particular, increased expression of *OsALBA1* was detected upon drought stress accompanied by a protein re-localization from the cytoplasm to the nucleus. Moreover, a similar gene response was revealed in the samples treated by osmotic stress. Both conditions activate pathways of oxidative stress response to oxygen peroxide united by ABA signalization, indicating ALBA1 involvement in DNA maintenance and adaptation (Verma et al., 2014). The expression levels of other *OsALBA* genes changed under stress conditions and hormonal treatments, while most of them were significantly elevated. Collectively, these findings implicate several members to similar physiological processes (Verma et al., 2018).

Correspondingly, transcriptomic changes in *ALBA4* and *ALBA5* were recorded upon stress treatments in cotton. Both genes were upregulated in wild-type seedlings exposed to drought and osmotic stresses. Moreover, *ALBA4* and *ALBA5* knockdown plants are more sensitive to the treatments that are likely caused by stress-induced gene downregulation and reduced activity of ROS scavenging enzymes. In tomato, the unique gradual elevation of *ALBA6* activity reached a maximum 24 h upon salt treatment despite the declining expression of other homologs. Interestingly, drought stress treatment elevated *ALBA3* in contrast to the significant downregulation of other members. Finally, tomato *ALBA* genes exhibited shared response patterns to ABA treatment (Magwanga et al., 2019), which were further supported by the identification of stress-responsive elements in their promoters (Wai et al., 2021). Additionally, *ALBA* genes and proteins were closely linked to temperature-induced responses. Under cold stress, the Alba family in rice is equally divided according to expression patterns, with three genes being upregulated and four downregulated. *ALBA9* possesses a unique pattern of mixed response to cold (Verma et al., 2018). In tomato, the transcription levels of seven genes were influenced by exposure to a low temperature. From the cold-sensitive genes, significantly elevated expression was detected solely in *ALBA8,* though the predominant number of homologs was downregulated (Wai et al., 2021).

1.7.1. Heat stress

High or extreme temperatures unfavorably affect plant growth and significantly reduce reproduction ability (Hasanuzzaman et al., 2013). Therefore, plants adopted specific pathways to cope with damaged protein structures and ROS by activation of HS transcription factors (HSFs) that

promote HS-responsive gene transcription, primarily chaperones and ROS scavengers (Ding et al., 2020). The HSFs are precisely regulated at multiple levels by alternative splicing, micro open reading frames in the *5′ UTR* and post-translation modifications that influence protein stability and localization (Guo et al., 2016; Nakaminami et al., 2018). According to some studies, *ALBA* genes are regulated similarly in response to HS (Verma et al., 2018; Magwanga et al., 2019; Wai et al., 2021; Tong et al., 2022). In rice seedlings, a significant part of the homologs respond to HS (42 °C). Almost all *ALBA* gene activity is elevated, but *ALBA4* is downregulated (Verma et al., 2018). In tomato, five *ALBA* genes are downregulated, and only the *ALBA4* and *ALBA5* transcript levels are upregulated 24 h after HS (Wai et al., 2021). In Arabidopsis, the Rpp25-like subfamily's response to HS has been thoroughly investigated. In seedlings, all three homologs are randomly localized in the cytoplasm under standard conditions, although they relocalize into heat-induced aggregates. This process is mediated by the phase separation of ALBA proteins, which enable the sequestration of mRNAs into SGs and PBs. Accumulated transcripts, including *HSF,* are stored and protected from degradation in these particles. ALBA4-6 can form heterodimers or oligomers and directly bind to PB and SG counterparts, DECAPPING 5 (DCP5) and POLY (A)-BINDING PROTEIN 2 (PAB2) upon HS. Additionally, seedlings of *alba456* triple mutants are hypersensitive to high temperatures, which highlights their impact on thermotolerance adaptation (Tong et al., 2022).

1.7.2. Heat stress during reproduction

Elevated temperatures harmfully influence plant growth and development from the juvenile to the reproductive phases. The final consequences of the environment depend on several factors, including exact temperature, period length, and character of induction (Yeh et al., 2012). Sensing of temperature fluctuation is tightly connected with the photoperiod and collectively promotes plant transition to flowering (Kazan et al., 2016). Nevertheless, the severity of the temperature stress varies throughout flower and seed development. Two particularly sensitive windows include the synchronized meiosis of megasporocytes and microsporocytes, as well as fertilization with early embryo formation. Moreover, the inequality of temperature impact on reproductive organs clearly highlights male germline hypersensitivity in cereals, tomato and Arabidopsis (Sato et al., 2006; Bac-Molenaar et al., 2015). High temperatures cause pollen abortion and elevate humidity in flower buds, which has a synergistic effect on anther dehiscence and postponed grain release (Kim et al., 2001; Sakata et al., 2010). These processes cause anthers and stigma development asynchrony, leading to a loss of the pollination cross-point in self-fertilizing plants (Bac-Molenaar et al., 2015).

The number of molecular mechanisms responds for the equalization of master regulators and flowering promotion upon high temperatures. In various plant species, HSF/HSP homologs reportedly regulate flowering, which directly connects reproduction with defense processes (Majee et al., 2023).

These HS genes were identified to provide thermotolerance during the reproductive phase of development (Giorno et al., 2013). Nevertheless, their involvement in response to various abiotic stress conditions underlined their importance for reproduction, especially seed germination and anther development (Queitsch et al., 2000; Zinn et al., 2010). At the molecular level, unfolded protein responses and ROS scavengers cope with damaged proteins and excessive ROS through both canonical and non-canonical pathways (Li et al., 2018). Members of two HSP classes, HSP101 and HSP90, are involved in the aggregation of key flowering master regulators to coordinate flowering induction (Margaritopoulou et al., 2016; Qin et al., 2021). Moreover, overexpression of the grape homolog *HSFA9* in Arabidopsis promotes seed germination but delays flowering (Li et al., 2015).

Heat stress affects flower size, introduces morphological abnormalities of floral organs and tissues, and causes the production of completely sterile flowers. Changes in floral architecture have a detrimental impact on successful pollination and fertilization that inevitably reduce the quality and number of progeny (Resentini et al., 2023). Developing anthers and processes resulting in mature pollen production represents a fragile compound that is extremely sensitive to elevated temperatures and connected environmental factors (Kim et al., 2001). Elevated temperatures cause pollen and ovule abortion or a reduction in quantity and disrupting pollen morphology and metabolism, resulting in reduced viability (Young et al., 2004; Zinn et al., 2010; Chaturvedi et al., 2021). Mature pollen undergoes desiccation permitted by specialized cell wall, transcript protection and storage in aggregates, which are also formed upon stress (Sze et al., 2024). Activated thermotolerance pathways connect multiple cellular adaptations mediating metabolic stability upon HS. Hence, PBs are present in the cytoplasm under normal conditions, whereas SGs are formed in response to stress treatment (Guzikowski et al., 2019). Both types of aggregates are involved in transcript regulation by storage or localized translation connected by the partial sharing of compounds and positions (Xu et al., 2020). Moreover, SGs include mRNAs, RNA-binding proteins (RBP47, PABs), translation initiation factors, and HSP17 (Weber et al., 2008).

Although *ALBA* genes were characterized and connected to various processes in sporophytic tissues, their description in reproductive tissues and their impact on plant reproduction remain poorly understood. The primary study of rice revealed significantly enriched levels of *OsALBA3*, *OsALBA6,* and *OsALBA8* in the reproductive tissues, which are responsible for seed nourishment and protection against dehydration and temperature stress (Zhang et al., 2012). In Arabidopsis, *alba3-1* (K46E) single mutant fertility is reduced upon HS. Although the mutant phenotype does not significantly affect the development of pollen grains or pollen tube growth, it could influence pollen adhesion to the stigma. In *alba3-2 (*L90S), the pollen tube guidance is most probably disrupted, leading to a higher number of untargeted ovules observed specifically upon HS. According to these findings,

the RNA affinity of ALBA3 is essential for fertility in pollen progamic phase regulation upon HS (Ci et al., 2025).

2. Aims and hypotheses

The presented doctoral thesis aims to elucidate the importance of *ALBA* genes for Arabidopsis growth, especially its reproductive phase. Moreover, the description of their behavior in pollen development under standard conditions and upon heat stress provides improved knowledge of their significant value for plant fertility. The first goal was to elucidate the localization of ALBA proteins in pollen nuclei by strong NLS. Next, the connection of *ALBA* genes to the HS response in pollen was studied at the levels of gene activity and fused protein tracking. Therefore, further attention was devoted to the link of Arabidopsis Alba family with various types of RNPs by colocalization assays with PABP3, PABP5, GAF1 and ALBA proteins. Finally, the impact of ALBA protein homeostasis on plant growth and development was investigated by specific overexpression of *ALBA* genes in the pollen vegetative and sperm cells followed by widespread sporophytic overexpression.

H01: ALBA proteins localize in the pollen nuclei

Although AtALBA proteins were initially localized in the cytoplasm (Náprstková, 2016), their role could be at least partially situated in the nuclei (Verma et al., 2014; Dupé et al., 2015; Goyal et al., 2016). Moreover, some *AtALBA* coding regions possess a weak nuclear localization signal (NLS) and nuclear export signals, supporting their possible shuttling between the nuclei and the cytoplasm. Therefore, a strong NLS was used for the preferential localization of the ALBA-YFP fusion proteins into the pollen nuclei. Surprisingly, most of them were localized in the cytoplasm despite nuclear targeting, except for ALBA3-YFP, which was detected in the VC nucleus. Consequently, the hypothesis was proven only for ALBA3.

H02: The role of ALBA proteins in the male gametophyte is connected with the HS response

ALBA proteins are involved in sporophytic stress responses in plants (Verma et al., 2018; Wai et al., 2021), though pollen is sensitive to temperature fluctuations. Therefore, the expression analysis of *ALBA* genes was performed in generative organs under standard and heat-stressed conditions. In *Leishmania*, the Alba-family members ensure developmental processes even in a stress-dependent manner (Dupé et al., 2015). Therefore, the potential dynamics of ALBA-GFP throughout pollen development and upon HS were selected for the detailed investigation. During pollen development, detected signal pattern accumulates in foci toward pollen maturation and desiccation, which is further enhanced upon HS. Altogether, the activity of the *ALBA* genes and the proteins encoded by them were involved in the HS response.

H03: ALBA proteins are a part of the RBPs in the male gametophyte.

ALBA proteins are components of RNPs in sporophytic tissues of Arabidopsis, specificaly related to stress responses (Fan et al., 2024). Therefore, markers of multiple RNPs with natural presence in mature pollen were selected for colocalization assays. ALBA-GFP fusion proteins were colocalized with the mRNA markers PABP3-RFP and PABP5-RFP. Partial colocalizations were detected in the predominant number of samples. ALBA proteins preferably share the localization pattern with PABP3. Furthermore, ALBA proteins are subunits of RNase P/MRP in animals, but the investigated AtALBA colocalization with the RNase P marker did not indicate a connection. Finally, the presumed cooperation of subfamily-limited members revealed partial co-occurrence in pollen. Overall, the acquired results suggest the potential role of ALBA proteins in various types of RNPs.

H04: Does ALBA overexpression affect reproduction?

The loss of *ALBA* genes does not severely influence the plant phenotype most likely due to their high similarity and functional redundancy. Therefore, the *ALBA* pool could be disrupted by overexpression in tissues with the native presence, VC (*LAT52* promoter) and SCs (*DUO1* promoter) in pollen and in the sporophyte (*CsWMV* promoter). First, ALBA-GFP/YFP localization revealed atypical patterns created by the aggregated foci, suggesting the disruption of cytoplasmic homeostasis. Although fertility was not reduced by *ALBA* overexpression in pollen, the members of the Rpp25-like subfamily regulated by *proCsWMV* activity can surprisingly harm the reproductive ability. The severe defects included growth delay, flowering retardation, and abnormal seed production. Finally, detailed molecular analysis revealed the affected pathways involved in flowering promotion. Hence, strong overexpression induces the accumulation of ALBA proteins within the cytoplasm and detrimentally alters plant physiology, leading to fertility reduction, which supports the initial hypothesis.

3. Materials and Methods

3.1. Plant material and growth conditions

All generated lines of *Arabidopsis thaliana* were based on the background of the Col-0 ecotype. Only plants of the *proPabp3:PABP3-RFP* and *proPabp5::PABP5-RFP* marker lines were based on the mutant backgrounds, *pab3-1* T-DNA insertion line SAIL_783_D04 and *pab5* gabiKat line GK-324H01-015976. All seeds were stored in -20 °C for three days before sowing, followed by sterilization and placement in a medium. Seeds were sterilized by 20% (w/v) SAVO solution for 7-10 min, the solution was removed and the seeds were washed four times with ddH_2O. Sterilized seeds were immediately transferred on 0.5× Murashige and Skoog (MS) medium containing 1% (w/v) sucrose, and 1% (w/v) agar, modified according to Murashige et al. 1962, by a pipette tip and enclosed by a tape. Agar plates with seeds were stored at 4 °C for 3 days to promote and synchronize germination. Seeds were germinated *in vitro* in a cultivation room under standard conditions of 21 °C and a long day regime (16-h light/8-h dark photoperiod). Seeds germinated on a plate in the vertical position and grew for 7 to 14 days. Seedlings with first true leaves primordia (usually 10-14-day-old) were transferred into soil Jiffy7 (Jiffy International AS, Kristiansand, Norway) and further cultivated under standard growth conditions of a long day regime at 21 °C, 60% relative humidity (RH) to reach the developmental stage of interest in a cultivation chamber (Conviron® model PGC20 plant growth chamber, Conviron®, Winnipeg, Canada).

3.2. DNA extraction

Leaves from 14-day-old plants were harvested in 2 mL tubes containing sterilized sea sand stones and immediately frozen in liquid nitrogen. The samples were grinded twice for one minute using FastPrep-24™ 5G Homogenizer (MP Biomedicals, CA, USA) at 4,000 rpm. Homogenized tissues were stabilized by 250 µL of CTAB extraction buffer (1.4 M NaCl, 20 mM EDTA, 100 mM Tris-Cl pH 8, 3% w/v cetyl trimethylammonium bromide – CTAB) with a modification of the standard protocol (Doyle et al., 1990). The obtained solution was vortexed and incubated for 20 min at room temperature (RT). Further, 250 µL mixture of chloroform:isoamyl alcohol (24:1 v/v) was added, thoroughly mixed by vortexing and centrifuged at 17,000 × g, RT for 10 min. The aqueous phase containing the dissolved DNA was transferred to a fresh tube. Isolated DNA was precipitated by a 0.7 × volume of isopropanol, mixed, and incubated for at least 10 min at 4 °C. Precipitated DNA was centrifuged at 17,000 × g for 7 min. The supernatant was discarded and the pellet was washed with 1 ml of 70% (w/v) ethanol, mixed by brief vortexing and centrifuged at 17,000 × g for 2 min. Ethanol was removed by a vacuum pipette and the pellet was dried at 42 °C by a vacuum concentrator

(Eppendorf® Concentrator Plus with rotor F-45-48-11, Eppendorf, Hamburg, Germany) at 1400 rpm for 1 h. The pellet was resuspended in 50 µL of ddH_2O and thoroughly dissolved DNA concentration was measured (NanoDrop One instrument, Thermo Fisher Scientific, Waltham, MA, USA). The isolated DNA samples were frozen at -20 °C and stored for further use.

3.3. Polymerase chain reaction (PCR) and primer hybridization

The PCR mixtures were used for further molecular cloning and verification steps. The individual reactions contained buffer, free nucleotide mixture (dNTPs), specific primers (Table 1), DNA template, and DNA-dependent DNA polymerase. Fragment amplification for further cloning was mediated by the Phusion® HighFidelity DNA Polymerase with proofreading activity (Thermo Fisher Scientific, Waltham, MA, USA). The final 20µL PCR contained HF buffer (Thermo Fisher Scientific, Waltham, MA, USA), 0.2 µM dNTPs, 0.2 µM of each primer, and 0.5 U Phusion Polymerase. Reactions were initiated at 98 °C for 30 s followed by 30 cycles of denaturation at 98 °C for 10 s, annealing (Ta of primers) for 30 s and extension at 72 °C, 30 s per 1 kb. The reactions were finalised by enhanced extension at 72 °C for 5 min followed by cooling to 4 °C. The DNA fragments were isolated directly using a QIAquick PCR purification kit (Qiagen, Valencia, CA, USA). In brief, five volumes of PB Buffer were added to each PCR sample, mixed, and transferred to a QIAquick column with a collection tube. The samples were centrifuged at 17,900 × g for 30 s and the supernatant was discarded. The membrane was washed by 750 µ of PE buffer and centrifuged at 17,900 × g for 30 s. The flow-through was discarded and the membrane with bound DNA was dried by another round of centrifugation. DNA was eluted by 30 µl of Elution Buffer (10 mM Tris-Cl, pH 8.5).

The initial step of vector verification was based on general amplification by Merciáza Taq polymerase (Merci, Brno, Czech Republic). The PCR mixtures contained 1× Merciáza buffer (Merci, Brno, Czech Republic), 0.2 µM dNTPs, 0.2 µM of each primer, and 0.5 U of Taq polymerase. Reactions were initiated by 95 °C denaturation for 2 min followed by 25-30 cycles of denaturation at 95 °C for 10 s, annealing for 30 s at the temperature according to the specific primer pair and extension at 68 °C for 1 min per kb. The final extension at 68 °C for 5 min completed the reaction followed by cooling to 4 °C. All reactions were loaded on agarose gel electrophoresis for fragment separation and visualized by ethidium bromide.

PCRs and enzymatic DNA digestion reactions were loaded onto an agarose gel electrophoresis for fragment separation. All samples were mixed with 10× Orange G loading dye (containing 45% sucrose and 0.02–0.05% of Orange G) before loading. Fragments were separated by a gel prepared from 1% agarose dissolved in 1× TAE Buffer (PanReac AppliChem, Darmstadt, Germany), which was microwaved until complete dissolution. The gel solution was cooled by running water, and one drop of

Ethidium bromide (SigmaAldrich®, Burlington, MA, USA) was added. Gel hardened in a container with a comb, producing sample positions. Samples and an appropriate ladder were loaded, and the electrophoresis run in 1× TAE Buffer at 80 V. Stained DNA fragments were detected and recorded by a trans-illuminator Gel and Blot Imager (UVP ChemSolo Auto Imager - Versatile Bioimaging System equipped with UVP Elite 302nm UV Transilluminator and the broad band filter, AnalytikJena, Jena, Germany).

Primer hybridization was carried out for a pair of primers from Table 1 (GBA3_CAFN and GBA3_CARN). Equimolar amount of oligonucleotides was incubated at 95 °C for 5 min to remove secondary structures and hydrogen bonds. The sample was sequentially cooled down to 4 °C. Annealed oligonucleotides were used directly or stored for further use at -20 °C up to two weeks.

Primers for *ALBA* domestication		
P	GBA1_p1F	GCGCCGTCTCGCTCGGGAGCCACCATATAGTCCCAAAGAC
P	GBA1_p1R	GCGCCGTCTCGGCCTCGTACGATACAGCCGA
P	GBA1_p2F	GCGCCGTCTCGAGGCGGATTCAGTTACGCCT
P	GBA1_p2R	GCGCCGTCTCGCTCAAGTAAACTTGAAATGCCAAACGACATC
G	GBA1_C1F	GCGCCGTCTCGCTCGAATGATGGAAGAGATCACGGAAGG
G	GBA1_C1R	GCGCCGTCTCGCTCACGAAgcGTTTTGCTCTTGGGCTTC
P	GBA2_p1F	GCGCCGTCTCGCTCGGGAGAATATAAAACAAGAATTGGTCCAATG
P	GBA2_p1R	GCGCCGTCTCGCTCAAGTAACGCTTGTGAAATCGGGTCA
G	GBA2_C1F	GCGCCGTCTCGCTCGAATGATGGAAGAGATCACCGATGG
G	GBA2_C1R	GCGCCGTCTCGCTCACGAAGCGTTCTGCACCTGAGCTTC
P	GBA3_p1F	GCGCCGTCTCGCTCGGGAGTGTTTGATTTGTTTAAGCTGTTGG
P	GBA3_p1R	GCGCCGTCTCGTAAGACCAATCTCGTTGAAGG
P	GBA3_p2F	GCGCCGTCTCGCTTATGTATTGTGGTCTGTGG
P	GBA3_p2R	GCGCCGTCTCGATACCACTATGCTTGTGAGGT
P	GBA3_p3F	GCGCCGTCTCGGTATCTCTCCGTCATTCGCT
P	GBA3_p3R	GCGCCGTCTCGCTCAAGTAAAAACCGTTACGACGCTTAAC
G	GBA3_C1F	GCGCCGTCTCGCTCGAATGATGGCGATGGAAGTAGCAAC
G	GBA3_C1R	GCGCCGTCTCGCTGTCTCTGCACTGGCTTCC
G	GBA3_C2F	GCGCCGTCTCGACAGAAGCTTCCGTGGAAGC
G	GBA3_C2R	GCGCCGTCTCGCTCACGAAGCGACCTCGGTGGCAGCGGC
P	GBA4_p1F	GCGCCGTCTCGCTCGGGAGAAACAGAAATTGTAATACATGGCAAT
P	GBA4_p1R	GCGCCGTCTCGCTCAAGTATCTGATATATATCAGCCGCAC
G	GBA4_C1F	GCGCCGTCTCGCTCGAATGATGGATAAGTATCAACGAGTGG
G	GBA4_C1R	GCGCCGTCTCGCTCACGAAgcAGCAGCTGCCTGGACTGGTG
P	GBA20_p1F	GCGCCGTCTCGCTCGGGAGATTTCTTGAAATGAATGTTTATCCATG
P	GBA20_p1R	GCGCCGTCTCGGCGACGCTATACTGCAAAGA
P	GBA20_p2F	GCGCCGTCTCGTCGCAAGAGGAGTCTCCGCG
P	GBA20_p2R	GCGCCGTCTCGCTCAAGTATCGATTTCCGGTTTTTAAGTTTTTAC
G	GBA20_C1F	GCGCCGTCTCGCTCGAATGATGGATAAGTATCAGAGAGTTGAG
G	GBA20_C1R	GCGCCGTCTCGTGATCTCAATTCTTCAGGAGAAAA

G	GBA20_C2F	GCGCCGTCTCGATCACGAGGCATGTGTCGAT
G	GBA20_C2R	GCGCCGTCTCGCTCACGAAGCTGCAGCAGCCTGGATAGG
P	GBA6-12_p1F	GCGCCGTCTCGCTCGGGAGTCAGATGAAACATCTGACAGAAG
P	GBA6-12_p1R	GCGCCGTCTCGGCGACCAGCAAAAAAATGTTG
P	GBA6-12_p2F	GCGCCGTCTCGTCGCATGAGTCAGTGCTAATG
P	GBA6-12_p2R	GCGCCGTCTCGCTCAAGTACGCTTCAAAACGGGTCAGAT
C	GBA6-12_C1F	GCGCCGTCTCGCTCGAATGATGGATAGATACCAGAGAGTC
C	GBA6-12_C1R	GCGCCGTCTCGCATCTCTTCCTCCACCATACctgt
C	GBA6-12_C2F	GCGCCGTCTCGGATGACGGGTATGGTGGAGGaa
C	GBA6-12_C2R	GCGCCGTCTCGCTCACGAAGCGGCTTCGTTTTGGTTACT
PU	GBA1_p1F	GCGCCGTCTCGCTCGGGAGCCACCATATAGTCCCAAAGAC
PU	GBA1_p1R	GCGCCGTCTCGGCCTCGTACGATACAGCCGA
PU	GBA1_p2F	GCGCCGTCTCGAGGCGGATTCAGTTACGCCT
PU	GBA1_5U1R	GCGCCGTCTCGCTCACATTTGAATCTAACTCAGAAAAATTAAAACTTCTCCTCTCG
PU	GBA2_p1F	GCGCCGTCTCGCTCGGGAGAATATAAAACAAGAATTGGTCCAATG
PU	GBA2_5U1R	GCGCCGTCTCGCTCACATTGCTTGCTAATCGGAATCCGT
PU	GBA3_p1F	GCGCCGTCTCGCTCGGGAGTGTTTGATTTGTTTAAGCTGTTGG
PU	GBA3_p1R	GCGCCGTCTCGTAAGACCAATCTCGTTGAAGG
PU	GBA3_p2F	GCGCCGTCTCGCTTATGTATTGTGGTCTGTGG
PU	GBA3_p2R	GCGCCGTCTCGATACCACTATGCTTGTGAGGT
PU	GBA3_p3F	GCGCCGTCTCGGTATCTCTCCGTCATTCGCT
PU	GBA3_5U1R	GCGCCGTCTCGCTCACATTCTTTCTCCGATCGATCACTC
PU	GBA4_p1F	GCGCCGTCTCGCTCGGGAGAAACAGAAATTGTAATACATGGCAAT
PU	GBA4_5U1R	GCGCCGTCTCGATACGAAGATTGAGATAAAACGAAAA
PU	GBA4_5U2F	GCGCCGTCTCGGTATCTTTCGAAAGATCTAACCAC
PU	GBA4_5U2R	GCGCCGTCTCGCTCACATTCTGAATCAACCCCAAAATGGA
PU	GBA20_p1F	GCGCCGTCTCGCTCGGGAGATTTCTTGAAATGAATGTTTATCCATG
PU	GBA20_p1R	GCGCCGTCTCGGCGACGCTATACTGCAAAGA
PU	GBA20_p2F	GCGCCGTCTCGTCGCAAGAGGAGTCTCCGCG
PU	GBA20_5U1R	GCGCCGTCTCGCTCACATTCTGAAAAGCAACACAAAATCAGAA
PU	GBA6-12_p1F	GCGCCGTCTCGCTCGGGAGTCAGATGAAACATCTGACAGAAG
PU	GBA6-12_p1R	GCGCCGTCTCGGCGACCAGCAAAAAAATGTTG
PU	GBA6-12_p2F	GCGCCGTCTCGTCGCATGAGTCAGTGCTAATG
PU	GBA6-12_u1R	GCGCCGTCTCGCTCACATTTTTACCAGAAGATGAAAAGATCGA
PU	GBpD1_1F	GCGCCGTCTCGCTCGGGAGCGTCCGAAGTTTCCCTCTTG
PU	GBpD1_1R	GCGCCGTCTCGCTCACATTTTCCTCATCGCTAATCGATC
G	GBA3_C2FN	GCGCCGTCTCGACAGAAGCTTCCGTGGAAGCACAAGAAGAAGTTGCCGCTGCCACCGAGGTCGCTTCGTGAGCGAGACGGCGC
G	GBA3_C2RN	GCGCCGTCTCGCTCACGAAGCGACCTCGGTGGCAGCGGCAACTTCTTCTTGTGCTTCCACGGAAGCTTCTGTCGAGACGGCGC

Primers for *GAF1* domestication		
PU	GBGAF1_P5U1F	GCGCCGTCTCGCTCGGGAGATGAGTAAAGTTGGTTAAAGCTTC
PU	GBGAF1_P5U1R	GCGCCGTCTCGGCCTCATCTACGAGGAGACA
PU	GBGAF1_P5U2F	GCGCCGTCTCGAGGCCACTAATACGCTTGAC

PU	GBGAF1_P5U2R	GCGCCGTCTCGCTCACATTTAGTGAGTCGGAGAGAACAG
G	GBGAF1_c1F	GCGCCGTCTCGCTCGAATGATGGGATTCTTCGATCTTAGC
G	GBGAF1_c1R	GCGCCGTCTCGGCGACCCAAGAGTGAGAAGA
G	GBGAF1_c2F	GCGCCGTCTCGTCGCTAATCAAAGTCGCTCC
G	GBGAF1_c2R	GCGCCGTCTCGTAAGACGCGTGTACTGCCGA
G	GBGAF1_c3F	GCGCCGTCTCGCTTACAGTTCATGTGGAGAGT
G	GBGAF1_c3R	GCGCCGTCTCGCTCACGAAGCATGTTTTCTTTTTTTACTGATCC

Primers for *pDuo1* domestication		
PU	pDuo1_ F	GCGCCGTCTCGCTCGGGAGCGTCCGAAGTTTCCCTCTTG
PU	pDuo1_1R	GCGCCGTCTCGCTCACATTTTCCTCATCGCTAATCGATC

Table 1: List of primers used for fragment´s domestication. P = promoter sequence, G = genomic sequence, C = cDNA sequence, PU = promoter and *5 'UTR* sequences

3.4. GoldenBraid cloning and fragment domestication

Initially, all TUs were assembled by SnapGene® software (from Dotmatics; available at snapgene.com), and all required plasmids were created *in silico*. Designed constructs were created by the GoldenBraid (GB) cloning system based on Type IIS restriction enzymes (Sarrion-Perdigones et al., 2011; Sarrion-Perdigones et al., 2013). Primer sequences for domestication were obtained from GoldenBraid 3.0 domestication tool (https://goldenbraidpro.com/do/domestication/) and are listed in Table 1. The final vectors were achieved through following three cloning steps: domestication into pUPD2, TU assembly in the pDB1 backbone, and combination of TUs in the binary destination vector pDGB3, suitable for stable transgenic plant production. The initial domestication step removes internal Type IIS restriction sites from target sequences by introducing point mutations in specific parts of primers that are elongated by adapters. Gene fragments were amplified according to chapter 3.3 by PCR using Phusion High-Fidelity DNA Polymerase and purified with the QIAquick PCR purification kit. Domestication restriction-ligation reactions were prepared according to the GB domestication protocol. Equimolar amount of all fragments was added to a ligation reaction containing 75ng/µL of pUPD2 (Vazquez-Vilar et al., 2017) domestication vector with chloramphenicol resistance marker, 5 U of BsmBI/Esp3I restriction enzyme (Thermo Scientific, Waltham, MA, USA) and 3 U of T4 DNA ligase (Thermo Scientific, Waltham, MA, USA) dissolved in 1×Ligase Buffer and filled by ddH_2O up to 10 µL. In the event of unsuccessful ligation, the concentration of the domestication vector was elevated to 100 ng/µL, and equimolar amounts of all fragments were recalculated. Reactions were run by modified GB domestication protocol initiated by 37 °C for 10 min, followed by 30 cycles of a 2-step cycle; 37 °C for 2 min and ligation at 16 °C for 5 min. The reactions were finalised at 37 °C for 30 mins and terminated at 65 °C for 20 min. The reactions were immediately transformed into cells or stored in -20 °C.

3.5. Plasmid amplification and isolation

All cloning reactions were transformed into *E. coli* cells (One Shot® TOP10 Chemically Competent, Thermo Fisher Scientific, Waltham, MA, USA), selected by blue/white screening and verified. Heat shock-mediated transformation of *E. coli* cells by 1 µL of the reaction was induced at 42 °C for 30 s. Treated mixtures were immediately placed on ice for 2 min to enhance transformation efficiency. The cells were incubated at 37 °C for 45 mins with 250 µL of SOC medium containing 2 % (w/v) tryptone, 0.5 % Yeast extract, 10 mM sodium chloride, 2.5 mM potassium chloride, 10 mM magnesium chloride, and 20 mM α-D-glucose. Induced cultures were transferred to LB agar low salt plates supplemented with 1 mM IPTG (Isopropyl β-D-1-thiogalactopyranoside, SigmaAldrich®, Burlington, MA, USA) and 100 µg/mL X-Gal (5-bromo-4-chloro-3-indolyl-β-D-galactopyranoside, SigmaAldrich®, Burlington, MA, USA), inducing lacZ expression, which enables colonies blue/white selection with correctly assembled constructs from the original vectors. LB agar plates were additionally supplemented with 25-30 µl/mL Chloramphenicol (SigmaAldrich®, Burlington, MA, USA) for pUPD2 vector-containing colonies selection or 50 µg/mL Kanamycin (Duchefa Biochemie B.V., Haarlem, The Netherlands) for pDB1 vector-containing colonies selection, or 100 µg/mL Spectinomycin (Spectinomycin HCl pentahydrate, Duchefa Biochemie B.V., Haarlem, The Netherlands). Cells on solid medium were incubated overnight at 37 °C and moved to 4 °C until the next day to enhance the blue signal. Only white colonies were selected for a transfer to the fresh LB plate with the same selection agents and incubated at 37 °C overnight. New colonies were selected for PCR verification using a 10µL pipette tip and transferred into a PCR mixture containing backbone-specific primers listed in Table 2.

Backbone-specific primers	
pUPD2_F	CCGATCAACTCGAGTGC
pUPD2_R	TGTTCTTTCCTGCGTTATCC
LB_F	TGGCAGGATATATTGTGGTG
RB_R	GTTTACCCGCCAATATATCC
AlphaOmega_F	GAAAGGCGGCAACCTC
pLX_F	CGGCGCAGTTCTGCGTAG
pLX_R	ATCACCAAGGTAGTCGGC
DUO1_F3	ACTTAGTGAGTGCATCTGC
Seq_pCsVMV_F	GATAAGGTCGGTGATTGTG
YFP/GFP_R	GAAGTTCACCTTGATGCCG
Seq_YFP_F	CTGAGCTACCAGTCCGC
GFPseq_R	TGAAGCACTGCACGCCGTA
sGFP_middle_F	TACGTCCAGGAGCGCAC
Seq_Kan_R1	CCATGATGGATACTTTCTCG

Table 2: List of primers for verification by PCR.

Plasmids were extracted and purified by the GeneJET Plasmid Miniprep Kit (Thermo Fisher Scientific, Waltham, MA, USA). Liquid cultures were grown in 5 ml LB broth containing ddH_2O and LB broth low salt (Tryptone 10 g/ L, Sodium chloride 5 g/ l, Yeast extract 5 g/ l) supplemented with 25-30 µl/mL chloramphenicol, or 50 µg/mL kanamycin or 100 µg/mL spectinomycin according to the inserted-vector resistance. The cultures were cultivated at 37 °C while shaking at 250 rpm. Cells were harvested by centrifugation at 6,800 × g for 2 min at RT. The supernatant was completely removed, and the cells were immediately resuspended in 250 µL of Resuspension Solution. Cells were disrupted by adding 250 µL of Lysis Solution and gently mixed until a partial clarity was achieved. Lysed cells were mixed with 350 µL of Neutralisation Solution by immediate tube inversion and left to precipitate at 4 °C for at least 10 min. Cell debris with chromosomal DNA was pelleted by centrifugation at 14,000 × g for 5 min. The supernatant was transferred to a GeneJET™ spin column and centrifuged at 14,000 × g for 1 min. The DNA was washed twice with 500 µL of Wash Solution at 14,000 × g for 1 min, followed by additional centrifugation at the same conditions to remove residual Wash Solution. DNA was incubated with 30 µL of Elution Buffer for 2 min and eluted at 14,000 × g for 2 min into a new tube. Plasmid concentration was immediately measured (NanoDrop One instrument, Thermo Fisher Scientific, Waltham, MA, USA) and stored at -20 °C.

Isolated plasmids were validated by the digestion reaction and gel electrophoresis separation. The 10 µL digestion reaction contained one or two conventional restriction enzymes, according to manufacturer´s protocol (Thermo Fisher Scientific, Waltham, MA, USA), which included 1× selected Buffer for highest enzyme activity diluted with ddH_2O, 300 ng/µL of verified plasmid, and the restriction enzyme. Only vectors with correct fragment sizes were sent for Sanger sequencing (Eurofins Genomics, Ebersberg, Germany) with specific primers listed in Table 3.

Sequencing primers	
A1SP1F	TCGGATTAGAAGGAGGAGG
A1SPV2F	TGAGCCGTCACCAATTG
A1SPV3F	ACGTCAATCTCGCCAAG
A1SPV4F	GGCTTTGCTGTTGAAAAG
A2SPV2F	CCACACTCTTCCCATGG
A2SPV3F	GGAAGAGATCACCGATGG
A2SPV4F	TGCAGCCATTGCAACTG
A3SP1F	TATTTAACCCGTCACAGGC
A3SPV2F	GGTCCAACAAATGGTCCC
A3SPV3F	TCCCGCTAGAGAGAGAGAG
A3SPV4F	TTTCTGCACTTGGAATGGG
A4SPV2F	GATAACATAGACACGTTCTCC
A4SPV3F	CTTCCTGGGCAACAAAAC
A4SPV4F	AAGGCAATGGGAAGAGC
A4SPV5F	GAATCTCCCTTGTACTTGC

A4SPV6F	CGCCGTGGTTATGATGG
A5SPV2F	GCGCAGTAGGAGAATTTCG
A5SPV3F	AACAACCGCCTCTTAGG
A5SPV4F	TCTCGCTGCTTGCTATTC
A5SPV5F	GGTACATTGTCTCCAATGC
A5SPV6F	CGGACAAGTGTTTGATTGG
SPA6var_F	CATTGTCATTGAGCGAGC
SPA6var_R	TAGCTTCGTCCACCACG

Table 3: List of primers used for Sanger sequencing.

3.6. GB cloning at pDB1 and pDGB3 levels

In the next step, TUs were formed by combining the domesticated sequences and GB parts in pDB1 α11 and pDB1 α12 backbones with the kanamycin resistance cassette (Sarrion-Perdigones et al., 2013). All combined vectors (pUPD2, MoClo, backbone) were added to a reaction in the same concentration set to 75ng/µL with 5 U of BsaI restriction enzyme (Thermo Scientific, Waltham, MA, USA) and 3 U of T4 DNA ligase (Thermo Scientific, Waltham, MA, USA) in 1×Ligase Buffer and ddH_2O. The assembled TUs comprised of promoters (native, *proDUO1*, *proLAT52*, *proCsWmV*), N-tag (NLS containing *5′ UTR*, ω (Tobacco Mosaic Virus) + nuclear localisation signal (Simian Virus 40) (Engler et al., 2014), full-gene fragments starting by *ATG* signature without stop codon (*ALBA1-5*, *GAF1, GFP, YFP*), and pollen-specific cDNA *ALBA6-4*, C-tags (*GFP, YFP, mCherry*), and terminator *nosT* obtained from the MoClo Tool kit (Weber et al., 2011; Werner et al., 2012). Plasmids containing the required TUs were transformed into *E. coli* One Shot® TOP10 Chemically Competent cells as described in chapter 3.5. Colonies containing created plasmids were selected on LB plates supplemented with 1 mM IPTG, 100 µg/mL X-Gal, and 50 µg/mL kanamycin. Plasmids were purified and validated by digest reaction and Sanger sequencing.

The last GB cloning reaction ensures the combination of selected TUs in the destination pDGB3 ω2 binary backbone with a spectinomycin resistance cassette (Sarrion-Perdigones et al., 2013). The reaction was prepared according to the same protocol as described above for pDB1 α level cloning, with a modification in the restriction enzyme used, BsmBI. This reaction combines TUs formed in pDB1 α11 and α12 backbones with pDB1 α11-14 vectors containing 35-bp stuffer sequences and pDGB3 α2 carrying plant selection cassette (KanFastR), conferring resistance to the kanamycin antibiotic, and a FastRed cassette (*proOLE::RFP*) active in mature embryos. Specific adapter sequences create an order of selected TUs from α11 to α14 and α2. The final binary vectors created TU or TUs connected to the plant markers by short sequences at the background of high-copy pDGB3 ω2. Low-copy pDGB3 pLX B3ω2 backbone (Pasin et al., 2017) was used when

a restriction-ligation reaction to the high-copy plasmid was unsuccessful. The obtained vectors were amplified, purified, and validated according to chapter 3.5.

3.7. Transcription units and their combinations

3.7.1. Experimental design for ALBA proteins targeting to the nuclei

Vectors containing *proAlba::NLS-ALBA-YFP::nosT* were used for nuclear-targeted ALBA localization presented in chapter 4.1. These TUs were created by domesticated promoter sequences of *ALBA* genes in pUPD2::*proALBA* combined with *NLS* for N-terminal fusion from the MoClo, *ALBA* gene sequences starting with *ATG* signature without stop codon, pUPD2::*ALBA*; *YFP* sequence for C-terminal fusion, and strong terminator sequence *nosT*. The TUs were formed in the pDG1 α12 backbone and further inserted into a high-copy pDGB3 ω2 backbone with the cassette for plant selection (KanFastR) and stuffer sequences. The binary vectors were transferred to the wild-type Col-0 plants by Agrobacterium-mediated transformation.

3.7.2. Colocalization assays of ALBA proteins and RBP markers

Pollen grains coexpressing various pairs consisting of *ALBA* genes (*proALBA:ALBA-GFP*) and a RBP marker (*proPabp3:PABP3-RFP* or *proPabp5:PABP5-RFP*) are presented in chapter 4.3.1 and 4.3.2. Transcription units of *proALBA:ALBA1-5-GFP,* carried by destination vectors pFASTR07, were created during my master´s studies (Náprstková, 2016). Combinations of ALBA1-6-GFP on PABP3-RFP and PABP5-RFP backgrounds were created by Agrobacterium-mediated transformation. Selected pairs were included in a manuscript presented in chapter 4.2. (Náprstková et al., 2021).

For a further experiment, the *GAF1* marker (*proGAF1::GAF1-mCherry::nosT*) was created in the pDB1 α13 backbone. The *GAF1* TU consisted of a domesticated promoter and *5′ UTR* sequences of *GAF1* in pUPD2::*proGAF1-5' UTR,* followed by a domesticated *GAF1* coding sequence starting with *ATG* signature without stop codon, pUPD2::*GAF1*, *mCherry* sequence for C-terminal fusion, and strong terminator sequence *nosT*. The *GAF1* TU was combined with 35-bp stuffer fragments and the cassette for plant selection KanFastR in the destination vector pDGB3 ω2. The destination vector was inserted in the wild-type Col-0 and transgenic ALBA-GFP plants. Colocalization results are shown in chapter 4.3.3.

Pair assembly within Rpp20-like and Rpp25-like subfamilies was created by a systematic α-level design (pDB1), pDB1 α11 (TUs with mCherry), and pDB1 α12 (TUs with YFP). To obtain *proALBA::ALBA-mCherry::nosT,* TUs were combined by domesticated promoter and *5′ UTR* sequences of *ALBA* genes in pUPD2::*proALBA-5' UTR*, domesticated sequence of *ALBA* coding

region starting by *ATG* signature without stop codon, pUPD2::*ALBA*, *mCherry* sequence for C-terminal fusion and strong terminator sequence *nosT*. These functional units were combined with prepared TUs *proALBA::ALBA-YFP::nosT*. These TUs were created by domesticated promoter and *5' UTR* sequences of *ALBA* genes in pUPD2::*proALBA-5' UTR* fused with domesticated genomic sequence of *ALBA* genes starting with *ATG* signature without stop codon, pUPD2::*ALBA*, *YFP* sequence for C-terminal fusion, and strong terminator sequence *nosT*. Formed destination vectors carrying *ALBA-mCherry* and *ALBA-YFP* TUs are based on pDGB3 ω2 (ALBA1-mCherry and ALBA2-YFP, ALBA2-mCherry and ALBA3-YFP, ALBA3-mCherry and ALBA1-YFP, ALBA6-mCherry and ALBA5-YFP, ALBA6-mCherry and ALBA5-YFP) or pDGB3 pLX B3ω2 (ALBA4-mCherry and ALBA5-YFP) backgrounds. All couples containing the mCherry-containing and YFP-containing TUs were combined with 35-bp stuffer fragments and the cassette for plant selection KanFastR. The created destination vectors were inserted in the wild-type Col-0 plants, and colocalization results are shown in chapter 4.3.4. Control plants harbouring *proLAT52::YFP* and *proLAT52::mCherry* were obtained from the Laboratory collection.

3.7.3. Overexpression of ALBA proteins in SCs

Vectors used for *ALBA* gene overexpression contained a single TU assembled in the pDB1 α12 backbone. The *ALBA* gene overexpression in pollen SCs was achieved by promoter of *DUO1* sequence domestication (Table 1, Primers for *proDUO1* domestication) in pUPD2 and TUs formation (*proDUO1::ALBA-GFP::nosT)*. The pUPD2::*pDUO1* was combined with domesticated genomic sequences of *ALBA* genes, starting with *ATG* signature without stop codon, pUPD2::*ALBA, GFP* sequence for C-terminal fusion and strong terminator sequence *nosT*. Localization control was created by promoter *DUO1*, pUPD2::*proDUO1,* and *GUS* genomic sequence fused *in frame* with *GFP* sequence for C-terminal fusion, finalised with strong terminator *nosT*. Obtained TUs were inserted into a high-copy destination vector pDGB3 ω2 (*ALBA1, ALBA4,* and *ALBA6*) or the low-copy pDGB3 pLX B3ω2 backbone (*ALBA2, ALBA3,* and *ALBA5)*. Formed destination vectors contained one *ALBA* TU combined with 35-bp stuffer fragments and the cassette for plant selection KanFastR. Verified destination vectors were inserted into the wild-type Col-0 plants used for the experiment presented in chapter 4.4.1.

3.7.4. Overexpression of ALBA proteins in VC

The widely used *LAT52* promoter was used for *ALBA* gene overexpression in mature pollen VCs caused by TUs containing *proLAT52::ALBA-YFP::nosT*. The *proLAT52* sequence obtained from the MoClo Tool kit (Weber et al., 2011; Werner et al., 2012) was combined with domesticated genomic sequences of *ALBA* genes, starting with *ATG* signature without stop codon, pUPD2::*ALBA,*

YFP sequence for C-terminal fusion, and strong terminator sequence *nosT*. Each TU was combined with 35-bp stuffer fragments and the cassette for plant selection KanFastR in one of the destination vectors pDGB3 ω2 or pDGB3 pLX B3ω2. A low-copy pDGB3 pLX B3ω2 backbone was used for *ALBA5* and *ALBA6 TUs*. The created destination vectors were inserted in the wild-type Col-0 plants, and the results are shown in chapter 4.4.2.

3.7.5. Overexpression of ALBA proteins in sporophytic tissues

Sporophytic overexpression of *ALBA* genes was achieved by the activity of *CsWmV* promoter and assembly of *proCsWMV::ALBA-GFP::nosT* TUs. Sequence of *proCsWMV* was obtained from the MoClo Tool kit (Weber et al., 2011; Werner et al., 2012), followed by domesticated genomic sequences of *ALBA* genes starting with *ATG* signature without stop codon, pUPD2::*ALBA, YFP* sequence for C-terminal fusion, and strong terminator sequence *nosT*. Triple mutant seedlings of *alba456* were acquired by my student, Mgr. Helena Kočová in homozygous state for *alba4*$^{(+A119)}$ and *alba6*$^{(+T76)}$ and heterozygous state in *ALBA5*$^{(+T76)}$. The triple homozygous line *alba456* $^{+A/+A,\ +T/+T,\ +T/+T}$ was identified by Sanger sequencing and used in this study. All sequences for a control TU were obtained from the MoClo Tool kit (*pCsWMV, GUS, GFP, nosT*). All TUs were assembled in the pDGB3 ω2 destination vector with 35-bp stuffer fragments and the cassette for plant selection KanFastR. Final plasmids were inserted into the wild-type Col-0 plants and are further shown in chapter 4.4.3.

3.8. *Agrobacterium tumefaciens* transformation by electroporation

Vector samples were diluted, and 2 µL of each reaction was used for *Agrobacterium tumefaciens*, strain GV3101 (pMP90RK) transformation. Cells were let thawed on ice, gently mixed with the isolated plasmid, and electroporated using an eporator (Eppendorf™ Eporator™, Hamburg, Germany) set to 2.0 kV for 5.4–5.6 s. Bacterial cultures were incubated in 950 µL of YEB medium (6 g/ L Yeast extract, 5 g/ L Peptone from casein, 5 g/ L Sucrose, 0.5 g/ L Magnesiumsulfat-Heptahydrat) for 1.5–2 h in the Incubator Hood TH 30 at 28 °C, 180 rpm. Suspensions were 1,000× diluted by ddH_2O and transferred on 20 mL YEB agar (6 g/ L Yeast extract, 5 g/ L Peptone from casein, 5 g/ L sucrose, 0.5 g/ L Magnesiumsulfat-Heptahydrat and 12 g/ L agar with selection 100 ng/ µL spectinomycin 50 ng/ µL rifampicilin (Rifampicilin (13292-46-1); Duchefa Biochemie B.V., Haarlem, The Netherlands) and 50 ng/ µL gentamycin (Gentamycin sulphate (1405-41-0); Duchefa Biochemie B.V., Haarlem, The Netherlands). Cells on the solid medium were cultivated at 28 °C for 2 to 3 days. Several colonies were transferred to a fresh YEB plate with the identical selection and left at 28 °C overnight. The colonies were verified by PCR using gene-specific and backbone-specific primers (Table 1 and Table 2) to confirm the presence of the vector.

3.9. Plant transformation and crossing

Stable transgenic plants were obtained by floral dipping; pots of five flowering individuals were used for Floral dipping (Clough et al., 1998). Liquid cultures of *A. tumefaciens* cells containing a sole destination vector were cultivated in 5 mL of YEB medium containing 50 ng/ µL rifampicillin, 50 ng/ µL gentamycin, and 100 ng/ µL spectinomycin and grown at 28 °C overnight, 120 rpm. For further propagation, 1 mL of the culture was inoculated into 500 mL of the same YEB medium with the selection and cultivated at the same conditions overnight. The cells were harvested by centrifugation at 5,500 × g for 20 min, and the supernatant was removed. Pellet was resuspended by infiltration medium (2.17 g/ L Murashige and Skoog Basal Salt Mixture, 1 mL/ L Gamborg B5 vitamin mixture, 0.5 g/ L MES (2-(N-Morpholino) ethanesulfonic acid, 50 g/ L sucrose), 10 µL/ L 6-BAP (6-Benzylaminopurine, SigmaAldrich®)). Meanwhile, siliques and opened flowers from vital inflorescences were removed. Inflorescence tips containing flower buds were dipped for 45 s into the infiltration solution containing 300 µL/L Silwet L-77 to increase the wettability of plant tissues. Transformed plants were cultivated under standard growth conditions until maturation. Various plant lines were used for the floral dip procedure: wild-type Col-0, *proPabp3:PABP3-RFP*/*pab3-1,* and *proPabp5::PABP5-RFP*/*pab5,* and plants harbouring *proGAF1:GAF1-mCherry:nosT* cassette.

Multiple experimental materials were prepared by plant crossing. Donor plants of both genotypes were grown simultaneously. Independent donors were selected; emasculated flowers were obtained from *proPabp3:PABP3-RFP*/*pab3-1*, *proPabp5:PABP5-RFP*/*pab5,* and Col-0 plants. Mature anthers were isolated from *proALBA:ALBA-GFP* and *proCsWMV::ALBA-GFP* transgene-harbouring plants. In one inflorescence, one or two buds with immature anthers were selected for emasculation, and all anthers were removed under a Stereomicroscope. Plants were further cultivated at standard conditions, and stigma development was monitored for two to four days. Mature papillae cells were covered by released pollen grains and pollinated plants were cultivated until the pistil´s maturation.

3.10. Plant selection and heat stress

Transformed plants were selected by specific markers, including resistance to antibiotics dissolved in 0.5× MS medium kanamycin (GoldenBraid 3.0 vectors) or hygromycin (Hygromycin B Gold™, San Diego, CA, USA) (Gateway vectors), which were later found to reduce the germination ratio of the transgenic seeds. Therefore, the seeds were preselected by a needle according to RFP signal presence controlled by KanFastR cassette activity by the fluorescence Stereomicroscope Leica M205FA with Leica DMC6200 100 with filter set RFP ET546/10x ET605/70 (Leica Microsystems, Wetzlar, Germany). Representative transformed seeds of wild-type and aberrant phenotypes were detected using a Leica DMC6200 colour camera with a 2.2MP resolution (Leica Microsystems,

Wetzlar, Germany). Selected seeds were grown without antibiotics on 0.5× MS medium, as described in chapter 3.1. 7-day-old seedlings harboring FPs controlled by native and sporophytic promoters were screened using the fluorescent stereomicroscope for the presence of specific signals.

Plants were further selected based on the presence of the signal in pollen when presented. The pollen grains were harvested, and mounted in DAPI solution (0.8 µg/mL DAPI (4′-6-Diamidino-2-phenylindole, Merck KGaA, Darmstadt, Germany) in GUS buffer) for 10 min according to an adjusted protocol (Park, Howden, and Twell 1998). Pollen phenotype and signal localization uniformity were observed. The first two generations after transformation (T1 uniform and T2 segregating) emitted sufficient signal intensity for microscopic analysis. More than 15 plants were screened for each obtained construct in the T1 generation to identify transgenic plants with the most similar patterns of expression and protein localization. Segregating plants of the T2 generation were used for most of the experiments due to gene silencing in the following generation.

Heat stress treatment (37 °C for 3 hours, 70% RH, light) was performed on 6-leaf stage juvenile rosettes grown under standard conditions in Jiffy7. Stems were collected by a razor immediately after the treatment and frozen in liquid nitrogen. The samples were further processed for RNA isolation and RNA sequencing (described in chapters 3.13and 3.15), and the results are presented in chapter 4.4.3.7.

3.11. Fluorescence microscopy

Colocalization and localization results in mature pollen grains were investigated and presented in chapters 4.1, 4.3, 4.4. Pollen grains were harvested from opened flowers and stained with DAPI solution. Stained samples were prepared for light and confocal microscopy. The solution containing pollen grains was transferred to a slide and covered with a cover slip. Only grains with sufficient signal in two (localization) or three (colocalization) channels were documented by the inverted confocal microscope (Zeiss LSM880 equipped with an Airyscan detector and Plan-Apochromat 100×/1.46 Oil objective, Carl Zeiss, Jena, Germany). For excitation of DAPI, GFP, and RFP/mCherry, argon ion laser lines at 405 nm and 488 nm, and a DPSS laser at 561 nm were used in a sequential scanning mode. Emitted signals were selected by the fluorescence filter cubes BP 420-480 + LP 605 and BP 495-550 + LP 570, and detected by the 1× high-resolution Airyscan detector. Within the experiment, all images were captured using the same imaging setup, acquired with adjusted settings that reflected the various signal intensities of individual samples. Raw files were immediately calculated by an Airyscan Processing in ZEN black software (Carl Zeiss, Jena, Germany).

Seedlings, leaves, sepals, and other parts except pollen were mounted in water and processed for further analysis, as shown in chapter 4.4.3.2, chapter 4.4.3.3, and chapter 4.4.3.4. Screens of seedlings were performed on closed MS plates using the fluorescence stereomicroscope. Seedlings

and larger organs were harvested, mounted in water on a slide, covered with a cover slip and observed under the fluorescence stereomicroscope (Leica M205FA with Leica DMC6200, illuminated by HXP120 V Illuminator/HAL 100 with filter set ET GFP Ex470/40x Em525/50 and detected by the Leica DMC6200 colour camera 2.2Mp, Leica Microsystems, Wetzlar, Germany) in transmitted light (TL) and green channels. Samples for detailed inspection were prepared under the stereomicroscope and imaged by the wide-field fluorescence microscope (Zeiss AxioImager with ApoTome2 by EC Plan-Neofluar 20x/0.50 DIC M27 objective or C-Apochromat 40x/1.2 W Kor DIC M27 objective illuminated by HXP120 V Illuminator/VIS LED with FS38/GFP BP (Ex 470/40 Em BP 525/50) and detected by the CCD Axiocam 506 mono 6Mpix (2752x2208), 19 fps, pixel size 4,5 mm, Carl Zeiss, Jena, Germany) in TL, blue and green channels. Individual cells and selected tissues were captured by the Zeiss LSM880 with C-Apochromat 40x/1.2 W Kor FCS M27 objective in the green channel selected by FS38/GFP BP (Ex 470/40 Em BP 525/50), detected by a standard PMT detector or Plan-Apochromat 100×/1.46 Oil objective selected by the fluorescence filter cube BP 495-550 + LP 570 and detected by the 1× high resolution Airyscan detector and TL captured by PMT detector (Carl Zeiss, Jena, Germany).

Signal was detected in 7DAG seedlings, epidermal cells of cotyledons, and hypocotyl and rhizodermal cells of meristematic, transition, elongation, and differentiation root zones. True leaves were cut from juvenile rosettes and epidermal pavement cells on abaxial side of the leaf were captured by the inverted confocal laser scanning microscope (Zeiss LSM880 with C-Apochromat 40x/1.2 W Kor FCS M27 objective or Plan-Apochromat 100×/1.46 Oil objective in the green channel selected by FS38/GFP BP (Ex 470/40 Em BP 525/50) and TL detected by standard PMT detectors, Carl Zeiss, Jena, Germany). Discs cut from true leaves were captured by a lambda scan excited by the argon ion laser 488 nm in the green channel selected by FS38/GFP BP (Ex 470/40 Em BP 525/50), detected by the standard PMT detector. The signal was also localized in floral organs; epidermal cells of the sepal and mature pollen stained in DAPI solution and additionally captured in the blue channel described above. All data acquired by the Zeiss microscopes were further processed in ZEN blue software (Carl Zeiss, Jena, Germany). Z-stacks were selected and fused using maximum intensity projection, and individual channels were artificially colored and merged. Scale bars were added. All figures were created in the Photoshop CS6 software.

3.12. Phenotypic Analysis

A comprehensive study of phenotypic aberrations observed in *proCsWMV::ALBA-GFP::nosT* transgenic plants is presented in chapter 4.4.3.3 and chapter 4.4.3.4. Seeds were germinated on agar plates according to the chapter 3.1 and 4DAG seedlings were scanned with a ruler at high resolution. Image data were processed in Photoshop CS6 software, and scale bars were added. Collected 7DAG

seedlings were mounted in water on a slide and overlaid with a cover slip. Prepared samples were captured by the stereomicroscope (Leica M205FA with LasX Premium software, Leica Microsystems, Wetzlar, Germany) in green and TL channels. Flowering plants were selected, and their inflorescences were fixed using tweezers on the stereomicroscope table and captured. Flowers were collected on a slide and captured in multiple focal planes using the stereomicroscope in green and TL channels. Images were immediately processed in the software by extended depth of focus, and scales were added in Leica Application Suite X 3.7.4.23463 version.

The 7DAG seedling samples were further captured in detail. Root zones and cotyledons with youngest green tissues were captured by the fluorescence microscope (Zeiss AxioImager with ApoTome2 with C-Apochromat 40x/1.2 W Kor DIC M27 objective, Carl Zeiss, Jena, Germany) in the green channel. Later developmental stages were collected, and adult rosettes were cut by a razor above the hypocotyl, and all leaves were removed. Cleansed rosette stems were poured into 5% Agarose gel and allowed to solidify in a fridge. The prepared blocks were cut by a microtome in the longitudinal direction; slices were mounted in water on a slide and covered with coverslip. Imaging was performed by the fluorescence microscope (Zeiss AxioImager with ApoTome2, equipped with an EC Plan-Neofluar 20x/0.50 DIC M27 objective) in the green channel and the TL. Ovules were isolated from the pistil, mounted in water on a slide and captured in the TL by the fluorescence microscope. Acquired images were processed in the Zen Blue software. Pictures for phenotypic analyses of juvenile rosettes and adult flowering plants were acquired using a Canon camera (Tokyo, Japan); scaling of images was achieved by capturing a ruler within the acquisition. Raw data and final figures were created using Photoshop CS6 software, which included scale bars.

3.12.1. Analysis of flowering delay and seed aberrations

Populations of Col-0 and transgenic plants harbouring *proCsWmV::GFP*, *proCsWmV::ALBA4-GFP*, *proCsWmV::ALBA5-GFP,* and *proCsWmV::ALBA6-GFP* plants were grown in populations at standard conditions. Individual populations of independent lines for each genotype were considered biological replicas (BRs), and populations grown at different times represented technical replicas (TRs). Plants of control and sample genotypes were used for the following experiments. Co-0 populations were grown in 6 TRs and 4 BRs, *proCsWmV::GFP* in 5 TRs and 4 BRs, *proCsWmV::ALBA4-GFP* in 5 TRs and 4 BRs, *proCsWmV::ALBA5-GFP* in 6 TRs and 4 BRs, and *proCsWmV::ALBA6-GFP* in 3 TRs and 5 BRs. Individuals were cultivated up to adult rosettes, and on the day of first opened flower, they were considered to be flowering. Each population was observed daily, and the numbers of juvenile and flowering plants were counted until the day when the last plant began to flower. Further statistics were calculated using the R software with the ggplot2 package (R Core Team, 2018). Data from all grown populations were separately tested using the Shapiro-Wilk

normality test, and the impact of outliers was indicated by Cook´s distance. Outliers with a possible impact were removed. Normality was tested again, with no significant difference. Therefore, the data without a normal distribution were evaluated using two nonparametric tests: Kruskal-Wallis and Dunnett´s test. A two-sided Kruskal-Wallis test revealed significant differences between the medians of all populations. Therefore, Dunnett´s test, a nonparametric pairwise multiple-comparison procedure, was used to identify exact pairs of populations with distant medians, adjusted by the Bonferroni correction (Dinno, 2015). Acquired data calculations were visualized by box plots overlaid by violin graphs, which indicated data variability in chapter 4.4.3.5.

Cultivation of the obtained flowering plants continued until the individuals reached the precise maturation stage. When the 6th silique on the main inflorescence stem became yellowish, the 6th to 8th siliques were harvested and fixed with both-side tape to a slide. The style and fruit base were removed using a needle, and the valves were carefully cut along the replum and attached to the tape. Developing seeds were uncovered and counted based on their observed phenotype using the stereomicroscope. The acquired data were divided and visualized by bar charts in Microsoft Office Excel 2010. Graphs are presented in chapter 4.4.3.6.

3.13. RNA extraction

Total RNA was extracted from 7DAG seedlings of T1, T2, and T3 generations of plants as well as backcrossed lines from uniform (BC1) and segregating (BC2) generations. RNA isolation was performed using the RNeasy Mini Kit (Qiagen, Valencia, CA, USA) from approximately 100 mg of the deeply frozen tissue, which was collected in a tube containing autoclaved sea sand grains. The samples were powdered through two to three rounds of homogenization (FastPrep-24™ 5G Homogenizer, MP Biomedicals, CA, USA) at 4,000 rpm with RLT Buffer, which is responsible for cell lysis and RNA stabilization. The homogenized solution was loaded onto the QIAshredder spin column to filter out cell debris through centrifugation. The collected supernatant was transferred to the RNeasy spin column for RNA binding. The procedure continued with multiple washes by two Buffers, RW1 Buffer and RPE Buffer to remove contaminants.

The purified RNA was eluted with RNase-free water and treated with DNAaseI according to the modified RQ1 RNase Free DNaseI protocol (Promega, Madison, WI, USA). Each sample was gently mixed with the reaction mixture containing RNase-free water, 1× RQ1 RNAse-free DNase RB, and RQ1 RNAse-free DNase and incubated at 37 °C for 30 min. The treatment was arrested with 2 µL of DNase Stop solution at 65 °C for 10 min. The samples were centrifuged and the liquid phase was transferred to a fresh tube. The obtained purified RNA was used for further procedures, RT-qPCR and RNA sequencing.

3.14. RT-qPCR analysis

DNAseI-treated RNA served as template for complementary DNA (cDNA) synthesis. Reverse transcription was ensured by the ImProm-II™ Reverse Transcription System (Promega, Madison, WI, USA), initiated by an oligo-d$(T)_{20}$ primer, according to the manufacturer´s protocol. The reaction mixtures were placed in a heat block equilibrated to 25 °C for 5 min to anneal the primers, followed by extension at 42 °C for 1 hour and finalized by enzyme inactivation at 70 °C for 15 min. RNA quantity and quality were measured (NanoDrop One instrument, Thermo Fisher Scientific, Waltham, MA, USA). RNA integrity was verified by gel electrophoresis in a 2% agarose gel in 1× TAE (40 mM Tris base, 20 mM acetic acid, 1 mM EDTA, pH 8.0) to achieve 28S and 18S rRNA bands visualization.

RT-qPCR measurements of *ALBA1-5* expression levels in *oexALBA4*, *oexALBA5,* and *oexALBA6* samples were obtained using GoTaq Q-PCR Master Mix (Promega, Madison, WI, USA). Measurements of *ALBA6* expression in *oexALBA6* samples were achieved using GoTaq 1-Step RT-qPCR System (Promega, Madison, WI, USA). Transcripts were selectively amplified by gene specific primers (Table 4) on a LightCycler 480 (Roche, Basel, Switzerland). There were prepared single BR and two TRs for each sample. All connected samples were run simultaneously. Cycle threshold values (Ct values) for *ALBA4* and *ALBA5* were normalized according to *GAPC1* (At3g04120). Ct values obtained by GoTaq 1-Step RT-qPCR for *ALBA6* were normalized according to *EIF1a4* (At5g60390). Results are presented in chapter 4.4.3.1.

Primers for Q-PCR	
A1-q1	GAGTTAACAACATGAACTTGGCTGTT
A1-q2	CATTGTTCTTCAATATCTCAGCGACC
A2-q1	CGATGGAGTGAACAACATGAACTTAGCCACC
A2-q2	CTTCTCAACAGCAAAACCATTGTTCTTCAGTATTTCAGTA
A4-q1	GAGGTTACGGTTACGATGCTCCTC
A4-q2	CATCATAACCACCACGGCCTTG
A5-q1	GGAGGAAGGGGAAGAGGTGG
A5-q2	TCCATCTTGTTGAGCTTCATAGTAAGG
A6-q1	CCAAGGGAGTTATGAAGGAAAAGACC
A6-q2	CCCCATACCCGTCATTTCTCC
GAPC1_f	GACTACAGTCCACTCAATCACTGC
GAPC1_rv	AAGAGCTGGAAGCACCTTTCCG
eIF1a4_f	TGAGCACGCTCTTCTTGCTTTCA
eIF1a4_rv	GGTGGTGGCATCCATCTTGTTACA

Table 4: List of gene-specific primers used for Q-PCR

3.15. RNA sequencing and data analysis

To obtain transcriptomic data, RNA was isolated from juvenile rosettes, adult rosettes, and flowering plants. Whole stems were collected from juvenile rosettes (sample 1), and adult rosettes (sample 2), followed by old internodia cut from inflorescence stems (sample 3), and main inflorescence tips including all developing organs and tissues without opened flowers (sample 4,) grown under standard conditions. Furthermore, juvenile rosettes were heat-treated (37 °C for 3 hours), and whole stems were immediately collected (sample 5). Three BRs per genotype were collected at the same time of a day, 11-13h. RNA quality and quantity, as well as RNase-Free DNAse treatments, were performed as described above. For cDNA library construction, total RNA was poly (A)-enriched and sequenced by Illumina. The sequencing generated at least 20 million 150-bps long read pairs.

Rough reads were quality-filtered using Rcorrector and Trim Galore scripts (Song et al., 2015). Gene expression levels (aggregated transcript abundances quantified as transcripts per million— TPM) were gained by Salmon (Patro et al., 2017) with parameters --posBias, --seqBias, --gcBias, --numBootstraps 30. The reference index was created by the *Arabidopsis thaliana*, TAIR10 CDS library, version 20101214. Visualization, quality control of data analysis, and determination of differentially expressed genes were selected using the sleuth (version 0.29.0) package in R (Pimentel et al., 2017). Genes with q-value ≤ 0.05 and log2 fold change ≥ 1 (upregulated) or ≤ −1 (downregulated) were considered to be significantly differentially expressed (Kubalová et al., 2025). The obtained data were filtered according to upregulated and downregulated results and further analyzed by Panther 19.0 Overrepresentation test to annotate Gene Ontology processes according to the *Arabidopsis thaliana* reference list (Mi et al., 2019; Thomas et al., 2021). Obtained results are presented in chapter 4.4.3.7.

4. Results

The experimental part is divided into four chapters, reflecting the original hypotheses. The initial experiment focused on elucidating the role of ALBA proteins role in the nuclei of mature pollen. The previous results of ALBA distribution in pollen cytoplasm, presented in my Diploma thesis initiated further experimental work, which is described in the following chapters. Initially, the clarification and elucidation of ALBA distribution in pollen nuclei were achieved by their targeted localization, further described in chapter 4.1. Detailed insights into Arabidopsis *ALBA* genes were provided by gene expression experiments and protein localization and colocalization experiments, creating a comprehensive study when combined with heat stress treatments. These depicted experiments were finalized in the published manuscript presented in chapter 4.2. Nevertheless, further colocalization experiments with specific markers for RBPs were performed in chapter 4.3 to clarify the distribution of ALBA throughout various types of aggregates in pollen grains. Disruption of cell homeostasis was induced by the significant upregulation of *ALBA* genes in mature pollen and sporophytic tissues as depicted in chapter 4.4.

4.1. Targeted localization of ALBA proteins to pollen nuclei

To investigate ALBA proteins´ nuclear localization, a strong NLS sequence containing the *5′ UTR* (Tobacco Mosaic Virus), and nuclear localization signal (Simian Virus 40) was used for their predominant targeting and stabilization in nuclei (for detailed comments, see chapter 3.7.1). Genomic DNA of *ALBA1-5* and cDNA originated from *ALBA6* were fused with the *NLS* sequence and *YFP* in functional TU *proALBA::NLS-ALBA-YFP*. Obtained transgenic plants were grown, and the FP signal was detected in the mature pollen grains stained with a DAPI solution.

The detected signal varied in strength intensity depending on the sample. The emission pattern of most samples was unexpectedly detected in the cytoplasm (Figure 7A, 7C, 7D, 7E), though ALBA3-YFP accumulation was specifically localized in the nuclei (Figure 7B, Merge). Inconsistent signal distribution within Rpp20-like subfamily is demonstrated by two members, ALBA1 and ALBA3. Emission signal of NLS-ALBA1-YFP was very weakly localized in the VC cytoplasm without any distinctive pattern (Figure 7A). Unfortunately, the localization pattern of NLS-ALBA2-YFP could not be detected due to a lack of signal in the male gametophyte, despite precise seed selection. Surprisingly, the most distinct homolog of the subfamily, NLS-ALBA3-YFP, was localized in VC nuclei (Figure 7B). In SCs, the signal was not detected in nuclei even though ALBA3 is naturally present in the cytoplasm of SCs.

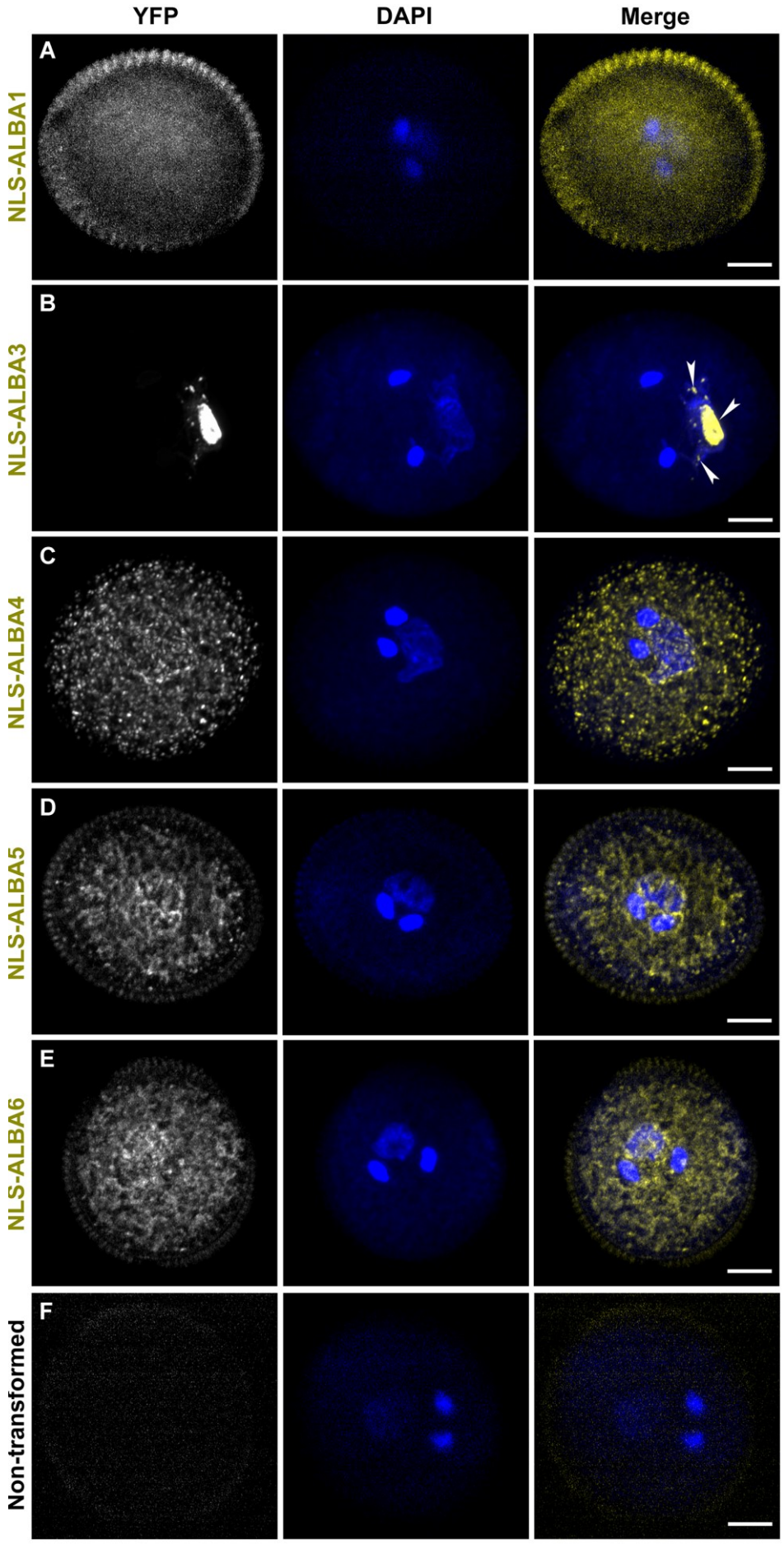
YFP
DAPI
Merge
A
NLS-ALBA1
B
NLS-ALBA3
C
NLS-ALBA4
D
NLS-ALBA5
E
NLS-ALBA6
F
Non-transformed

Figure 7: Subcellular localization of NLS-ALBA-YFP in transgenic pollen. Sequences of *ALBA1, ALBA3, ALBA4,* and *ALBA5* coding regions and cDNA encoding the pollen-expressed isoform of *ALBA6-4* were N-terminally fused with NLS, C-terminally tagged with YFP, and expressed in pollen under native promoter control (YFP column). Collected pollen from transgenic plants and Col-0 was stained in DAPI solution for nuclei visualization (DAPI column), and the channels were overlapped in post-processing (Merge column). Imaging was performed the same way, scale bar = 5 μm.

On the other hand, all members of the Rpp25-like subfamily share a localization pattern distinct from the expected results. All three NLS-ALBA4-6-YFP fusion proteins are localized in the VC cytoplasm, distributed in a reticular-like pattern similar to their native localization, though with a higher intensity of very clear round foci (Figure 7C, 7D, 7E). NLS-ALBA4-YFP distribution differs only in the absence of typical signal enrichment, aligning possible membranes and nuclei of SCs, although it is present around VC nuclei (Figure 7C). NLS-ALBA5-YFP and NLS-ALBA6-YFP share natural characteristic signal enrichment surrounding the whole MGU, foci accumulation around VC nuclei and possible membranes of SCs, including aggregation tightly associated with SC nuclei (Figure 7D, 7E). The experiment is completed with a negative control, where wild-type Col-0 mature pollen is visualized and processed in the same manner to exclude a non-specific signal (Figure 7F).

4.2. Detailed characterization of *ALBA* genes in generative organs of *Arabidopsis thaliana* and their response to heat stress

Published in: Náprstková A, Malínská K, Záveská Drábková L, Billey E, Náprstková D, Sýkorová E, Bousquet-Antonelli C, Honys D., 2021 **Characterization of ALBA Family Expression and Localization in *Arabidopsis thaliana* Generative Organs** *International Journal of Molecular Sciences* 22(4): p.1–23. DOI: 10.3390/ijms22041652.

Summary

Available information about *ALBA* genes in plant species persist limited. Predicted roles in cellular processes and regulatory pathways were based on high sequence similarity to homologs from more investigated species. The main objective of the study was to provide an elementary description of *ALBA* genes in generative organs at the expression and protein localization levels, with a focus on the male gametophyte. Furthermore, heat treatment enabled the first connection of Arabidopsis homologs to stress responses at both investigated regulatory processes.

The illustration of the *AtALBA* gene phylogeny was based on pollen transcript homology and expression level analysis using RNA sequencing. Expression analysis of *ALBA* genes in inflorescences was performed by specific GUS staining complemented by fusion protein ALBA-GFP localization in pollen stages, microspores, bicellular and mature pollen. These results were further extended by detecting gene activity in inflorescences under standard conditions and following heat treatments (37 °C for 3 hours and 42 °C for 1 hour), as measured by RT-qPCR one hour after the treatment. The alteration of the ALBA-GFP signal pattern was studied in mature pollen under both stress conditions, and the intensity of the stress response was calculated by quantifying signal accumulation of selected ALBA4-GFP, together with PABP3-RFP. Colocalization analysis was quantified for two pairs, ALBA4-GFP and PABP3-RFP, and ALBA6-GFP and PABP3-RFP, in mature pollen at standard conditions and heat-treated at 37 °C for 3 hours. Colocalization assay was completed by ALBA4-mCherry and ALBA6-YFP visualization in mature pollen.

Achieved results demonstrate the structural plasticity of the Rpp25-like subfamily and variability in expression patterns throughout pollen development, which is typically enriched in SCs. Visualization of gene activities in inflorescences revealed patterns shared by the two subfamilies, represented by highly active *ALBA1* and *ALBA4*, predominantly detected in sporophytic tissues, and *ALBA3* and *ALBA6*, with almost exclusive transcription in anthers. Detailed focus on both gametophytes showed the presence of all *ALBA* genes in bicellular pollen, although most of them are active in mature pollen. Only *ALBA1*, *ALBA4*, and *ALBA5* are active in ovules and developing seeds. All ALBA-GFP fusion variants were localized in dispersely in the bicellular pollen cytoplasm. In mature pollen, they created a reticular-like pattern with distinct foci, which are even more

pronounced upon HS treatments. Promoter activity is weakly affected by HS, though ALBA4-GFP and ALBA6-GFP quantification of signal accumulation detected significant changes. Moreover, colocalization of ALBA4-GFP with PABP3-RFP marker is very strong after the HS treatment. Nevertheless, ALBA6 colocalize with PABP3 and ALBA4 only partially.

Achieved results supported an initial hypothesis of the Alba family involvement in pollen development, particularly in later stages of pollen maturation. Moreover, the ALBA protein aggregation in mature pollen was connected with the response to heat treatment. Overall, achieved data further correspond with previous publications about ALBA proteins.

My major contribution to this publication consisted of experimental design and realization, including data processing (except for RNA sequencing), draft writing, and formation. My partial participation was further connected with phylogeny tree creation, R statistics calculation, accumulation analysis, and PCC calculations.

Original research article including all Supplements is a constituent part of this thesis in the form of the Supplementary PDF file; Supplementary_S1 (original research article), Supplementary_S2 (Supplementary Figures and Tables), Table S1 – S4.

4.3. Connection of ALBA proteins with a role in RBPs

4.3.1. ALBA-GFP proteins colocalization with PABP3-RFP marker

The colocalization analysis continued and expanded the published pairs ALBA4 and PABP3, as well as ALBA6 and PABP3, a class I member of the PABP family (Belostotsky, 2003). Agrobacterium-mediated transformation of a *proPabp3:PABP3-RFP*-harbouring line by *proALBA1-6:ALBA1-6-GFP* constructs established the colocalization of ALBA-GFP and PABP3-RFP markers. First uniform and second segregating generations were used for imaging, as signal weakening or loss occurred in further offspring. The obtained transgenic plants were grown under standard conditions, as described in chapter 3.1, and the FP signal was detected in mature pollen grains stained with a DAPI solution.

Originally, all combinations of ALBA1-6-GFP and PABP3-RFP were intended to obtain. Nevertheless, this plan could not be fully achieved due to the lack of seeds carrying both fusion proteins in certain combinations. A signal localization pattern was observed in both channels, with no variation compared to pollen grains expressing single transgenic TUs (Figure 8). The signal emission of the marker PABP3-RFP is broadly distributed in the VC cytoplasm, with its characteristic pattern consisting of foci with variable signal intensity enriched in the MGU region (Náprstková et al., 2021). A similar pattern was observed in the ALBA-GFP localization analysis. GFP emission patterns of ALBA2, ALBA3, and ALBA5 are not affected and remain unmodified except for the ALBA1 and PABP3 combination, which completely lacks the characteristic subcellular signal distribution in mature pollen (data not shown).

Two colocalization lines with the brightest signals and similar signal distributions within the Rpp25-like subfamily were selected for extended imaging and further analysis (Náprstková et al., 2021). ALBA1-GFP, ALBA2-GFP, and ALBA5-GFP emit a low intensity signal, which is more dissimilar to the PABP3-RFP distribution. For these reasons, the samples of PABP3 and ALBA with very weak GFP emission were not used for advanced examination. Three *ALBA* genes exhibited stable localization patterns when colocalized with the PABP3-RFP marker. In the ALBA2 sample, the channel´s projection uncovered at least partial overlap (Figure 8A). Pattern, which is located in the cytoplasm, is irregularly accumulated in VC and even more pronounced around MGU. The characteristics of signal fluctuations are more dissimilar. Both channels are overlapped only in bright foci of the VC cytoplasm as well as aligned with VC nuclei (Figure 8A, Merge + DAPI).

In contrast, ALBA3-GFP emits a strong signal in pollen grains comparable with the red signal of PABP3-RFP (Figure 8B). Both detected signal intensities and cytoplasmic distributions are quite similar, but the merge displays a portion of single-channel foci. There are partially overlapped foci

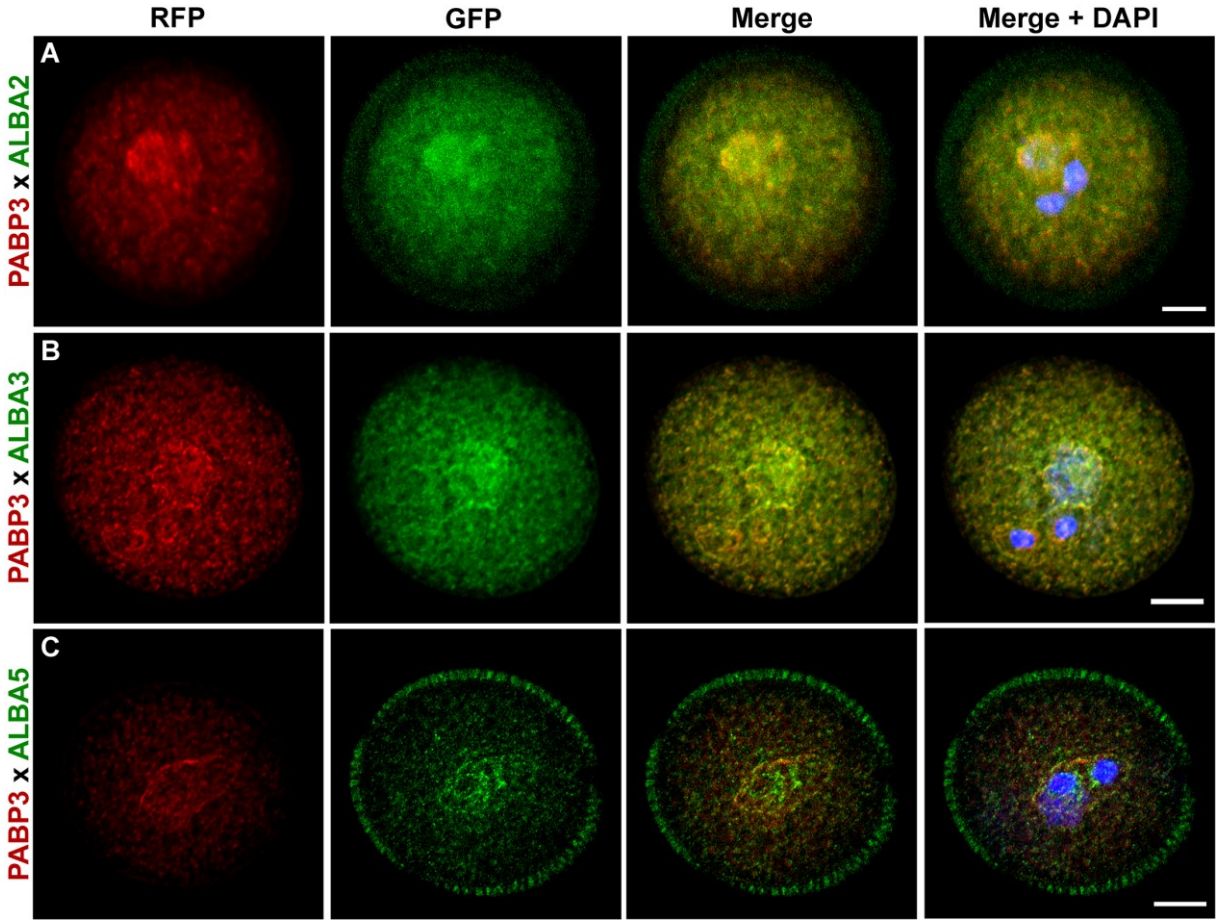

Figure 8: Subcellular colocalization of ALBA1, 2, 6 with PABP3 marker. Genomic DNA fragments of *ALBA2*, *ALBA3*, and *ALBA5* were C-terminally fused with GFP (ALBA) in the green channel, driven by their native promoters, respectively. Mature pollen coexpressing ALBA fusion proteins and PABP3-RFP marker (red) was harvested and stained with DAPI (Merge + DAPI). Imaging was performed in the same manner, except for 561 and 488 LPs, with scale bars set at 5 µm.

in the VC cytoplasm, possible SC membranes, and even more superimposed with the VC nuclei border (Figure 8B, Merge + DAPI). In the last combination of ALBA5-GFP and PABP3-RFP, the visualized signals co-occur very weakly in the VC cytoplasm, which could be influenced by differences in both signal intensities, despite the localization pattern appearing to be quite similar (Figure 8C). Nevertheless, there is a visible partial overlap of the channels in bright foci surrounding possible SC plasma membranes that is even more enhanced in areas where these round particles are accumulated (Figure 8C, Merge + DAPI). A very similar overlay is detected in the possible SC membrane region in the aligned pattern of gathered patches. Although the colocalization and accumulation analyses revealed strong overlap of PABP3-RFP and ALBA4-GFP in the VC nucleus, the data vary between ALBA members, with partial signal overlap between PABP3-RFP and ALBA6-GFP. The results of PABP3-RFP colocalization with ALBA5-GFP and two members of the Rpp20-like subfamily, ALBA2 and ALBA3, were not sufficient for further analysis. Therefore, the connection of ALBA

with PABP3-containing particles is not permanent, suggesting their involvement in multiple cellular processes.

4.3.2. ALBA-GFP proteins colocalization with PABP5-RFP marker

Another marker from the PABP class I, PABP5 specifically expressed in developing floral organs; tapetum, pollen, ovules and seeds, was selected for further colocalization assay (Belostotsky, 2003). Therefore, plants harbouring *proPabp5:PABP5-RFP* transgene were transformed by Agrobacterium with *proAlba1-6:ALBA1-6-GFP* constructs. Transgenic plants were grown under standard conditions, as described in chapter 3.1. Signal detection was performed on pollen stained with DAPI in the first uniform and second segregating generations to assess signal weakening or loss in the next generation.

A colocalization experiment was set up for PABP5-RFP and ALBA-GFP harboring pollen grains. Although checked signals were of good quality, only some combinations were obtained in the progeny. Therefore, only samples that were positive for the presence of both channels in mature pollen are shown: two members of the Rpp20-like family (ALBA1 and ALBA2), and ALBA6 from the Rpp25-like subfamily. The detected signal pattern was comparable to that reported in the research article (Náprstková et al., 2021) and remained stable between solo TU-harboring and ALBA coexpressing plants. However, in all presented combinations, the signal intensity pattern was at least minimally altered (Figure 9). The colocalization of ALBA1-GFP with PABP5-RFP was influenced by a low intensity of the GFP signal, which made the final result more challenging. Nevertheless, the captured pattern persists, distributed randomly in the VC cytoplasm. The signal enrichment aligned with the nucleus almost completely disappears, as well as the significant pattern attached to SC nuclei (Figure 9A). A co-occurrence of the PABP5-RFP and ALBA1-GFP was detected in a few foci surrounding SC nuclei, where the red signal is most prominent, indicated by an arrow (Figure 9A, Merge + DAPI).

Interestingly, ALBA2-GFP localization pattern changes in the presence of PABP5-RFP marker (Figure 9B). While ALBA2-GFP characteristic cytoplasmic signal distribution, including nuclear shape alignment, is almost lost in VC, there is an enriched signal in SC. The strongest signal is clearly visible, divided into two parts, most likely localized in the SC cytoplasm, which could cause its loss at the possible SC membranes. The green and red channels overlay revealed their co-occurrence in parts of the pattern, with the brightest foci localized in SCs (Figure 9B, Merge). Specifically, the tightly overlapping regions surrounding SC nuclei accumulated to form irregular shapes, as indicated by the arrows (Figure 9B, Merge + DAPI). An analogous result was achieved for the last obtained combination coexpressing *proPabp5:PABP5-RFP* and *proAlba6:ALBA6-GFP*. The detected signal pattern alters in the cytoplasm and around the VC nucleus in the green channel. Although the ALBA-GFP cytoplasmic signal is one of the strongest in the Alba family (Figure 9C), PABP5-RFP

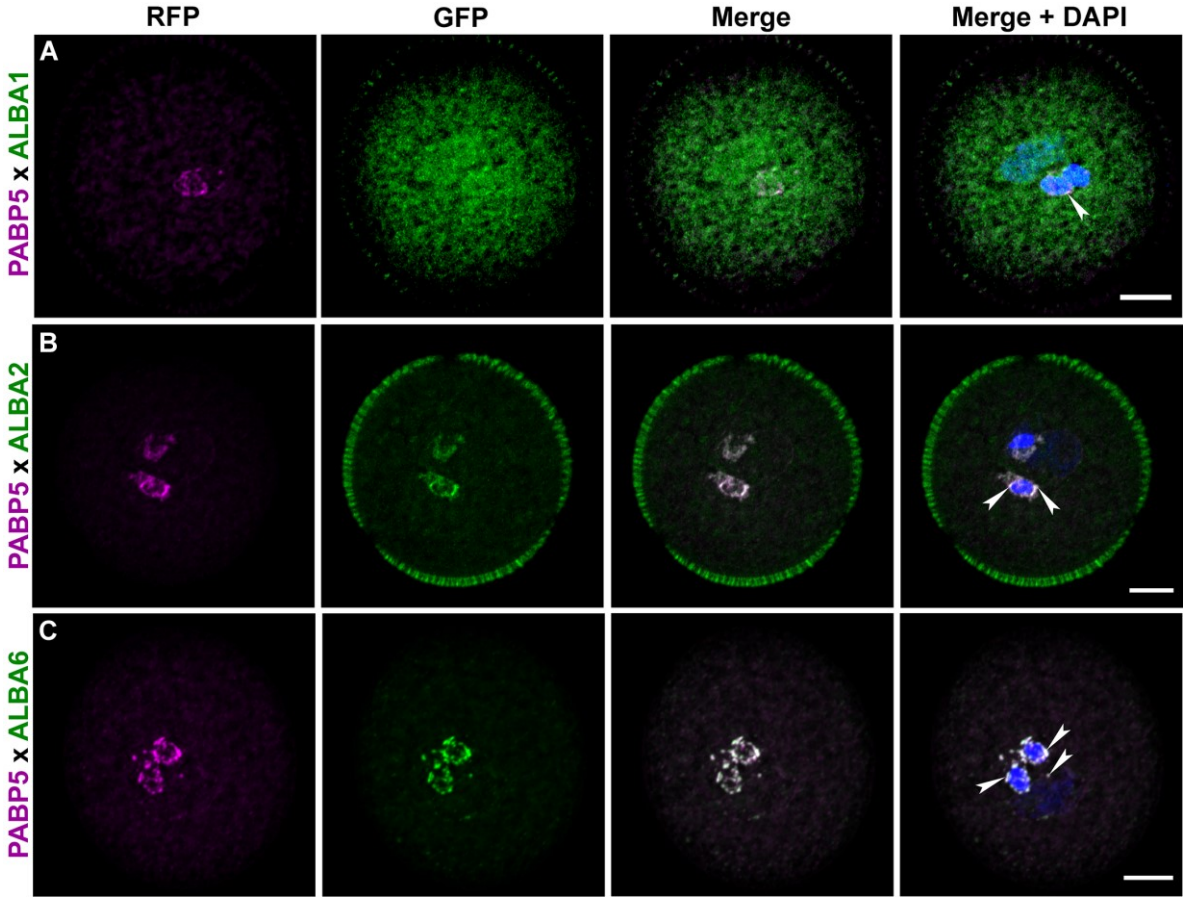

Figure 9: Subcellular colocalization of ALBA1-GFP, ALBA2-GFP, and ALBA6-GFP with PABP5-RFP marker. Genomic DNA fragments of *ALBA1*, *ALBA2*, and *ALBA6* cDNA isolated from mature pollen were C-terminally fused with *GFP* (green) controlled by their native promoters, respectively. Pollen grains from stable transgenic plants coexpressing *proALBA:ALBA-GFP* with *proPabp5:PABP5-RFP* marker (magenta) were harvested and stained in DAPI (Merge + DAPI). Imaging was performed the same way except for 561 and 488 LPs, post-processing included Airyscan processing followed by z-stack range selection covering all nuclei, maximum intensity projection and scale bar (5 µm).

coexpression decreases its intensity. It enhances the accumulation in SCs the same way as described in ALBA2 on the PABP5 background. Merged channels reveal signal co-occurrence in the VC cytoplasm only in most intensive foci (Figure 9C, Merge). Signal fluctuations are detectable in MGU, characterized by a few stronger aggregates aligned with VC nuclei (arrow, Figure 9C, Merge + DAPI). Both channels are enriched around SC nuclei, with almost complete overlay, likely due to recruited accumulation, as indicated. Colocalization with PABP5-RFP, which marked specific mRNA aggregations, revealed a similar localization to ALBA2-GFP and ALBA6-GFP, with variable signal intensities within the pattern. The most pronounced RFP signal, which tightly surrounds SC nuclei, predominantly overlaps with GFP emission, suggesting that the observed proteins cooperate in this area.

4.3.3. ALBA-GFP colocalization with RNAse P subunit GAF1

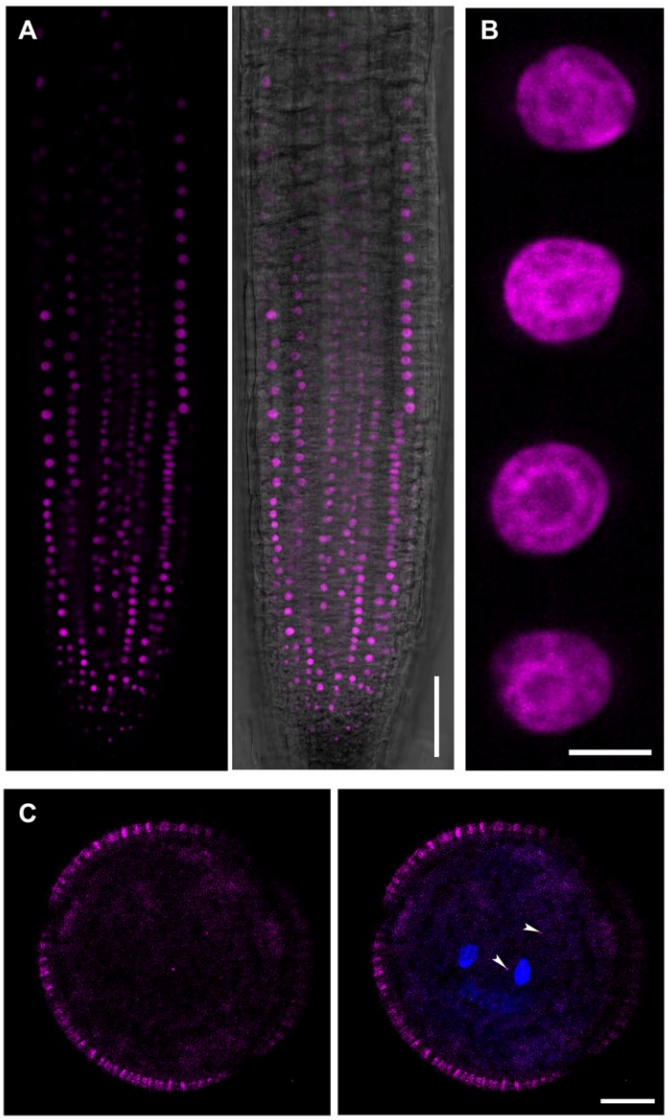

Figure 10: Subcellular localization of GAF1-mCherry marker. The genomic sequence of *GAF1* was C-terminally fused with mCherry under native promoter control and terminated by *nosT*. Specific emission in the red channel was detected in a root tip (**A**). A detail of four cells revealed a round pattern in the nuclei, with a signal-enriched surrounding area, possibly nucleoli, and bright areas lining the outer shape (**B**). Mature pollen was harvested and stained in DAPI solution (**C**). The signal was captured in weak cytoplasmic foci. Nuclei position is indicated by DAPI (blue) in the channels overlay (Merge). Z-stacks from both channels (**B, C**) were processed using Airyscan processing followed by maximum intensity projection. White arrows indicate the specific mCherry signal. Scale bar = 50 µm (**A**), 5 µm (**B, C**).

ALBA proteins are associated with various roles in nuclear processes across multiple organisms. Therefore, GAF1/RPP30 was picked for colocalization with ALBA proteins, also for a similar expression pattern in Arabidopsis developmental stages, especially in young seedling root tips and later in mature pollen. Initially, a novel marker, *proGAF1:GAF1-mCherry::nosT*, was created and localized in root tips and mature pollen on a wild-type Col-0 background (Figure 10). According to a previous study (Wang et al., 2012), *GAF1* activity was detected in root tips, lateral root primordia, shoot meristematic zones, ovules, and pollen by GUS staining. A screen of the transformed seedlings revealed strong signal emission in all layers of root tip cells, especially in the root meristematic and transition zones, with a specific subcellular localization pattern (Figure 10A). According to the morphology, position, and the publication, the marked structures are considered cell nuclei (Figure 10B) Nevertheless, localization of GAF1-mCherry signal in mature pollen changes to cytoplasmic foci that

were difficult to capture (Figure 10C, right). The signal emission was very weak and could only be detected by the inverted confocal microscope (Zeiss LSM880, equipped with an Airyscan detector). Captured signal was sequestered into a few weak cytoplasmic foci usually concentrated around MGU (visualized by DAPI), indicated by arrows.

Coexpression of ALBA-GFP proteins with the introduced GAF1-mCherry marker was established. Marker transgene *proGAF1:GAF1-mCherry* was introduced to plants expressing *proALBA1-6:ALBA1-6-GFP* by Agrobacterium-mediated transformation. Grown plants of the first generation were used for this experiment to ensure sufficient signal detection in the green channel. Most studied pairs, GAF1 × ALBA1, GAF1 × ALBA2, GAF1 × ALBA3, GAF1 × ALBA4, and GAF1 × ALBA5 were colocalized in mature pollen (Figure 11). Present results show transgenic pollen containing GAF1-mCherry (magenta) and ALBA-GFP (green). The experiment is concluded by a picture of control wild-type Col-0 pollen (Figure 11F), which emits a weak autofluorescence in the red channel without distinct foci. The control sample was imaged with the same setup that supports the following experiment. Localization patterns of ALBA1-GFP, ALBA3-GFP, and ALBA5-GFP signal distribution are comparable to their sole appearance characteristic by their reticular-like cytoplasmic pattern with bright foci in VC, accompanied by the typical enrichment around MGU (Figure 11A, 11C, 11E). Nevertheless, the typical native signal enrichment around MGU was completely lost in ALBA2-GFP and ALBA4-GFP samples, and only the cytoplasmic distribution persisted. These signal localizations more closely resemble the pattern of pollen 24 hours after a 42 °C, 1-hour stress period (Figure 11B and D). The GAF1-mCherry signal in the studied colocalization samples is characteristically sequestrated to a low number of miniature foci surrounding MGU, particularly VC nuclei.

The channels overlay revealed different patterns without any overlap in mature pollen. Diverged patterns of ALBA emission signal and GAF1 marker suggest distinct roles of inspected fusion proteins. According to the obtained data, the ALBA-GFP connection to GAF1/RPP30, RNAse P/MRP subunit in Arabidopsis, remains elusive. Though selected colocalization pairs resemble similar expression patterns in metabolically active tissues, the obtained localization patterns are divergent. The GAF1-mCherry localization in root tips is restricted to the nuclei, while the ALBA pattern is typically distributed in the cytoplasm in all studied cell types (Náprstková et al., 2021; Tong et al., 2022), which supports the achieved results and reduces the plausibility of common features.

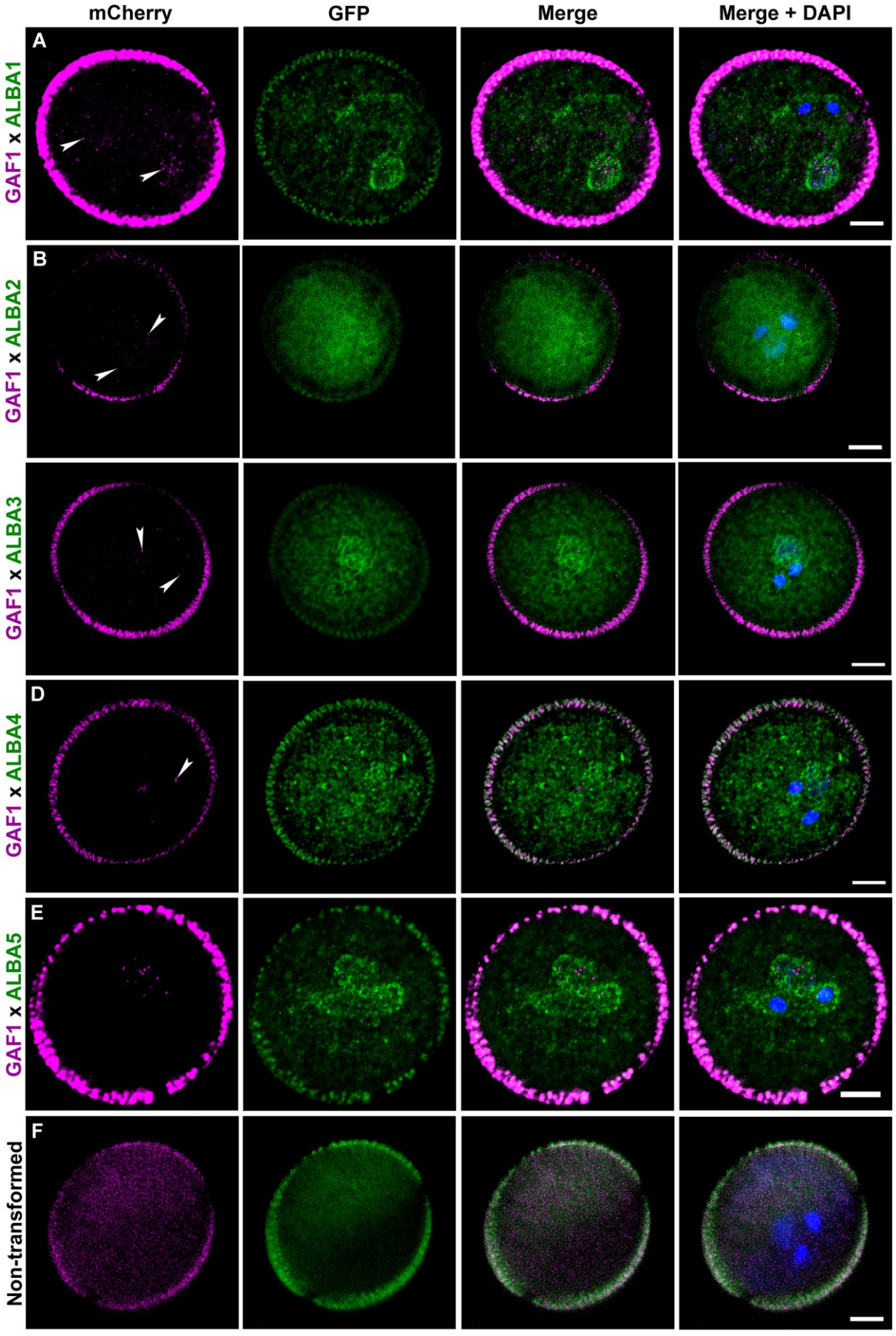
mCherry
GFP
Merge
Merge + DAPI
A
GAF1 x ALBA1
B
GAF1 x ALBA2
GAF1 x ALBA3
D
GAF1 x ALBA4
E
GAF1 x ALBA5
F
Non-transformed

Figure 11: Subcellular colocalization of ALBA1-6-GFP and GAF1 marker in mature pollen. Genomic DNA fragments of *GAF1, ALBA1-5*, and *ALBA6* cDNA isolated from mature pollen were C-terminally fused with *GFP* (*ALBA*) and *mCherry* (*GAF1*). All TUs were controlled by native promoters and terminated by the *nosT* terminator. Mature pollen from transgenic plants was harvested and stained in DAPI solution. Colocalization patterns of ALBA-GFP (green) and GAF1-mCherry (magenta) were captured and the overlay is shown (Merge). Nuclei positions are indicated by DAPI (blue) in the three channels overlay (Merge + DAPI). All samples were imaged identically, except for the 561 and 488 LPs. Z-stacks from all channels were calculated using Airyscan processing followed by maximum intensity projection. Scale bar = 5 μm.

4.3.4. Colocalization of Alba subfamilies in mature pollen

The last analysis extends published data based on the colocalization of ALBA4-mCherry and ALBA6-YFP in mature pollen. These experiments were based on the coexpression of ALBA pairs within individual subfamilies Rpp20-like (ALBA1-mCherry and ALBA2-YFP, ALBA2-mCherry and ALBA3-YFP, ALBA3-mCherry and ALBA1-YFP) and Rpp25-like (ALBA4-mCherry and ALBA5-YFP, ALBA6-mCherry and ALBA5-YFP) according to chapter 3.7.2. Formed TUs were combined in a destination vector and introduced into the wild-type Col-0 plants by Agrobacterium-mediated transformation. Transgenic plants were prepared according to chapter 3.1, and the first uniform and second segregating generations were used for imaging, as signal weakening or loss was observed in subsequent progeny.

ALBA-ALBA colocalization analysis was performed within Rpp20-like and Rpp25-like subfamilies according to their similar behavior (Yuan et al., 2019; Náprstková et al., 2021; Tong et al., 2022). The order of TUs within vector was based on fluorescent tag characteristics (ALBA-mCherry followed by ALBA-YFP). Actually, ALBA proteins colocalization in mature pollen influenced localization patterns of some members (Figure 12) compared to the previously published results acquired from GFP fusions (Náprstková et al., 2021). Native distribution of the signal was detected in the pollen cytoplasm of *proALBA1:ALBA1-mCherry/YFP*, *proALBA2:ALBA2-YFP*, *proALBA3:ALBA3-mCherry*, *proALBA4:ALBA4-mCherry,* and *proALBA6:ALBA6-mCherry*-harboring samples. However, altered signal patterns were recorded in *proALBA2:ALBA2-mCherry* and *proALBA3:ALBA3-YFP* coexpressing pollen grains. Interestingly, *proALBA5:ALBA5-YFP*-harboring samples exposed both native and altered signal patterns according to the colocalizing partner. Moreover, the alternative signal distributions are more similar to the respective HS patterns.

The first captured combination of ALBA1-mCherry and ALBA2-YFP revealed almost identical signal distributions compared to the native patterns (Figure 12A, mCherry, YFP). Moreover, ALBA1 and ALBA2 colocalization revealed marginal signal overlap in the whole pollen volume, especially

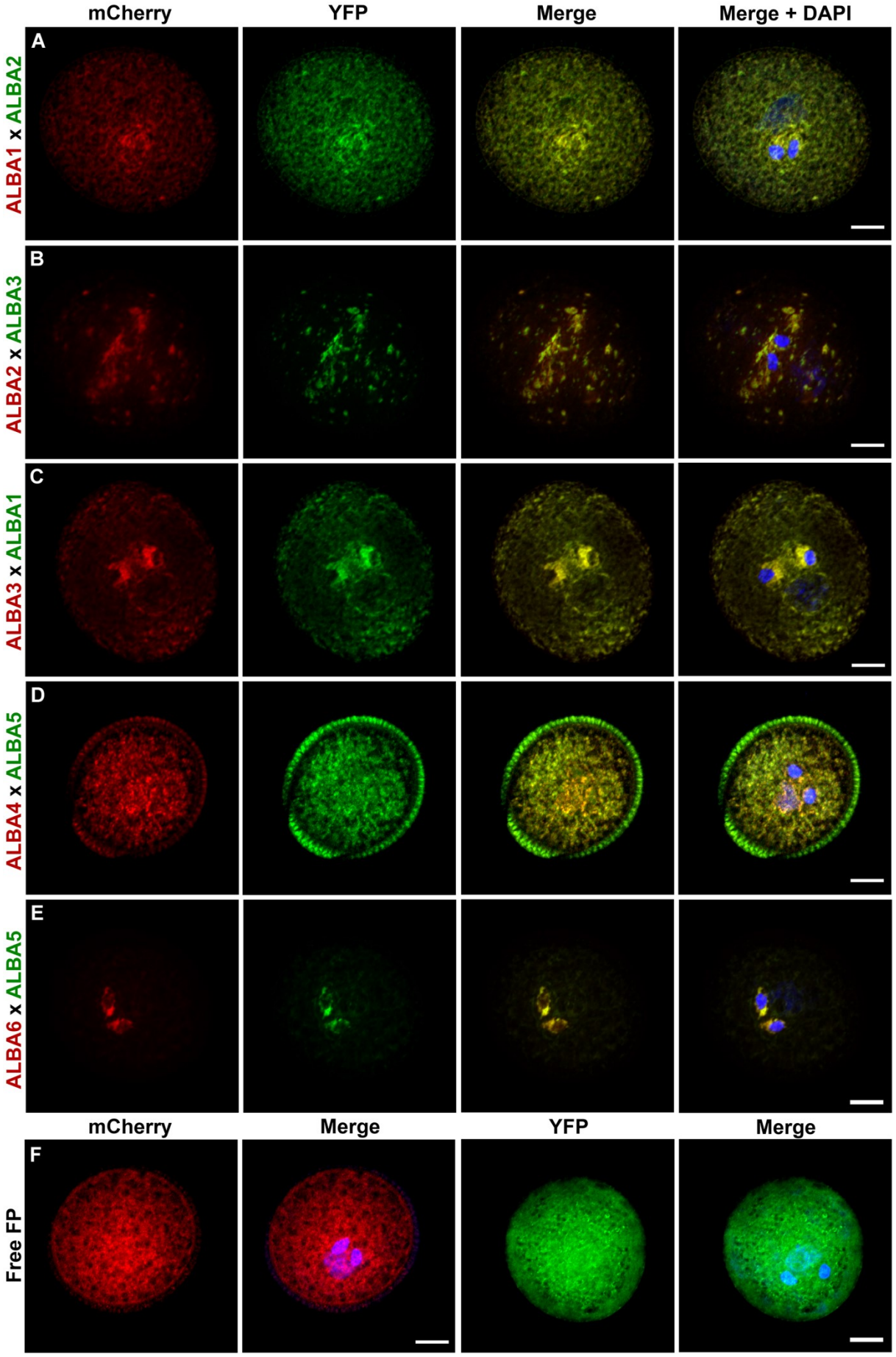
mCherry
YFP
Merge
Merge + DAPI
A
ALBA1 x ALBA2
B
ALBA2 x ALBA3
C
ALBA3 x ALBA1
D
ALBA4 x ALBA5
E
ALBA6 x ALBA5
mCherry
Merge
YFP
Merge
F
Free FP

Figure 12: Subcellular colocalization of Rpp20-like and Rpp25-like subfamily members in transgenic mature pollen grains. Genomic DNA fragments of the Rpp20-like subfamily (*ALBA1*, *ALBA2*, and *ALBA3*) and Rpp25-like subfamily (*ALBA4*, *ALBA5*) and cDNA encoding the pollen-isolated isoform of *ALBA6-4* were C-terminally fused with mCherry (red) or YFP (green). The TUs were controlled by their respective native promoters and terminated by the *nosT*. Both channels overlay indicates FP-emitted signal colocalization (Merge). Next, FPs' coding regions were expressed under the pollen-specific promoter *LAT52*, with mCherry (red) and YFP (green) serving as controls for fused protein localization. Nuclei position and morphology are indicated by DAPI staining (Merge + DAPI). Imaging was performed in the same manner, except for 561 and 488 LPs, with scale bars set at 5 µm.

in cytoplasmic foci accompanied by increased signals' co-occurrence in areas with higher intensities surrounding SC nuclei (Figure 12A, Merge + DAPI). The next analyzed pair of ALBA2-mCherry and ALBA3-YFP revealed alternative localization patterns in both channels that are more similar to the stress-induced distribution in both channels (Figure 12B, mCherry, YFP). Nevertheless, minimal alteration within signal patterns is demonstrated by the red signal's unspecific low intensity distribution, despite the green signal targeting enlarged foci of irregular shapes. Although the samples did not match the single-gene expression distribution, the overlap of the channels is prominent not only in the characteristic SC nuclei and proximal structures, but also in the vegetative cell cytoplasm. However, there are detectable solely green foci (Figure 12B, Merge + DAPI). The last analyzed pair of Rpp20-like subfamily members is ALBA3-mCherry and ALBA1-YFP, with localization patterns similar to the normal GFP signal distribution in mature pollen (Figure 12C, mCherry, YFP). The signal patterns marginally overlap in the VC cytoplasm. Both signals even more colocalize in the enlarged, irregular structures that tightly surround a considerable part of SC nuclei and a thin layer around the VC nucleus (Figure 12C, Merge + DAPI).

Colocalization of Rpp25-like subfamily members was initiated by fusion proteins ALBA4-mCherry and ALBA5-YFP, which coexpressed with similar signal patterns to those of the single-expressed TUs (Figure 12D). The ALBA4-mCherry signal pattern is enriched within MGU, roughly visible in red, while ALBA5-YFP signal intensity distribution is more pronounced exclusively around VC nuclei. The signal patterns partially overlap in the VC cytoplasm, with more prominent green signal intensity, which contrasts with the red channel's MGU-enriched areas. Unexpectedly, the last investigated pair of *ALBA* genes emitted a native pattern in the red channel and altered green signal distribution, compared to native samples. ALBA6-mCherry and ALBA5-YFP detected signals were significantly enriched in SCs (Figure 12E). Within these areas, both channels overlap massively, although they are reduced in the VC cytoplasm. On the contrary, the ALBA5-YFP signal in the green channel is visible at the border of MGU, aligned with the VC nucleus and possible membranes of SCs (Figure 12E, Merge + DAPI). The experiment was accompanied by a single localization of free fluorescent proteins used for

visualization of the targeted proteins, free mCherry, and free YFP (Figure 12F). The emission signal was detected in the cytoplasm and nuclei of both combinations, although the data show non-homogeneous signal distribution in the pollen grains.

Collectively, the coexpression and visualization of ALBA proteins within subfamilies revealed variable behavior, as observed in previous chapters. The ALBA1-ALBA2 and ALBA1-ALBA3 colocalizations were detected in the cytoplasm of VC, accompanied by enriched signal accumulations around SC nuclei. Although the localization patterns of ALBA2-mCherry and ALBA3-YFP samples displayed artificial, pronounced signal accumulation, these areas are marginally shared. Colocalization of ALBA4-mCherry and ALBA5-YFP corresponds to the pattern of ALBA4-YFP and ALBA6-mCherry presented in the journal article (Náprstková et al., 2021). Strong signal accumulation of ALBA6-mCherry in SCs is the same in both samples. However, the localization pattern of ALBA5-YFP varies according to the coexpressed partner; its characteristic distribution is maintained in combination with ALBA4-mCherry, but unusual SCs' ALBA5-YFP accumulation was detected when combined with ALBA6-mCherry. Finally, two distinct populations of results were identified within the experiment. Major samples revealed native localization, creating partially shared patterns. Nevertheless, distinct areas without signal overlay indicate variability and probable promiscuity within studied pairs. On the contrary, samples with an affected localization of the studied homologs predominantly display signal overlay, suggesting a stronger relation between the respective pairs, ALBA2-ALBA3, and ALBA5-ALBA6.

4.4. Targeted overexpression of *ALBA* genes in *Arabidopsis thaliana*

4.4.1. Overexpression of ALBA-GFP in the male germ line

Specific overexpression of *ALBA* genes in the male gametophyte, particularly in the GC and its mitotic products, was induced by the specific activity of the *DUO1* promoter. The promoter sequence was domesticated from the Arabidopsis genome for this experiment. Sample TUs *proDUO1::ALBA-GFP::nosT* and a control TU *proDUO1::GUS-GFP::nosT* were formed by the *proDUO1* sequence followed by genomic sequences of *ALBA* genes fused with GFP. Created TUs were inserted into the destination vector and further imported into the wild-type Arabidopsis plants. Transformed seeds were harvested, germinated, and cultivated under standard conditions until the reproductive stage of development, as described in chapter 3.7.3. Observation and imaging were accomplished using first- and second-generation transformed plants to detect signal loss in the following generation. Pollen was harvested and stained with DAPI for nuclei detection.

Initially, control samples were observed to ensure the precise adjustment of the microscopic setup. Therefore, pollen from the positive control, which harboured *proDUO1::GUS-GFP::nosT*, and the negative control, untransformed wild-type Col-0, were imaged (Figure 13). A strong signal of the GUS-GFP marker was detected in SCs concentrated predominantly in bright foci randomly distributed in the cytoplasm (Figure 13A, GFP). The non-specific accumulations of the signal are most likely caused by a GFP fusion with GUS, which creates a larger protein that is unable to freely diffuse to the nucleus (Figure 13A, Merge). The next imaged sample presented a negative control, non-transformed wild-type Col-0, which completely lacked a specific green signal (Figure 13B). Collectively, selected controls enabled precise microscope adjustment before the experimental procedure with the investigated samples.

A strong signal was detected in all pollen grains carrying *proDUO1::ALBA-GFP::nosT* expression cassette exclusively localized to the possible SCs cytoplasm (Figure 14). Unspecific structures of various shapes and sizes were observed around SC nuclei in the green channel and all three nuclei in the blue channel. Interestingly, the detection of DAPI signal revealed changes in SC chromatin organization, as presented by nuclear shape irregularities in most samples. According to these characteristics, the samples were divided into three classes: samples containing typical, marginally oval-shaped nuclei in SCs, samples containing nuclei with a curved outer surface, and samples having SC nuclei with long protrusions stained by DAPI. The only sample with an unaffected SC nucleus structure, *proDUO1::ALBA2-GFP*, emitted a signal localized to cytoplasmic foci that accumulated around the SC nuclei (Figure 14B). The signal was completely lost from the cytoplasm and SC membranes. Two samples, *proDUO1::ALBA1-GFP* and *proDUO1::ALBA4-GFP*, shared a predominant number of SC nuclei with mild shape variations, typically harbouring few chromatin

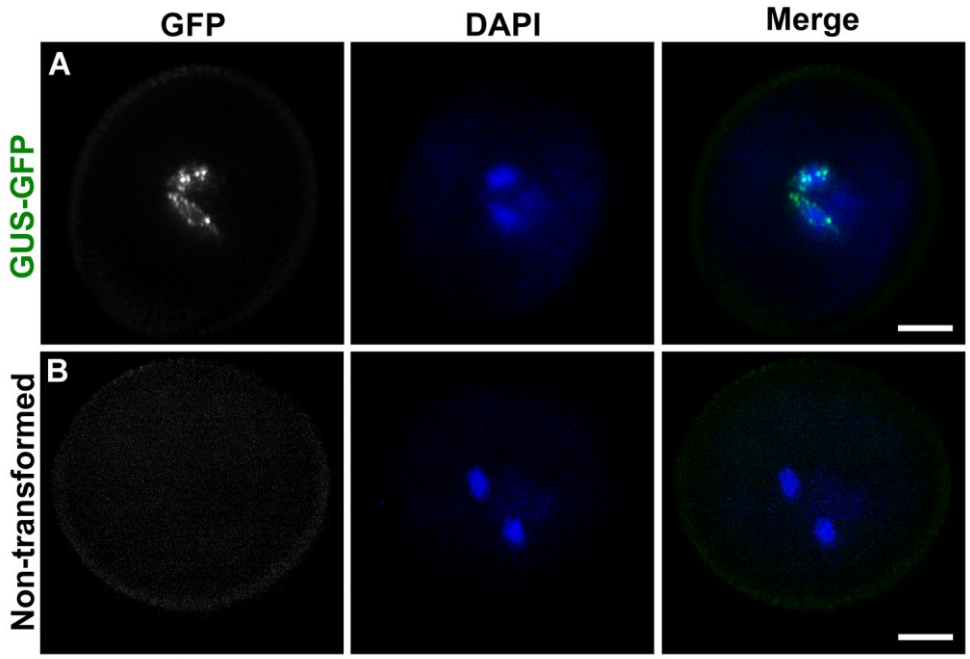

Figure 13: Signal detection in transgenic *proDUO1::GUS-GFP* and Col-0 pollen. Control plants harboring *proDUO1::GUS-GFP::nosT* transgene (GUS-GFP) and wild-type Col-0 (Non-transformed) were cultivated up to the flowering stage. Open flowers were collected, and mature pollen was stained in a DAPI solution. Prepared samples were captured in green (GFP column) and blue (DAPI column) channels. Overlapped channels (Merge) were created by post-processing. Imaging was performed in the same manner, with scale bars equal to 5 µm.

lobes and changing nuclear surface (Figure 14A, 14D). Interestingly, all DAPI-stained excessive curvatures were completely covered by the signal emitted in the green channel, indicated by arrows. These foci were further distributed among the SC cytoplasm. In *proDUO1::ALBA5-GFP* and *proDUO1::ALBA6-GFP* samples, the last class of SC nuclei showed phenotypic variation with a few long chromatin protrusions. Moreover, *proDUO1::ALBA3-GFP*-harboring pollen grains contained SC nuclei of a completely hairy surface (Figure 14C, 14E, 14F). All chromatin prominences are completely covered by the specific green fluorescence indicated by arrows. These atypical aggregations could cause almost complete signal loss in the cytoplasm.

According to the acquired results, the specific overexpressionn of *ALBA* genes in SC apparently changes their typical localization pattern. Their localization is sequestrated to a tight proximity of nuclear chromatin. Their signal diminishes from the cytoplasm and SC plasma membrane. Moreover, overexpression of several members presumably influences nuclear architecture. According to these data, some members may be involved in nuclear shape regulation, particularly in processes that influence chromatin compaction. Although the nuclear defect is specific to SC overexpression, the precise regulation of *ALBA* genes appears to be crucial for maintaining the three-dimensional structure of SC nuclei. While VC transcriptome and proteome profiles correspond more to the sporophytic

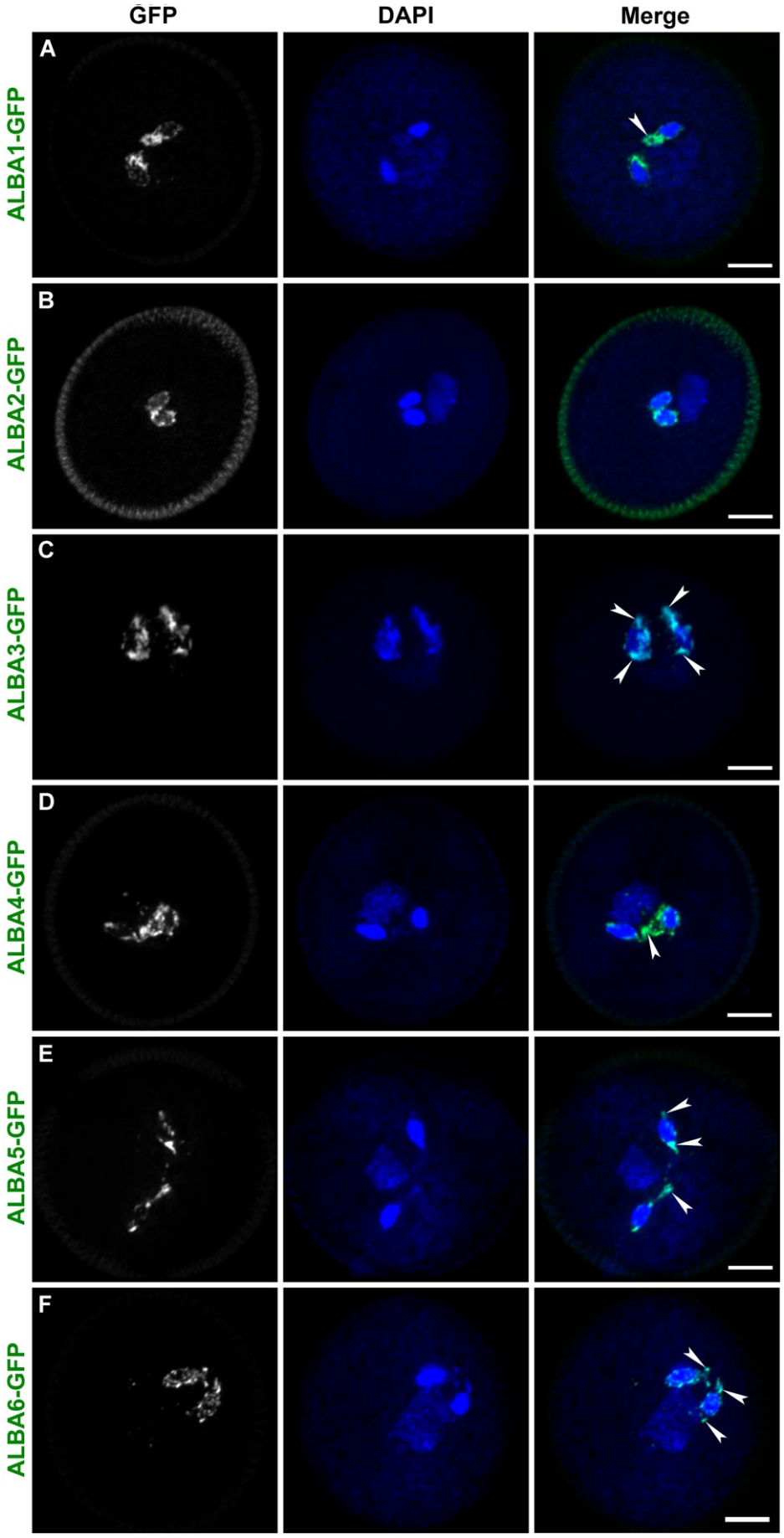
GFP
DAPI
Merge
A
ALBA1-GFP
B
ALBA2-GFP
C
ALBA3-GFP
D
ALBA4-GFP
E
ALBA5-GFP
F
ALBA6-GFP

Figure 14: Subcellular localization of ALBA-GFP controlled by the GC-specific promoter *DUO1* in mature pollen. *ALBA1-5* coding regions and cDNA encoding the pollen-expressed isoform of *ALBA6-4* were C-terminally fused in frame with *GFP* and expressed in mature pollen under *DUO1* promoter control (GFP column). Collected pollen was stained in DAPI solution for nuclei visualization (DAPI column), and the channels were overlapped in post-processing (Merge column). Sample imaging was performed in the same way; scale bars = 5 μm.

tissues than to the specific SC transcription. The role of ALBA proteins may vary in pollen grains based on the cell type, which could explain the differences in ALBA localization in SCs under their native promoters and overexpression caused by *the DUO1* promoter, accompanied by detectable subcellular changes. Nevertheless, the fertility of the transgenic plants, neither the length of siliques nor the number of seeds within siliques, was not affected.

4.4.2. Overexpression of *ALBA-YFP* in the pollen VC

Excessive overexpression of *ALBA* genes in the male gametophyte was targeted explicitly to VC by the broadly used *LAT52* promoter. TUs containing *proLAT52::ALBA-YFP::nosT* were created by fusing the *proLAT52* sequence and genomic sequences of *ALBA* genes with *YFP*, as described in chapter 3.7.4. Obtained TUs were cloned into a destination vector and inserted to wild-type Col-0 plants, which were cultivated at standard conditions until maturation. Pollen was collected from adult individuals of uniform and segregating generations and stained with a DAPI solution.

Although it was expected to have a pronounced signal intensity of the native pattern in VC, the overexpression of the Alba family caused a surprising variation. The *LAT52* promoter is used for pollen-targeted assays, as its activity is considered exclusive for the VC of mature pollen, although it was later also found in SCs. Native ALBA signal distribution in pollen has been demonstrated (Náprstková et al. 2021), and the described pattern is remarkably distinct from the predominant number of *proLAT52*-induced lines. A yellow fluorescent signal accumulates to form enormous particles localized in mature pollen (Figure 15A, 15B, 15C, 15D, 15E). Moreover, the compact structure of MGU was dislocated by SCs' deviation from the central position in a portion of screened pollen grains (data not shown). Sample control of free YFP localization in mature pollen is shown in chapter 4.3.4.

All Rpp20-like and Rpp25-like subfamily members emitted signal was distributed in bright foci accompanied by larger aggregation in distinct elongated cytoplasmic aggregates of irregular shapes (Figure 15A, 15B, 15C, 15D, 15E). Moreover, this highlighted pattern included one or two enormous abnormal structures of various shapes and sizes, and a trace of inner structures. Interestingly, these patterns completely lack typical nuclei-enriched areas and a reticular-like distribution in the VC

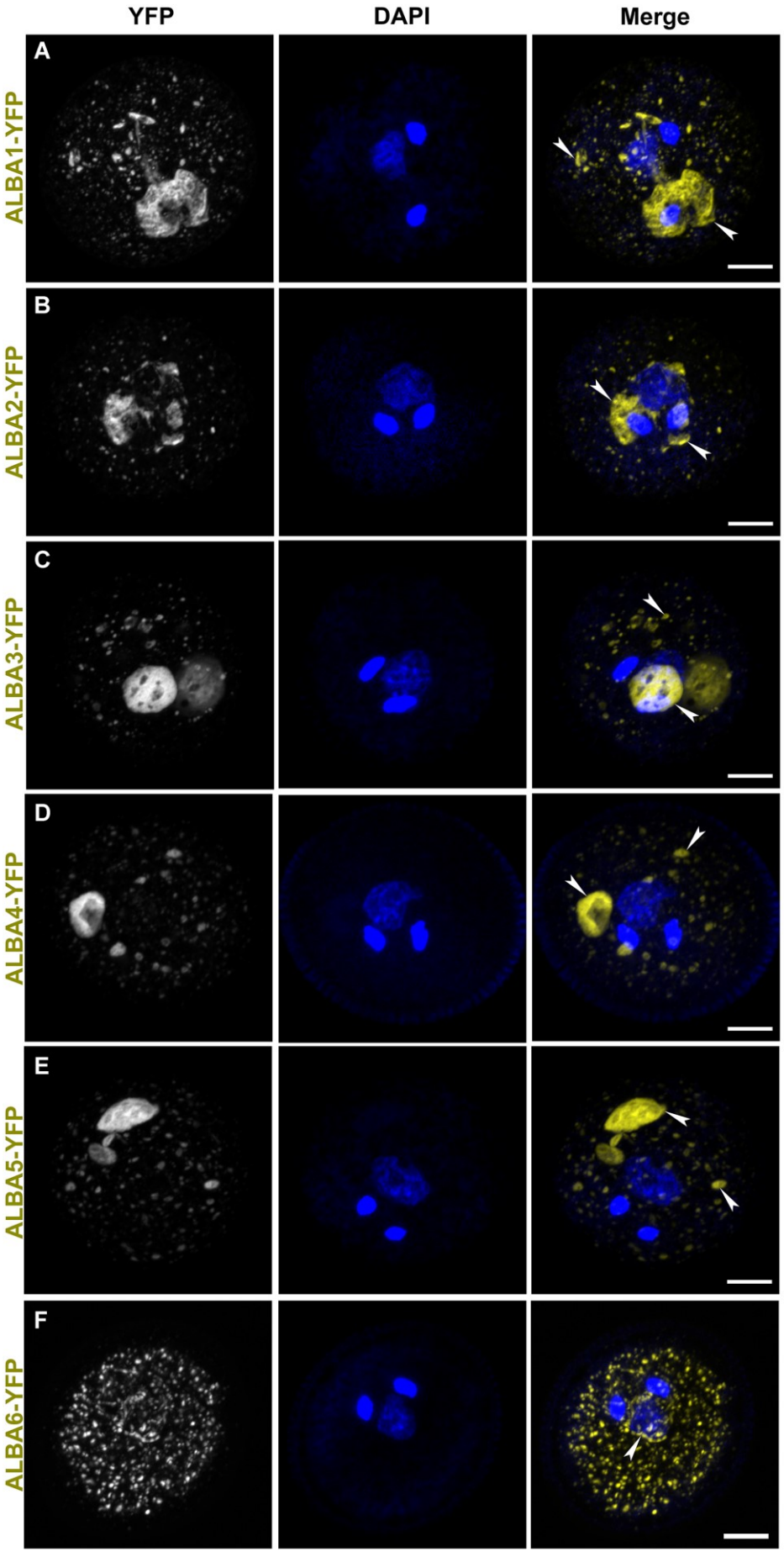
YFP
DAPI
Merge
A
ALBA1-YFP
B
ALBA2-YFP
C
ALBA3-YFP
D
ALBA4-YFP
E
ALBA5-YFP
F
ALBA6-YFP

Figure 15: Subcellular localization of ALBA-YFP under *LAT52* promoter control with specific activity in mature pollen. *ALBA1-5* coding regions and cDNA encoding the pollen-expressed isoform of *ALBA6-4* were C-terminally fused in frame with *YFP* and expressed in pollen under *LAT52* promoter control (YFP column). Collected pollen was stained in DAPI solution for nuclei visualization (DAPI column). Z-stacks were processed using maximum intensity projection, and channels were overlapped in post-processing (Merge column). Samples were imaged in the same manner, except for the 488 LP, where scale bars represent 5 µm.

cytoplasm. In *proLAT52::ALBA6-YFP*-expressing pollen grains, a unique ALBA-like localization pattern was detected. The recorded distribution character was characterized by round granules-filled cytoplasm, enhanced by their accumulation aligned with VC nuclei, indicated by arrows (Figure 15F). The characteristic signal accumulation tracing of the SC plasma membrane is lost, which could be caused by the low or no presence of ALBA6-YFP in SCs.

Although the accumulations are unique to this experiment, there is no evidence of their function. However, they are likely stock aggregates of ALBA-YFP in enormous quantities. This experiment had a dramatic effect on the signal emission pattern, most likely caused by the overexpression of single ALBA proteins in the VC. The possible explanation for the abnormal localization pattern could be a cell response to the dose effect or a poisonous amount of the protein in the cytoplasm, resulting in the storage of fusion proteins in secluded granules. Though the massive amount of ALBA proteins in the cytoplasm is accumulated in cytoplasmic foci, their formation does not significantly affect the fertility of transgenic plants.

4.4.3. Characterization of Alba family overexpression in sporophyte

4.4.3.1. Identification of *ALBA* transcripts levels

The last experiment of *ALBA* gene overexpression included a broad spectrum of cell types, tissues, and organs throughout plant development. For the sporophytic overexpression, a novel viral *CsWMV* promoter was selected. Therefore, control TUs *proCsWMV::GFP::nosT* (*oexGFP*) and *proCsWMV::GUS-GFP::nosT (oexGUS-GFP)* were created for the description of promoter activity. Studied transgenic lines were created by forming *ALBA*-harbouring TUs through *proCsWMV::ALBA-GFP::nosT* (*oexALBA*) and inserting them into destination vectors. The obtained plasmids were introduced into wild-type Col-0 Arabidopsis plants using Agrobacterium-mediated transformation. Plants of the first uniform and second segregating generations were used for most of the experiments, especially imaging, phenotypic observations, and RNA sequencing.

First, 10-14-day-old transgenic seedlings were used for overexpression verification in sporophytic tissues. The transgene expression levels were measured to identify genuine excessive transcription

in the T2 generation, and the same experiment was later performed in subsequent generations and backcross (BC) lines. These measurements were realized by reverse transcription quantitative PCR (RT-qPCR) using gene-specific primers in a single BR and two TRs per line. Measured Ct values of *oexGFP, oexGUS-GFP, oexALBA4*, and *oexALBA5* expression were acquired by GoTaq Q-PCR and standardised to *GAPC1* level within samples. Expression levels of *oexALBA6* were measured by GoTaq 1-Step RT-qPCR and standardised to *EIF1a4.* Standardised ratios of *ALBA* genes standardised in *oexALBA* samples were further normalised to the wild-type Col-0 levels for visualization and easier understanding. A Col-0 value was set to 1, and all samples were related to this level. For control samples (*oexGFP* and *oexGUS-GF), f*our independent lines were tested, three of which were from the T2 segregating generation for better comparison with *ALBA* samples, and one sample was collected from the homozygous T5 generation (Figure 16A). The measurements revealed strong overexpression of *GFP*, highly exceeding the threshold value, with a 2.5-fold elevation above the set level. Moreover, these results correspond to microscopic observations of the samples, revealing intense emission of the fluorescent protein. Seven independent *oexALBA4* lines were selected for the expression level quantification in the segregating generation, characterized by the strongest green signal when present (Figure 15B, left). There was confirmed overexpression of *ALBA4* transcripts in three of the selected transgenic lines: *oexALBA4* Line 2, *oexALBA4* Line 6, and *oexALBA4* Line 7. Only the verified lines were used for further experiments, signal localization, phenotype analysis, and RNA sequencing.

Nevertheless, expression levels were measured the same way throughout generations to reveal the intensity of signal silencing. Therefore, seedlings of the following generations were harvested, processed, and measured in an independent experiment with a focus on variation within lines. Two lines, *oexALBA4* Line 2 and *oexALBA4* Line 7, were selected for this experiment. Transgenic seedlings of segregating T2 and following T3 generations were harvested for the experiment. *OexALBA4* BC lines were created by Col-0 pistil pollination by *oexALBA4* pollen grains. Transgenic 7DAG seedlings of the first uniform *oexALBA4* BC T1 and second segregating *oexALBA4* BC T2 generations were collected. A portion of the T2 generation seedlings was transferred to Jiffy and further cultivated at standard conditions until maturation. Severe developmental abnormalities were observed in the sporophytic tissues throughout plant development, further described in chapter 4.4.3.4. Mature seeds were harvested separately and selected based on the presence of the KanFastR cassette-mediated RFP emission. The ratio of transformed (red) seeds and non-transformed (brown) seeds was roughly calculated, yielding an expected segregation ratio of 3:1 (data not shown). The seeds of the T3 generation were germinated, and the presence of a green signal was observed using a stereomicroscope (Leica M205FA). There was almost no signal observed in these seedlings that corresponded to the RT-qPCR data, confirming a decreased transcript level. Therefore, pollen from the segregating generation was used for pollination of Col-0 pistils, resulting in the generation of BC lines. Expression levels

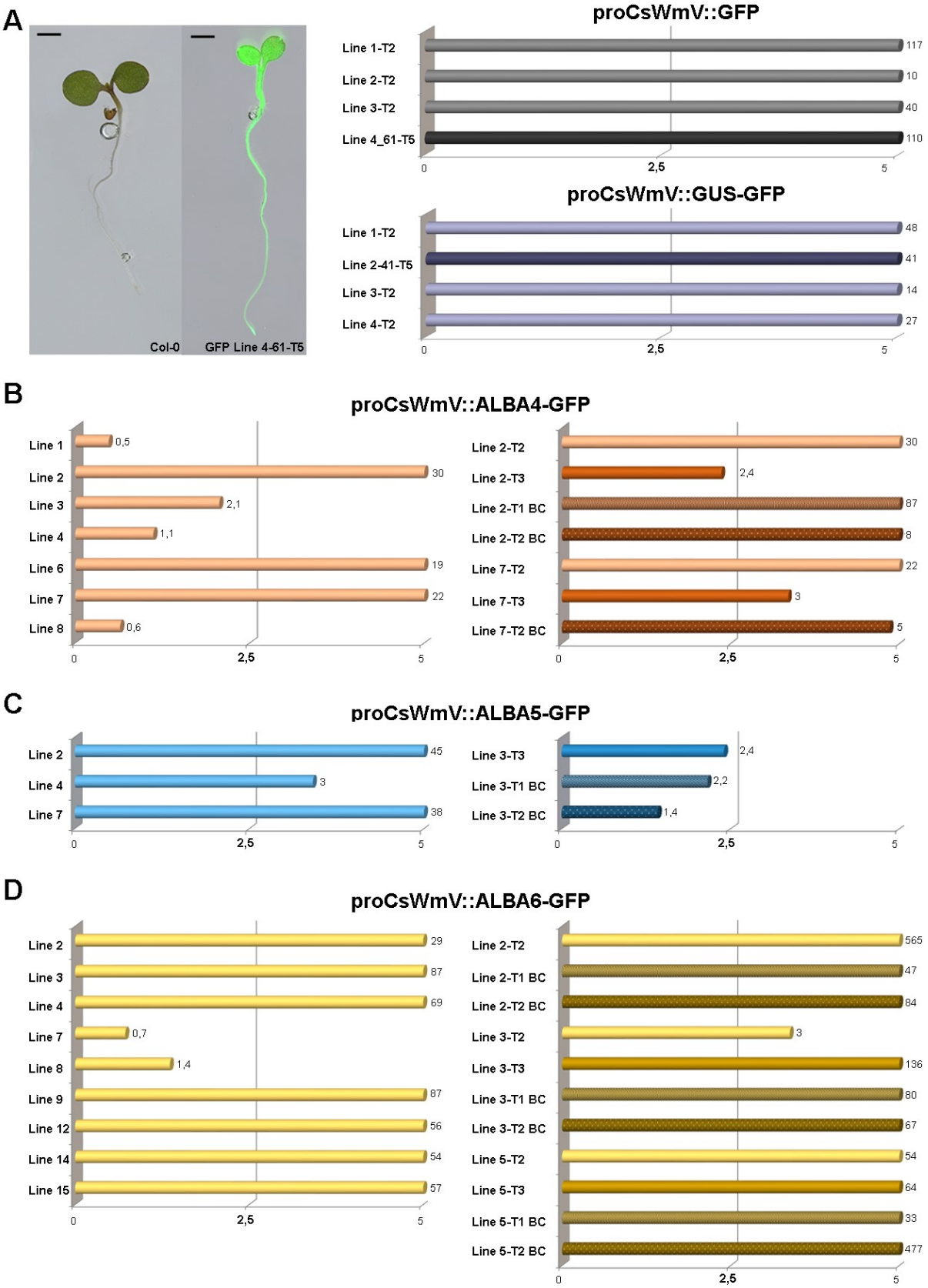

Figure 16: Evaluation of *oexGFP*, *oexGUS-GFP* and *oexALBA4-6* relative expression levels by RT-qPCR in seedlings. Transgenic seeds were germinated on vertical plates, and 10-14-day-old seedlings were checked for the presence of the green signal. Transgenic seedlings were harvested.

Initially, negative individuals (Col-0) and positive (*oexALBA4* Line 4-61-T5) control seedlings were observed and used for individual selection (**A**); scale bars = 1 cm. Two positive controls were introduced (*oexGFP* and *oexGUS-GFP*), and the *r*elative *GFP* expression levels of the created lines insegregating (T2) and homozygous (T5) generations were recorded. Relative expression of *ALBA-GFP* constructs was checked in the created lines of segregating generation (**B, C, D**, left panel) by the *ALBA*-specific primers. The relative mRNA levels were tracked between segregating, T3, and BC generations. *oexGFP, oexGUS-GFP, oexALBA4* and oex*ALBA5* Ct values (measured by GoTaq Q-PCR) are standardized to *GAPC1*, *oexALBA6* Ct values (measured by GoTaq 1-Step RT-qPCR) are standardized to *EIF1a4*. All represented numbers are normalized to Col-0 Ct values run at the same time. Independent transgenic lines are marked on the y-axis, with the level of transgene overexpression set to 2.5 relative expression (Sample: Col-0) on the x-axis, and shown up to 5-fold upregulation.

of *ALBA4* transcripts were highly elevated in both *oexALBA4* T2 samples, confirming previous measurements (Figure 16B, right). However, the overexpression level of the measured transgene dropped significantly in the following generation, even in homozygous seedlings of the T3 generation. Interestingly, backcrossing of the *oexALBA4* lines with the wild-type Col-0 resulted in an elevation of *ALBA4* transcript levels in a uniform generation, accompanied by the presence of phenotypic defects (data not shown).

Not many lines carrying the *proCsWmV::ALBA5-GFP* transgene were obtained. From three tested lines in the T2 generation with green signal presence, all were verified by RT-qPCR using *ALBA5*-specific primers. All three lines, *oexALBA5* Line 2, *oexALBA5* Line 4, *oexALBA5* Line 7, were considered to be overexpressing for exceeding the 2.5-fold threshold of Col-0 level (Figure 16C, left). Seedlings selected by the green signal emission were transferred to Jiffy and cultivated under standard conditions, resulting in the same developmental defects observed in the *oexALBA4* lines. Unfortunately, the very low germination ability of seeds led to populations of a few seedlings, which are usually insufficient for RT-qPCR. Therefore, only the *oexALBA5* Line 3 was used for expression quantification throughout generations, according to the presence of the green signal in the T2 generation. A sufficient number of *oexALBA5* Line 3 seedlings was obtained only in the T3 and BC generations, and the measurements showed identical results, lacking transgene overexpression (Figure 15C, right). Moreover, the *ALBA5* level in *oexALBA5* BC1 was even lower than in *oexALBA5* T3, which continued the trend of decreasing to the lowest level in oexALBA5 BC T2. Nevertheless, *ALBA4* and *ALBA5* decreased expression in the following generations could be caused by the simple position effect of the transgene insertion.

Lastly, *proCsWmV::ALBA6-GFP* seedlings were obtained, and the *ALBA6* transcription level was tested in 10-14-day-old seedlings using specific primers. Nevertheless, within a pool of first-obtained

oexALBA6 lines, none exceeded the threshold of overexpression. Therefore, the transgene was introduced again to the wild-type Col-0 plants. The transgenic seeds were germinated, and a sufficient number of seedlings with the green signal were harvested and processed for RT-qPCR. *ALBA6* transcription level was detected in nine plant lines by the 1-Step RT-qPCR System (Figure 16D, left). In seven lines, *ALBA6* overexpression was verified: *oexALBA6* Line 2, *oexALBA6* Line 3, *oexALBA6* Line 4, *oexALBA6* Line 9, *oexALBA6* Line 12, *oexALBA6* Line 14, and *oexALBA6* Line 15. Individuals of these plant lines were grown until maturation. The transgenic seeds, identified by the presence of a red signal, were selected and then germinated. All collected seedlings of the T3 generation were grown and processed simultaneously for 1-Step RT-qPCR. This experiment verified *ALBA6* overexpression in all tested samples, although with varying trends (Figure 16D, right). Measured levels of *ALBA6* in T2 and T3 generations revealed an increasing trend in *oexALBA6* Line 3 and *oexALBA6* Line 5. Interestingly, backcrossing with wild-type Col-0 resulted in *ALBA6* downregulation, from *oexALBA6* BC1 to *oexALBA6* BC2. In *oexALBA6* Line 2, the expression level trend increased towards segregating generation but decreased in the uniform *oexALBA6* BC1 population.

Consequently, independent plant lines with excessive upregulation of the target gene were identified and used for further research by RT-qPCR. Homozygous lines were obtained only for control genotypes *oexGFP* and *oexGUS-GFP*. Sample lines harbouring *ALBA4* and *ALBA5* transgenes gradually loosened transcript levels, which led to a complete loss in the T3 generation, except for *ALBA6*, which exhibited distinct behaviour. Most likely, the elevated *ALBA* expression caused severe conditions at the cellular level, leading to subsequent loss at the transcript level. Therefore, for further research were exclusively used plant lines in the segregating T2 generation with confirmed overexpression. The transgene activity was confirmed before every subsequent step of the experiment or analysis based on the presence of the green signal observed by the stereomicroscope.

Moreover, transcription levels of other Alba-family members were investigated in the overexpression backgrounds and Col-0. A few samples were selected, and RT-qPCR was used to measure *GFP* and other *ALBA* transcript levels with gene-specific primers. The data were standardized according to *GAPC1* Ct values, and the calculated measurements were normalized to transcription in Col-0. Nine lines were tested, including the newly achieved *alba456*$^{+A/+A,\ +T/+T,\ +T/+T}$ homozygous triple mutant, as well as *oexGFP, oexALBA4, oexALBA5,* and *oexALBA6* samples (Figure 17). The activity of six genes (*ALBA1, ALBA2, ALBA4, ALBA5, ALBA6*, and *GFP*) was measured in each sample, as *ALBA3* level was not successfully measured. The evaluated data revealed strong *GFP* overexpression in all transgenic samples harboring *GFP*-containing TUs. However, the amplified transcript was measured at a minimal level in the wild-type Col-0 (Figure 17, grey columns). This unspecific product value was filtered out of all samples. Nevertheless, the massive overexpression of the specific product in GFP-harboring samples completely masks this background.

Further examination of the *alba456* mutant revealed significant downregulation of the two mutated genes, *ALBA4* and A*LBA5*. The relative expression level of Rpp25-like subfamily members *ALBA4* (Figure 17, orange columns) and *ALBA5* (Figure 17, blue columns) is significantly below the threshold for gene downregulation set at 0.5 fold, and clearly confirms the absence of transcripts. Although the sequence of *ALBA6* (Figure 17, yellow columns) is mutated in the sample as well, the transcription level approaches the threshold. This result can be explained by the very low relative expression level of *ALBA6* in the wild-type Col-0, as illustrated by both measured and calculated values. Original absolute Ct numbers are identical to relative expression levels. Relative expression levels of the Rpp20-like subfamily *ALBA1* (Figure 17, green columns) and *ALBA2* (Figure 17, purple columns) are not significantly affected in the investigated samples, including the *alba456* triple mutant and *oexALBA4-6* lines. However, some trends in transcript quantities were observed. *ALBA2* dynamic activity is illustrated by a weak downregulation in the triple mutant and mild elevation in *oexALBA6* Line 12.

Similar results were observed for the relative expression levels of the Rpp25-like subfamily members *ALBA4, ALBA5,* and *ALBA6* in the overexpressing lines, although exceptions were noted. Relative numbers representing *ALBA4* activity at *oexGFP* and *oexALBA6* backgrounds were comparable to the wild-type sample. However, relative values of *ALBA4* were reduced in both tested *oexALBA5* lines. Very similar behavior was demonstrated by the relative expression level of ALBA5 in the samples. *ALBA5* relative expression in *oexGFP*, *oexALBA6,* and *oexALBA4* Line 2 was comparable to wild-type Ct values. Interestingly, *ALBA5* is mildly decreased in *oexALBA4* Line 6 and *oexALBA4* Line 7. Levels of *ALBA1*, *ALBA2*, *ALBA4,* and *ALBA5* transcripts were typically reduced, although not significantly, in all tested *oexALBA* samples, except for *ALBA6,* which is more dynamic. It is strongly downregulated in *oexALBA4* Line 2 and *oexALBA5* Line 7, approaches the downregulation threshold in *oexALBA4* Line 6, and is significantly affected in *oexALBA4* Line 7. Interestingly, elevated relative expression of *ALBA6* was recorded in *oexALBA5* Line 2. Therefore, the sporophytic overexpression of a single member of the Rpp25-like subfamily does not significantly affect transcript levels of other tested members.

Nevertheless, there were indicated trends in the activity of measured genes in distinct samples, represented by the predominant downregulation of *ALBA4* in *oexALBA5* lines and *ALBA5* in *oexALBA4* lines. These results suggest that *ALBA4* and *ALBA5* are connected through gene activities. However, apparent variability between tested lines generates unclear results, and the plausible mechanism would need to be studied in detail. Collectively, the obtained data on *GFP* and the relative expression of most *ALBA* genes in seedlings confirmed a significant elevation of *GFP* in all overexpressing samples. Levels of the *GFP* are similar to those of *ALBA4* transcripts in all three *oexALBA4* lines. However, in *oexALBA5* and *oexALBA6* samples, relative value of the respective

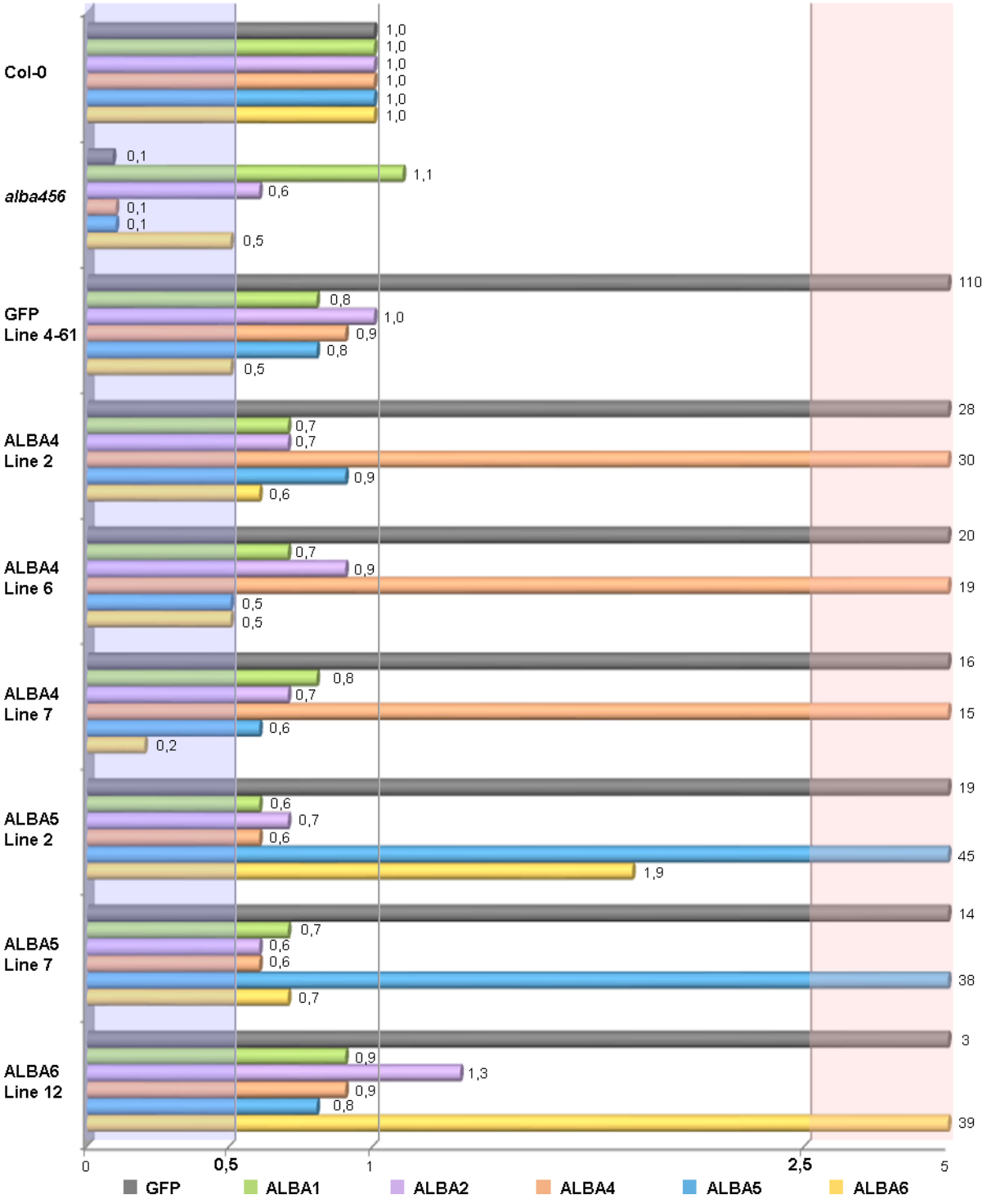

Figure 17: Evaluation of *GFP*, *ALBA1, ALBA2, ALBA4, ALBA5*, and *ALBA6* relative expression levels in Col-0, *alba456* triple mutant, *oexGFP*, and *oexALBA* seedlings by RT-qPCR. Gene-specific primers (Table 4) were used for relative expression measurement in isolated RNA samples from several verified lines using the GoTaq Q-PCR kit in the experiment. The obtained Ct values were standardized to *GAPC1* and related to Col-0 numbers (Sample : Col-0). The threshold for significant downregulation is set to 0.5, and the threshold for transgene overrepresentation is set to 2.5 relative expression on the x-axis, shown up to 5-fold upregulation.

targeted gene activity (*ALBA5* or *ALBA6*) is much higher compared to *GFP* level which could be caused by enhanced upregulation of the native TU in plant genome. Interestingly, targeted gene overexpression in *oexALBA4* lines causes downregulation of the native *ALBA4* transcript, resulting in excessive overexpression mediated by the transgenic cassette. At this level, the *alba456* triple-homozygous line exhibited significantly reduced values of *ALBA4* and *ALBA5*, except for *ALBA6,* which is at the threshold level, likely due to the native extremely low gene activity in the wild-type control. Moreover, the verified overexpression of *ALBA4, ALBA5*, and *ALBA6* does not severely affect the gene regulation of other Alba-family members.

4.4.3.2. Localization of oexALBA in sporophyte

Transgenic seedlings of the homozygous T5 generation, harboring the *oexGFP* cassette, were used for FP marker localization. From the initial population of generated lines, *oexGFP* Line 4-61 was selected and used for protein localization. Transgene overexpression was verified by RT-qPCR and is presented in chapter 4.4.3.1. Initial observations were focused on the description of promoter activity through GFP visualization at subcellular, cellular, and tissue levels across multiple developmental stages. The seedlings were selected in the T3 generation based on the presence of the green signal, and the subcellular localization was repeatedly investigated in their progeny. There were no recorded signal intensities or phenotypic differences between generations of control plants. A very strong green signal was detected in seedlings across generations, with no significant differences (data not shown). Homogenity of green signal distribution in 7DAG seedlings was observed by the stereomicroscope. The collected seedlings were mounted in water on a slide, covered with a coverslip, and immediately captured. Specific strong GFP signal emission was almost equally distributed in all organs, including cotyledons, true leaves, hypocotyl, main root, and lateral roots, with enrichment in the main root tip (Figure 18A).

The subcellular localization of GFP was investigated using a fluorescence microscope with higher magnification. The first observation focused on localization in roots using the fluorescence microscope, and the root differentiation zone was imaged in the green channel (Figure 18B). The signal was observed in all root layers, including root hairs, with enrichment in the central part of the root. Next, the main root tip detail was captured by the confocal microscope (Figure 18C). The GFP-specific signal was detected in all captured cells, exhibiting a pattern similar to that observed in the root elongation, transition, and meristematic zones. Channel merge indicates visible structures overlap with the FP signal localization. The subcellular localization was captured throughout cell growth and differentiation. Within a cell of root hair, GFP signal is randomly distributed in the cytoplasm, aligned with the cell membrane and tonoplast (Figure 18D) as well as in the root differentiation zone cell cytoplasm and nucleus (Figure 18E). The signal is further equally distributed in the cytoplasm and nuclei of the root elongating cell (Figure 18F) and cells from the root

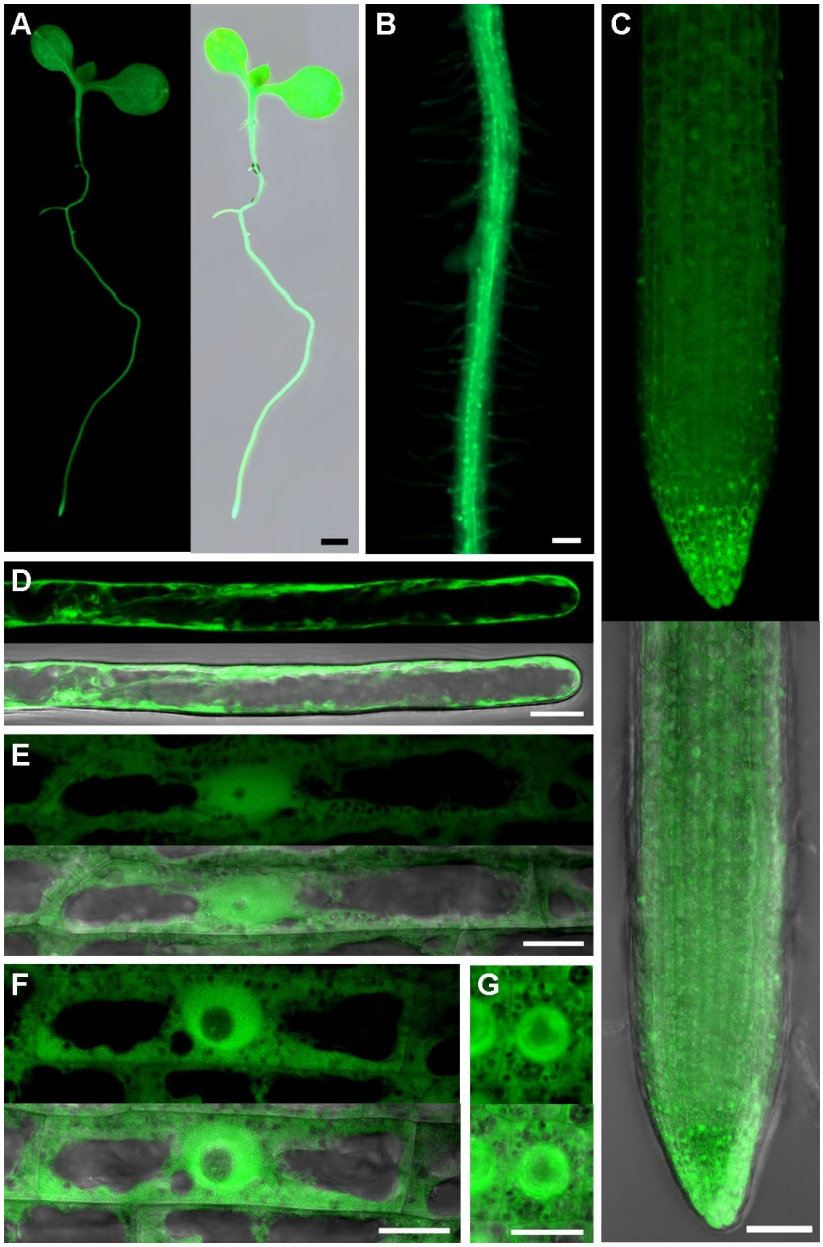

Figure 18: Subcellular localization of free GFP in organs and tissues of 7DAG *oexGFP* seedlings. The *GFP* sequence from the GB collection was expressed under the control of the strong sporophytic promoter *CsWmV*. One-week-old seedlings were screened for the presence of GFP signal in green and TL using a Leica M205FA stereomicroscope (**A**). Channels were merged during post-processing. Detailed visualization of the root differentiation zone was captured using the fluorescence microscope Zeiss AxioImager (**B**). Details of decent root parts were imaged by the confocal microscope Zeiss LSM 880 with Airyscan in GFP and TL channels; root tip (**C**), root hair (**D**), cells from root differentiation zone (**E**), root elongation zone (**F**), and root meristematic zone (**G**). Airyscan processing, z-stack maximum intensity projection, and channel merge were created by post-processing. Scale bars represent 1mm (**A**), 100 µm (**B**), 50 µm (**C**), 10 µm (**D - G**).

meristematic zone (Figure 18G). Dark areas in nuclei are most likely nucleoli, which occupy a significant volume of nuclei in meristematic and elongation cells. However, they occupy only a minor portion of the nuclei in differentiating cells.

The GFP distribution was documented in green parts of the sporophyte and pollen grains. In the 7DAG seedling, a detail of the SAM zone with true leaf primordia was captured in the green channel. It revealed a homogeneous distribution of the signal within all captured organs, including young true leaves, cotyledon basal parts, and hypocotyl (Figure 19A). Cotyledon pavement cells were imaged by the confocal microscope, and green emission was detected in the cytoplasm aligned with the cell plasma membrane and nuclei with very strong intensities (Figure 19B). The same cytoplasmic signal pattern was recorded in epidermal cells of hypocotyl (Figure 19C) and rosette true-leaf pavement cells (Figure 19D). The investigation continued in later developmental stages of plant individuals by the confocal microscope observation and imaging. Flowers were collected, and their floral organs were isolated and mounted in water covered with a slip. Promoter activity was indicated by a specific GFP emission in epidermal cells of a sepal randomly distributed in the cytoplasm aligned with the cell shape (Figure 19E). Mature pollen was mounted in DAPI solution and incubated for a few minutes. Although nuclei were visualized in the blue channel, there was almost no signal detected in the GFP emission window (Figure 19F). According to these observations, the activity of the *CsWMV* promoter was recorded in all inspected tissues and cells, from seedlings to flowering adults, in developing tissues as well as in the fully differentiated cells of sporophytic organs. The absence of intensive signal emission in mature pollen indicates a lack of promoter activity in the male gametophyte. Therefore, the promoter was considered active only in the plant sporophyte throughout all developmental stages.

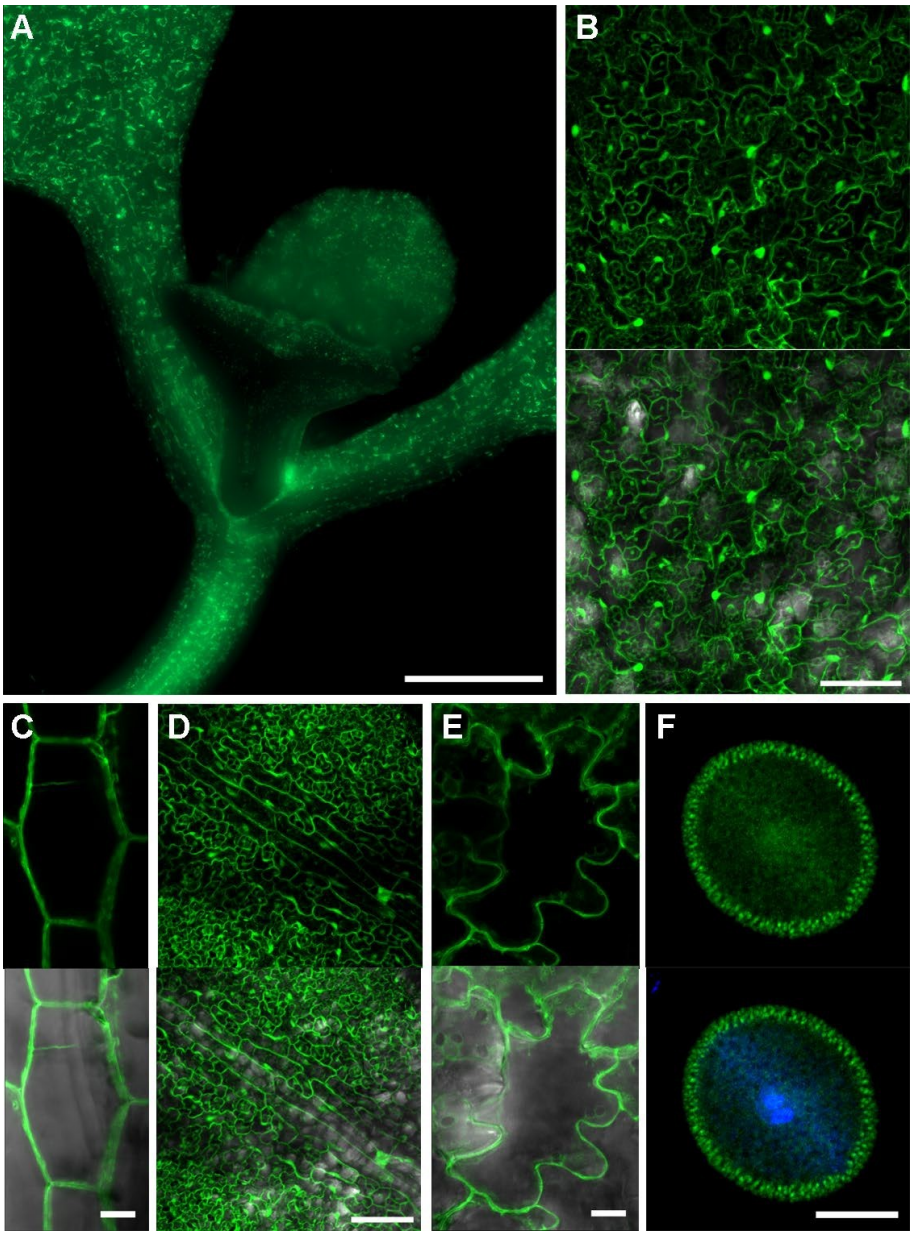

Figure 19: Subcellular localization of free GFP in green parts of *oexGFP* plant and pollen grains. A 7DAG transgenic seedling was mounted in water, and the green part of the plant was imaged in the green channel using the fluorescence microscope (**A**). Detailed images were obtained by the confocal microscope in green and TL channels. Epidermal cells of 7DAG seedlings are shown in the cotyledon (**B**) and hypocotyl (**C**). A disc from juvenile rosette leaf was collected, and epidermal pavement cells of the abaxial side were captured (**D**). Floral organs were harvested, and epidermal cells of a sepal leaf were captured (**E**). Mature pollen grains were harvested, stained in DAPI, and captured in green (GFP) and blue (DAPI) channels (**F**). Images were processed by the z-stack maximal intensity projection, and signal overlaps were created by post-processing. Images acquired by the confocal microscope underwent Airyscan processing (**C, E, F**). Scale bars 500 µm (**A**), 100 µm (**B, D**), 10 µm (**C, E, F**).

4.4.3.3. Visual characterization of the Rpp20-like subfamily

Selected transgenic seeds were germinated, and individuals from the segregating T2 generation were used for phenotypic analysis. A description of *oexGFP* on the wild-type background enabled a detailed portrait illustration of *oexALBA* plants. Seeds of Rpp20-like subfamily members were obtained and selected by the presence of the red signal. Seedlings harboring *proCsWMV::ALBA1-GFP* were collected, and the green signal distribution was documented using a fluorescence microscope. The specific signal was detected in the green parts of the 7DAG seedling, specifically in the cotyledons, and a weak fluorescence was recorded in the emerging true leaves. Signal intensity enrichment was detected around SAM and in the hypocotyl (Figure 20A). The same pattern is visible in the primary root differentiation zone; the green signal is enriched in the central part of the root (Figure 20B). In the differentiated zone, the signal is very weak and strengthens toward the root tip. It emerges in the central part of a root elongation zone and significantly increases in the meristematic zone except for the root cap (Figure 20C).

The unexpected observation was made early in the plant development. Seedlings transferred to the soil started losing the green colour in the cotyledons. Within the following days, further true leaves emerged with significantly light green or completely colourless leaves. Therefore, a leaf disc was cut from a juvenile rosette leaf, and the morphology of the chloroplasts was briefly observed, focusing on the colour and number in the TL, and compared with the wild-type sample (data not shown). No significant difference was observed in the organelle number. Surprisingly, the pale phenotype was presumably caused by the presence of yellowish chloroplasts in the investigated leaves, compared to the dark green shade typical of wild-type plants. Therefore, signal quality was measured in a true leaf cut from a transgenic pale juvenile rosette by the confocal microscope lambda scan. The actual GFP pattern is shown in blue-green in lambda scan mode. It localizes exclusively to the pavement cell cytoplasm on a background of chloroplast-specific emission in deep carmine (Figure 20D). Although the green signal intensity seemed stronger compared to the TU driven by native promoters, the pattern differed from the experimental control *oexGFP* results in the absence of emission in nuclei. Unexpectedly, the GFP signal was detected in mature pollen collected from open flowers of adult plants, stained with a DAPI solution, and captured in three channels. The detected green signal distribution was very similar to the localization controlled by the native promoter, characterized by a reticular-like pattern in the VC cytoplasm with enrichment surrounding MGU (Figure 20E).

In the absence of further phenotypic aberrations, the plants' morphology and development were not affected by the pale phenotype. The juvenile rosettes were comparable in terms of development timing, leaf size, and shape to the control plants, wild-type Col-0, and *oexGFP*. Regularly fertilized, simultaneously cultivated populations of wild-type Col-0 and *oexALBA1* plants matured at the same time, although transgenic individuals typically grew with light green inflorescence stems and pale

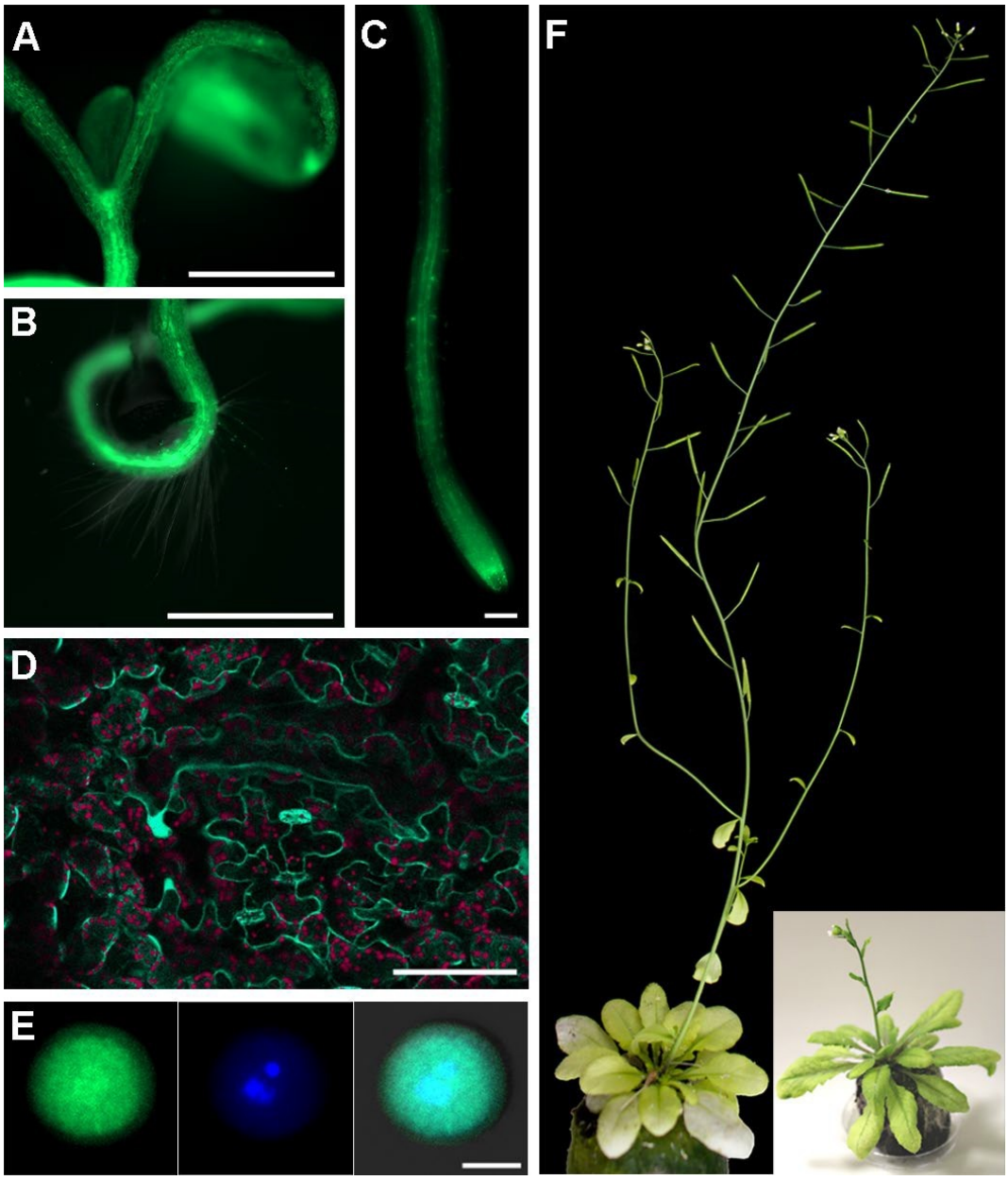

Figure 20: Subcellular localization of ALBA1-GFP and an effect of its overexpression to sporophyte development. *ALBA1* genomic sequence was C-terminally tagged with *GFP* and expressed under strong sporophytic promoter *CsWmV* control. Seedlings obtained from transformed seeds were screened for GFP signal presence in cotyledons (**A**, GFP), root hairs (**B**, GFP and TL) and root tips (**C**, GFP) using the fluorescence microscope. Rosette leaves were collected and cells of the abaxial side were captured in lambda scan mode using the confocal microscope (**D**). GFP is shown in blue-green, and chlorophyll is depicted in deep carmine. Pollen from adult plants was collected and stained in a DAPI solution for nuclear visualization (**E**, middle) and GFP detection in green (**E**, left) using the confocal microscope. The acquired image was processed using Airyscan, with Maximum intensity projection of z-stacks, and the channels were overlapped (**E**, right). Transgenic plants possess usually light green or almost white sporophyte (**F**). Scale bars 1 mm (**A, B**), 100 µm (**C, D**), 10 µm (**E**).

leaves. Despite phenotypic differences, these plants produce enough flowers, siliques, and seeds (Figure 20F). The length of lateral inflorescence stems and flower numbers were usually non-significantly reduced.

Some plants in the segregating generation and some lines in the T3 generation started to lose the pale phenotype during plant development gradually. The phenotype disappearance is obligatorily connected with a reduction in transgene expression below the threshold for overexpression verification, as illustrated by the Rpp25-like subfamily expression analysis (see Figure 16). However, the phenotypic aberration is not dependent on the red seed marker. Therefore, a disc was cut from the green part of the transgenic leaf. The GFP signal was captured in pavement cells using the confocal microscope, in a lambda scan mode. The GFP signal was not detected, as no blue-green or green signal was present; however, the unspecific chloroplast autofluorescence was very strong compared to the results achieved from pale leaves (Figure 21A). This indicates gradual transgene silencing during plant development, resulting in the recovery of the wild-type phenotype. The plants are regaining their original phenotype by producing new structures that counteract weakened phenotypic abnormalities. Moreover, later-emerging organs are produced with the wild-type phenotype, e.g., young true leaves surrounding the SAM area, as presented in Figure 21B, down.

Populations of transgenic and control plants were captured at the rosette stage. The individuals differed in the phenotype of the oldest pale leaves, while the youngest leaves in the rosette center almost completely regained their green color. This phenomenon was observed in adult plants, sometimes with a clean border between the pale and green parts of the leaf (Figure 21C). Moreover, the inflorescence stem usually quickly adopted the original colour by the production of new organs (Figure 21C, 21D). Although a slight reduction in fertility was observed, mature pollen harvested from opened flowers exhibits the same phenotype as that of wild-type plants (Figure 21E). Pollen grains were stained in DAPI solution and captured by the confocal microscope in GFP, DAPI, and TL channels. The green signal was localized to unspecific foci in the VC cytoplasm and enriched around MGU, though the intensity was much weaker compared to the pollen harvested from pale plants.

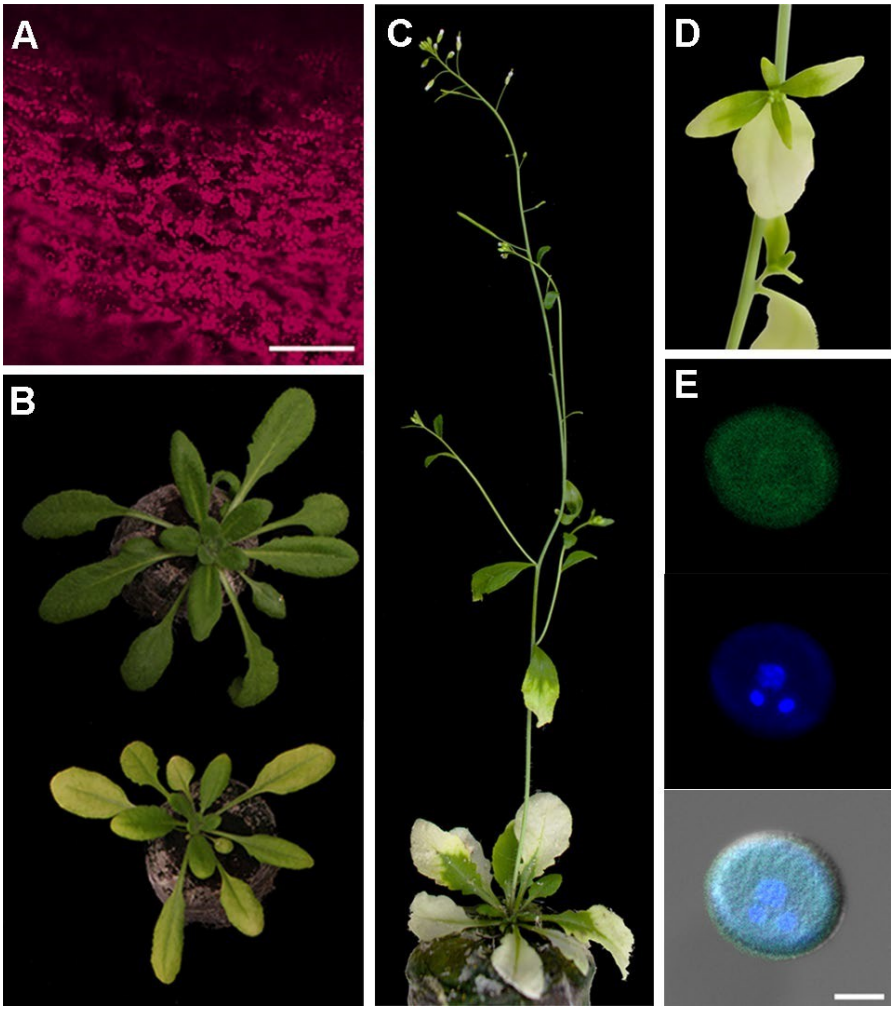

Figure 21: Phenotypic expression of o*exALBA1 i*n the following generation. The green part of an actual leaf was collected, and pavement cells of the abaxial side were captured in the lambda scan mode (**A**). GFP is absent in blue-green, and chlorophyll is visible in deep carmine. Juvenile plants in the rosette stage were captured by a camera (**B**), with Col-0 at the top and *oexALBA1* at the bottom. Adult plants in the T3 generation regain the green color in the central parts of the rosette (**C**), as well as in the inflorescence stem and leaves (**D**). Pollen was harvested from almost entirely green inflorescences, stained in DAPI (**E**, middle), GFP signal was captured (**E**, up), and images were overlapped with TL (**E**, down). Scale bars 100 µm (**A**), 10 µm (**E**).

Next, plants harbouring *proCsWMV::ALBA2-GFP* transgene were characterized. According to the high sequence identity between ALBA1 and ALBA2 amino acid sequences, it was expected that the transgenic plants would exhibit a similar phenotype. Grown 7-day-old seedlings were collected and captured in the green channel using the fluorescence microscope. Investigated individuals exhibited high signal intensity in the primary root differentiation zone, which was gradually decreasing in lateral roots and at the root tip (Figure 22A, 22C).

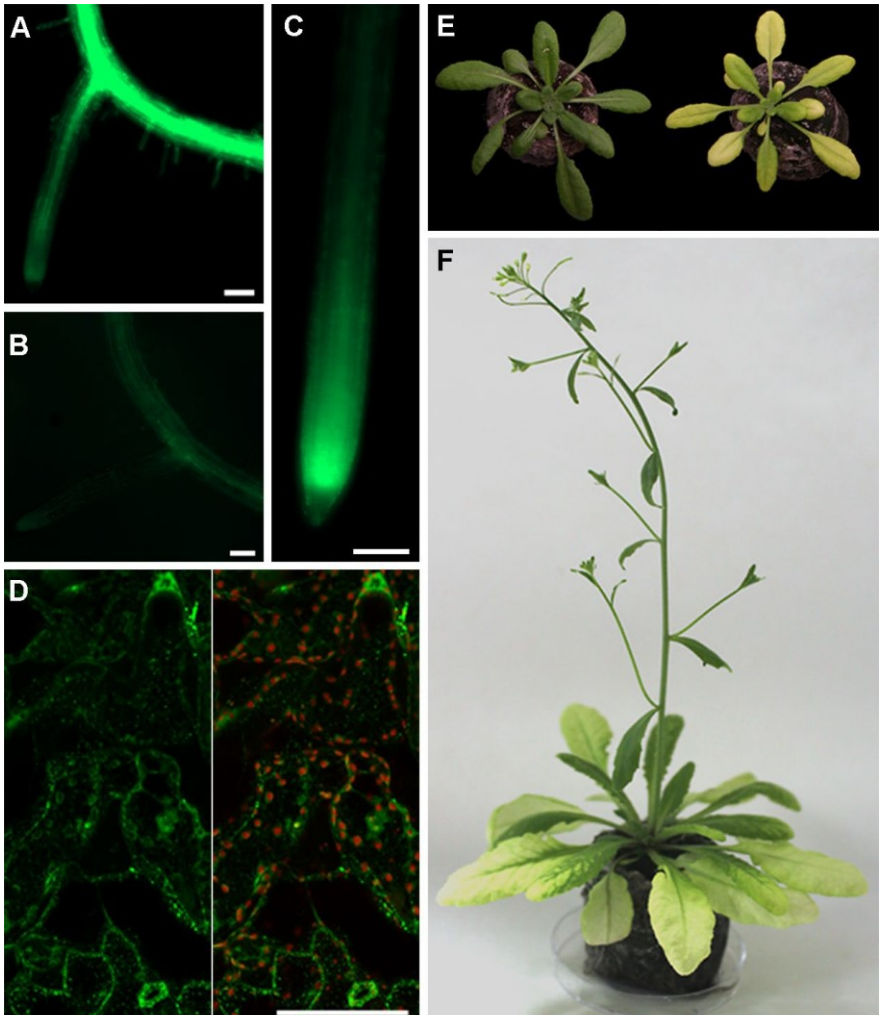

Figure 22: Subcellular localization of ALBA2-GFP and the effect of the overexpression on sporophyte development. The *ALBA2* coding region was C-terminally tagged with *GFP* and expressed under strong sporophytic promoter *CsWmV* control. Transgenic seeds were selected based on the presence of a red signal, germinated, and seedlings were screened for the presence of a GFP signal in the root differentiation zone, yielding positive (**A**) or negative (**B**) results using the fluorescence microscope. Further, GFP signal was visualized in root tips (**C**). The white part of the rosette true leaf was captured from the abaxial side in the GFP channel (**D**, left) and the red channel for chlorophyll emission using the confocal microscope; the overlap of the channels is shown (**D**, right). Adult rosettes and the flowering plant were captured by a camera. The *exALBA2* adult rosette lack dark green color (**E**, right) and is paler than the control plant (**E**, left). Flowering plants of *oexALBA2* regain the dark green color in developing inflorescence stem (**F**). Scale bars 100 µm.

On the other hand, seedlings with a very low signal in the primary root were identified with enriched intensity around lateral root protrusions (Figure 22B). Furthermore, the presence of the signal was investigated in the juvenile rosette stage. A true leaf was harvested, and a leaf disc was mounted in water. The leaf's abaxial side was then captured in green and red channels using the confocal microscope. The green signal was homogenously distributed in the pavement cell cytoplasm (Figure 22D), though the localization pattern was accompanied by a quite high number of very bright foci (Figure 22D, left). The channel was merged with the autofluorescence of the chloroplasts in the red channel (Figure 22D, right). Juvenile, Col-0 and *oexALBA2,* plants were captured at the same age and time on camera. From the early stages of rosette development, the transgenic plants were noticeably paler compared to the commonly cultivated control plants. The change in phenotype was very similar to that of *oexALBA1* lines, although the pale, early-developed true leaves gradually regained color, almost restoring the dark green in the rosette center (Figure 22E). Interestingly, transgenic rosettes were nonsignificantly delayed in leaf development. Adult plants were very similar to the previously described plant phenotype, with rapid recovery of the wild-type phenotype in stems and stem leaves (Figure 22F).

Sporophytic overexpression of the last member of the Rpp20-like subfamily was also investigated in detail. The sequence similarity of the almost identical *ALBA1* and *ALBA2* pair sets the *ALBA3* gene to the same subfamily, despite being the most diversified (Náprstková et al., 2021). Obtained seeds were selected, germinated, and grown. 7DAG seedlings were collected and observed using the stereomicroscope. A weak green fluorescence signal was detected in whole individuals enriched in distinct tissues. Overlaid images enabled the identification of tissues at cotyledon ends, hypocotyl, and root tips (Figure 23A). Details of the root differentiation and elongation zones were imaged using the fluorescence microscope, revealing a novel signal pattern (Figure 23B, 23C). Green signal in the investigated tissues is predominantly dispersed over the root layers in large foci with very strong intensity. Homogenous distribution of the signal was detected only in the primary root meristematic zone (Figure 23C). Plants of Col-0 and *oexALBA3* lines were grown together without fertilizer for the first few weeks. Obtained transgenic plants exhibited the same pale phenotype typical of the Arabidopsis Rpp20-like subfamily, although most of them died before reaching the rosette stage. Therefore, the rest of the population was treated with fertilizer and finally flowered a long time after the wild-type Col-0 control plants (Figure 23D). The transgenic pale plants were tiny, producing inflorescences with a reduced number of flowers and smaller silique sizes. However, the low number of surviving plants was not sufficient for any phenotypic evaluation of the observed phenotypes.

Collectively, high activity of the *CsWMV* promoter elevates levels of Rpp20-like subfamily members in sporophytic tissues, as indicated by the signal intensity detected even under a stereomicroscope. The sole member overexpression causes changes in the plant phenotype, manifested by the production

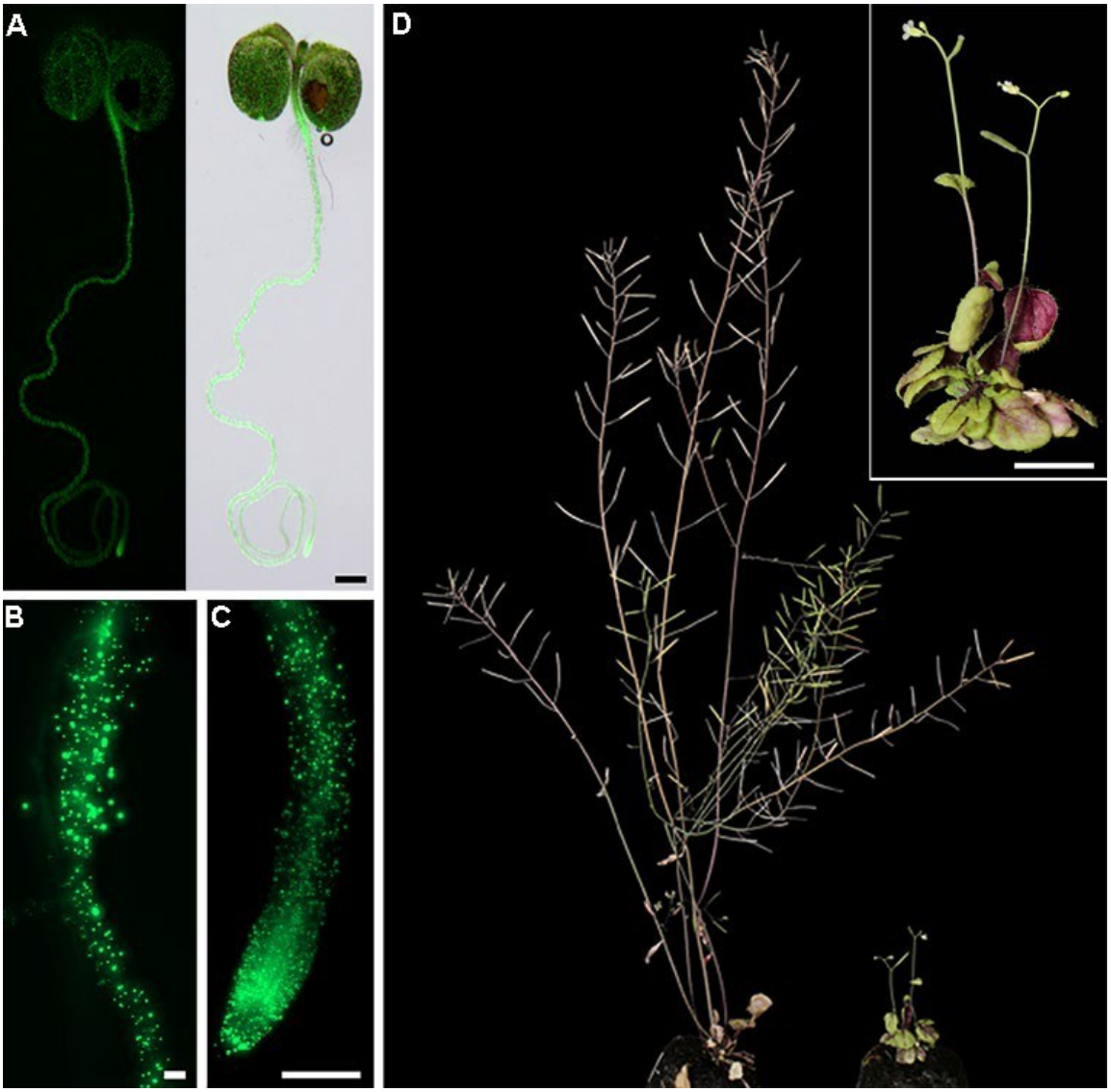

Figure 23: Subcellular localization of ALBA3-GFP and the effect of the overexpression on sporophyte development. *ALBA3* coding region was C-terminally tagged with *GFP* and expressed under the strong sporophytic promoter *CsWmV* control. Seedlings were screened for green signal presence (**A**) by the stereomicroscope Leica. The GFP signal localization was detected in the root differentiation zone (**B**) and root tip (**C**) by the fluorescence microscope. Adult plants lack dark green color and are delayed in development (**D**) compared to Col-0 wild-type. Scale bars 1 mm (**A**, **D**), 100 µm (**B**, **C**).

of pale organs in the juvenile stage of development and light green inflorescences with fully fertile flowers. Even though the GFP signal intensity is reduced compared to *oexGFP* plants, it is above the level that the plant can cope with. This theory is further supported by a gradual loss of GFP signal in subsequent generations, accompanied by a loss of phenotype. Therefore, the subfamily is probably involved in energetic metabolism and ROS regulation. According to these data, the Rpp20-like level and maintenance of homeostasis are crucial for plant growth and development.

4.4.3.4. Visual characterization of Rpp25-like subfamily

The investigation continued with a description of Rpp25-like subfamily overexpression controlled by the sporophytic promoter *CsVMW* in Arabidopsis wild-type, Col-0 plants. Transgenic seeds of the T2 generation were germinated, and the resulting seedlings were used for the experimental procedures described in this chapter. Only *oexALBA* lines with verified transgene overexpression were used.

Obtained *oexALBA4* seedlings were examined, and only 7-day-old individuals with the green signal presence were captured by the stereomicroscope in green and TL channels (Figure 24A). A seedling was mounted in water and overlaid with a cover slip. A weak green signal was detected in whole individuals, with enrichment in the root differentiation zone and a brighter area in the oldest part of the root, close to the hypocotyl. Nevertheless, the most intensive signal emission was clearly concentrated in the root tip meristematic zone, gradually decreasing towards the elongation and transition zones (Figure 24B). Although the signal distribution is smooth between tissues, precise localization revealed a non-homogeneous pattern consisting of large, bright foci across root cell layers. The most vigorous intensity was observed in the primary root, although the pattern gradually disappeared in the lateral roots and 2nd lateral roots (Figure 24C). A detail of the root tip revealed a weak, homogenous signal distribution around the root transition zone, which was accompanied by several pronounced foci. The signal quantity accumulated towards the root tip (Figure 24D). The subcellular localization of the GFP signal was achieved through confocal microscopy of single cells at various developmental and differentiation stages. Nevertheless, the cytoplasmic signal distribution was very similar between the investigated cell types, which were characterized by a weak cytoplasmic signal distribution accompanied by round or oval-shaped aggregations. This localization pattern was detected in a fully differentiated cell of a root hair (Figure 24E), an elongating root cell (Figure 24F), and a small root meristematic cell (Figure 24G). An identical pattern was revealed even in differentiated pavement cells of cotyledon leaves (Figure 24H).

Seedlings were transferred to soil and cultivated at standard conditions. Stems from juvenile rosettes were collected, fixed in agar, and sliced by a microtome. A central part of the stem, including the SAM, was captured by the fluorescence microscope in green and TL channels (Figure 25A). The image was processed and merged using the Zen software, as described in chapter 3.11, and revealed a green signal in all tissues presented, including the SAM zone, young leaves, buds, and stem. According to the microscopic details, the rosette was in the intermediate stage, slowly developing its primary inflorescence and flower primordia. The detail of the meristem revealed the presence of the green signal in all captured layers, visible in the merged image (Figure 25B). The plants were cultivated to the flowering stage, and the flowers were collected. The presence of the green signal was analyzed using the stereomicroscope. Floral organs were collected and mounted in water to be captured in detail by the confocal microscope, which revealed a specific GFP signal in petal epidermis

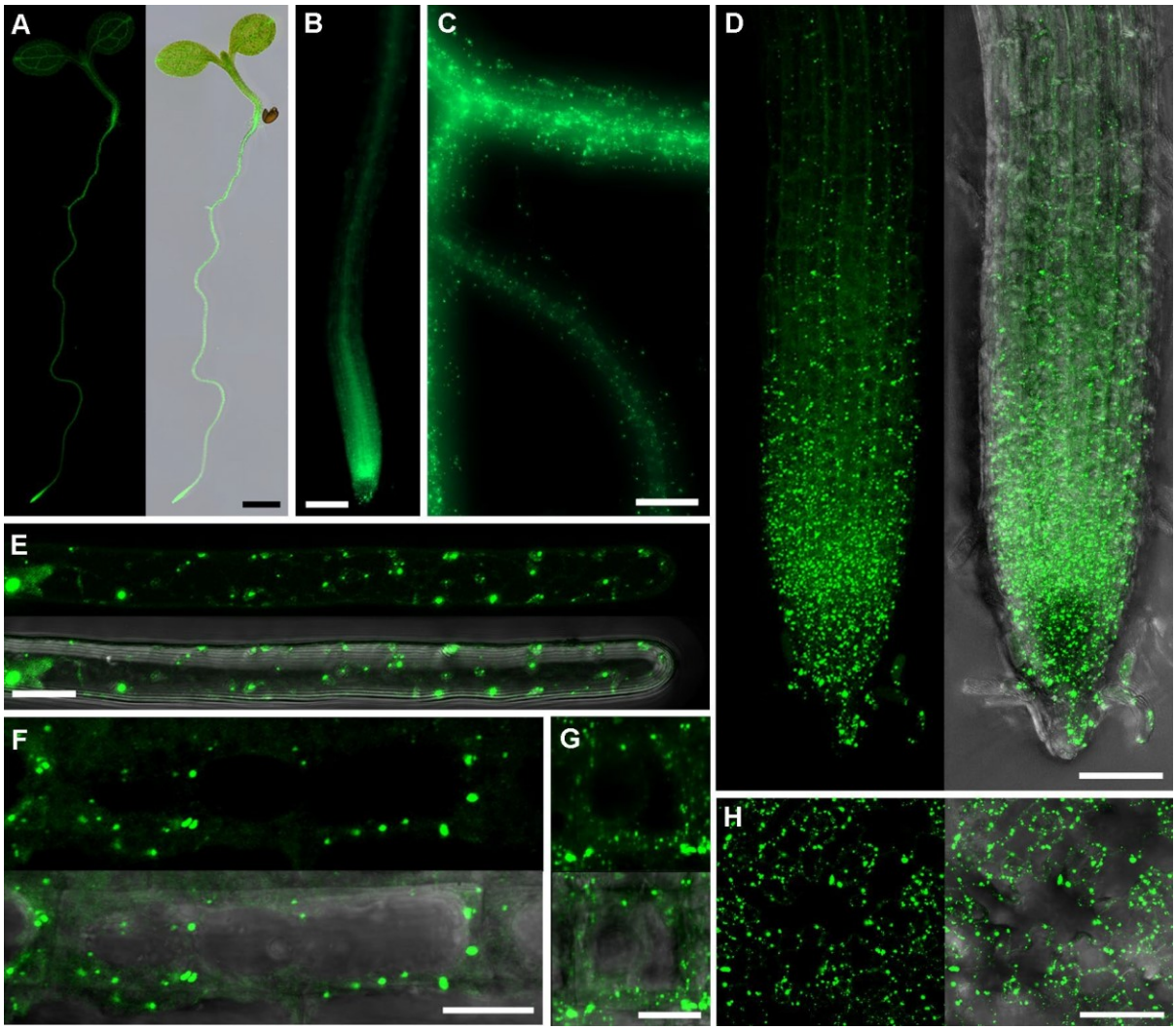

Figure 24: Subcellular localization of ALBA4-GFP in *oexALBA4* seedlings. The *ALBA4* coding region was C-terminally fused with *GFP* and expressed under the control of a strong sporophytic promoter, *CsWmV* control. One-week-old seedlings were screened for the presence of a GFP signal (**A**) in green and BF using the Leica stereomicroscope and processed in LasX software, including channel overlay. 10DAG seedlings were collected and the root tip (**B**) and root differentiation zone with lateral roots (**C**) were captured by the fluorescence microscope in the green channel. 7DAG old seedling detail of the root tip (**D**), root hairs (**E**), elongation zone cell (**F**), meristematic cell (**G**), and cotyledon epidermal cells (**H**) were captured by the confocal microscope. Images were processed by Z-stack maximum intensity projection and channel overlap. Scale bars 1mm (**A**), 50 µm (**B – D, H**), 10 µm (**E – G**).

localized predominantly to foci of various sizes, followed a weak distribution in the cytoplasm (Figure 25C). The observation was followed by imaging of mature pollen in water and documentation

using the fluorescence microscope. The signal was presented in a reticular-like pattern in VC with enrichment in the area of possible SCs (Figure 25D).

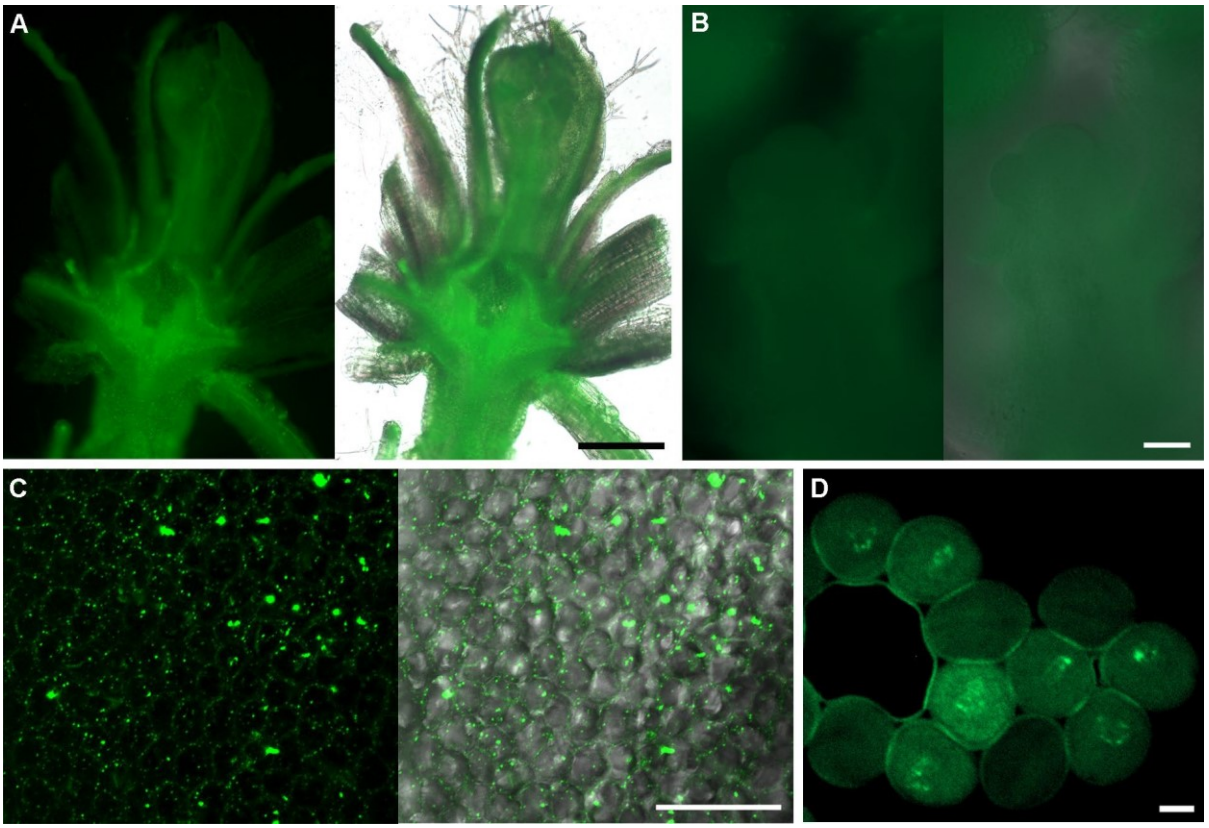

Figure 25: Subcellular localization of ALBA4-GFP in juvenile and adult in *oexALBA4*. A rosette was cut above the hypocotyl; all leaves were removed with a razor. A longitudinal slice of rosette stem was cut by a microtome and the whole stem was captured in GFP and TL channels by the fluorescence microscope (**A**), accompanied by the SAM detail (**B**). Channels′ overlap was created by image post-processing (**A, B**, right). Flower organs were collected, and the petal epidermis was captured using the confocal microscope in green, overlapped with the TL channel in post-processing (**C**). Mature pollen was collected from open flowers and screened for GFP signal localization by the fluorescence microscope (**D**). Scale bars 500 µm (**A**), 50 µm (**B, C**), 10 µm (**E–G**).

Although the ALBA family proteins are highly similar, their overexpression in the sporophyte, controlled by the *CsWmV* promoter, causes two distinct phenotypes. While the Rpp20-like subfamily characteristically produces plant organs with pale colour, the phenotypic defects of the Rpp25-like subfamily are more apparent. Obtained *oexALBA4* seeds were sewn and germinated together with wild-type Col-0 on MS/2 media with 1% Sucrose in vertical orientation (for details see chapter 3.1), and the germination efficiency was observed according to plate scan 4DAG (Figure 26A). There are displayed germinating seeds of segregating generation *oexALBA4* Line 7 (left) and wild-type Col-0

seedlings (right) grown on the same plate. While Col-0 seeds are all germinated, only a portion of *oexALBA4* seeds are germinating. There is a clearly visible germination delay of *oexALBA4* transgenic seeds compared to the wild-type. Moreover, the growth of transgenic seedlings is usually slowed down, as displayed by abnormally short primary roots and underdeveloped cotyledons. The growth delay is even more pronounced in the subsequent developmental stages, accompanied by abnormal morphology of the produced organs

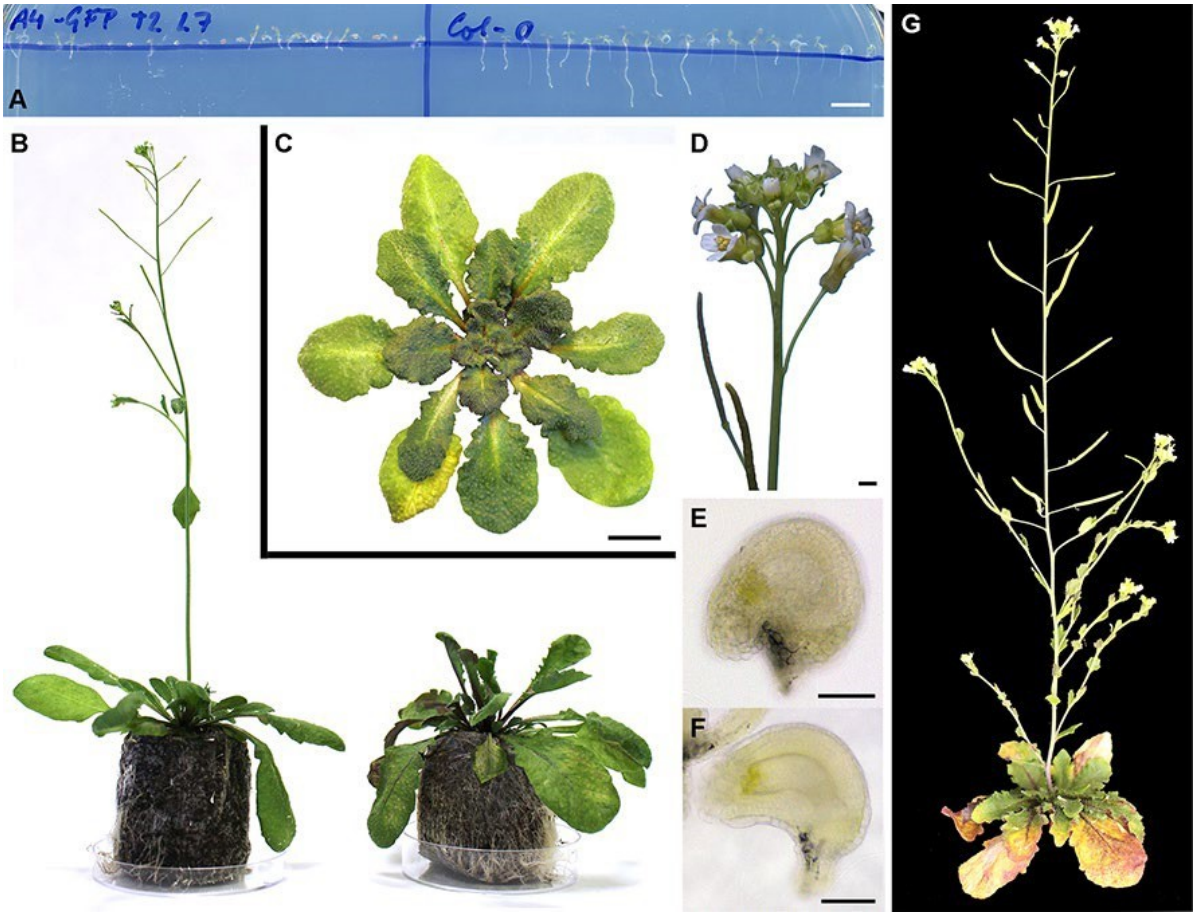

Figure 26: Manifestation of *oexALBA4* throughout plant development. Selected transgenic red and wild-type Col-0 seeds were germinated on a plate with MS/2 media with 1% sucrose in vertical orientation. The plate of 4-day-old seedlings was scanned (**A**). Control Col-0 (left) and *oexALBA4* (right) plants were grown together, and the side view was captured by a camera at the same time for comparison (**B**). Juvenile *oexALBA4* rosette was captured from an upper view to detect aberrant leaf shapes by a camera (**C**). Inflorescence detail with visible alternative flower and inflorescence morphology was obtained using the stereomicroscope Leica (**D**). Seeds from transgenic plants were isolated, and two phenotypes were recorded by the fluorescence microscope: wild-type amphitropous (**E**) and aberrant hemianatropous (**F**). A flowering transgenic plant with early lateral inflorescence protrusions (**G**) was imaged using a camera. Scale bars: 1mm (**A, D**), 1 cm (**C**), 50 µm (**E, F**).

Differences between the investigated and control genotypes are gradually increasing with age. Seedlings transferred to soil grow and produce true leaves, creating juvenile rosettes that secure inflorescence stem production with precise timing depending on energetic state, plant age, hormonal balance, and other factors. The wild-type (left) and transgenic *oexALBA4* plants were cultivated and captured together at the same time (Figure 26B). Although the control plants were flowering, producing main and lateral inflorescences, the transgenic plants remained in juvenile rosettes, growing true leaves at the same time. A detailed study of the transgenic individuals could reveal the possible origin of the phenotypic alteration. Therefore, fully developed rosettes were captured from above (Figure 26C). Variations in organ development, stem, and leaves were observed. The precise architecture of these organs is crucial for transitioning to the generative stage. Recorded alterations in leaf number, size, and thickness in transgenic plants could disrupt processes involved in flowering promotion. At transition, inflorescence stems elongate, grow leaves with pronounced lobes, and produce early, protruding lateral branches before the first flower opens. The diameter of developing inflorescences is enlarged, which is not caused by the number but by flower morphology. Growing sepals usually cover and protect inner floral organs. However, sepal tops are already bowed out in buds of the transgenic plants. This causes the bud cavity to open and the development of inner floral organs, especially the underdeveloped anthers and pistil, without protection against mechanical damage and moisture loss (Figure 26D). Plants were fertile, and the predominant number of seeds within seed set originated from fully developed amphitropous ovules (Figure 26E). However, a low number of seeds in siliques was developed from immature hemianatropous ovules (Figure 26F). Transgenic adult plants were characterized by developmental delay, with early lateral inflorescences protrusions, nonsignificantly shorter siliques, and shorter main stems compared to the wild-type Col-0 (Figure 26G). Finally, the growth delay resulted in the maturation of the investigated plants from 3 to 4 months after germination, which is almost twice the time required for the generation of the wild-type and *oexGFP* controls.

Further study of the Rpp25-like subfamily was accomplished through the characterization of *oexALBA5* plants. Initially, transgenic seeds were germinated in the vertical orientation, and 7DAG seedlings were captured by the stereomicroscope in blue and BF channels (Figure 27A). Seedlings were collected into a water drop on the slide, overlaid with a cover slip, and captured. A green signal was recorded through all seedling organs, with enrichment in the root differentiation zone and root tip. The observed pattern was identical to that of the previously inspected *oexALBA4* seedlings. The signal was homogenously distributed with a weak intensity in the root tip meristematic and elongation zones, accompanied by large aggregates in the meristematic zone and the root cap (Figure 27B). Subcellular localization pattern of ALBA5-GFP was investigated in the differentiated root hair (Figure 27C), developing epidermal cell of elongation zone (Figure 27D), and epidermal meristematic cell (Figure 27E) by the confocal microscope in green and BF channels. The revealed GFP pattern is stable across

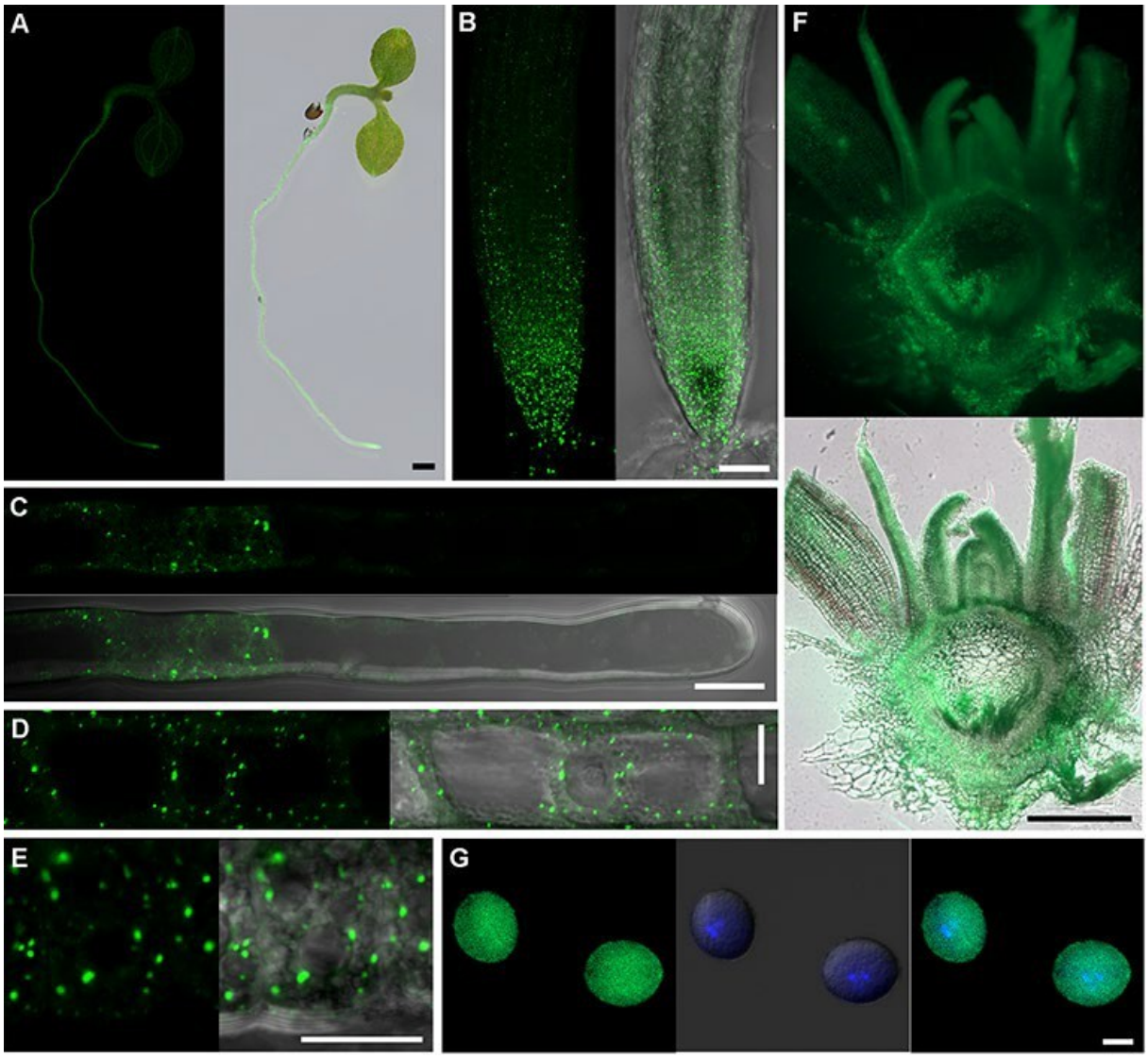

Figure 27: Subcellular localization of ALBA5-GFP controlled by sporophytic *proCsWmV* promoter. *ALBA5* genomic region was C-terminally fused with *GFP* and expressed under strong sporophytic promoter *CsWmV* control. One week old seedlings were screened for GFP signal presence (**A**) in green channel by the stereomicroscope Leica. Seedlings were collected and root tip (**B**), root hairs (**C**), cell of the root elongation zone (**D**) and meristematic zone (**E**) were captured by the confocal microscope. Juvenile plants were cut above hypocotyl and all leaves were removed by a razor. Obtained stems were cut in longitudinal direction by a microtome and captured in the GFP channel (**F**) by the fluorescence microscope and overlapped with TL. Mature pollen from adult flowering plants was collected and stained in DAPI solution for nuclei visualization. The confocal microscope was used for imaging of transgenic pollen grains in green channel for GFP detection (**G**, left), blue channel for DAPI visualization (**G**, middle overlapped with TL). Channels´ overlaps were created by post-processing. Scale bars 1mm (**A**), 500 µm (**F**), 50 µm (**B**), 10 µm (**C - E, G**).

various cell types and differentiation levels, characterized by a weak signal in the cytoplasm, enhanced by a high number of round and elongated foci. The selected seedlings were transferred to soil and cultivated at standard conditions. The signal detection was repeated in juvenile rosettes by the fluorescence microscope in the green and TL channels. The rosette stem was isolated and cut by a microtome in the longitudinal direction. The GFP signal was detected in all sectioned organs of the rosette stem except for a tissue in the central enlarged part filled with dead cells (Figure 27F). However, the transgenic stem´s morphology was distinct from that of the control plants. The diameter of rosette stems is much broader and vigorous compared to wild-type (data not shown). Plants were further cultivated at standard conditions until the flowering stage, and pollen grains were harvested from open flowers. Pollen was stained in DAPI solution and imaged by the confocal microscope with Airyscan in green, blue, and TL channels. The observation revealed a weak GFP signal, randomly distributed throughout the VC cytoplasm and probably the SC cytoplasm, without any pronounced foci being detected (Figure 27G).

Confirmed transgene overexpression in *oexALBA5* seedlings, rosettes, and adult plants influenced the phenotype of the plants. The first unusual phenotype expression of the plant individuals was observed early in development during seed germination on MS/2 media supplemented with 1% sucrose, grown in a vertical orientation. Reaction of transgenic *oexALBA5* Line 7 seeds to rehydration was slower in comparison to wild-type seeds grown together (Figure 28A). Emerged transgenic seedlings were smaller (left) in contrast to the wild-type (right) of the same age. The seedlings were grown together, and the delay in plant development was even more pronounced in later stages—juvenile rosettes produced typically abnormal true leaves with an enlarged size and lobed shape. Moreover, the true leaves were thinner than wild-type (Figure 28C). Transgenic and control plants were grown together and reached adulthood at different times due to *oexALBA5*-induced developmental delay. At the time of image acquisition, wild-type plants were almost fully mature, with only a few last flowers left on lateral branches (Figure 28B, left).

In contrast, the transgenic plants rapidly flowered and produced new flowers (Figure 28B, right). *OexALBA5* grew characteristically wide and solid primary inflorescence stems at the base and produced early lateral inflorescence protrusions. Moreover, the main inflorescences were shorter than those of the wild-type. Evolved inflorescences consisted of flowers with abnormal sepal tip bend observed already in young buds (Figure 28D). This morphological deformation could lead to altered morphology of inner floral organ, which could influence the development of siliques and result in decreased seed set.

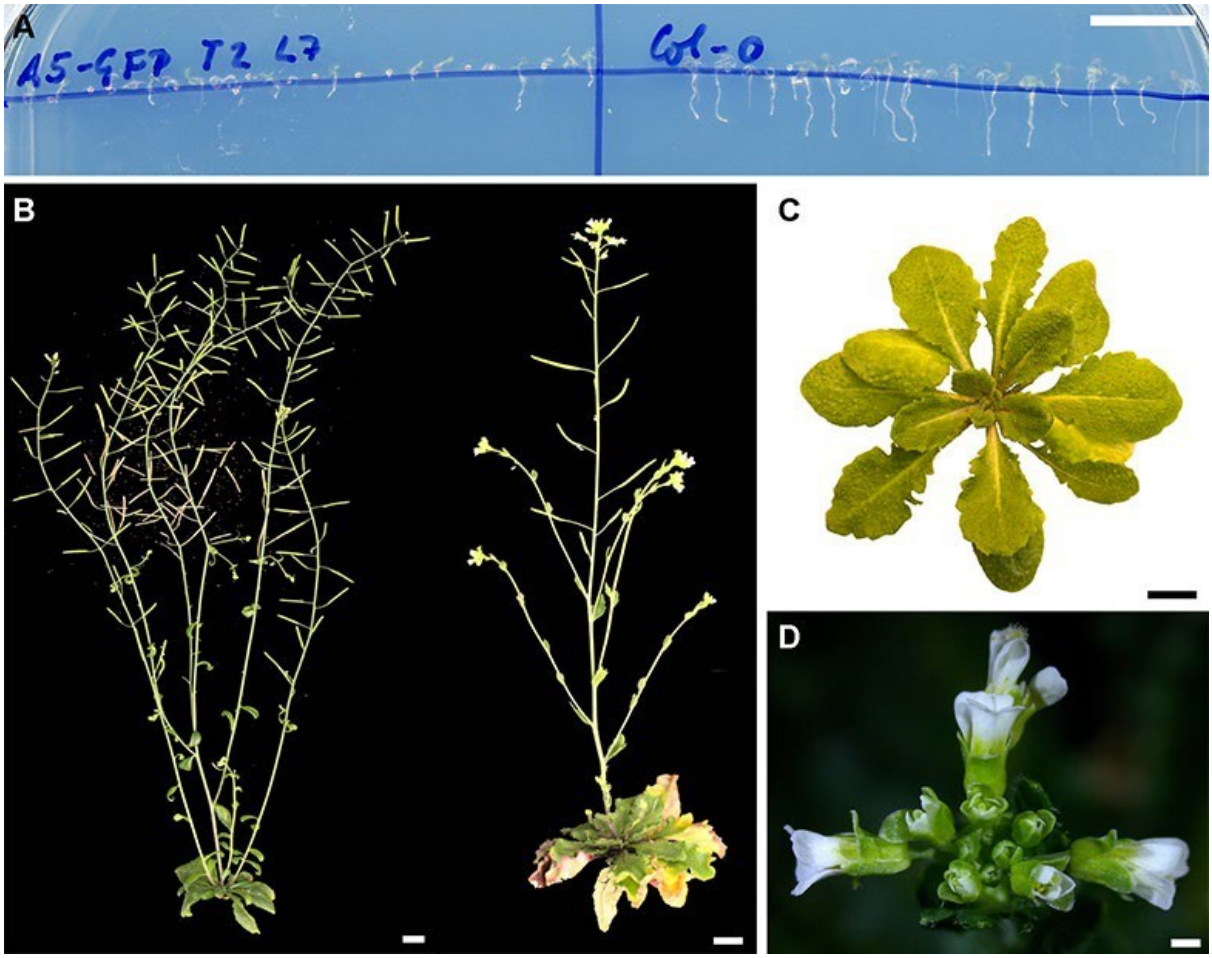

Figure 28: Phenotypic defects caused by *oexALBA5* in sporophyte development. Selected transgenic and wild-type Col-0 seeds were germinated on MS/2 media with 1% sucrose in vertical orientation. Germinating seeds were imaged 4DAG by a plate scan (**A**). Adult wild-type Col-0 (**B**, left) and *oexALBA5* Line 7 (**B**, right) plants of the same age were photographed simultaneously to visualize growth and developmental differences. A juvenile rosette was captured from an upper view (**C**) for leaf morphology visualization by a camera. An inflorescence detail was captured using the stereomicroscope Leica M205FA in TL for visualization of flower developmental stages and morphology of floral organs (**D**). Scale bars represent 1cm (**A-C**) and 1 mm (**D**).

Further, overexpression of the most distant Rpp25-like subfamily member, *oexALBA6,* was investigated. Initially, the GFP signal was detected in all seedlings´ organs with enrichment in the root differentiation zone, lateral root primordia, and root tips (Figure 29A). Further study revealed that the strongest signal distribution was homogenously dispersed in the root tip, with a gradual loss

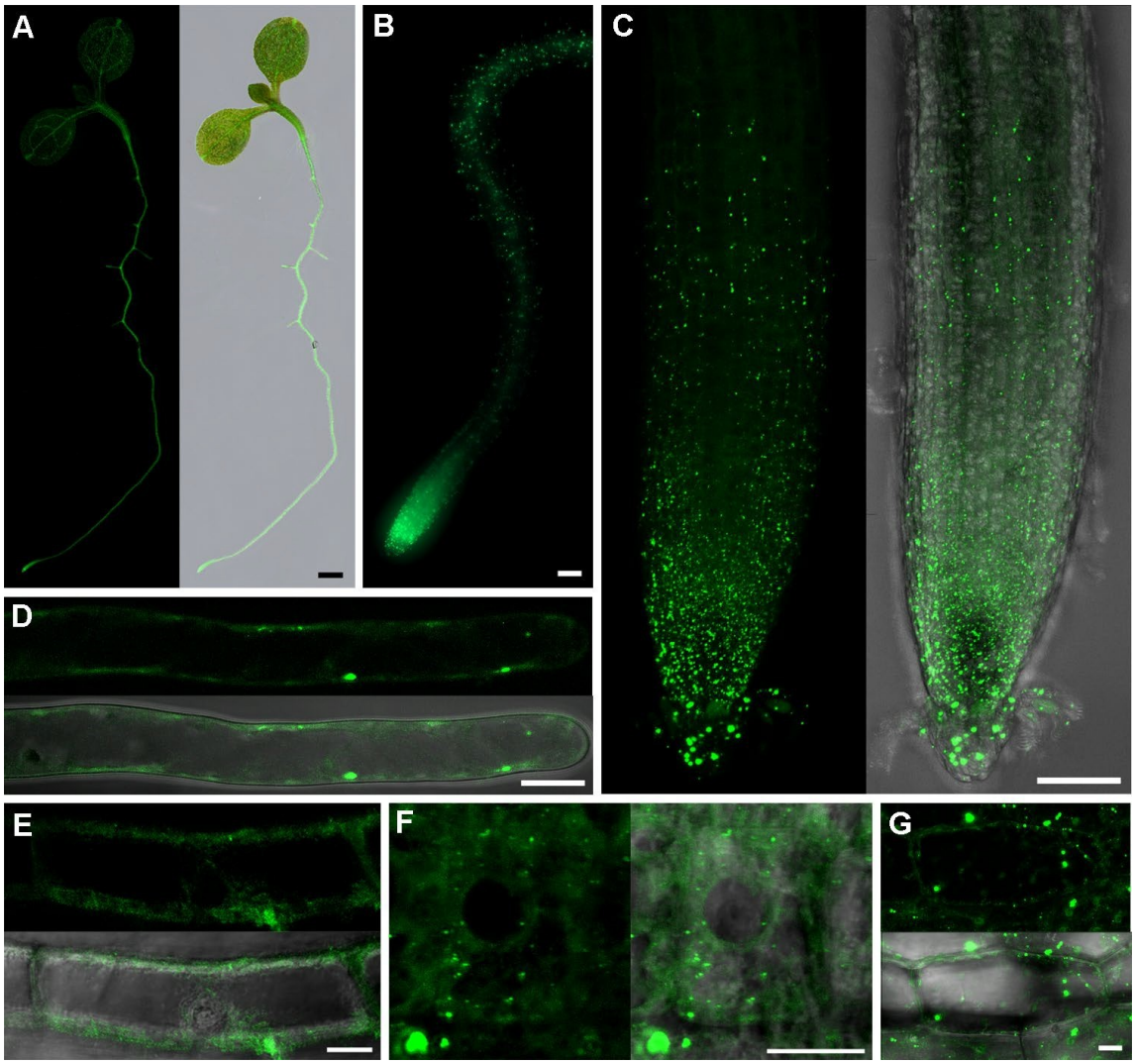

Figure 29: Subcellular localization of ALBA6-GFP controlled by the sporophytic *proCsWmV* promoter. Genomic sequence of *ALBA6* was C-terminally fused in frame with *GFP* and expressed under strong sporophytic promoter *CsWmV* control. One-week-old seedlings were collected, mounted in water, and screened for the presence of a GFP signal (**A**) in the green channel using a Leica M205FA stereomicroscope. Prepared samples were further imaged in detail of root tip (**B**), root hairs (**C**), root elongation zone cell (**D**), root meristematic cell (**E**), and hypocotyl epidermal cell (**G**). The data were captured using the fluorescence microscope (**B**) and the confocal microscope with an Airyscan detector (**C–G**). Maximum intensity projection of z-stacks and images overlap was mediated by post-processing. Scale bars 1mm (**A**), 50 µm (**B, C**), 10 µm (**D - G**).

towards the elongation zone. The localization pattern was characteristically enriched by pronounced larger foci (Figure 29B, 298C). The foci are clearly identified against the weak cytoplasmic background in the root tip, with the highest number concentrated around the cell proliferation center, and a gradual decline in their number towards the root elongation zone (Figure 29C). Details of the subcellular signal localization were imaged in various cell types. The acquired data were comparable to the previously documented characterization of other subfamily members, though they differed in the number and size of foci. The GFP emission of *oexALBA6*-harbouring cells is distributed predominantly in the cytoplasm, accompanied by several small foci followed by a few bright elongated accumulations identified in differentiated root hair (Figure 29D) and the root elongation cell (Figure 29E). A more granular pattern was detected in the metabolically active meristematic cell. Although the predominant signal localization was homogenously distributed in the cytoplasm, miniature foci were gathered in a few populations (Figure 29F). Large foci accompanied by a weak signal distribution in the cytoplasm were also recorded in hypocotyl epidermal cells, representing another type of differentiated tissue (Figure 29G).

The observed phenotypic defects described in *oexALBA4* and *oexALBA5* plants were partially recorded in *oexALBA6* individuals. Juvenile rosettes were grown in soil at standard conditions until the adult rosette stage. A rosette stem was isolated, fixed in agar, and cut in the longitudinal direction by a microtome. Individual slices were mounted in water and observed by the fluorescence microscope. The GFP emission was detected in all tissues except for the central part of the stem (Figure 30A). A detail of the SAM area was captured in the same way and revealed a homogenously dispersed green signal in all cell layers and developing organs (Figure 30B). The plants were cultivated at standard conditions and revealed similar phenotypic alterations characteristic of the subfamily, including early lateral inflorescence appearance (not shown) and alterations in inflorescence size and shape caused by non-standard flowers (Figure 30C). The sepals in all captured buds and developing flowers were bending outward, which caused the underdeveloped pistils and anthers to be exposed to outer conditions. Localization of the GFP marker was further investigated in flowering individuals. Floral organs were collected and mounted in water on a slide, and the epidermal cells of the sepals were captured by the confocal microscope in green and red channels. Green emission was predominantly detected, aligned with pavement cell borders, and homogeneously distributed in the cytoplasm, accumulating in small foci. The green channel is presented overlaid with chloroplast autofluorescence in the red channel (Figure 30D). Pollen grains were collected from open flowers and investigated in detail. Pollen was mounted in DAPI solution and imaged in green and blue channels using the confocal microscope Zeiss LSM 880 with an Airyscan detector. A weak cytoplasmic signal in VC was detected with the characteristic pattern of a reticular-like localization (Figure 30E) enriched by a few stronger foci partially aligning MGU and SC nuclei (Figure 30F). Although some alterations are

typical for all members of the Rpp25-like subfamily, others are shared only by the two closest homologs.

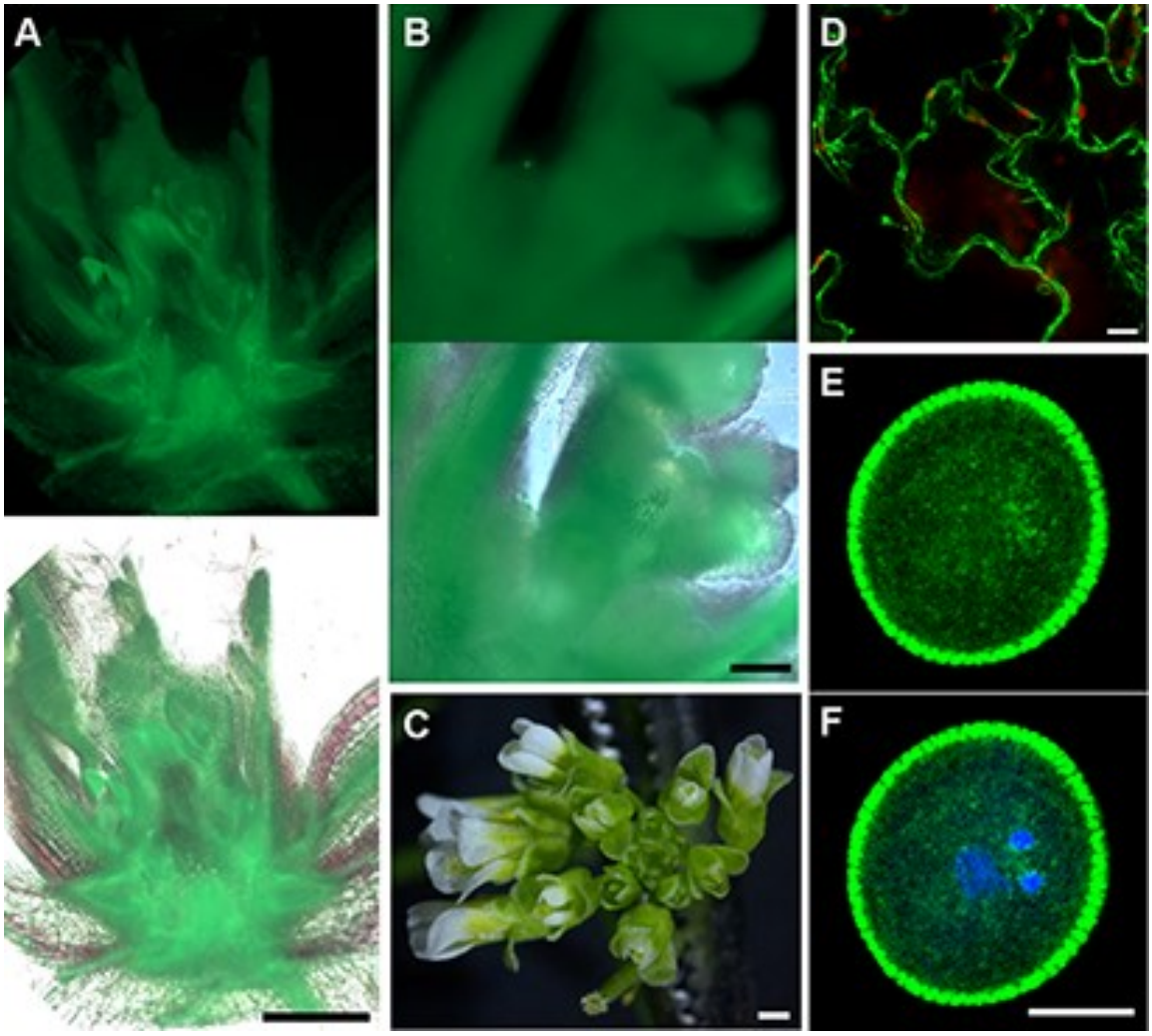

Figure 30: GFP signal localization and phenotypic defects caused by *oexALBA6* to sporophyte development. Juvenile rosettes were cut above the hypocotyl, and all true leaves were removed with a razor. A rosette stem was cut in the longitudinal direction using a microtome into slices and then captured by the fluorescence microscope in green and TL channels. Stem sections were captured, and GFP distribution was visualized (**A**). The detail of SAM was imaged in green, and the TL channel (**B**). Inflorescence detail was captured using the stereomicroscope from the top for visualization of flower developmental stages (**C**). Sepals from an opened flower were removed and imaged using the confocal microscope in the GFP channel and the red channel for chlorophyll emission; the overlap of the channels is shown (**D**). Mature pollen was harvested from open flowers, stained in DAPI solution for nuclei visualization, and GFP signal emission was captured (**E**). The signals from the green (GFP) and blue (DAPI) channels were overlapped by post-processing (**F**). Scale bars 500 µm (**A**), 100 µm (**B**), 1mm (**C**), 10 µm (**D**, **F**).

4.4.3.5. Evaluation of the Rpp25-like subfamily flowering delay

A considerable number of seeds were sown to produce sufficient populations; however, the low seed germination ratio often affected the size of the growing population. Therefore, more populations and independent lines with verified transgene overexpression were grown, and the transition to the generative phase was measured for each individual. Plants were cultivated under the same conditions and regularly watered with fertilizer. Juvenile and flowering individuals considered by the first opened flower presence were counted every day. Plants of six genotypes were selected for the experiment: the *alba456* homozygous mutant line, wild-type Col-0 controls, and *oexGFP* and tested *oexALBA4-6* lines. Acquired measurements were analysed by R software with the ggplot2 package (R Core Team, 2018) and visualized by violin and box plot graphs (Figure 31).

Although primary datasets were reasonably sufficient, their size was decreased by further statistical analyses. The data were tested for normality using the Shapiro-Wilk test, and it was revealed that they were drawn from a normal distribution (p-value 0.01611) at a 0.05 confidence interval. Simultaneously, Cook´s distance indicated that suspicious measurements had an impact. These tests were repeated until a few unreliable values were removed. The analysis continued according to the Shapiro-Wilk test result. A non-parametric Kruskal-Wallis test was used for comparing population medians. A significant difference in medians was indicated by a p-value of 2×10^{-16} with the 0.05 confidence interval. Therefore, exact population pairs with statistically significant differences were identified by Dunnett´s test with the Bonferroni correction (Dinno, 2015). Firstly, control populations, including wild-type Col-0 and *oexGFP*, were tested and showed no statistical differences. Therefore, a single control sample merging these two populations was created, with a median of 27 days after plant germination. According to Dunnett´s test, the same result was calculated for the *alba456* triple mutant (median at 28 days) and *oexALBA6* (median at 33 days). Although variability and slowed flowering induction were observed in these two plant populations, the calculated median values did not reveal a significant difference compared to the Control sample. According to the observed developmental delay, the *oexALBA4* and *oexALBA5* populations were assumed to be statistically distant from the Control. This hypothesis was confirmed by the pairwise Dunnett´s test for both tested populations. A significant difference at a 0.05 confidence interval was revealed between the Control (median at 27 days) and *oexALBA4* (median at 47 days) populations, followed by the same result for Control and *oexALBA5* (median at 48 days). Violin graphs with inserted box plots were created for each genotype and the Control sample (x-axis), indicating the flowering period of each genotype in days (y-axis). Box plots indicate medians, quartiles, minimal and maximal values, accompanied by outliers that have no impact. The violin graphs display considerable variability between populations and clearly illustrate the dispersion of the populations.

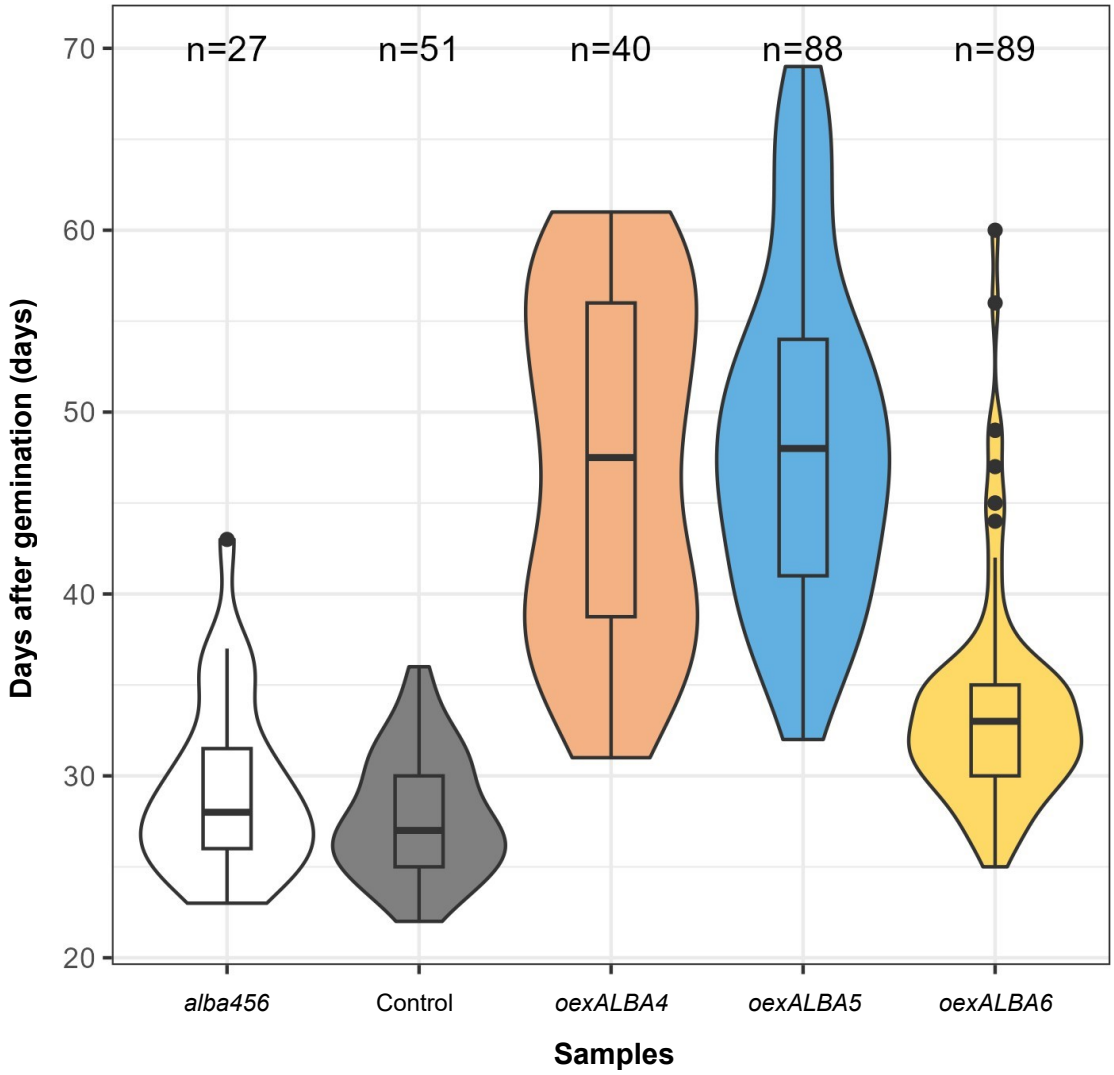

Figure 31: Violin and box plot graphs of flowering individuals in the studied samples. Populations of the investigated samples were grown under standard conditions, and measurements were taken each day from the first opened flower until all individuals reached the flowering stage. Boxplots were merged with violin graphs to show medians (back bars), quartile ranges, and outliers, while violin graphs indicate data variability. Numbers of counted individuals per sample are displayed above (n).

4.4.3.6. Evaluation of seed malformations in Rpp25-like subfamily

Phenotypic characterization of the Rpp25-like subfamily revealed reduced seed sets in fully developed siliques. Therefore, the flowering plants were observed, and distinct siliques at various stages of development were collected. Specifically, 6^{th}, 7^{th}, and 8^{th} siliques were cut from the main inflorescence stem together when the distal end of the oldest silique turned yellowish. At this stage, all seeds in the Control sample (Col-0, *oexGFP,* and *oexGUS-GFP*) are mature. Collected siliques were fixed on a slide, and valves were cut off for the seed set analysis. The first analysis indicated

the presence of seeds with distinct phenotypes, including wild-type and aberrant. While siliques of wild-type Col-0, *oexGFP,* and *oexGUS-GFP* individuals were collected and analyzed at approximately the same time, approximately 5 weeks after plant germination, plants with Rpp25-like subfamily overexpression cassettes were grown for almost two months to reach the same stage of development.

A predominant seed population was developed according to the standard program and exhibited a shared wild-type phenotype in all samples (Figure 32). However, variability in the frequencies of the wild-type and aberrant seed phenotypes was revealed. Initial analysis showed similar results of wild-type Col-0, *oexGFP* Line 4-61, and *oexGUS-GFP* Line2-41 measurements. Data from these control samples were merged due to their insufficient number. Both control lines share a homozygous genotype and frequencies of seed set phenotypes. The investigated samples are more distinct in terms of the wild-type and aberrant seeds ratio. Analysed seed sets included a genotype mixture

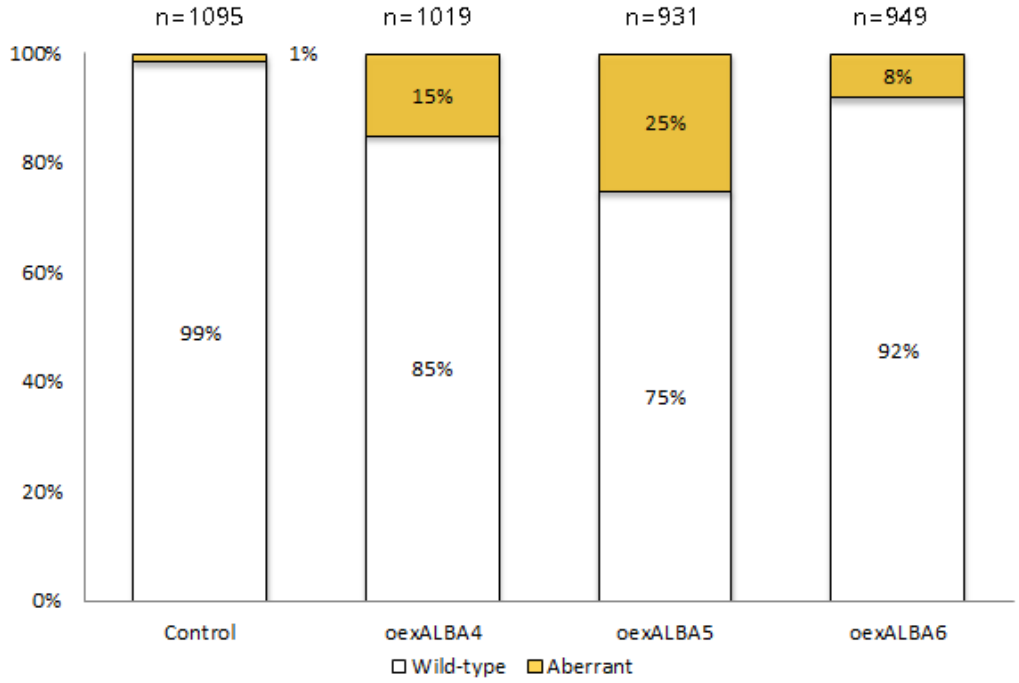

Figure 32: Graphical visualization of wild-type and aberrant seeds observed in the *oexALBA* and Control. Three siliques of the main inflorescence stem were harvested from each sample plant. Every 6th to 8th silique was collected when the oldest pistil green color faded. Siliques were fixed by both-side tape on a slide and placed under the stereomicroscope Leica M205FA. Each silique was cut by a needle along both sides of replum, valves were opened and fixed by the tape. Wild-type (white) and aberrant seeds (yellow) were counted and frequencies of the observed phenotypes were calculated for each sample. Control sample contains wild-type (Col-0), *oexGFP* Line 4-61 and *oexGUS-GFP* Line2-41 and segregating samples *oexALBA4* (Line 2 and Line 7), *oexALBA5* (Line 2 and Line 7) and *oexALBA6* (Line 2 and Line 12). Seed counts are displayed (n).

of segregating generations, homozygous, and heterozygous offspring. Two lines were analyzed for each sample, with verified overexpression confirmed by RT-qPCR (see Figure 16), and exhibited very similar phenotypic aberrations during plant development. Although the timing of transition to the generative phase is postponed and floral organ development is affected, pollination and seed production are not severely affected. Seed sets of *oexALBA4* Line 2 and *oexALBA4* Line 7 consist of 85 % wild-type and 15 % aberrant seeds. Seed production is mostly affected in the *oexALBA5* sample, represented by two lines (*oexALBA5* Line 2 and *oexALBA5* Line 7), with a drop to only 75% wild-type seed production. The least affected sample is *oexALBA6*, represented by *oexALB6-GFP* Line 2 and *oexALBA6* Line 12, which rarely differ from the Control. The affected germination rate displayed in chapter 4.4.3.4 stimulated the study of the particular seed morphology.

Aberrant seeds were investigated in detail, which initiated their separation into individual phenotypic classes. Four aberrant phenotypes were recorded in mature seeds (Figure 33). Three of these classes usually result in reduced seed sets in mutant plants, including aborted ovules, aborted seeds, and white seeds. The fourth class of "hemianatropous seeds" is not typical. The first class includes unfertilised ovules which were not reached by any pollen tube and degrade during silique development into rudimental structures attached to funiculi. The second class consists of fertilized ovules that develop into seeds but are arrested early in embryo development, forming small, white, aborted seeds. The third class of phenotypic defects involves immature seeds arrested in later developmental stages. Their size is similar to that of mature seeds, and the typical white or brown colour is caused by a small embryo occupying only a portion of the volume. These seeds usually contain embryos in the heart or torpedo stages. The last observed phenotype was probably induced early in ovule development. Angiosperm ovules originate straight and, during successful development, curve and finish in amphitropous orientation. The curvature of a micropylar entrance to the funiculus is very narrow, typically less than 45°. The seed sac curvature in "hemianatropous seeds" identified in *oexALBA* samples varies from straight (180°) to the hemianatropous orientation (90°).

Frequencies of the aberrant phenotypic classes in the three investigated samples and the control are shown graphically. A sole phenotypic aberration, aborted seeds, was recorded in the Control sample, while the other three classes were not observed at all. Aborted seeds represented half of the non-standard seeds and ovule derivates in the *oexALBA4* sample and less than 20 % in *oexALBA5* lines. Investigated seed sets typically possessed a higher number of aborted seeds in siliques that were rapidly growing, ranging from 14% in the *oexALBA4* sample to almost 60% in the *oexALBA5* and 71% in the *oexALBA6* sample, as calculated from the total aberrant seed counts. White seeds with embryos arrested in the heart or torpedo stages were found only in *oexALBA5* and *oexALBA6* individuals in up to 6 % of the abnormal seed population. The most specific class was found in the *oexALBA* samples with almost uniform distribution varying between 25 % in *oexALBA4,* 18 % in *oexALBA5*,

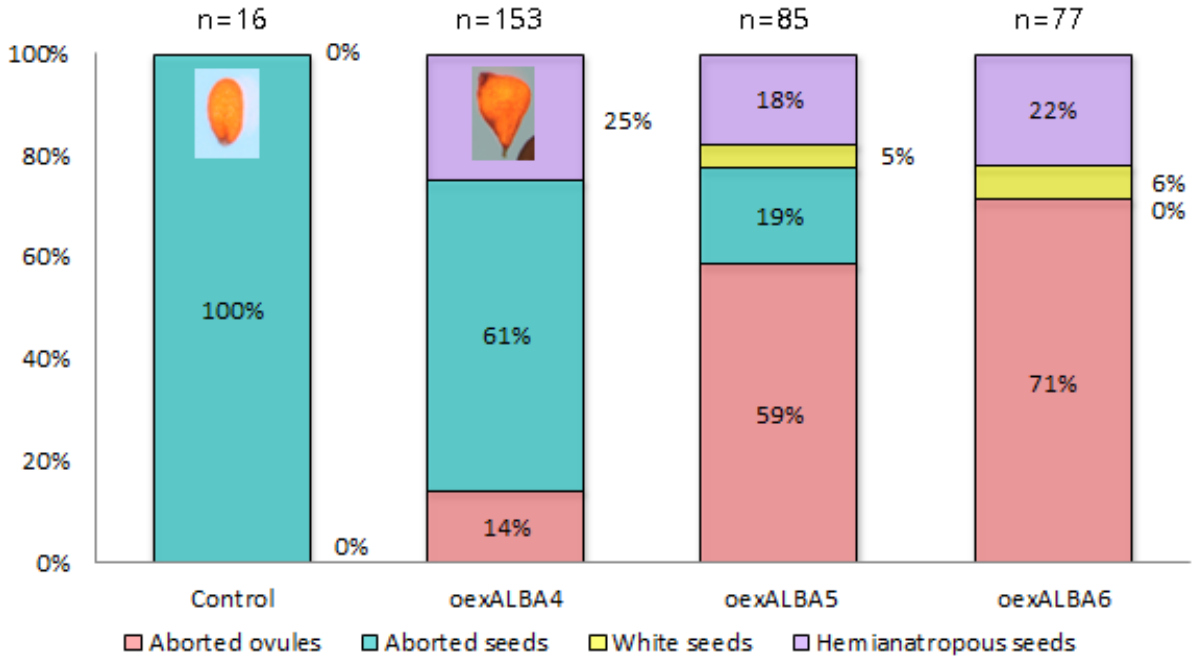

Figure 33: Graphical visualization of individual seed defects detected in the *oexALBA* and Control samples. Collected siliques were fixed on a slide using both-sided tape. Aberrant seeds were counted and distributed into four classes: aborted ovules, aborted seeds, white seeds, and "Hemianatropous seeds". Examples of wild-type seeds in the Control column and hemianatropous seeds in the *oexALBA4* column are displayed. Images were captured using the stereomicroscope Leica M205FA in red and TL channels, which were then merged in LasX software. The frequencies were calculated for all investigated genotypes: homozygous Control (Col-0, *proCsWmV::GFP* Line 4-61) and segregating samples *oexALBA4* (Lines 2 and 7), *oexALBA5* (Lines 2 and 7), and *oexALBA6* (Lines 2 and 12). Total counts of aberrant seeds are displayed (n).

and 22 % in *oexALBA6*. Although silique length is not affected by sporophytic overexpression of the Rpp25-like subfamily genes, the produced seeds possess a few phenotypic abnormalities that could influence the germination ratio. All detected aberrations could be caused by underdeveloped ovules, which create asynchrony in ovule and pollen development and decrease the probability of fertilization. Moreover, even the fertilized ovules and developing seeds can be delayed by slowed growth, which could result in desiccation of seeds with immature embryos. These seeds do not have to possess significant phenotypic defects; however, desiccation of the underdeveloped embryo could affect their ability to germinate, which may explain the observed germination rates.

The only severely affected seed production was recorded in *oexALBA5* lines, with only 75% of wild-type seeds and 25% of aberrant phenotypes, including all four observed classes of defects. In contrast, the *oexALBA4* sample did not produce "white seeds," and the *oexALBA6* line lacked the "aborted

seeds" phenotype. Therefore, the impact of Rpp25-like subfamily members on seed development presumably differs. The recorded variability could be explained by their implementation in various processes at distinct stages, resulting in specific phenotypic alterations that are manifested either before or after fertilization.

4.4.3.7. Molecular characterization of flowering delay in Rpp25-like subfamily

The most severe effect induced by the Rpp25-like members' overexpression influences the timing of flowering, an essential time point for plant reproduction. The origin of this phenotype was investigated on the molecular level. Only lines with verified overexpression of *oexGFP* control and *oexALBA* samples were grown under standard conditions and their distinct parts were collected when the developmental stage of interest was reached. Collectively, four samples were gathered from three developmental stages. The first two samples were collected from young and adult rosettes. Whole stems, including SAM, were collected from juvenile (6-leaf stage) developing rosettes (first sample) and adult rosettes (second sample). The following two samples were harvested from flowering individuals and separated into meristematic and non-meristematic tissues of a stem. The oldest parts of the stem internodia lacking apical meristems (third sample) were harvested from flowering plants at the same time as main inflorescence tips containing active meristems and developing buds up to the first opened flower (fourth sample). All samples were collected within a 3-hour window at the same time of day. Harvested tissues were immediately frozen in liquid nitrogen. Total RNA was extracted and treated with DNase according to chapter 3.13. RNA integrity was checked by running a portion of it on a 2% agarose gel. Prepared RNA samples were sent for RNA sequencing in three BRs. The raw data were processed and controlled (not shown). Transcript levels of each *oexALBA* sample were normalized by the control *oexGFP* sample isolated from the same developmental stage and tissue, resulting in background elimination. The filtered data were analysed by Panther 19.0 Overexpression test to identify distinct pathways grouping significantly affected genes by Gene Ontology processes. Relations of commonly dysregulated genes were visualized by DiVenn diagrams.

Firstly, the investigation of *ALBA* genes' transcription level did not show any significant changes throughout the family in any of the samples. Moreover, overexpression of *ALBA4*, *ALBA5*, and *ALBA6* was once more confirmed in all respective samples, with the exclusion of *ALBA6* overexpression in adult rosette stems. Then, a transcriptome analysis was performed to identify genes differentially affected in the context of the investigated genotypes across distinct developmental stages and organs responsible for signal integration leading to flowering promotion. Although *ALBA4* and *ALBA5* are highly related, whereas *ALBA6* is more evolutionarily distant, their overexpression shares some features and plausibly indicates variable phenotypic expression between the *oexALBA* tissues. There were commonly identified larger portions of upregulated genes than downregulated genes; moreover, some samples had no downregulated genes at all. At the level of investigated *oexALBA* genotypes,

655 transcript levels were significantly dysregulated in *oexALBA4*, 2730 in *oexALBA5*, and only 179 genes were affected in *oexALBA6*. A prevailing part of these transcript levels was related to timing and the transition to the flowering stage, particularly with pathways involved in regulating the circadian rhythm. Schematic relations of the commonly and solely dysregulated genes between developmental stages and tissues are displayed on three DiVenn diagrams (Figure 34).

The most common upregulated molecular processes across all investigated tissues were found in *oexALBA4* samples (Figure 34A). All identified pathways were connected with sensing of light (response to red light, regulation of photoperiodism and flowering) and temperature (response to cold and abscisic acid). Adult rosettes and flowering plants showed additional upregulated genes that encode proteins involved in the blue light response, the transition to the reproductive phase of development, and the regulation of flower development. In stems taken from adult rosettes and older inflorescences, genes that are significantly upregulated and related to leaf senescence, reactive oxygen species (ROS), and salicylic acid responses were identified. On the other hand, within these tissues, there were significantly downregulated genes involved in photosynthesis, regulation of stomatal closure, and response to light (red light and far-red light).

The most genes with affected expression were recorded in *oexALBA5* samples. Nevertheless, from a pool of affected genes, only compounds related to the circadian rhythm were upregulated in all tissues and developmental stages (Figure 34B). In juvenile rosette stems and samples collected from flowering individuals, elevated transcript levels of light response compounds (red light and blue light), which facilitate the transition to the reproductive phase of development, as well as photoperiodically induced flowering activators and factors controlling flower development, were identified. Nevertheless, genes encoding proteins involved in leaf senescence were already upregulated in young rosettes and persisted until the flowering stage in old stems, accompanied by enhanced regulators of response to abscisic acid. Interestingly, genes encoding products involved in photosynthesis (light-harvesting complex (LHC) of photosystems I and II), including those involved in ROS biosynthesis, were downregulated in the stems of adult rosettes and flowering stem internodia.

Lastly, the *oexALBA6* does not induce a dramatic effect on plant growth and development, including flowering, as indicated by the previously presented results (chapter 4.4.3.4) and data from RNA sequencing, which support the previous observations and analyses (Figure 34C). In the RNA sequencing dataset, the low number of dysregulated genes was not associated with any pathway or developmental process that would be similarly influenced across all *oexALBA6* samples. Nevertheless, a few modulators of the circadian rhythm, factors involved in red light sensing, and florigens, which depend on photoperiod, were significantly upregulated in stems isolated from juvenile rosettes and flowering plants. However, their impact on flowering promotion was probably not sufficient, according to the insignificance of the quantified measurements in chapter 4.4.3.5.

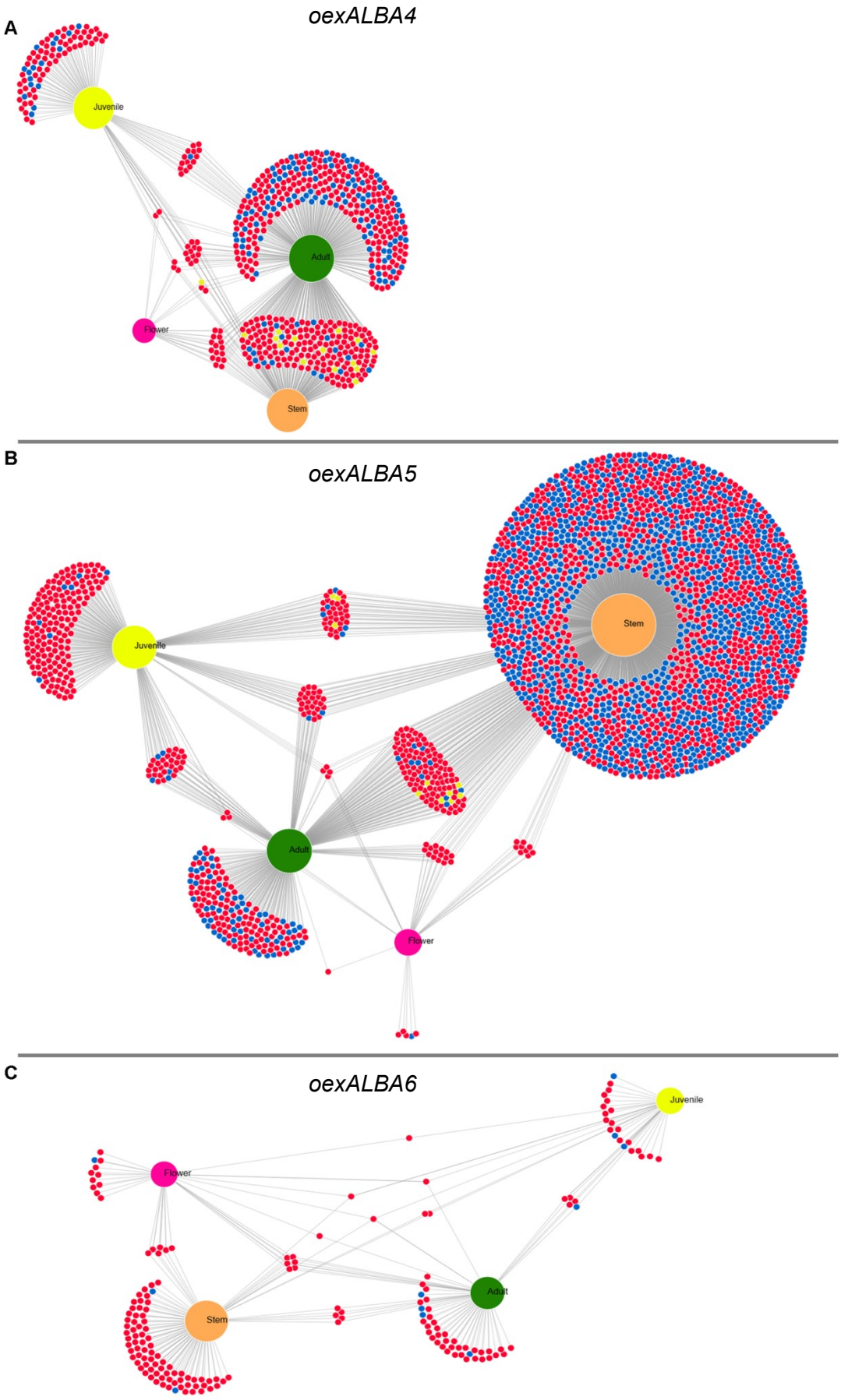
A
oexALBA4
Juvenile
Adult
Flower
Stem
B
oexALBA5
Stem
Juvenile
Adult
Flower
C
oexALBA6
Juvenile
Flower
Adult
Stem

Figure 34: DiVenn diagrams of dysregulated genes in stems throughout plant development on *oexALBA4*, *oexALBA5*, and *oexALBA6* backgrounds. Total RNA was extracted from harvested stems of juvenile and adult rosettes, old stem internodes, and inflorescence tips, and processed for RNA sequencing in three BRs. The acquired data were processed, and changes in overexpressing samples were revealed by normalization to the *oexGFP* control. All significantly affected genes were filtered, and DiVenn diagrams were created by https://divenn.tch.harvard.edu/. Individual samples of the investigated stages are shown: juvenile (juvenile rosette, yellow), adult (adult rosette, dark green), stem (old stem of a flowering plant, orange), and flower (inflorescence tip, pink). The diagrams were created separately for *oexALBA4* (**A**), *oexALBA5* (**B**), and *oexALBA6* (**C**). Upregulated genes are shown in red, downregulated genes are in blue, and up- and down-regulated genes are in yellow.

Overall, these data indicate that the oex*ALBA* plants showed a rapid transition to the generative stage of development compared to the control. Although the sampling was dependent on plant stage, up-regulation of the mentioned factors most likely enabled a much earlier achievement of flowering competence.

The obtained normalised data were further compared according to harvested tissue and developmental stage. Therefore, four DiVenn diagrams were created to illustrate genes with a change in regulation within one plant organ in the investigated *oexALBA* samples (Figure 35). A total of 324 uniquely expressed genes in transgenic juvenile rosettes, 685 regulated transcripts in adult rosettes, 2,389 genes with significant changes in old inflorescence stems, and 49 affected genes in inflorescence tips were identified.

Although all juvenile rosettes solely overexpressing Rpp25-like subfamily members share 13 genes that are significantly upregulated, only six genes were affected in the same way in *oexALBA5* and *oexALBA6* samples, and 65 genes were shared by *oexALBA4* and oexALBA5. Surprisingly, no genes were found to be shared between *oexALBA4* and *oexALBA6* in juvenile rosettes. Further, no pathway or molecular process regulating flowering in later stages was identified, which can be attributed to the low number of affected genes at this stage (Figure 35A). The same result was recorded in stems isolated from adult rosettes. All transgenic genotypes share a group of 33 genes that are affected. An additional five genes are identically upregulated in *oexALBA4* and *oexALBA6,* followed by two genes that are significantly influenced by both *oexALBA5* and *oexALBA6* (Figure 35B). The only *oexALBA4* and *oexALBA5* samples share a sufficient number of affected genes, with 211 upregulated and 33 downregulated, which are connected to flowering regulation. Within the elevated transcripts, genes encoding regulators of the circadian rhythm, cold acclimation, and response to ROS

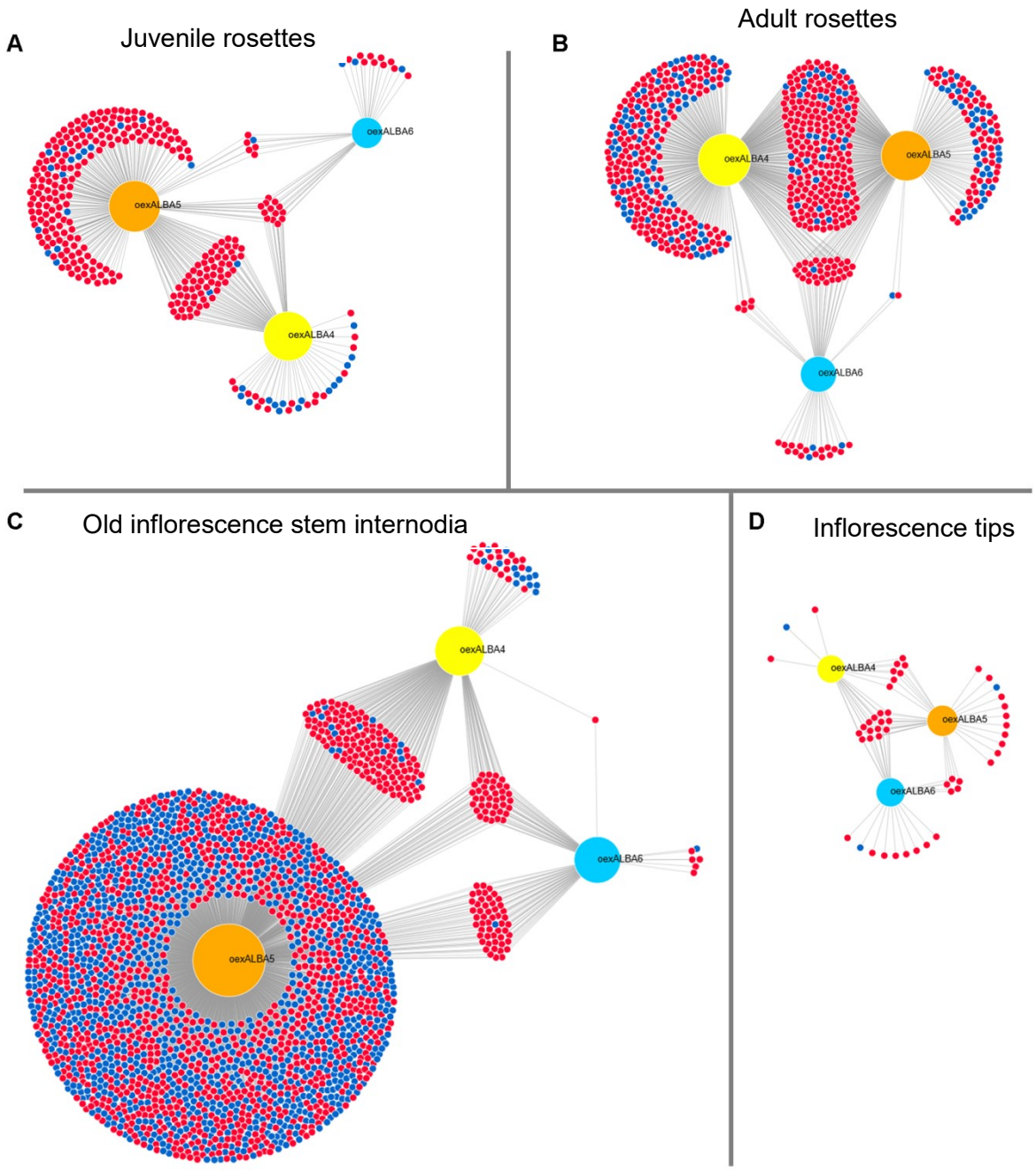

Figure 35: DiVenn diagrams of significantly dysregulated genes in *oexALBA4*, *oexALBA5*, and *oexALBA6* samples in distinct tissues and developmental stages. Samples were prepared from stems of juvenile and adult rosettes, old stem internodia, and inflorescence tips, including buds up to the first opened flower. Collected material was frozen and processed for RNA sequencing in three BRs. The acquired data were processed, and significant changes in the samples were revealed by normalization to the *oexGFP* control. Transcripts with variable abundancy were selected, and DiVenn diagrams were created by https://divenn.tch.harvard.edu/. Tissues collected in individual developmental stages are shown separately; stems from juvenile rosettes (**A)** and adult rosettes (**B**), old stem of flowering plant (**C**), and main inflorescence tip (**D**). Genotypes are shown in yellow (*oexALBA4*), orange (*oexALBA5*), and blue (*oexALBA6*). Upregulated genes are shown in red, downregulated genes are in blue.

were identified, which are connected with pathways involved in leaf senescence and response to salicylic acid. On the other hand, within genes with downregulated activity, members of LHC-regulated photosynthesis, light quality, and ROS responses were identified. Even in the generative stage of all six samples, some of these factors persist (regulators of circadian rhythm and response to cold), while others change significantly (Figure 35C, D). In the old stems of inflorescence internodia, the hyperactivation of ROS response genes continues in all samples, whereas the upregulation is lost in inflorescence tips. Moreover, there are significantly upregulated genes encoding mediators that sense blue, red, and far-red light in old stem internodia, in contrast to younger stages (Figure 35C). Although activation of genes involved in the blue light pathway persists only in *oexALBA4* and *oexALBA5* inflorescence tips, all samples share upregulated genes of photoperiodically-induced florigens (Figure 35D). Nevertheless, downregulated levels of LHC compounds were identified in *oexALBA4* and *oexALBA5* internodia, though no downregulated genes were significantly affected in inflorescence tips at all.

Although the phenotypic characteristics caused by Rpp25-like subfamily overexpression are visible from the earliest phases of plant development, such as seed germination delay, the first morphological changes appear in juvenile rosettes. An accumulated dysregulation of targeted genes may mediate the observed phenotypic aberrations. Nevertheless, affected comprehensive pathways responding to the physiological state of individuals by effectors promoting plant competence to flowering were found later, in adult rosettes. Interestingly, among the downregulated genes, functionally related groups involved in energetic metabolism and maintenance of homeostasis were identified, two fundamental processes essential for plant fitness. Nevertheless, compounds involved in pathways for coping with ROS were upregulated across all created genotypes in flowering stem internodes, highlighting the instability of the cells' inner state. Moreover, a significant elevation of genes involved in light quality sensing was found in *oexALBA4* and *oexALBA5* samples. All collected inflorescence tips, consisting of rapidly developing flower buds, shared upregulated genes controlling the expression of florigens in a photoperiodically dependent manner, marking exceptional sensitivity to their perception. On the other hand, instead of early flowering promotion caused by the competence achievement before control plants, the targeted individuals presumably do not respond or integrate signals correctly. Therefore, all highlighted connections require further investigation through independent experiments. The suggested implications propose new, detailed hypotheses that need to be validated.

Meanwhile, *oexALBA* and *oexGFP* juvenile rosettes were treated at 37 °C for 3 hours. The acquired data from treated *oexALBA* samples were normalized to the heat-treated *oexGFP* control, and significantly affected transcripts were identified. The upregulated and downregulated transcripts from the genotypes of interest were visualized by a DiVenn diagram (Figure 36). A total

of 418 affected genes were identified, with an equal distribution between upregulated and downregulated genes in *oexALBA4* juvenile rosette stems compared to the *oexGFP* heat-treated control. From 386 dysregulated genes in *oexALBA5,* 277 transcripts were upregulated while 109 were downregulated. In heat-treated *oexALBA6,* only 40 genes were significantly affected; of these, 12 genes were upregulated, and 28 genes were downregulated. The diagram clearly shows a remarkable group of transcripts shared by the closest homologs (*ALBA4* and *ALBA5*) comprising 118 upregulated and 29 downregulated genes. Among upregulated genes, factors associated with heat response and acclimation pathways were identified, including compounds involved in chaperone-mediated protein folding. These enhanced processes were followed by another interlinked symphony, maintaining redox homeostasis through elevated levels of genes encoding factors for protein oligomerization processes, as well as responses to hydrogen peroxide and hypoxia. On the other hand,

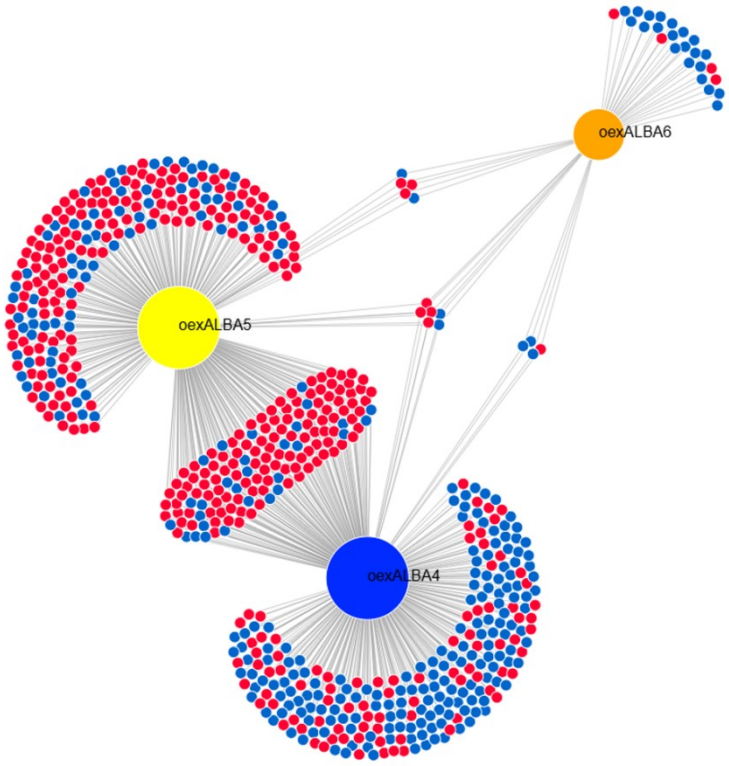

Figure 36: DiVenn diagram of significantly affected transcripts isolated from juvenile rosette stems of *oexALBA* treated by HS. Juvenile rosettes were heat-stressed by (37 °C/ 3 hours), and stems were immediately harvested and frozen. Total RNA was isolated, processed, and sent for sequencing in three BRs. Acquired data were normalized to the heat-treated *oexGFP* control. Significantly affected transcripts were filtered and are presented in a DiVenn diagram (https://divenn.tch.harvard.edu/). The three samples, *oexALBA4* (blue), *oexALBA5* (yellow), and *oexALBA6* (blue), are shown, with upregulated (red dots) and downregulated (blue dots) genes visualized.

downregulated transcripts shared by *oexALBA4* and *oexALBA5*, as well as all groups of transcripts, including those affected by *oexALBA6*, were probably too narrow and inconsistent for involvement in a complex pathway (4 to 6 genes). In the *oexALBA4* sample, downregulated transcripts related to three pathways influencing flowering competence were identified. These include activators of leaf senescence and regulators of vegetative phase termination, along with factors crucial for maintaining intermediate meristem identity, specifically *SOC1*.

According to the acquired data, the most sensitive sample to the applied HS is *oexALBA4,* followed by *oexALBA5,* whereas *oexALBA6* exhibits a reduced number of affected genes. The difference between the closest homologs and *oexALBA6* was enhanced by the predominant number of downregulated genes, although no common downregulated pathway was identified within the two related genotypes. On the other hand, genes involved in response to HS and acclimating to ease redox homeostasis were significantly upregulated within *oexALBA4* and *oexALBA5* juvenile rosette stems. In the *oexALBA4* background, unique pathways were upregulated, connected by an antagonistic role against the transition to the generative phase of development. Overall, acquired data needs to be further processed and investigated in detail. Although significantly dysregulated pathways connected to flowering promotion were presented, a deeper study of the comprehensive data collection could reveal new directions of interest. Furthermore, the mentioned significantly affected pathways correspond to the observed phenotypic aberrations; the direct involvement of ALBA proteins in these processes needs to be proven by targeted methods.

5. Discussion

Flowering represents a crucial developmental stage of Angiosperm plants facilitating germ lines identification and gametophytes production. From seed germination to successful reproduction, each individual must cope with environmental changes. Long-term stress-induced disruption of cell processes gradually remodels the morphology and physiology of tissues and organ structure. These modifications promote obstacles in later developmental stages and reduce the likelihood of successful offspring. Throughout last years, the RBPs gained increasing significance in molecular, cellular and physiological processes maintaining homeostasis secured by RNA stability, translatability, localization, storage and protection along with the metabolic machineries. This study revealed similar characteristics of Alba-family proteins' behavior to RPBs and suggested their plausible connection.

5.1. Elucidation of the ALBA role in pollen nuclei

Although specific targeting of ALBA-YFP was expected to stabilize suspected protein shuttling in the nucleus, the obtained results revealed two localization patterns: nuclear and cytoplasmic. Within the Rpp20-like subfamily, only NLS-ALBA3-YFP was targeted explicitly to pollen nuclei of stable transgenic lines. Interestingly, the revealed nuclear pattern was partially shared with the distribution of transiently expressed ALBA1 and ALBA2 in mesophyll protoplasts (Yuan et al., 2019). For this similarity, the extensive stabilization of ALBA3 in VC nuclei could be attributed to active sites of chromatin, where hybrid molecules, R-loops, are formed by the characteristic massive transcription of the VC. The transcriptionally active sites are susceptible to DNA damage, especially oxidative DNA damage (Ljungman et al., 1992). Moreover, these sites are recognized by the ALBA1/ALBA2 heterodimer *in vivo* (Yuan et al., 2019). Nevertheless, the ALBA3-YFP significant signal accumulations can be attributed only to ample storage of excessive protein. A recent study focused on *ALBA3*, revealing its important role in male fertility, particularly in the presence of HS (Ci et al., 2025). Hence, only ALBA3 can be localized in both the nucleus and cytoplasm; its role in pollen integrity is therefore supposed to be more distinct from that of other subfamily members. The specific regulation of *ALBA3* and its products in mature pollen (Náprstková et al., 2021) indicates a comprehensive regulatory network that facilitates pollen development and functional phases. The individual or interconnected processes could be united by specific *ALBA3*-dependent transcriptional regulation (Ci et al., 2025). Although correlations between achieved results and several publications were found, further experimental procedures are needed to verify them.

Interestingly, the inability of the whole Rpp25-like subfamily to target pollen nuclei could indicate the importance of their cytoplasmic targeting. Moreover, a recorded pronounced cytoplasmic signal pattern depicts disruption of their precise control. The substitution of native *5′ UTR* for viral *5′ UTR*-

NLS likely removed or abolished regulatory cis elements in *5′ UTRs*, leading to the accumulation of translated proteins. Consequently, the Rpp25-like subfamily appears to be preferentially targeted to the cytoplasm, which suggests that its nuclear role has a minor impact on pollen maturation.

5.2. ALBA proteins are localized in cytoplasmic RPBs

5.2.1. Some ALBA proteins partially colocalize with PABP3

Since the initial study in eukaryotes, the preferential affinity of ALBA proteins for RNA molecules has expanded their functional differentiation (Mani et al., 2011; Lemieux et al., 2016; Reichel et al., 2016; Verma et al., 2018). A specific interlink of molecular processes underlies their implementation in growth and development, often in a stress-dependent manner (Mair et al., 2010; Subota et al., 2011). Obtained and investigated pairs of ALBA proteins and PABP3-RFP marker revealed partial colocalization varying throughout the cytoplasmic pattern. Similarly, all ALBA homologs were found in plasmodial P granules, which are associated with eIF4E and PABP, standard components of SGs (Anderson et al., 2009). These aggregates serve for the temporal translational inactivation of specific transcripts by reversible deadenylation, mediated by particular forms of PABPs, which could reflect the variability of the ALBA potential roles. Male-specific *PABP3* is active exclusively in the tapetum and pollen, where PABP3-RFP intensively accumulates along VC nuclei and possibly the plasma membrane of SCs, in conjunction with several investigated ALBA-GFP proteins (Belostotsky, 2003). Although the ALBA and PABP3 colocalization patterns vary among distinct samples, the partial overlap of red and green signal was recorded in all samples. The Alba-family members are unevenly distributed across various types of particles in distinct regions of VC and SCs, indicating mRNA particle compartmentalization and content diversification. Moreover, the partial colocalization of PABP3-RFP and ALBA4-GFP is greatly enhanced by HS treatment (Náprstková et al., 2021). This result is in agreement with the involvement of the Rpp25-like subfamily in heat adaptation via HSF transcription regulation in Arabidopsis (Tong et al., 2022).

5.2.2. ALBA proteins colocalize with PABP5 around SC nuclei

PABP5-RFP enables marking another specific mRNA-containing particle in the male gametophyte (Belostotsky, 2003). In mature pollen, the ALBA2-GFP and ALBA6-GFP identically colocalize with PABP5-RFP in accumulated ring-like structures surrounding SC nuclei, indicating their possible involvement in the same RPBs. On the other hand, the marker localization is different from ALBA1-GFP within mature pollen. Therefore, this colocalization assay distinguishes the subcompartmentalization of ALBA1, ALBA2, and ALBA6 in the VC, as well as the distinct localization of ALBA1 from ALBA2 and ALBA6 in SCs. A possible connection between ALBA

proteins and various types of RBPs, mediated through a selective mRNA interactome, could indicate their regulatory role in translational control, as described (Szostak et al., 2013; Reichel et al., 2024). This potential remark is further supported by the activity of *AtALBA* genes in growing tissues throughout plant development (Náprstková et al., 2021) and the function of protozoal homologs in temperature-dependent and independent translation repression (Chêne et al., 2012; Dupé et al., 2014; Pérez-Díaz et al., 2017). Nevertheless, elucidation of ALBA protein incorporation into these processes needs to be further studied due to the absence of direct evidence in Arabidopsis.

5.2.3. ALBA proteins do not colocalize with GAF1 in Arabidopsis mature pollen

The *GAF1* marker was used for RNAse P/MRP localization in an Arabidopsis colocalization assay at the beginning of this study. This selection was based on the connection of ALBA homologs, human RPP20/RPP25, and yeast POP6/POP7 to RNase P/MRP roles (Dupé et al., 2015; Chan et al., 2018). The experimental setup was further supported by *GAF1* expression activity in identical tissues with *ALBA* genes, especially in developing gametophytes (Wang et al., 2012; Náprstková et al., 2021). Hence, the co-occurrence of the studied genes with the marker was not expected to be absolute. However, there was an assumption for at least partial correlation and possible cooperation of GAF1 with ALBA proteins. Nevertheless, almost any shared position within the correlated patterns was observed in Arabidopsis pollen. Therefore, the initial hypothesis does not imply an ALBA role connected to RNase P/MRP via its subunit GAF1, and the detected diversification of the Alba family throughout evolution most probably prioritized alternative functions in Arabidopsis.

5.2.4. Colocalization of ALBA within subfamilies in mature pollen

In view of ALBA homologs' ability to form homodimers, heterodimers, and even multimers across archaeal-eukaryotic studied species, their relationships were investigated *in vivo* in pollen grains. Results of colocalization assays within subfamilies revealed unexpected difficulties. Acquired data show a colocalization mask related to the HS-induced pattern, as indicated by ALBA signal accumulation. Nevertheless, these observations enhance the indication of their differentiation conditioned to the actual physiological circumstances within cells. The unusual localization patterns characteristic for some pairs could be influenced by the ALBA protein content in the mature pollen. Colocalization hotspots vary among pairs, underlining preferential affinities in distinct parts of the cytoplasm. Therefore, the multiplication of the Alba family could enable actual dimer specialization by the targeted localization. This regulatory step could integrate various processes by the specific pair and translate acquired information to effectors, which is in agreement with their presence in multiple types of mRNA-containing granules mentioned above.

The substantial colocalization overlap of ALBA1 and ALBA2, indicating dimer formation, was later confirmed (Yuan et al., 2019). As a result, this pair was selected for the introduction of a Ribo-BiFC method to the Arabidopsis model. The data have been compiled, and the manuscript is currently under peer review by Plant Methods. At the same time, my two master's students examined other interactions and presented their findings in their theses for master's degrees (Kočová, 2020; Popelářová, 2021). They demonstrated ALBA1-ALBA3 interaction using the Bimolecular Fluorescence Complementation system (BiFC) in transiently transformed tobacco cells, indicated by the overlap of signals obtained by the colocalization assay. Unfortunately, no other interaction partners within subfamilies were detected, although they are likely to form homodimers (ALBA5 and ALBA3). According to BiFC and yeast-two-hybrid system (Y2H) results, heterodimers could be formed between Rpp20-like and Rpp25-like subfamily members. Nevertheless, the obtained colocalization results in pollen could indicate indirect interaction or localization in the same type of RBP without interaction. Therefore, Alba family-binding partners can define the position and content of accumulated material, determining the character of the formed aggregate in mature pollen.

Collectively, ALBA colocalization assays with selected RBP markers revealed sequestration of individual Alba-family members to various types of aggregates. Their existence is further supported by ALBA4's interaction with the m^6A reader ECT2, creating an efficient complex for mRNA recognition in sporophytic tissues. Interestingly, both proteins possess IDRs in their structure responsible for interactions with PABP2, PABP4, and PABP8 (Reichel et al., 2024). Therefore, the RGG domain may be responsible for sequestration of the Rpp25-like subfamily to PABP-containing RBPs. However, the association of ALBA proteins with PABP3-containing particles is not permanent, suggesting their involvement in multiple cellular processes.

5.3. Overexpression of *ALBA* genes in pollen

The importance of a gene and its encoded product's role are usually elucidated by a targeted loss-of-function mutation and its effect on the plant phenotype. However, due to high sequence similarity and probable functional redundancy, single *alba* knock-outs do not exhibit any visible aberrations. Therefore, three promoters with specific activity in the male gametophyte and sporophyte were used to disrupt *ALBA* homeostasis. According to the achieved results, the particular overexpression of *ALBA* genes in SCs can cause severe changes in nuclear shape. The altered morphology suggests a significant role for the members in SCs, particularly in processes related to the specifically packed chromatin. Interestingly, the most affected nuclear shape was detected in *proLAT52::ALBA3-YFP*-transgenic pollen, which corresponds with its impact on fertility, as it regulates genes essential for pollen function, according to multiple publications (Becker et al., 2003; Borg et al., 2011; Wang et al., 2021). The genotype-induced gene overexpression generates a global imbalance disrupting

a fragile homeostasis of the male gametophyte. Therefore, the supernumerary compounds must be neutralized by the cellular machinery to maintain fertility efficiency. The pronounced alteration in ALBA3-GFP distribution and its effect on SC nuclei highlight its protective role under stress. ALBA3 binds and stabilizes mRNAs essential for male fertility in Arabidopsis and rice and sequestrates them into SGs under elevated temperatures. Moreover, loss of the *ALBA*3 homolog in rice severely affects male fertility upon HS (Ci et al., 2025).

The significance of *ALBA* genes' precise regulation in the male gametophyte was further elucidated by their visualization in the VC, controlled by a highly active *LAT52* promoter. The excess of proteins in the VC cytoplasm may disrupt the localization of ALBA proteins. This alteration could arise from proteins with IDRs that effectively sequester or from the mediated accumulation of Rpp20-like subfamily members. Nevertheless, the subcellular structure of the male gametophyte does not imply noticeable shifts. Therefore, the generated disproportion of ALBA proteins is likely blocked by storage in large foci.

5.4. Characterization of *ALBA* sporophytic overexpression

Interestingly, the overexpression of Alba-family proteins in sporophytic tissues, caused by a constitutively active promoter, resulted in the most harmful developmental consequences observed throughout plant growth. Even more surprising was the manifestation of individual gene overexpression, highlighting their variability between subfamilies and partial redundancy within the three closest homologs. While the plants remained fertile, the loss of color in the Rpp20-like subfamily sporophyte indicates an alteration in energetic metabolism that disrupts redox potential and prevents reserve accumulation. Nonetheless, Alba-family members are known for their involvement in processes crucial for plant growth and reproduction, which is predominantly manifested by the Rpp25-like subfamily phenotype. Induced abnormalities influence cellular processes from seed germination to progeny production, resulting in various morphological changes observed in *oexALBA4* and *oexALBA5* individuals. The upregulated level of these transcripts primarily affects young, rapidly dividing tissues, as their loss in *alba456* mutants leads to growth inhibition (Kočová, 2020; Tong et al., 2022).

Analysis of *ALBA* gene activity in the Rpp25-like subfamily overexpression background indicated cooperation among the subfamily members. Acquired data revealed a connection between the closest Rpp25-like homologs, *ALBA4* and *ALBA5*, in terms of regulation. Interestingly, *ALBA6* activity consistently influences only *ALBA4*. Moreover, dysregulation caused by either overexpression or absence of Rpp25-like subfamily members results in developmental defects, such as reduced fresh weight of seedlings, slowed root growth, and abnormal leaf morphology, although elevated transcript levels present especially severe conditions (Tong et al., 2022). Analysis of the *alba456* transcriptome

revealed a significant number of dysregulated genes related to metabolic pathways associated with nutrient deficiency, which likely cause rosette size reduction (Wang et al., 2019; Tong et al., 2022). This finding correlates with the observed phenotype expression by enlarged rosettes typical of *oexALBA4* and *oexALBA5*. At a larger scale, similar characteristics were revealed for *alba4* and *alba5* T-DNA insertion mutants, with the *Mpalba* mutant producing shortened root hairs and rhizoids, respectively. This conservation between moss and evolutionarily advanced Angiosperms in one-celled root structures indicates a mechanism similarity that could be shared with related structures, such as pollen tubes (Honkanen et al., 2016).

OexALBA-GFP-induced effects detrimentally influence fertility, such as delayed flowering, abnormal flower production, and distorted ovule development, demonstrating RBPs' involvement in flowering control and gametophyte development (Cho et al., 2019; Steffen et al., 2019). An excessive amount of Rpp25-like family members influences multiple key factors for the transition to the generative phase, activates circadian cycle regulation, but negatively affects the energetic state. The crucial effect of flowering delay may be based on the downregulation of genes encoding proteins involved in energy metabolism and photosynthesis, which can lead to energetic stress and excessive ROS production. Detected dysregulation of these dangerous processes in *oexALBA4* and *oexALBA5* disrupts essential subcellular structures and results in cell death. Wide loss of cells promotes leaf senescence, a process regulated by abscisic acid (Saibo et al., 2009; Qin et al., 2011; Banerjee et al., 2017; Wai et al., 2021) , a pathway with significantly upregulated compounds in *oexALBA4* and *oexALBA5* samples. Flowering induction depends on vernalization, which consequently inhibits *FLC* transcription. Significantly elevated activity of *FLC* could be one of the factors maintaining the juvenile stage in all samples of *oexALBA4* and *oexALBA5*, except in juvenile rosettes. These data also correlate with the proposed relationship of ALBA to DNA R-loops, which are well known for their role in regulating *FLC* activity (Sun et al., 2013). The flowering is simultaneously stimulated by the upregulation of GI and CO in all genotypes. The effect is likely even more pronounced due to the downregulation of the *COL9*, which is uniquely and significantly affected in all collected samples. Interestingly, the cumulative effect could downregulate transcription of SAM transition master regulators *SOC1* and *LFY* in *oexALBA4*. The massive dysregulation of energetic metabolism can slow or arrest flowering achievement. Even though the significant upregulation of circadian rhythm genes and flowering activators strongly promotes flowering simultaneously with repressor downregulation, the transition to the generative phase is probably decelerated by the induced stress. *ALBA* genes control processes also in later stages of fruit development; particularly, *ALBA5* promotes fruit enlargement and ripening in tomato (Wai et al., 2021; Tong et al., 2022). These data enhance the seriousness of recorded seed phenotypic defects at the *oexALBA4-6-GFP* background in Arabidopsis. These morphological abnormalities are most likely caused by impaired RNA metabolism, significantly affecting a wide range of physiological processes (Fan et al., 2024).

Therefore, it can be assumed that sporophytic overexpression induces similar stress-related conditions within plant tissues. Molecular effectors of the response are connected with cytoplasmic RBPs, which sequester several ligands, including specific mRNAs and proteins (Tong et al., 2022). Following the recent surge in publications describing various types of RNA-binding proteins, their core compounds have been identified. Among conventional RBPs, proteins with Cold-shock domains, Alba domains, and Yth domains are known for their mutual connections in seed germination and root growth (Tiang et al., 2012), which are affected in *oexALBA* lines. Interestingly, a compound of RPBs, glycine-rich RBP7 (GRP7), is significantly upregulated in the *oexALBA4* and *oexALBA5* samples, with the exception of juvenile rosettes. ALBA5 binds various types of RNA *in vitro*, typically at their 3' ends, to regulate plant development and stress responses *in vivo*. GRP7 aggregates with the cold-induced mRNA chaperones and the EUKARYOTIC INITIATION FACTOR 4E1(eIF4E1) into cytoplasmic SGs to disrupt translation upon HS (Fan et al., 2024). In *oexALBA* lines, pathways related to cold response and acclimation were found to be upregulated, making the aggregation even more complex and dependent on individual factors, which have been previously reported in tomato (Wai et al., 2021).

A relationship between the Rpp25-like subfamily and the HS response was revealed by RNA sequencing in *oexALBA* lines. Although there are missing experimental procedures that prove a direct connection, the acquired data correlate with previous publications (Wai et al., 2021; Náprstková et al., 2021; Tong et al., 2022). The most sensitive genotype to HS is *oexALBA4*, followed by *oexALBA5,* according to the results of RNA sequencing and reported HS-induced upregulation in tomato (Wai et al., 2021). Consistently, these two heat-treated genotypes shared elevated expression of genes involved in HS response and thermotolerance, which maintain redox homeostasis within the tested tissue. Both HS-treated *oexALBA4* and *oexALBA5* samples exhibit significantly elevated transcripts that encode compounds involved in the response to hypoxia, a process that aggregates RNA helicases in SGs and PBs (Tong et al., 2022; Fan et al., 2024). HS-induced SGs and PBs include ALBA4-6, which protect specific transcripts against XRN4 exonuclease, causing hypersensitivity to HS at the *alba456* background (Tong et al., 2022). Consistently, a functional complex, ALBA-ECT2, binds m^6A-modified transcripts and relocates to SGs upon heat and osmotic stresses (Arribas-Hernández et al., 2018; Scutenaire et al., 2018). The *ALBA6* contribution to thermotolerance is much weaker, but its sensitivity arises from another type of stress factor (Wai et al., 2021). Altogether, cytoplasmic aggregates are formed under variable stress conditions to create multiple populations of functional complexes that cope with detected stress factors. Consequently, their impact on plant reproduction is considerable, enhancing survival and offspring production across a wide range of conditions.

6. Conclusions

This thesis provides a comprehensive study of the Alba-family members in Arabidopsis, focusing on their characteristics during reproductive development. The research reveals their functional diversification based on phenotypic differences, explicitly categorizing them into the Rpp20-like and Rpp25-like subfamilies. Within each subfamily, two homologs demonstrate a close relationship by sequence similarity, expression and localization patterns, while the most distinct member stands out as distinctly divergent. Notably, *ALBA3* plays a pivotal role in the male gametophyte, exhibiting dominance and unique stability within VC nuclei, as well as remarkable presence in SCs. This highlights its essential contribution to male gametophyte development, with particular importance for MGU integrity. The relationship between ALBA1 and ALBA2 is underscored in their colocalization and identical responses to induced cell stresses. Although the cooperation of the Rpp20-like subfamily in the pollen RBP granules is evident, further exploration is needed to fully understand this aspect.

Members of the Rpp25-like subfamily are essential for plant reproduction, accumulating through self-activity based on their molecular characteristics. Their cytoplasmic distribution is intricately associated with various types of RBPs, which comprise a distinct group of molecules forming separate populations. This dynamic allows for the effective sequestration of bound materials within the concentrated pollen cytoplasm. Moreover, the phenomenon of aggregation is significantly enhanced by HS, further increasing the roles of ALBA4-6 in the storage and protection of crucial molecules against damage or degradation. This subfamily interconnects molecular processes across various cell types, tissues, and developmental stages, highlighting its fundamental importance in maintaining cellular homeostasis. Beyond this, its importance extends to complex processes that facilitate essential physiological changes necessary for flowering and gametophyte production.

While functional differences exist among the Rpp20-like and Rpp25-like subfamilies and their individual members, they collectively exhibit crucial characteristics underscoring their shared significance. The overdose-induced disruption to their natural regulation can induce detrimental imbalances that severely impact cellular homeostasis. Such disturbances can lead to profound alterations in both the morphology and developmental pathways of the plant, underscoring the critical nature of these proteins in plant health and reproductive success.

7. Bibliography

Acharya, D, Bavikatte, AN, Ashok, VV, Hegde, SR, Macpherson, CR, Scherf, A, Vembar, SS, 2025. **During Asexual Blood Development**. *Microbiology Spectrum* 13(3): p.1–20. DOI: 10.1128/spectrum.00885-24.

Aizer, A, Kalo, A, Kafri, P, Shraga, A, Ben-Yishay, R, Jacob, A, Kinor, N, Shav-Tal, Y, 2014. **Quantifying mRNA targeting to P-bodies in living human cells reveals their dual role in mRNA decay and storage**. *Journal of Cell Science* 127(20): p.4443–4456. DOI: 10.1242/jcs.152975.

Altman, T, Altman, S, 2001. **Protein-protein interactions with subunits of human nuclear RNase P**. *Proceedings of the National Academy of Sciences of the United States of America* 98(3): p.920–925. DOI: 10.1073/pnas.021561498.

Anderson, P, Kedersha, N, 2009. **RNA granules: post-transcriptional and epigenetic modulators of gene expression.** *Nature reviews. Molecular cell biology* 10(6): p.430–436. DOI: 10.1038/nrm2694.

Aravind, L, Iyer, LM, Anantharaman, V, 2003. **The two faces of Alba: the evolutionary connection between proteins participating in chromatin structure and RNA metabolism.** *Genome biology* 4(10): p.R64. DOI: 10.1186/gb-2003-4-10-r64.

Aravind, L, Koonin, E V., 2001. **THUMP - A predicted RNA-binding domain shared by 4-thiouridine, pseudouridine synthases and RNA methylases**. *Trends in Biochemical Sciences* 26(4): p.215–217. DOI: 10.1016/S0968-0004(01)01826-6.

Arribas-Hernández, L, Rennie, S, Köster, T, Porcelli, C, Lewinski, M, Staiger, D, Andersson, R, Brodersen, P, 2021. **Principles of mRNA targeting via the Arabidopsis m6A-binding protein ECT2**. *eLife* 10: p.1–33. DOI: 10.7554/eLife.72375.

Arribas-Hernández, L, Bressendorff, S, Hansen, MH, Poulsen, C, Erdmann, S, Brodersen, P, 2018. **An m6A-YTH module controls developmental timing and morphogenesis in arabidopsis**. *Plant Cell* 30(5): p.952–967. DOI: 10.1105/tpc.17.00833.

Bac-Molenaar, JA, Fradin, EF, Becker, FFM, Rienstra, JA, van der Schoot, J, Vreugdenhil, D, Keurentjes, JJB, 2015. **Genome-wide association mapping of fertility reduction upon heat stress reveals developmental stage-specific QTLs in Arabidopsis Thaliana**. *Plant Cell* 27(7): p.1857–1874. DOI: 10.1105/tpc.15.00248.

Banani, SF, Lee, HO, Hyman, AA, Rosen, MK, 2017. *Biomolecular condensates: Organizers of cellular biochemistry*. DOI: 10.1038/nrm.2017.7.

Banerjee, A, Roychoudhury, A, 2017. **Abscisic-acid-dependent basic leucine zipper (bZIP) transcription factors in plant abiotic stress**. *Protoplasma* 254(1): p.3–16. DOI: 10.1007/s00709-015-0920-4.

Barnabás, B, Jäger, K, Fehér, A, 2008. **The effect of drought and heat stress on reproductive**

processes in cereals. *Plant, cell & environment* 31(1): p.11–38. DOI: 10.1111/j.1365-3040.2007.01727.x.

Baron, KN, Schroeder, DF, Stasolla, C, 2012. **Transcriptional response of abscisic acid (ABA) metabolism and transport to cold and heat stress applied at the reproductive stage of development in Arabidopsis thaliana**. *Plant Science* 188–189: p.48–59. DOI: 10.1016/j.plantsci.2012.03.001.

Becker, D, Boavida, LC, Carneiro, J, Haury, M, Feijo, A, 2003. **Transcriptional Profiling of Arabidopsis Tissues**. *Plant Physiology* 133: p.713–725. DOI: 10.1104/pp.103.028241.the.

Becker, JD, Feijó, JA, 2007. **How many genes are needed to make a pollen tube? Lessons from transcriptomics**. *Annals of Botany* 100(6): p.1117–1123. DOI: 10.1093/aob/mcm208.

Bedinger, P, 1992. **The remarkable biology of pollen**. *Plant Cell* 4(8): p.879–887. DOI: 10.1105/tpc.4.8.879.

Bell, SD, Botting, CH, Wardleworth, BN, Jackson, SP, White, MF, 2002. **The interaction of Alba, a conserved archaeal chromatin protein, with Sir2 and its regulation by acetylation**. *Science* 296: p.148–151. DOI: 10.1126/science.1070506.

Belostotsky, DA, 2003. **Unexpected complexity of poly(A)-binding protein gene families in flowering plants: Three conserved lineages that are at least 200 million years old and possible auto- and cross-regulation**. *Genetics* 163(1): p.311–319. DOI: 10.1093/genetics/163.1.311.

Berger, F, Twell, D, 2011. **Germline specification and function in plants.** *Annual review of plant biology* 62: p.461–84. DOI: 10.1146/annurev-arplant-042110-103824.

Biou, V, Shu, F, Ramakrishnan, V, 1995. **X-ray crystallography shows that translational initiation factor IF3 consists of two compact a / i domains linked by an a-helix**. *EMBO Journal* 14(16): p.4056–4064. DOI: 10.1002/j.1460-2075.1995.tb00077.x.

Blümel, M, Dally, N, Jung, C, 2015. **Flowering time regulation in crops—what did we learn from Arabidopsis?** *Current opinion in biotechnology* 32: p.121–129. DOI: 10.1016/j.copbio.2014.11.023.

Boisvert, F-M, van Koningsbruggen, S, Navascués, J, Lamond, AI, 2007. **The multifunctional nucleolus.** *Nature reviews. Molecular cell biology* 8(7): p.574–585. DOI: 10.1038/nrm2184.

Bokszczanin, KL, Fragkostefanakis, S, 2013. **Perspectives on deciphering mechanisms underlying plant heat stress response and thermotolerance.** *Frontiers in plant science* 4: p.315. DOI: 10.3389/fpls.2013.00315.

Borg, M, Berger, F, 2015. **Chromatin remodelling during male gametophyte development.** *The Plant journal : for cell and molecular biology* 83(1): p.177–188. DOI: 10.1111/tpj.12856.

Borg, M, Brownfield, L, Khatab, H, Sidorova, A, Lingaya, M, Twell, D, 2011. **The R2R3 MYB Transcription Factor DUO1 Activates a Male Germline-Specific Regulon Essential for Sperm Cell Differentiation in Arabidopsis**. *The Plant Cell* 23(2): p.534–549. DOI:

10.1105/tpc.110.081059.

Borges, F, Gomes, G, Gardner, R, Moreno, N, McCormick, S, Feijó, JA, Becker, JD, 2008. **Comparative transcriptomics of arabidopsis sperm cells**. *Plant Physiology* 148(2): p.1168–1181. DOI: 10.1104/pp.108.125229.

Boulila, Y, Tomavo, S, Gissot, M, 2014. **A RGG motif protein is involved in Toxoplasma gondii stress-mediated response**. *Molecular and Biochemical Parasitology* 196(1): p.1–8. DOI: 10.1016/j.molbiopara.2014.07.009.

Brownfield, L, Hafidh, S, Borg, M, Sidorova, A, Mori, T, Twell, D, 2009. **A plant germline-specific integrator of sperm specification and cell cycle progression**. *PLoS Genetics* 5(3). DOI: 10.1371/journal.pgen.1000430.

Buchan, JR, Parker, R, 2009. **Eukaryotic Stress Granules : The Ins and Out of Translation What are Stress Granules ?** *Molecular cell* 36(6): p.932.

Cao, S, Ye, M, Jiang, S, 2005. **Involvement of GIGANTEA gene in the regulation of the cold stress response in Arabidopsis**. *Plant Cell Reports* 24(11): p.683–690. DOI: 10.1007/s00299-005-0061-x.

Čapková, V, Hrabětová, E, Tupý, J, 1988. **Protein synthesis in pollen tubes: preferential formation of new species independent of transcription**. *Sexual Plant Reproduction* 1(3): p.150–155. DOI: 10.1007/BF00193745.

Cassola, A, De Gaudenzi, JG, Frasch, AC, 2007. **Recruitment of mRNAs to cytoplasmic ribonucleoprotein granules in trypanosomes**. *Molecular Microbiology* 65(3): p.655–670. DOI: 10.1111/j.1365-2958.2007.05833.x.

Chan, CW, Kiesel, BR, Mondragón, A, 2018. **Crystal Structure of Human Rpp20/Rpp25 Reveals Quaternary Level Adaptation of the Alba Scaffold as Structural Basis for Single-stranded RNA Binding**. *Journal of Molecular Biology* 430(10): p.1403–1416. DOI: 10.1016/j.jmb.2018.03.029.

Chao, Y, Zhang, T, Yang, Q, Kang, J, Sun, Y, Yvonne, M, Qin, Z, 2014. **Plant Science Expression of the alfalfa CCCH-type zinc finger protein gene MsZFN delays flowering time in transgenic Arabidopsis thaliana**. *Plant Science* 215–216: p.92–99. DOI: 10.1016/j.plantsci.2013.10.012.

Chaturvedi, P, Wiese, AJ, Ghatak, A, Záveská Drábková, L, Weckwerth, W, Honys, D, 2021. **Heat stress response mechanisms in pollen development**. *New Phytologist* 231(2): p.571–585. DOI: 10.1111/nph.17380.

Chêne, A, Vembar, SS, Rivière, L, Lopez-Rubio, JJ, Claes, A, Siegel, TN, Sakamoto, H, Scheidig-Benatar, C, Hernandez-Rivas, R, Scherf, A, 2012. **PfAlbas constitute a new eukaryotic DNA/RNA-binding protein family in malaria parasites**. *Nucleic Acids Research* 40(7): p.3066–3077. DOI: 10.1093/nar/gkr1215.

Cho, H, Cho, HS, Hwang, I, 2019. **Emerging roles of RNA-binding proteins in plant development**. *Current Opinion in Plant Biology* 51: p.51–57. DOI: 10.1016/j.pbi.2019.03.016.

Chou, CC, Lin, TW, Chen, CY, Wang, AHJ, 2003. **Crystal structure of the hyperthermophilic archaeal DNA-binding protein Sso10b2 at a resolution of 1.85 Angstroms**. *Journal of Bacteriology* 185(14): p.4066–4073. DOI: 10.1128/JB.185.14.4066-4073.2003.

Ci, D, Liu, Y, Wang, L, Zhu, R, Chen, Y, Bai, G, Xu, Z, Zhou, H, Zhou, X, Fan, LM, Qian, W, 2025. **ALBA3 maintains male fertility under heat stress in plants**. *Journal of Integrative Plant Biology* 67(5): p.1413–1427. DOI: 10.1111/jipb.13846.

Clough, SJ, Bent, AF, 1998. **Floral dip: A simplified method for Agrobacterium-mediated transformation of Arabidopsis thaliana**. *Plant Journal* 16(6): p.735–743. DOI: 10.1046/j.1365-313X.1998.00343.x.

Conrath, U, 2011. **Molecular aspects of defence priming.** *Trends in plant science* 16(10): p.524–531. DOI: 10.1016/j.tplants.2011.06.004.

da Costa, KS, Galúcio, JMP, Leonardo, ES, Cardoso, G, Leal, É, Conde, G, Lameira, J, 2017. **Structural and evolutionary analyses of Leishmania Alba proteins**. *Molecular and Biochemical Parasitology* 217: p.23–31. DOI: 10.1016/j.molbiopara.2017.08.006.

Cui, Q, Tong, Y, Xue, H, Huang, L, Feng, Y, Wang, J, 2003. **Two conformations of archaeal Ssh10b: The origin of its temperature-dependent interaction with DNA**. *Journal of Biological Chemistry* 278(51): p.51015–51022. DOI: 10.1074/jbc.M308510200.

Darnell, JC, Jensen, KB, Jin, P, Brown, V, Warren, ST, Darnell, RB, 2001. **Fragile X mental retardation protein targets G quartet mRNAs important for neuronal function**. *Cell* 107(4): p.489–499. DOI: 10.1016/S0092-8674(01)00566-9.

Decker, CJ, Parker, R, 2012. **P-bodies and stress granules: possible roles in the control of translation and mRNA degradation.** *Cold Spring Harbor perspectives in biology* 4(9): p.a012286. DOI: 10.1101/cshperspect.a012286.

Ding, Y, Shi, Y, Yang, S, 2020. **Molecular Regulation of Plant Responses to Environmental Temperatures.** *Molecular plant* 13(4): p.544–564. DOI: 10.1016/j.molp.2020.02.004.

Dinno, A, 2015. **Nonparametric pairwise multiple comparisons in independent groups using Dunn's test**. *The Stata Journal* 15(1): p.292–300. DOI: 10.1177/1536867x1501500117.

Doyle, JJ, Doyle, JI, 1990. **Isolation of Plant DNA from Fresh Tissue**. *Focus* 12(1): p.13–15.

Dresselhaus, T, Franklin-Tong, N, 2013. **Male-female crosstalk during pollen germination, tube growth and guidance, and double fertilization**. *Molecular Plant* 6(4): p.1018–1036. DOI: 10.1093/mp/sst061.

Dresselhaus, T, Sprunck, S, 2012. **Plant fertilization: Maximizing reproductive success**. *Current Biology* 22(12): p.R487–R489. DOI: 10.1016/j.cub.2012.04.048.

Drews, GN, Lee, D, Christensen, CA, 1998. **Genetic analysis of female gametophyte development and function**. *Plant Cell* 10(1): p.5–17. DOI: 10.1105/tpc.10.1.5.

Dupé, A, Dumas, C, Papadopoulou, B, 2014. **An Alba-domain protein contributes to the stage-regulated stability of amastin transcripts in Leishmania.** *Molecular microbiology* 91(3):

p.548–561. DOI: 10.1111/mmi.12478.

Dupé, A, Dumas, C, Papadopoulou, B, 2015. **Differential Subcellular Localization of Leishmania Alba-Domain Proteins throughout the Parasite Development**. *PLoS ONE* 10(9): p.e0137243. DOI: 10.1371/journal.pone.0137243.

Eady, C, Lindsey, K, Twell, D, 1995. **The significance of microspore division and division symmetry for vegetative cell-specific transcription and generative cell differentiation**. *Plant Cell* 7(1): p.65–74. DOI: 10.2307/3869838.

Van Eenennaam, H, Vogelzangs, JHP, Lugtenberg, D, Van Den Hoogen, FHJ, Van Venrooij, WJ, Pruijn, GJM, 2002. **Identity of the RNase MRP- and RNase P-associated Th/To autoantigen.** *Arthritis and rheumatism* 46(12): p.3266–3272. DOI: 10.1002/art.10673.

Eimert, K, Wang, SM, Lue, WL, Chen, J, 1995. **Monogenic recessive mutations causing both late floral initiation and excess starch accumulation in arabidopsis**. *Plant Cell* 7(10): p.1703–1712. DOI: 10.2307/3870031.

Emenecker, RJ, Holehouse, AS, Strader, LC, 2020. **Emerging Roles for Phase Separation in Plants**. *Developmental Cell* 55(1): p.69–83. DOI: 10.1016/j.devcel.2020.09.010.

Engler, C, Youles, M, Gruetzner, R, Ehnert, TM, Werner, S, Jones, JDG, Patron, NJ, Marillonnet, S, 2014. **A Golden Gate modular cloning toolbox for plants**. *ACS Synthetic Biology* 3(11): p.839–843. DOI: 10.1021/sb4001504.

Fagerlund, RD, Perederina, A, Berezin, I, Krasilnikov, AS, 2015. **Footprinting analysis of interactions between the largest eukaryotic RNase P/MRP protein Pop1 and RNase P/MRP RNA components.** *RNA (New York, N.Y.)* 21(9): p.1591–1605. DOI: 10.1261/rna.049007.114.

Fan, S, Zhang, Y, Zhu, S, Shen, L, 2024. **Plant RNA-binding proteins: Phase separation dynamics and functional mechanisms underlying plant development and stress responses**. *Molecular Plant* 17(4): p.531–551. DOI: 10.1016/j.molp.2024.02.016.

Fetzer, CP, Hogan, DJ, Lipps, HJ, 2002. **A PIWI homolog is one of the proteins expressed exclusively during macronuclear development in the ciliate Stylonychia lemnae**. *Nucleic Acids Research* 30(20): p.4380–4386. DOI: 10.1093/nar/gkf579.

Forterre, P, Confalonieri, F, Knapp, S, 1999. **Identification of the gene encoding archeal-specific DNA-binding proteins of the Sac10b family**. *Molecular Microbiology* 32(3): p.669–670. DOI: 10.1046/j.1365-2958.1999.01366.x.

Fowler, S, Lee, K, Onouchi, H, Samach, A, Richardson, K, Morris, B, Coupland, G, Putterill, J, 1999. **GIGANTEA: a circadian clock-controlled gene that regulates photoperiodic flowering in Arabidopsis and encodes a protein with several possible membrane-spanning domains.** *The EMBO journal* 18(17): p.4679–4688. DOI: 10.1093/emboj/18.17.4679.

Fray, RG, Simpson, GG, 2015. **The Arabidopsis epitranscriptome**. *Current Opinion in Plant Biology* Oct(27): p.17–21. DOI: 10.1016/j.pbi.2015.05.015.

Freitas-Junior, LH, Hernandez-Rivas, R, Ralph, SA, Montiel-Condado, D, Ruvalcaba-Salazar, OK, Rojas-Meza, AP, Mâncio-Silva, L, Leal-Silvestre, RJ, Gontijo, AM, Shorte, S, Scherf, A, 2005. **Telomeric heterochromatin propagation and histone acetylation control mutually exclusive expression of antigenic variation genes in malaria parasites.** *Cell* 121(1): p.25–36. DOI: 10.1016/j.cell.2005.01.037.

Geula, S, Moshitch-Moshkovitz, S, Dominissini, D, Mansour, AA, Kol, N, Salmon-Divon, M, Hershkovitz, V, Peer, E, Mor, N, Manor, YS, Ben-Haim, MS, Eyal, E, Yunger, S, Pinto, Y, Jaitin, DA, Viukov, S, Rais, Y, … Hanna, JH, 2015. **m6A mRNA methylation facilitates resolution of naïve pluripotency toward differentiation.** *Science (New York, N.Y.)* 347(6225): p.1002–1006. DOI: 10.1126/science.1261417.

Giorno, F, Wolters-Arts, M, Mariani, C, Rieu, I, 2013. **Ensuring reproduction at high temperatures: The heat stress response during anther and pollen development**. *Plants* 2(3): p.489–506. DOI: 10.3390/plants2030489.

Gissot, M, Walker, R, Delhaye, S, Alayi, TD, Huot, L, Hot, D, Callebaut, I, Schaeffer-Reiss, C, Dorsselaer, A Van, Tomavo, S, 2013. **Toxoplasma gondii Alba Proteins Are Involved in Translational Control of Gene Expression**. *Journal of Molecular Biology* 425(8): p.1287–1301. DOI: 10.1016/j.jmb.2013.01.039.

Gomes, E, Shorter, J, 2019. **The molecular language of membraneless organelles**. *Journal of Biological Chemistry* 294(18): p.7115–7127. DOI: 10.1074/jbc.TM118.001192.

Gosai, SJ, Foley, SW, Wang, D, Silverman, IM, Nelson, ADL, Beilstein, MA, Daldal, F, Deal, RB, Gregory, BD, 2016. **Secondary Structure Landscapes of the Arabidopsis Nucleus**. 57(2): p.376–388. DOI: 10.1016/j.molcel.2014.12.004.Global.

Goyal, M, Alam, A, Iqbal, MS, Dey, S, Bindu, S, Pal, C, Banerjee, A, Chakrabarti, S, Bandyopadhyay, U, 2012. **Identification and molecular characterization of an Alba-family protein from human malaria parasite Plasmodium falciparum**. *Nucleic Acids Research* 40(3): p.1174–1190. DOI: 10.1093/nar/gkr821.

Goyal, M, Banerjee, C, Nag, S, Bandyopadhyay, U, 2016. **The Alba protein family: Structure and function**. *Biochimica et Biophysica Acta - Proteins and Proteomics* 1864(5): p.570–583. DOI: 10.1016/j.bbapap.2016.02.015.

Guerrier-Takada, C, Eder, PS, Gopalan, V, Altman, S, 2002. **Purification and characterization of Rpp25, an RNA-binding protein subunit of human ribonuclease P**. *Rna* 8(3): p.290–295. DOI: 10.1017/S1355838202027954.

Guo, F, Yoon, GM, McCubbin, AG, 2013. **PiSCP1 and piCDPK2 localize to peroxisomes and are involved in pollen tube growth in Petunia inflata**. *Plants* 2(1): p.72–86. DOI: 10.3390/plants2010072.

Guo, M, Liu, J-H, Ma, X, Luo, D-X, Gong, Z-H, Lu, M-H, 2016. **The Plant Heat Stress Transcription Factors (HSFs): Structure, Regulation, and Function in Response to Abiotic**

Stresses. *Frontiers in plant science* 7: p.114. DOI: 10.3389/fpls.2016.00114.

Guo, R, Xue, H, Huang, L, 2003. **Ssh10b, a conserved thermophilic archaeal protein, binds RNA in vivo**. *Molecular microbiology* 50(5): p.1605–1615. DOI: 10.1046/j.1365-2958.2003.03793.x.

Guo, W, Zhang, X, Peng, Q, Luo, D, Jiao, K, Su, S, 2019. **LOVE ON WINGS, a Dof family protein regulates floral vasculature in Vigna radiata**. *BMC Plant Biology* 19(495): p.1–12. DOI: 10.1186/s12870-019-2099-x.

Guzikowski, AR, Chen, YS, Zid, BM, 2019. **Stress-induced mRNP granules: Form and function of processing bodies and stress granules**. *Wiley Interdiscip Rev RNA* 10(3): p.1–30. DOI: 10.1002/wrna.1524.

Hada, K, Nakashima, T, Osawa, T, Shimada, H, Kakuta, Y, Kimura, M, 2008. **Crystal Structure and Functional Analysis of an Archaeal Chromatin Protein Alba from the Hyperthermophilic Archaeon Pyrococcus horikoshii OT3**. *Bioscience, Biotechnology, and Biochemistry* 72(3): p.749–758. DOI: 10.1271/bbb.70639.

Hafidh, S, Čapková, V, Honys, D, 2011. **Safe keeping the message: MRNP complexes tweaking after transcription**. *Advances in Experimental Medicine and Biology* 722: p.118–136. DOI: 10.1007/978-1-4614-0332-6_8.

Hafidh, S, Fíla, J, Honys, D, 2016. **Male gametophyte development and function in angiosperms: a general concept**. *Plant Reproduction* 29(1–2): p.31–51. DOI: 10.1007/s00497-015-0272-4.

Hafidh, S, Honys, D, 2021. **Reproduction Multitasking: The Male Gametophyte.** *Annual review of plant biology* 72: p.581–614. DOI: 10.1146/annurev-arplant-080620-021907.

Hafidh, S, Potěšil, D, Müller, K, Fíla, J, Michailidis, C, Herrmannová, A, Feciková, J, Ischebeck, T, Valášek, LS, Zdráhal, Z, Honys, D, 2018. **Dynamics of the Pollen Sequestrome Defined by Subcellular Coupled Omics**. *Plant Physiology* 178(1). DOI: 10.1104/pp.18.00648.

Hamada, T, Yako, M, Minegishi, M, Sato, M, Kamei, Y, Yanagawa, Y, 2018. **Stress granule formation is induced by a threshold temperature rather than a temperature difference in Arabidopsis**. *Journal of Cell Science* 131: p.jcs216051. DOI: 10.1242/jcs.216051.

Han, Y, Zhang, X, Wang, W, Wang, Y, Ming, F, 2013. **The suppression of WRKY44 by GIGANTEA-miR172 pathway is involved in drought response of Arabidopsis thaliana.** *PLoS ONE* 8(11): p.e73541. DOI: 10.1371/journal.pone.0073541.

Hands-Taylor, KLD, Martino, L, Tata, R, Babon, JJ, Bui, TT, Drake, AF, Beavil, RL, Pruijn, GJM, Brown, PR, Conte, MR, 2010. **Heterodimerization of the human RNase P/MRP subunits Rpp20 and Rpp25 is a prerequisite for interaction with the P3 arm of RNase MRP RNA**. *Nucleic Acids Research* 38(12): p.4052–4066. DOI: 10.1093/nar/gkq141.

Hasanuzzaman, M, Nahar, K, Alam, MM, Roychowdhury, R, Fujita, M, 2013. **Physiological, biochemical, and molecular mechanisms of heat stress tolerance in plants.** *International journal of molecular sciences* 14(5): p.9643–9684. DOI: 10.3390/ijms14059643.

He, Y, Amasino, RM, 2005. **Role of chromatin modification in flowering-time control.** *Trends in*

plant science 10(1): p.30–35. DOI: 10.1016/j.tplants.2004.11.003.

Hentze, MW, Castello, A, Schwarzl, T, Preiss, T, 2018. **A brave new world of RNA-binding proteins**. *Nature Reviews Molecular Cell Biology* 19(5): p.327–341. DOI: 10.1038/nrm.2017.130.

Honkanen, S, Jones, VAS, Morieri, G, Champion, C, Hetherington, AJ, Kelly, S, Proust, H, Saint-Marcoux, D, Prescott, H, Dolan, L, 2016. **The Mechanism Forming the Cell Surface of Tip-Growing Rooting Cells Is Conserved among Land Plants**. *Current Biology* 26(23): p.3238–3244. DOI: 10.1016/j.cub.2016.09.062.

Honys, D, Reňák, D, Feciková, J, Jedelský, PL, Nebesářová, J, Dobrev, P, Čapková, V, 2009. **Cytoskeleton-Associated Large RNP Complexes in Tobacco Male Gametophyte (EPPs) Are Associated with Ribosomes and Are Involved in Protein Synthesis , Processing , and Localization research articles**. *Journal of proteome research* 8(4): p.2015–2031. DOI: 10.1021/pr8009897.

Honys, D, Oh, SA, Reňák, D, Donders, M, Šolcová, B, Johnson, JA, Boudová, R, Twell, D, 2006. **Identification of microspore-active promoters that allow targeted manipulation of gene expression at early stages of microgametogenesis in Arabidopsis**. *BMC Plant Biology* 6: p.1–9. DOI: 10.1186/1471-2229-6-31.

Honys, D, Twell, D, 2004. **Transcriptome analysis of haploid male gametophyte development in Arabidopsis**. *Genome biology* 5(11): p.R85–R85. DOI: 10.1186/gb-2004-5-11-r85.

Hua, Y, Zhou, J, 2004. **Rpp20 interacts with SMN and is re-distributed into SMN granules in response to stress**. *Biochemical and Biophysical Research Communications* 314(1): p.268–276. DOI: 10.1016/j.bbrc.2003.12.084.

Huijser, P, Schmid, M, 2011. **The control of developmental phase transitions in plants.** *Development (Cambridge, England)* 138(19): p.4117–4129. DOI: 10.1242/dev.063511.

Irene Julca, Camilla Ferrari, María Flores-Tornero, Sebastian Proost, Ann-Cathrin Lindner, Dieter Hackenberg, Lenka Steinbachová, Christos Michaelidis, Sónia Gomes Pereira, Chandra Shekhar Misra, Tomokazu Kawashima, Michael Borg, Frédéric Berger, Jacob Goldberg, Mark Johnson, David Honys, David Twell, … Marek Mutwil, 2021. **Comparative transcriptomic analysis reveals conserved programmes underpinning organogenesis and reproduction in land plants**. *Nature Plants* 7: p.1153–1159. DOI: 10.1038/s41477-021-00958-2.

Iserman, C, Desroches Altamirano, C, Jegers, C, Friedrich, U, Zarin, T, Fritsch, AW, Mittasch, M, Domingues, A, Hersemann, L, Jahnel, M, Richter, D, Guenther, UP, Hentze, MW, Moses, AM, Hyman, AA, Kramer, G, Kreysing, M, … Alberti, S, 2020. **Condensation of Ded1p Promotes a Translational Switch from Housekeeping to Stress Protein Production**. *Cell* 181(4): p.818-831.e19. DOI: 10.1016/j.cell.2020.04.009.

Ito, S, Song, YH, Josephson-Day, AR, Miller, RJ, Breton, G, Olmstead, RG, Imaizumi, T, 2012. **FLOWERING BHLH transcriptional activators control expression of the photoperiodic**

flowering regulator CONSTANS in Arabidopsis. *Proceedings of the National Academy of Sciences of the United States of America* 109(9): p.3582–3587. DOI: 10.1073/pnas.1118876109.

Jagadeesh, J, Vembar, SS, 2024. **Evolution of sequence, structural and functional diversity of the ubiquitous DNA/RNA-binding Alba domain**. *Scientific Reports* 14(1): p.1–17. DOI: 10.1038/s41598-024-79937-4.

Jang, GJ, Yang, JY, Hsieh, HL, Wu, SH, 2019. **Processing bodies control the selective translation for optimal development of Arabidopsis young seedlings**. *Proceedings of the National Academy of Sciences of the United States of America* 116(13): p.6451–6456. DOI: 10.1073/pnas.1900084116.

Jang, S, Torti, S, Coupland, G, 2009. **Genetic and spatial interactions between FT, TSF and SVP during the early stages of floral induction in Arabidopsis.** *The Plant journal : for cell and molecular biology* 60(4): p.614–625. DOI: 10.1111/j.1365-313X.2009.03986.x.

Jelinska, C, Conroy, MJ, Craven, CJ, Hounslow, AM, Bullough, PA, Waltho, JP, Taylor, GL, White, MF, Ky, F, Court, F, Bank, W, Sheffield, S, 2005. **Obligate Heterodimerization of the Archaeal Alba2 Protein with Alba1 Provides a Mechanism for Control of DNA Packaging**. 13: p.963–971. DOI: 10.1016/j.str.2005.04.016.

Jung, C, Müller, AE, 2009. **Flowering time control and applications in plant breeding.** *Trends in plant science* 14(10): p.563–573. DOI: 10.1016/j.tplants.2009.07.005.

Kazan, K, Lyons, R, 2016. **The link between flowering time and stress tolerance**. *Journal of Experimental Botany* 67(1): p.47–60. DOI: 10.1093/jxb/erv441.

Kiledjian, M, Dreyfuss, G, 1992. **Primary structure and binding activity of the hnRNP U protein: Binding RNA through RGG box**. *EMBO Journal* 11(7): p.2655–2664. DOI: 10.1002/j.1460-2075.1992.tb05331.x.

Kim, SY, Hong, CB, Lee, I, 2001. **Heat shock stress causes stage-specific male sterility in Arabidopsis thaliana**. *Journal of Plant Research* 114(3): p.301–307. DOI: 10.1007/pl00013991.

Kim, W-Y, Fujiwara, S, Suh, S-S, Kim, J, Kim, Y, Han, L, David, K, Putterill, J, Nam, HG, Somers, DE, 2007. **ZEITLUPE is a circadian photoreceptor stabilized by GIGANTEA in blue light.** *Nature* 449(7160): p.356–360. DOI: 10.1038/nature06132.

Kim, W-Y, Ali, Z, Park, HJ, Park, SJ, Cha, J-Y, Perez-Hormaeche, J, Quintero, FJ, Shin, G, Kim, MR, Qiang, Z, Ning, L, Park, HC, Lee, SY, Bressan, RA, Pardo, JM, Bohnert, HJ, Yun, D-J, 2013. **Release of SOS2 kinase from sequestration with GIGANTEA determines salt tolerance in Arabidopsis.** *Nature communications* 4: p.1352. DOI: 10.1038/ncomms2357.

Kočová, H, 2020. *Funkční charakterizace proteinů rodiny Alba u huseníčku rolního*. Karlova Univerzita.

Koonin, E V., Wolf, YI, Aravind, L, 2001. **Prediction of the archeal exosome and its connections with the proteasome and the translation and transcription machineries by a comparative-genomic approach**. *Genome Research* 11(2): p.240–252. DOI: 10.1101/gr.162001.

Kouzuma, Y, Mizoguchi, M, Hisanori, T, Fukuhara, H, Tsukamoto, M, Numata, T, Kimura, M, 2003. **Reconstitution of archaeal ribonuclease P from RNA and four protein components**. *Biochemical and Biophysical Research Communications* 306: p.666–673. DOI: 10.1016/S0006-291X(03)01034-9.

Kramer, S, Queiroz, R, Ellis, L, Webb, H, Hoheisel, JD, Clayton, C, Carrington, M, 2008. **Heat shock causes a decrease in polysomes and appearance of stress granules in trypanosomes independently of eIF2α phosphorylation at threonine 169**. *Journal of Cell Science* 121(Pt 18): p.3002–14. DOI: 10.1242/jcs.031823.

Krasensky, J, Jonak, C, 2012. **Drought, salt, and temperature stress-induced metabolic rearrangements and regulatory networks.** *Journal of experimental botany* 63(4): p.1593–1608. DOI: 10.1093/jxb/err460.

Kubalová, M, Griffiths, J, Müller, K, Levenets, L, Tylová, E, Tarkowská, D, Jones, AM, Fendrych, M, 2025. **Gibberellin-deactivating GA2OX enzymes act as a hub for auxin-gibberellin cross talk in Arabidopsis thaliana root growth regulation**. *PNAS* 122(30). DOI: 10.1073/pnas.2425574122.

Laanen, P, Cuypers, A, Saenen, E, Horemans, N, 2023. **Plant Physiology and Biochemistry Flowering under enhanced ionising radiation conditions and its regulation through epigenetic mechanisms**. *Plant Physiology and Biochemistry* 196(June 2022): p.246–259. DOI: 10.1016/j.plaphy.2023.01.049.

Laurens, N, Driessen, RPC, Heller, I, Vorselen, D, Noom, MC, Hol, FJH, White, MF, Dame, RT, Wuite, GJL, 2012. **Alba shapes the archaeal genome using a delicate balance of bridging and stiffening the DNA**. *Nature Communications* 3: p.1328. DOI: 10.1038/ncomms2330.

Lemieux, B, Laterreur, N, Perederina, A, Noël, JF, Dubois, ML, Krasilnikov, AS, Wellinger, RJ, 2016. **Active Yeast Telomerase Shares Subunits with Ribonucleoproteins RNase P and RNase MRP**. *Cell* 165(5): p.1171–1181. DOI: 10.1016/j.cell.2016.04.018.

Li, B, Gao, K, Ren, H, Tang, W, 2018. **Molecular mechanisms governing plant responses to high temperatures**. *Journal of Integrative Plant Biology* 60(9): p.757–779. DOI: 10.1111/jipb.12701.

Li, Y, Altman, S, 2001. **A subunit of human nuclear RNase P has ATPase activity**. *Proceedings of the National Academy of Sciences of the United States of America* 98(2): p.441–444. DOI: 10.1073/pnas.98.2.441.

Li, Z, Tian, Y, Zhao, W, Xu, J, Wang, L, Peng, R, Yao, Q, 2015. **Functional characterization of a grape heat stress transcription factor VvHsfA9 in transgenic Arabidopsis**. *Acta Physiologiae Plantarum* 37(7): p.1–10. DOI: 10.1007/s11738-015-1884-x.

Lin, SY, Chen, PW, Chuang, MH, Juntawong, P, Bailey-Serres, J, Jauh, GY, 2014. **Profiling of translatomes of in vivo-grown pollen tubes reveals genes with roles in micropylar guidance during pollination in Arabidopsis**. *Plant Cell* 26(2): p.602–618. DOI: 10.1105/tpc.113.121335.

Liu, Q, Dreyfuss, G, 1995. **In Vivo and In Vitro Arginine Methylation of RNA-Binding Proteins**.

Molecular and Cellular Biology 15(5): p.2800–2808. DOI: 10.1128/mcb.15.5.2800.

Liu, Y, Guo, L, Guo, R, Wong, RL, Hernandez, H, Hu, J, Chu, Y, Amster, IJ, Whitman, WB, Huang, L, 2009. **The Sac10b homolog in Methanococcus maripaludis binds DNA at specific sites.** *Journal of bacteriology* 191(7): p.2315–2329. DOI: 10.1128/JB.01534-08.

Ljungman, M, Hanawalt, PC, 1992. **Efficient protection against oxidative DNA damage in chromatin**. *Molecular Carcinogenesis* 5(4): p.264–269. DOI: 10.1002/mc.2940050406.

Lu, YW, Huang, T, Tsai, CT, Chang, YY, Li, HW, Hsu, CH, Fan, HF, 2013. **Using single-molecule approaches to study archaeal DNA-binding protein Alba1**. *Biochemistry* 52(44): p.7714–7722. DOI: 10.1021/bi4010478.

Lurz, R, Grote, M, Dijk, J, Reinhardt, R, Dobrinski, B, 1986. **Electron microscopic study of DNA complexes with proteins from the Archaebacterium Sulfolobus acidocaldarius**. *The EMBO Journal* 5(13): p.3715–3721. DOI: 10.1002/j.1460-2075.1986.tb04705.x.

Ma, H, 2005. **Molecular genetic analyses of microsporogenesis and microgametogenesis in flowering plants.** *Annual review of plant biology* 56: p.393–434. DOI: 10.1146/annurev.arplant.55.031903.141717.

Magwanga, RO, Kirungu, JN, Lu, P, Cai, X, Xu, Y, Wang, X, Zhou, Z, Hou, Y, Agong, SG, Wang, K, Liu, F, 2019. **Knockdown of ghAlba_4 and ghAlba_5 Proteins in Cotton Inhibits Root Growth and Increases Sensitivity to Drought and Salt Stresses**. *Frontiers in Plant Science* 10(1292): p.1–20. DOI: 10.3389/fpls.2019.01292.

Mair, GR, Lasonder, E, Garver, LS, Franke-Fayard, BMD, Carret, CK, Wiegant, JCAG, Dirks, RW, Dimopoulos, G, Janse, CJ, Waters, AP, 2010. **Universal features of post-transcriptional gene regulation are critical for Plasmodium zygote development**. *PLoS Pathogens* 6(2): p.e1000767. DOI: 10.1371/journal.ppat.1000767.

Majee, A, Kumari, D, Sane, VA, Singh, RK, 2023. **Novel roles of HSFs and HSPs, other than relating to heat stress, in temperature-mediated flowering**. *Annals of Botany* 132(6): p.1103–1106. DOI: 10.1093/aob/mcad112.

Maldonado-Bonilla, LD, 2014. **Composition and function of P bodies in Arabidopsis thaliana**. *Frontiers in Plant Science* 5(May): p.1–11. DOI: 10.3389/fpls.2014.00201.

Mancio-Silva, L, Rojas-Meza, AP, Vargas, M, Scherf, A, Hernandez-Rivas, R, 2008. **Differential association of Orc1 and Sir2 proteins to telomeric domains in Plasmodium falciparum.** *Journal of cell science* 121(Pt 12): p.2046–2053. DOI: 10.1242/jcs.026427.

Mani, J, Güttinger, A, Schimanski, B, Heller, M, Acosta-Serrano, A, Pescher, P, Späth, G, Roditi, I, 2011. **Alba-Domain Proteins of Trypanosoma brucei are Cytoplasmic RNA-Binding Proteins That Interact with the Translation Machinery**. *PLoS ONE* 6(7): p.e22463. DOI: 10.1371/journal.pone.0022463.

Margaritopoulou, T, Kryovrysanaki, N, Megkoula, P, Prassinos, C, Samakovli, D, Milioni, D, Hatzopoulos, P, 2016. **HSP90 canonical content organizes a molecular scaffold mechanism**

to progress flowering. *The Plant journal : for cell and molecular biology* 87(2): p.174–187. DOI: 10.1111/tpj.13191.

Marsh, VL, Peak-Chew, SY, Bell, SD, 2005. **Sir2 and the acetyltransferase, Pat, regulate the archaeal chromatin protein, Alba.** *The Journal of biological chemistry* 280(22): p.21122–21128. DOI: 10.1074/jbc.M501280200.

Martin-Tryon, EL, Kreps, JA, Harmer, SL, 2007. **GIGANTEA acts in blue light signaling and has biochemically separable roles in circadian clock and flowering time regulation**. *Plant Physiology* 143(1): p.473–486. DOI: 10.1104/pp.106.088757.

Matiz-González, JM, Pardo-Rodriguez, D, Puerta, CJ, Requena, JM, Nocua, PA, Cuervo, C, 2024. **Exploring the functionality and conservation of Alba proteins in Trypanosoma cruzi: A focus on biological diversity and RNA binding ability**. *International Journal of Biological Macromolecules* 272(Pt 2). DOI: 10.1016/j.ijbiomac.2024.132705.

McCue, AD, Cresti, M, Feijó, JA, Slotkin, RK, 2011. **Cytoplasmic connection of sperm cells to the pollen vegetative cell nucleus: Potential roles of the male germ unit revisited**. *Journal of Experimental Botany* 62(5): p.1621–1631. DOI: 10.1093/jxb/err032.

Mi, H, Muruganujan, A, Huang, X, Ebert, D, Mills, C, Guo, X, Thomas, PD, 2019. **Protocol Update for large-scale genome and gene function analysis with the PANTHER classification system (v.14.0)**. *Nature Protocols* 14(3): p.703–721. DOI: 10.1038/s41596-019-0128-8.

Mizoguchi, T, Wright, L, Fujiwara, S, Cremer, F, Lee, K, Onouchi, H, Mouradov, A, Fowler, S, Kamada, H, Putterill, J, Coupland, G, 2005. **Distinct roles of GIGANTEA in promoting flowering and regulating circadian rhythms in Arabidopsis**. *Plant Cell* 17(8): p.2255–2270. DOI: 10.1105/tpc.105.033464.

Murashige, T, Skoog, F, 1962. **A Revised Medium for Rapid Growth and Bio Assays with Tobacco Tissue Cultures**. *Physiologia Plantarum* 15(3): p.473–497. DOI: 10.1111/j.1399-3054.1962.tb08052.x.

Nag, S, Banerjee, C, Goyal, M, Siddiqui, AA, Saha, D, Mazumder, S, Debsharma, S, Pramanik, S, Saha, SJ, De, R, Bandyopadhyay, U, 2024. **Plasmodium falciparum Alba6 exhibits DNase activity and participates in stress response**. *iScience* 27(4): p.109467. DOI: 10.1016/j.isci.2024.109467.

Nakaminami, K, Seki, M, 2018. **RNA Regulation in Plant Cold Stress Response.** *Advances in experimental medicine and biology* 1081: p.23–44. DOI: 10.1007/978-981-13-1244-1_2.

Náprstková, A, 2016. *Proteiny rodiny Alba a jejich úloha ve vývoji samčího gametofytu*. Karlova Univerzita.

Náprstková, A, Malínská, K, Záveská Drábková, L, Billey, E, Náprstková, D, Sýkorová, E, Bousquet-Antonelli, C, Honys, D, 2021. **Characterization of alba family expression and localization in arabidopsis thaliana generative organs**. *International Journal of Molecular Sciences* 22(4): p.1–23. DOI: 10.3390/ijms22041652.

Nepi, M, Franchi, GG, Pacini, E, 2001. **Pollen hydration status at dispersal: Cytophysiological features and strategies**. *Protoplasma* 216(3–4): p.171–180. DOI: 10.1007/BF02673869.

Ohama, N, Sato, H, Shinozaki, K, Yamaguchi-Shinozaki, K, 2017. **Transcriptional Regulatory Network of Plant Heat Stress Response**. *Trends in Plant Science* 22(1): p.53–65. DOI: 10.1016/j.tplants.2016.08.015.

Olson, MOJ, 2004. **Sensing cellular stress: another new function for the nucleolus?** *sci STKE* (224): p.pe10. DOI: 10.1126/stke.2242004pe10.

Ozdilek, BA, Thompson, VF, Ahmed, NS, White, CI, Batey, RT, Schwartz, JC, 2017. **Intrinsically disordered RGG/RG domains mediate degenerate specificity in RNA binding**. *Nucleic Acids Research* 45(13): p.7984–7996. DOI: 10.1093/nar/gkx460.

Pacini, E, 1996. **Types and meaning of pollen carbohydrate reserves**. *Sexual Plant Reproduction* 9(6): p.362–366. DOI: 10.1007/BF02441957.

Pacini, E, Guarnieri, M, Nepi, M, 2006. **Pollen carbohydrates and water content during development, presentation, and dispersal: A short review**. *Protoplasma* 228(1–3): p.73–77. DOI: 10.1007/s00709-006-0169-z.

Palm, D, Simm, S, Darm, K, Weis, BL, Ruprecht, M, Schleiff, E, Scharf, C, 2016. **Proteome distribution between nucleoplasm and nucleolus and its relation to ribosome biogenesis in Arabidopsis thaliana**. *RNA Biology* 13(4): p.441–454. DOI: 10.1080/15476286.2016.1154252.

Park, C, Hyun, Y, Lee, JY, 2024. **Female gametophyte development is required for nucellar-tip degeneration during Arabidopsis ovule development**. *Planta* 260(4): p.1–8. DOI: 10.1007/s00425-024-04519-7.

Park, DH, Somers, DE, Kim, YS, Choy, YH, Lim, HK, Soh, MS, Kim, HJ, Kay, SA, Nam, HG, 1999. **Control of circadian rhythms and photoperiodic flowering by the Arabidopsis GIGANTEA gene.** *Science* 285(5433): p.1579–1582. DOI: 10.1126/science.285.5433.1579.

Park, HJ, Kim, W, Pardo, JM, Yun, D, 2016. **Molecular Interactions Between Flowering Time and Abiotic Stress Pathways**. *International Review of Cell and Molecular Biology* 327: p.371–412. DOI: 10.1016/bs.ircmb.2016.07.001.

Park, SK, Howden, R, Twell, D, 1998. **The Arabidopsis thaliana gametophytic mutation gemini pollen1 disrupts microspore polarity, division asymmetry and pollen cell fate**. *Development* 125(19): p.3789–3799. DOI: 10.1242/dev.125.19.3789.

Parton, RM, Fischer-Parton, S, Watahiki, MK, Trewavas, AJ, 2001. **Dynamics of the apical vesicle accumulation and the rate of growth are related in individual pollen tubes**. *Journal of Cell Science* 114(14): p.2685–2695. DOI: 10.1242/jcs.114.14.2685.

Pasin, F, Bedoya, LC, Bernabé-Orts, JM, Gallo, A, Simón-Mateo, C, Orzaez, D, García, JA, 2017. **Multiple T-DNA Delivery to Plants Using Novel Mini Binary Vectors with Compatible Replication Origins**. *ACS Synthetic Biology* 6(10): p.1962–1968. DOI: 10.1021/acssynbio.6b00354.

Patro, R, Duggal, G, Love, MI, Irizarry, RA, Kingsford, C, 2017. **Salmon: fast and bias-aware quantification of transcript expression using dual-phase inference**. *Nature Methods* 14(4): p.417–419. DOI: 10.1038/nmeth.4197.

Pavlov, NA, Cherny, DI, Nazimov, I V, Slesarev, AI, Subramaniam, V, 2002. **Identification, cloning and characterization of a new DNA-binding protein from the hyperthermophilic methanogen Methanopyrus kandleri.** *Nucleic acids research* 30(3): p.685–694. DOI: 10.1093/nar/30.3.685.

Perederina, A, Esakova, O, Quan, C, Khanova, E, Krasilnikov, AS, 2010. **Eukaryotic ribonucleases P/MRP: the crystal structure of the P3 domain.** *EMBO Journal* 29(4): p.761–769. DOI: 10.1038/emboj.2009.396.

Pérez-Díaz, L, Silva, TC, Teixeira, SMR, 2017. **Involvement of an RNA binding protein containing Alba domain in the stage-specific regulation of beta-amastin expression in Trypanosoma cruzi**. *Molecular and Biochemical Parasitology* 211: p.1–8. DOI: 10.1016/j.molbiopara.2016.12.005.

Pimentel, H, Bray, NL, Puente, S, Melsted, P, Pachter, L, 2017. **Differential analysis of RNA-seq incorporating quantification uncertainty**. *Nature Methods* 14(7): p.687–690. DOI: 10.1038/nmeth.4324.

Pluk, H, van Eenennaam, H, Rutjes, SA, Pruijn, GJ, van Venrooij, WJ, 1999. **RNA-protein interactions in the human RNase MRP ribonucleoprotein complex.** *RNA* 5(4): p.512–524. DOI: 10.1017/s1355838299982079.

Popelářová, A, 2021. *Dynamics of ALBA proteins in Arabidopsis thaliana evaluated by fluorescence microscopy*. Karlova Univerzita.

Qin, F, Shinozaki, K, Yamaguchi-Shinozaki, K, 2011. **Achievements and challenges in understanding plant abiotic stress responses and tolerance**. *Plant and Cell Physiology* 52(9): p.1569–1582. DOI: 10.1093/pcp/pcr106.

Qin, F, Yu, B, Li, W, 2021. **Heat shock protein 101 (HSP101) promotes flowering under nonstress conditions.** *Plant physiology* 186(1): p.407–419. DOI: 10.1093/plphys/kiab052.

Queitsch, C, Hong, SW, Vierling, E, Lindquist, S, 2000. **Heat shock protein 101 plays a crucial role in thermotolerance in Arabidopsis**. *Plant Cell* 12(4): p.479–492. DOI: 10.1105/tpc.12.4.479.

R Core Team, 2018. **R: A language and environment for statistical computing.** *R Foundation for Statistical Computing, Vienna, Austria.*

Reichel, M, Tankmar, MD, Rennie, S, Arribas-Hernández, L, Lewinski, M, Köster, T, Wang, N, Millar, AA, Staiger, D, Brodersen, P, 2024. **ALBA proteins facilitate cytoplasmic YTHDF-mediated reading of m6A in Arabidopsis**. *EMBO Journal* 43(24): p.6626–6655. DOI: 10.1038/s44318-024-00312-0.

Reichel, M, Liao, Y, Rettel, M, Ragan, C, Evers, M, Alleaume, A, Horos, R, Hentze, MW, Preiss, T, Millar, AA, 2016. **In Planta Determination of the mRNA-Binding Proteome of Arabidopsis**

Etiolated Seedlings. *The Plant Cell* 28(10): p.2435–2452. DOI: 10.1105/tpc.16.00562.

Reiner, R, Ben-asouli, Y, Krilovetzky, I, Jarrous, N, 2006. **A role for the catalytic ribonucleoprotein RNase P in RNA polymerase III transcription**. *Genes & development* 20: p.1621–1635. DOI: 10.1101/gad.386706.Newly.

Reiner, R, Alfiya-Mor, N, Berrebi-Demma, M, Wesolowski, D, Altman, S, Jarrous, N, 2011. **RNA binding properties of conserved protein subunits of human RNase P.** *Nucleic acids research* 39(13): p.5704–5714. DOI: 10.1093/nar/gkr126.

Resentini, F, Orozco-Arroyo, G, Cucinotta, M, Mendes, MA, 2023. **The impact of heat stress in plant reproduction**. *Frontiers in Plant Science* 14(December): p.1–12. DOI: 10.3389/fpls.2023.1271644.

Riboni, M, Galbiati, M, Tonelli, C, Conti, L, 2013. **GIGANTEA Enables Drought Escape Response via Abscisic Acid-Dependent Activation of the Florigens and**. 162(July): p.1706–1719. DOI: 10.1104/pp.113.217729.

Rigden, DJ, Galperin, MY, 2008. **Sequence analysis of GerM and SpoVS, uncharacterized bacterial 'sporulation' proteins with widespread phylogenetic distribution**. *Bioinformatics* 24(16): p.1793–1797. DOI: 10.1093/bioinformatics/btn314.

Robinson-Beers, K, Pruitt, RE, Gasser, CS, 1992. **Ovule Development in Wild-Type Arabidopsis and Two Female-Sterile Mutants.** *The Plant Cell* 4(10): p.1237–1249. DOI: 10.1105/tpc.4.10.1237.

Russell, SD, Jones, DS, 2015. **The male germline of angiosperms: Repertoire of an inconspicuous but important cell lineage**. *Frontiers in Plant Science* 6(173): p.1–10. DOI: 10.3389/fpls.2015.00173.

Saibo, NJM, Lourenço, T, Oliveira, MM, 2009. **Transcription factors and regulation of photosynthetic and related metabolism under environmental stresses**. *Annals of Botany* 103(4): p.609–623. DOI: 10.1093/aob/mcn227.

Sakata, T, Oshino, T, Miura, S, Tomabechi, M, Tsunaga, Y, Higashitani, N, Miyazawa, Y, Takahashi, H, Watanabe, M, Higashitani, A, 2010. **Auxins reverse plant male sterility caused by high temperatures**. *Proceedings of the National Academy of Sciences of the United States of America* 107(19): p.8569–8574. DOI: 10.1073/pnas.1000869107.

Santos-Pereira, JM, Aguilera, A, 2015. **R loops: new modulators of genome dynamics and function.** *Nature reviews. Genetics* 16(10): p.583–597. DOI: 10.1038/nrg3961.

Sarrion-Perdigones, A, Falconi, EE, Zandalinas, SI, Juárez, P, Fernández-del-Carmen, A, Granell, A, Orzaez, D, 2011. **GoldenBraid: An iterative cloning system for standardized assembly of reusable genetic modules**. *PLoS ONE* 6(7). DOI: 10.1371/journal.pone.0021622.

Sarrion-Perdigones, A, Vazquez-Vilar, M, Palací, J, Castelijns, B, Forment, J, Ziarsolo, P, Blanca, J, Granell, A, Orzaez, D, 2013. **Goldenbraid 2.0: A comprehensive DNA assembly framework for plant synthetic biology**. *Plant Physiology* 162(3): p.1618–1631. DOI:

10.1104/pp.113.217661.

Sato, S, Kamiyama, M, Iwata, T, Makita, N, Furukawa, H, Ikeda, H, 2006. **Moderate increase of mean daily temperature adversely affects fruit set of Lycopersicon esculentum by disrupting specific physiological processes in male reproductive development**. *Annals of Botany* 97(5): p.731–738. DOI: 10.1093/aob/mcl037.

Scott, RJ, Spielman, M, Dickinson, HG, 2004. **Stamen structure and function**. *Plant Cell* 16(Suppl): p.46–61. DOI: 10.1105/tpc.017012.

Scutenaire, J, Deragon, JM, Jean, V, Benhamed, M, Raynaud, C, Favory, JJ, Merret, R, Bousquet-Antonelli, C, 2018. **The YTH domain protein ECT2 is an m6A reader required for normal trichome branching in arabidopsis**. *Plant Cell* 30(5): p.986–1005. DOI: 10.1105/tpc.17.00854.

Searle, I, He, Y, Turck, F, Vincent, C, Fornara, F, Kröber, S, Amasino, RA, Coupland, G, 2006. **The transcription factor FLC confers a flowering response to vernalization by repressing meristem competence and systemic signaling in Arabidopsis**. *Genes and Development* 20(7): p.898–912. DOI: 10.1101/gad.373506.

Simpson, GG, Dean, C, 2002. **Arabidopsis, the Rosetta stone of flowering time?** *Science* 296(5566): p.285–289. DOI: 10.1126/science.296.5566.285.

Skinner, DJ, Hill, TA, Gasser, CS, 2004. **Regulation of ovule development.** *The Plant Cell* 16 Suppl(Suppl): p.S32-45. DOI: 10.1105/tpc.015933.

Song, L, Florea, L, 2015. **Rcorrector: Efficient and accurate error correction for Illumina RNA-seq reads**. *GigaScience* 4(1): p.1–8. DOI: 10.1186/s13742-015-0089-y.

Steffen, A, Elgner, M, Staiger, D, 2019. **Regulation of Flowering Time by the RNA-Binding Proteins AtGRP7 and AtGRP8**. *Plant and Cell Physiology* 60(9): p.2040–2050. DOI: 10.1093/pcp/pcz124.

Suárez-López, P, Wheatley, K, Robson, F, Onouchi, H, Valverde, F, Coupland, G, 2001. **CONSTANS mediates between the circadian clock and the control of flowering in Arabidopsis.** *Nature* 410(6832): p.1116–1120. DOI: 10.1038/35074138.

Subota, I, Rotureau, B, Blisnick, T, Ngwabyt, S, Durand-Dubief, M, Engstler, M, Bastin, P, 2011. **ALBA proteins are stage regulated during trypanosome development in the tsetse fly and participate in differentiation**. *Molecular Biology of the Cell* 22(22): p.4205–4219. DOI: 10.1091/mbc.E11-06-0511.

Sun, Q, Csorba, T, Skourti-stathaki, K, Proudfoot, NJ, 2013. **R-Loop Stabilization Represses Antisense Transcription at the Arabidopsis FLC Locus**. *Science* 340(6132): p.619–621. DOI: 10.1126/science.1234848.

Sunkar, R, Chinnusamy, V, Zhu, J, Zhu, J-K, 2007. **Small RNAs as big players in plant abiotic stress responses and nutrient deprivation.** *Trends in plant science* 12(7): p.301–309. DOI: 10.1016/j.tplants.2007.05.001.

Sze, H, Klodová, B, Ward, JM, Harper, JF, Palanivelu, R, Johnson, MA, Honys, D, 2024. **A wave of**

specific transcript and protein accumulation accompanies pollen dehydration. *Plant Physiology* 195(3): p.1775–1795. DOI: 10.1093/plphys/kiae177.

Sze, H, Palanivelu, R, Harper, JF, Johnson, MA, 2021. **Holistic insights from pollen omics: Co-opting stress-responsive genes and ER-mediated proteostasis for male fertility**. *Plant Physiology* 187(4): p.2361–2380. DOI: 10.1093/plphys/kiab463.

Szostak, E, Gebauer, F, 2013. **Translational control by 3´-UTR-binding proteins**. *Brief Funct Genomics* 12(1): p.58–65. DOI: 10.1093/bfgp/els056.

Takeno, K, 2016. **Stress-induced flowering: the third category of flowering response.** *Journal of experimental botany* 67(17): p.4925–4934. DOI: 10.1093/jxb/erw272.

Tanaka, T, Padavattan, S, Kumarevel, T, 2012. **Crystal structure of archaeal chromatin protein alba2-double-stranded DNA complex from Aeropyrum pernix K1**. *Journal of Biological Chemistry* 287(13): p.10394–10402. DOI: 10.1074/jbc.M112.343210.

Tanou, G, Filippou, P, Belghazi, M, Job, D, Diamantidis, G, Fotopoulos, V, Molassiotis, A, 2012. **Oxidative and nitrosative-based signaling and associated post-translational modifications orchestrate the acclimation of citrus plants to salinity stress.** *The Plant journal : for cell and molecular biology* 72(4): p.585–599. DOI: 10.1111/j.1365-313X.2012.05100.x.

Teotia, S, Tang, G, 2015. **To Bloom or Not to Bloom: Role of MicroRNAs in Plant Flowering**. *Molecular Plant* 8(3): p.359–377. DOI: https://doi.org/10.1016/j.molp.2014.12.018.

Thandapani, P, O'Connor, TR, Bailey, TL, Richard, S, 2013. **Defining the RGG/RG Motif**. *Molecular Cell* 50(5): p.613–623. DOI: 10.1016/j.molcel.2013.05.021.

Thomas, PD, Ebert, D, Muruganujan, A, Mushayahama, T, Albou, LP, Mi, H, 2021. **PANTHER: Making genome-scale phylogenetics accessible to all**. *Protein Science* 31(1): p.8–22. DOI: 10.1002/pro.4218.

Tiang, C-L, He, Y, Pawlowski, WP, 2012. **Chromosome organization and dynamics during interphase, mitosis, and meiosis in plants.** *Plant physiology* 158(1): p.26–34. DOI: 10.1104/pp.111.187161.

Tong, J, Ren, Z, Sun, L, Zhou, S, Yuan, W, Hui, Y, Ci, D, Wang, W, Fan, L, Wu, Z, Qian, W, 2022. **ALBA proteins confer thermotolerance through stabilizing HSF messenger RNAs in cytoplasmic granules**. *Nature Plants* 8(July): p.778–791. DOI: 10.1038/s41477-022-01175-1.

Tonkin, CJ, Carret, CK, Duraisingh, MT, Voss, TS, Ralph, SA, Hommel, M, Duffy, MF, Silva, LM da, Scherf, A, Ivens, A, Speed, TP, Beeson, JG, Cowman, AF, 2009. **Sir2 paralogues cooperate to regulate virulence genes and antigenic variation in Plasmodium falciparum.** *PLoS biology* 7(4): p.e84. DOI: 10.1371/journal.pbio.1000084.

Tsuji, H, 2017. **Molecular function of florigen.** *Breeding science* 67(4): p.327–332. DOI: 10.1270/jsbbs.17026.

Tupý, J, 1982. **Alterations in polyadenylated RNA during pollen maturation and germination**. *Biologia Plantarum* 24(5): p.331–340. DOI: 10.1007/BF02909098.

Twell, D, 2011. **Male gametogenesis and germline specification in flowering plants.** *Sexual plant reproduction* 24(2): p.149–160. DOI: 10.1007/s00497-010-0157-5.

Vanderweyde, T, Youmans, K, Liu-Yesucevitz, L, Wolozin, B, 2013. **Role of stress granules and RNA-binding proteins in neurodegeneration: a mini-review.** *Gerontology* 59(6): p.524–533. DOI: 10.1159/000354170.

Vasilyev, N, Polonskaia, A, Darnell, JC, Darnell, RB, Patel, DJ, Serganov, A, 2015. **Crystal structure reveals specific recognition of a G-quadruplex RNA by a β-turn in the RGG motif of FMRP**. *Proceedings of the National Academy of Sciences of the United States of America* 112(39): p.E5391–E5400. DOI: 10.1073/pnas.1515737112.

Vazquez-Vilar, M, Quijano-Rubio, A, Fernandez-Del-Carmen, A, Sarrion-Perdigones, A, Ochoa-Fernandez, R, Ziarsolo, P, Blanca, J, Granell, A, Orzaez, D, 2017. **GB3.0: a platform for plant bio-design that connects functional DNA elements with associated biological data**. *Nucleic acids research* 45(4): p.2196–2209. DOI: 10.1093/nar/gkw1326.

Verma, JK, Gayali, S, Dass, S, Kumar, A, Parveen, S, Chakraborty, S, Chakraborty, N, 2014. **OsAlba1 , a dehydration-responsive nuclear protein of rice (Oryza sativa L. ssp. indica), participates in stress adaptation**. *Phytochemistry* 100: p.16–25. DOI: 10.1016/j.phytochem.2014.01.015.

Verma, JK, Wardhan, V, Singh, D, Chakraborty, S, Chakraborty, N, 2018. **Genome-Wide Identification of the Alba Gene Gamily in Plants and Stress-Responsive Expression of the Rice Alba Genes**. *Genes* 9(4): p.183. DOI: 10.3390/genes9040183.

Vijayan, A, Tofanelli, R, Strauss, S, Cerrone, L, Wolny, A, Strohmeier, J, Kreshuk, A, Hamprecht, FA, Smith, RS, Schneitz, K, 2021. **A digital 3D reference atlas reveals cellular growth patterns shaping the Arabidopsis ovule.** *eLife* 10. DOI: 10.7554/eLife.63262.

Voigt, B, Timmers, ACJ, Šamaj, J, Hlavacka, A, Ueda, T, Preuss, M, Nielsen, E, Mathur, J, Emans, N, Stenmark, H, Nakano, A, Baluška, F, Menzel, D, 2005. **Actin-based motility of endosomes is linked to the polar tip growth of root hairs**. *European Journal of Cell Biology* 84(6): p.609–621. DOI: 10.1016/j.ejcb.2004.12.029.

Wada, KC, Takeno, K, 2010. **Stress-induced flowering.** *Plant signaling & behavior* 5(8): p.944–947. DOI: 10.4161/psb.5.8.11826.

Wai, AH, Cho, LH, Peng, X, Waseem, M, Lee, D, Lee, JM, 2021. **Genome-wide identification and expression profiling of Alba gene family members in response to abiotic stress in tomato (Solanum lycopersicum L.)**. *BMC Plant Biology* 21(530): p.1–21. DOI: 10.1186/s12870-021-03310-0.

Wang, N, Jalajakumari, M, Miller, T, Asadi, M, Millar, AA, 2019. **The ALBA RNA-binding proteins function redundantly to promote growth and flowering in Arabidopsis.** *BioRxiv* 16(1): p.1–25. DOI: 10.1101/758946.

Wang, R, Dobritsa, AA, 2021. **Loss of THIN EXINE2 disrupts multiple processes in the**

mechanism of pollen exine formation. *Plant physiology* 187: p.133–157. DOI: 10.1093/plphys/kiab244.

Wang, SQ, Shi, DQ, Long, YP, Liu, J, Yang, WC, 2012. **GAMETOPHYTE DEFECTIVE 1, a putative subunit of rnases P/MRP, is essential for female gametogenesis and male competence in arabidopsis**. *PLoS ONE* 7(4). DOI: 10.1371/journal.pone.0033595.

Wardleworth, BN, Russell, RJM, Bell, SD, Taylor, GL, White, MF, 2002. **Structure of Alba: An archaeal chromatin protein modulated by acetylation**. *EMBO Journal* 21(17): p.4654–4662. DOI: 10.1093/emboj/cdf465.

Weber, C, Nover, L, Fauth, M, 2008. **Plant stress granules and mRNA processing bodies are distinct from heat stress granules**. *Plant Journal* 56(4): p.517–530. DOI: 10.1111/j.1365-313X.2008.03623.x.

Weber, E, Engler, C, Gruetzner, R, Werner, S, Marillonnet, S, 2011. **A modular cloning system for standardized assembly of multigene constructs**. *PLoS ONE* 6(2). DOI: 10.1371/journal.pone.0016765.

Welting, TJM, Kikkert, BJ, Van Venrooij, WJ, Pruijn, GJM, 2006. **Differential association of protein subunits with the human RNase MRP and RNase P complexes**. *Rna* 12(7): p.1373–1382. DOI: 10.1261/rna.2293906.

Welting, TJM, Peters, FMA, Hensen, SMM, Van Doorn, NL, Kikkert, BJ, Raats, JMH, Van Venrooij, WJ, Pruijn, GJM, 2007. **Heterodimerization regulates RNase MRP/RNase P association, localization, and expression of Rpp20 and Rpp25**. *Rna* 13(1): p.65–75. DOI: 10.1261/rna.237807.

Welting, TJM, van Verooij, WJ, Pruijn, GJM, 2004. **Mutual interactions between subunits of the human RNase MRP ribonucleoprotein complex**. *Nucleic Acids Research* 32(7): p.2138–2146. DOI: 10.1093/nar/gkh539.

Werner, S, Engler, C, Weber, E, Gruetzner, R, Marillonnet, S, 2012. **Fast track assembly of multigene constructs using Golden Gate cloning and the MoClo system.** *Bioengineered bugs* 3(1): p.38–43. DOI: 10.4161/bbug.3.1.18223.

Windari, EA, Ando, M, Mizoguchi, Y, Shimada, H, Ohira, K, Kagaya, Y, Higashiyama, T, Takayama, S, Watanabe, M, Suwabe, K, 2021. **Two aquaporins, SIP1;1 and PIP1;2, mediate water transport for pollen hydration in the Arabidopsis pistil.** *Plant biotechnology (Tokyo, Japan)* 38(1): p.77–87. DOI: 10.5511/plantbiotechnology.20.1207a.

Wuriyanghan, H, Zhang, B, Cao, W-H, Ma, B, Lei, G, Liu, Y-F, Wei, W, Wu, H-J, Chen, L-J, Chen, H-W, Cao, Y-R, He, S-J, Zhang, W-K, Wang, X-J, Chen, S-Y, Zhang, J-S, 2009. **The ethylene receptor ETR2 delays floral transition and affects starch accumulation in rice.** *The Plant Cell* 21(5): p.1473–1494. DOI: 10.1105/tpc.108.065391.

Xu, L, Liu, T, Xiong, X, Liu, W, Yu, Y, Cao, J, 2020. **AtC3H18L is a stop-codon read-through gene and encodes a novel non-tandem CCCH zinc-finger protein that can form cytoplasmic**

foci similar to mRNP granules. *Biochemical and Biophysical Research Communications* 528(1): p.140–145. DOI: 10.1016/j.bbrc.2020.05.081.

Xue, H, Guo, R, Wen, Y, Liu, D, Huang, L, 2000. **An abundant DNA binding protein from the hyperthermophilic archaeon Sulfolobus shibatae affects DNA supercoiling in a temperature-dependent fashion**. *Journal of Bacteriology* 182(14): p.3929–3933. DOI: 10.1128/JB.182.14.3929-3933.2000.

Yamaguchi, A, Kobayashi, Y, Goto, K, Abe, M, Araki, T, 2005. **TWIN SISTER OF FT (TSF) acts as a floral pathway integrator redundantly with FT.** *Plant & cell physiology* 46(8): p.1175–1189. DOI: 10.1093/pcp/pci151.

Yeh, C-H, Kaplinsky, NJ, Hu, C, Charng, Y, 2012. **Some like it hot, some like it warm: Phenotyping to explore thermotolerance diversity**. *Plant Science* 195: p.10–23. DOI: https://doi.org/10.1016/j.plantsci.2012.06.004.

Ying, L, Chen, H, Cai, W, 2014. **BnNAC485 is involved in abiotic stress responses and flowering time in Brassica napus.** *Plant Physiology and Biochemistry* 79: p.77–87. DOI: 10.1016/j.plaphy.2014.03.004.

Yoo, SY, Kim, Y, Kim, SY, Lee, JS, Ahn, JH, 2007. **Control of flowering time and cold response by a NAC-domain protein in Arabidopsis.** *PLoS ONE* 2(7): p.e642. DOI: 10.1371/journal.pone.0000642.

Young, LW, Wilen, RW, Bonham-Smith, PC, 2004. **High temperature stress of Brassica napus during flowering reduces micro- and megagametophyte fertility, induces fruit abortion, and disrupts seed production**. *Journal of Experimental Botany* 55(396): p.485–495. DOI: 10.1093/jxb/erh038.

Yuan, W, Zhou, J, Tong, J, Zhuo, W, Wang, L, Li, Y, Sun, Q, Qian, W, 2019. **ALBA protein complex reads genic R-loops to maintain genome stability in Arabidopsis**. *Science Advances* 5(5). DOI: 10.1126/sciadv.aav9040.

Zadow, ME, MacRaild, CA, Creek, DJ, Wilson, DW, 2025. **Alba protein-mediated gene and protein regulation in protozoan parasites**. *International Journal for Parasitology* 55(11): p.557–568. DOI: 10.1016/j.ijpara.2025.04.013.

Zhang, X, Li, J, Liu, A, Zou, J, Zhou, X, Xiang, J, Rerksiri, W, Peng, Y, Xiong, X, Chen, X, 2012. **Expression Profile in Rice Panicle: Insights into Heat Response Mechanism at Reproductive Stage**. *PLoS ONE* 7(11). DOI: 10.1371/journal.pone.0049652.

Zhao, K, Chai, X, Marmorstein, R, 2003. **Structure of a Sir2 substrate, Alba, reveals a mechanism for deacetylation-induced enhancement of DNA binding**. *Journal of Biological Chemistry* 278(28): p.26071–26077. DOI: 10.1074/jbc.M303666200.

Zhong, S, Li, H, Bodi, Z, Button, J, Vespa, L, Herzog, M, Fray, RG, 2008. **MTA is an Arabidopsis messenger RNA adenosine methylase and interacts with a homolog of a sex-specific splicing factor.** *The Plant Cell* 20(5): p.1278–1288. DOI: 10.1105/tpc.108.058883.

Zinn, KE, Tunc-Ozdemir, M, Harper, JF, 2010. **Temperature stress and plant sexual reproduction: Uncovering the weakest links**. *Journal of Experimental Botany* 61(7): p.1959–1968. DOI: 10.1093/jxb/erq053.